

**Experimental Studies on Machinability of Inconel Super Alloy during  
Electro-Discharge Machining: Emphasis on Surface Integrity and  
Metallurgical Characteristics of the EDMed Work Surface**

*Dissertation submitted in partial fulfillment*

*of the requirement of the degree of*

***Doctor of Philosophy***

*in*

***Industrial Design***

*By*

***Rahul***

**Roll Number: 513ID1087**

*based on the research carried out*

*under the supervision of*

***Dr. Saurav Datta***

*and*

***Prof. Bibhuti Bhusan Biswal***



March, 2017

Department of Industrial Design  
**National Institute of Technology**  
**Rourkela-769008, Odisha (INDIA)**



Department of Industrial Design

**National Institute of Technology Rourkela**

---

## **Certificate of Examination**

Roll Number: *513ID1087*

Name: *Rahul*

Title of Dissertation: *Experimental Studies on Machinability of Inconel Super Alloy during Electro-Discharge Machining: Emphasis on Surface Integrity and Metallurgical Characteristics of the EDMed Work Surface*

We the below signed, after checking the dissertation mentioned above and the official record book(s) of the student, hereby state our approval of the dissertation submitted in partial fulfillment of the requirements of the degree of *Doctor of Philosophy in Industrial Design* at *National Institute of Technology Rourkela*. We are satisfied with the volume, quality, correctness, and originality of the work presented therein.

---

**Bibhuti Bhusan Biswal (ID)**  
Co-Supervisor

---

**Saurav Datta (ME)**  
Principal Supervisor

---

Saroj Kumar Patel  
Member, DSC

---

Mohammed Rajik Khan  
Member, DSC

---

Anindya Basu  
Member DSC

---

External Examiner

---

Ranjit Kumar Sahoo  
Chairperson, DSC

---

Mohammed Rajik Khan  
Head of the Department, ID



**National Institute of Technology**  
**Rourkela-769008, Odisha, INDIA**

---

***Dr. Saurav Datta***

Assistant Professor (Mechanical Engineering)

***Prof. Bibhuti Bhusan Biswal***

Professor (Industrial Design)

Date: -----

-

## **Supervisors' Certificate**

This is to certify that the work presented in the dissertation entitled ***Experimental Studies on Machinability of Inconel Super Alloy during Electro-Discharge Machining: Emphasis on Surface Integrity and Metallurgical Characteristics of the EDMed Work Surface*** submitted by ***Rahul***, Roll Number: **513ID1087**, is a record of original research carried out by him under our supervision and guidance in partial fulfillment of the requirements of the degree of ***Doctor of Philosophy in Industrial Design***. Neither this dissertation nor any part of it has been submitted earlier for any other academic degree or diploma to any institute or university in India or abroad.

---

***Bibhuti Bhusan Biswal***

Co-Supervisor

---

***Saurav Datta***

Principal Supervisor

# *Dedication*

*This dissertation is dedicated to my family  
for their love, endless support and continuous encouragement*



# Declaration of Originality

I, **Sri Rahul**, (bearing Roll Number: **513ID1087**) from the **Department of Industrial Design**, National Institute of Technology Rourkela, hereby declare that this dissertation entitled *Experimental Studies on Machinability of Inconel Super Alloy during Electro-Discharge Machining: Emphasis on Surface Integrity and Metallurgical Characteristics of the EDMed Work Surface* presents my original work carried out as a doctoral student of National Institute of Technology Rourkela and, to the best of my knowledge, contains no material previously published or written by another person, nor any material presented by me for the award of any degree or diploma of National Institute of Technology Rourkela or any other institution. Any contribution made to this research by others, with whom I have worked at National Institute of Technology Rourkela or elsewhere, is explicitly acknowledged in the dissertation. Works of other authors cited in this dissertation have been duly acknowledged under the Chapter ‘References’. I have also submitted my original research records to the scrutiny committee for evaluation of my dissertation.

I am fully aware that in case of any non-compliance detected in future, the Senate of National Institute of Technology Rourkela may withdraw the degree awarded to me on the basis of the present dissertation.

RAHUL

# Acknowledgment

The dissertation entitled *Experimental Studies on Machinability of Inconel Super Alloy during Electro-Discharge Machining: Emphasis on Surface Integrity and Metallurgical Characteristics of the EDMed Work Surface* is a great achievement of my academic career. The execution of the dissertation work, would have not been possible without support and guidance that I received from different intellectuals at a regular interval. I am grateful to a number of persons who have guided, supported and motivated me throughout my research tenure at National Institute of Technology, Rourkela.

I would like to express my special appreciation and heartfelt thanks to my Principal Supervisor **Dr. Saurav Datta**, Assistant Professor, **Department of Mechanical Engineering**, National Institute of Technology, Rourkela, you have been a tremendous mentor for me. I would like to thank him for encouraging my research and for allowing me to grow as a research genius. His vast knowledge and extraordinary guidance helped me a lot in innumerable ways at each and every phase of my research work. I am overwhelmed and feeling felicitous for all his support, motivation and enthusiasm towards my research work. His advice on both research as well as on my career have been priceless.

I am also grateful to my Co-Supervisor **Prof. Bibhuti Bhusan Biswal**, Professor, **Department of Industrial Design**, National Institute of Technology, Rourkela (presently on lien; joined as **Director, National Institute of Technology Meghalaya**, Shillong, Meghalaya 793003) for his continuous support and encouragement during my research work. I must appreciate all his efforts and contribution to make my Ph. D. research work more productive.

I would like to thank the members of my Doctoral Scrutiny Committee (DSC); **Prof. Ranjit Kumar Sahoo** (Chairperson, DSC), Professor, Department of Mechanical Engineering, **Prof. Saroj Kumar Patel**, Associate Professor, Department of Mechanical Engineering, **Prof. Anindya Basu**, Associate Professor, Department of Metallurgical and Materials Engineering and **Prof. Mohammed Rajik Khan**, Assistant Professor and Head, Department of Industrial Design, National Institute of Technology, Rourkela, for their kind cooperation and insightful suggestions throughout my research work, which has been proved extremely fruitful for the success of this dissertation.

I am highly obliged to ***Prof. Animesh Biswas***, Honorable Director, and ***Prof. Banshidhar Majhi***, Dean (Academic Affairs), of National Institute of Technology, Rourkela for their academic support and continuous encouragement.

I do gratefully acknowledge ***Mr. AK Pradhan***, Sr. Manager (Production), **Central Tool Room and Training Centre (CTTC)**, Bhubaneswar-751024, and ***Dr. SK Swain***, Senior Scientific Officer of Central Instrumentation Facility, **Birla Institute of Technology (BIT Mesra)**, Ranchi, Jharkhand- 835215, for helping me to explore experimental facilities available therein.

Special thank goes to ***Prof. Siba Sankar Mahapatra***, Professor and Head, **Department of Mechanical Engineering**, ***Prof. Manoj Masanta***, Assistant Professor, **Department of Mechanical Engineering**, ***Prof. Raj Kishore Patel***, Associate Professor, **Department of Chemistry**, and ***Prof. Santosh Kumar Sahoo***, Assistant Professor, **Department of Metallurgical and Materials Engineering**, **National Institute of Technology Rourkela**, Odisha- 769008, for their kind support and motivation towards completion of the research work.

I enjoyed my stay at National Institute of Technology Rourkela in association with my friends and lab mates that really became a memorable part of my life. I am indebted to my friends, ***Kumar Abhishek, Chitrasen Samantra, Dilip Kumar Sen, Suman Chatterjee, Chandramani Upadhyay, Dileep Kumar Mishra, Thrinadh Jadam, Bignesh Kumar Sahu, Rahul Sharma, Anshuman Kumar Sahu, Amit Kumar Mehar, Raviteja Buddala and Akash Verma*** for their continuous support and motivation, and for always making me feel so welcome.

I am grateful to ***Ministry of Human Resource Development (MHRD)***, **Government of India**, for providing me financial support during my research tenure at National Institute of Technology Rourkela.

I would like to express a deep sense of gratitude to my parents, especially to my father, who has always stood beside me like a pillar in times of need and to whom I owe my life for his constant care, encouragement, moral support, blessings and active cooperation throughout the course of my doctoral work.

Above all, I bow to the ***Divine Power*** for granting me the wisdom, health and strength to undertake this research task and enabling me to complete it.

**Rahul**

# Abstract

Inconel alloys are Nickel-Chromium based high temperature super alloys widely applied in aerospace, marine, nuclear power generation; chemical, petrochemical and process industries. Execution of traditional machining operations on Inconel super alloy is quite difficult due to its very low thermal conductivity which increases thermal effects during machining operations. Inconel often exhibits strong work hardening behavior, high adhesion characteristics onto the tool face, and thereby alters cutting process parameters to a remarkable extent. Additionally, Inconel may contain hard abrasive particles and carbides that create excessive tool wear; and, hence, surface integrity of the end product appears disappointing. The extent of tool life is substantially reduced. Thus, Inconel super alloys are included in the category of ‘*difficult-to-cut*’ materials.

In view of the difficulties faced during conventional machining, non-traditional machining routes like Electro-Discharge Machining (EDM), Wire Electro-Discharge Machining (WEDM), micro-machining (micro-electro-discharge drilling) etc. are being attempted for processing of Inconel in order to achieve desired contour and intricate geometry of the end product with reasonably good dimensional accuracy. However, low material removal rate and inferior surface integrity seem to be a challenge.

In this context, the present dissertation has aimed at investigating machining and machinability aspects of Inconel super alloys (different grades) during electro-discharge machining. Effects of process control parameters (viz. peak discharge current, pulse-on time, gap voltage, duty factor, and flushing pressure) on influencing EDM performance in terms of Material Removal Rate (MRR), Electrode Wear Rate (EWR) and Surface Roughness (SR) of the EDMed Inconel specimens have been examined. Morphology along with topographical features of the EDMed Inconel work surface have been studied in view of severity of surface cracking and extent of white layer depth.

Additionally, X-Ray Diffraction (XRD) analysis has been carried out to study metallurgical characteristics of the EDMed work surface of Inconel specimens (viz. phases present and precipitates, extent of grain refinement, crystallite size, and dislocation density etc.) in comparison with that of ‘as received’ parent material. Results, obtained thereof, have been

interpreted with relevance to Energy Dispersive X-ray Spectroscopy (EDS) analysis, residual stress and micro-indentation hardness test data.

Effort has been made to determine the most appropriate EDM parameters setting to optimize MRR, EWR, along with  $R_a$  (roughness average), relative Surface Crack Density (SCD), as well as relative White Layer Thickness (WLT) observed onto the EDMed work surface of Inconel specimens.

Moreover, an attempt has been made to examine the ease of electro-discharge machining on Inconel work materials using Deep Cryogenically Treated (DCT) tool/workpiece. A unified attempt has also made to compare surface integrity and metallurgical characteristics of the EDMed Inconel work surface as compared to the EDMed A2 tool steel (SAE 304SS) as well as EDMed Titanium alloy (Ti-6Al-4V).

**Keywords:** Inconel; super alloy; Electro-Discharge Machining (EDM); Material Removal Rate (MRR); Electrode Wear Rate (EWR); Surface Roughness (SR); X-Ray Diffraction (XRD); Energy Dispersive X-ray Spectroscopy (EDS); Surface Crack Density (SCD); White Layer Thickness (WLT); A2 tool steel (SAE 304SS); Titanium alloy (Ti-6Al-4V).

# *Content*

Particulars	Page No.
Title Page	
Certificate of Examination	
Supervisors' Certificate	
Dedication	
Declaration of Originality	
Acknowledgment	
Abstract	
Content	
List of Figures	
List of Tables	
Abbreviations	
<b>1. Introduction</b>	<b>01-20</b>
1.1 Super Alloy Inconel	01
1.2 Machining Difficulties of Inconel	03
1.3 Literature Review	04
1.3.1 State of Art on Non-Traditional Machining of Inconel	04
1.3.2 Cryogenic Treatment (CT) of Material	09
1.3.3 Use of Cryogenically Treated Tool/Workpiece during Execution of EDM/WEDM Processes	10
1.4 Motivation and Objectives	13
1.5 Organization of the Present Dissertation	16
<b>2. Experimental Details</b>	<b>21-48</b>
2.1 Experiment (Phase I): Material and Methods	21
2.2 Experiment (Phase II): Material and Methods	29
2.3 Experiment (Phase III): Material and Methods	35
2.4 Experiment (Phase IV): Material and Methods	36
2.5 Experiment (Phase V): Material and Methods	40
2.6 Experiment (Phase VI): Material and Methods	42
<b>3. Analysis on Surface Characteristics of Electro-Discharge Machined Inconel 718</b>	<b>49-78</b>
3.1 Coverage	49
3.2 Scope of the Work	49
3.3 Results and Discussion	52
3.3.1 Analysis of SEM Micrographs: Results of EDS, XRD and Micro- Hardness Tests	52
3.3.2 Study of Parametric Influence	60
3.3.2.1 Parametric Influence on Surface Roughness	61
3.3.2.2 Parametric Influence on Surface Crack Density	64
3.3.2.3 Parametric Influence on White Layer Thickness	69
3.4 Optimization of Machining Responses	72
3.4.1 Methodology: Utility Theory Combined with Taguchi Method	72
3.4.2 Evaluation of Optimal Parameters Setting	75
3.5 Conclusions	76

<b>4. Electro-Discharge Machining of Inconel 825 using Cryogenically Treated Copper Electrode: Emphasis on Surface Integrity and Metallurgical Characteristics of the EDMed Part</b>	<b>79-98</b>
4.1 Coverage	79
4.2 Scope of the Work	80
4.3 Results and Discussion	81
4.3.1 Effects of Cryogenic Treatment of Tool Electrode	81
4.3.2 Effects of using CTT during EDM on Inconel 825	84
4.3.2.1 Surface Integrity: Emphasis on Surface Cracking and Formation of White Layer	84
4.3.2.2 Analysis of EDS and Micro-Hardness Test Data	87
4.3.2.3 Analysis of Residual Stress	90
4.3.2.4 XRD Tests: Metallurgical Analyses of the EDMed Inconel 825 Work Surface	90
4.3.3 Effects of Using CTT during EDM: Tool Wear and Tool Shape Retention Capability	94
4.4 Conclusions	96
 <b>5. Electro-Discharge Machining of Cryogenically Treated Inconel 825 Using Copper Tool Electrode</b>	 <b>99-122</b>
5.1 Coverage	99
5.2 Scope of the work	100
5.3 Results and Discussion	101
5.3.1 Effects of Cryogenic Treatment of Inconel 825 Work Material	101
5.3.2 Effects of using Cryogenically Treated Workpiece (as Compared to Normal Workpiece) during EDM on Inconel 825	102
5.3.2.1 Surface Topography: Emphasis on Surface Cracking and Formation of White Layer	102
5.3.2.2 EDS Analysis and Micro-Hardness Test	106
5.3.2.3 Analysis of Residual Stress	107
5.3.2.4 XRD Tests: Metallurgical Analyses (Phase Information, Crystallite Size, and Dislocation Density of the EDMed work surface of Inconel 825)	108
5.3.2.5 Effects of Cooling Rate (During DCT of workpiece) on EDMed surface of Inconel 825	113
5.4 Conclusions	119
 <b>6. Surface Integrity and Metallurgical Characteristics of the EDMed Work Surfaces of A2 Tool Steel (SAE 304SS), Inconel 601 and Ti-6Al-4V: A Comparative Analysis</b>	 <b>123-138</b>
6.1 Coverage	123
6.2 Properties and Applications of 304SS, Super Alloy Inconel 601 and Ti-6Al-4V	123
6.3 Scope of the Work	127
6.4 Results and Discussion	128
6.4.1 XRD Analysis (Metallurgical Observations)	128
6.4.2 Effects of Peak Discharge Current	133
6.5 Conclusions	138
 <b>7. Machining Performance Optimization during EDM of Inconel 718: Application of Satisfaction Function Approach Integrated with Taguchi Method</b>	 <b>139-158</b>
7.1 Coverage	139
7.2 Scope of the work	140
7.3 Data Analysis: Methodology	142

7.3.1 Satisfaction Function	142
7.3.2 Proposed Optimization Module	145
7.4 Results and Discussion	145
7.5 Comparative Analysis	150
7.6 Study of the characteristics of EDMed work surface of Inconel 718	154
7.7 Confirmatory Test	155
7.8 Conclusions	156
 <b>8. Machining Performance Optimization during Electro-Discharge Machining of Inconel 601, 625, 718 and 825 Super Alloys</b>	 <b>159-192</b>
8.1 Coverage	159
8.2 Scope of the Work	160
8.3 Data Analysis	163
8.3.1 Methodology	163
8.3.1.1 Fuzzy Inference System (FIS)	163
8.3.1.2 Taguchi Method	164
8.3.1.3 Proposed Optimization Route	167
8.3.2 Results and Discussion	169
8.3.2.1 Machining Performance Optimization	169
8.3.2.2 Analysis of SEM Micrographs	185
8.4 Conclusions	190
 <b>9. Summary and Contribution</b>	 <b>193-198</b>
9.1 Executive Summary	193
9.2 Research Contribution	196
9.3 Limitations of the Present Work	196
9.4 Future Scope	197
 <b>References</b>	 <b>199-216</b>
<b>Dissemination</b>	<b>217-218</b>
<b>Resume of Mr. RAHUL</b>	<b>219</b>



# List of Figures

Figure No./ Figure Caption	Page No.
Fig. 2.1: Copper tool electrode	22
Fig. 2.2: EDMed workpiece	25
Fig. 2.3: Measurement of Surface Crack Density (SCD) of the EDMed work surface obtained at parameters setting $A_2B_1C_2D_3E_4$ i.e. [OCV=60V, $I_p=3A$ , $T_{on}=200\mu s$ , $\tau=75\%$ and $F_p=0.5bar$ ]	27
Fig. 2.4: Cold mounted specimen	27
Fig. 2.5: Measurement of White Layer Thickness (WLT) for the EDMed Inconel 718 specimen obtained at parameters setting $A_5B_1C_5D_4E_3$ i.e. [OCV=90V, $I_p=3A$ , $T_{on}=500\mu s$ , $\tau=80\%$ and $F_p=0.4 bar$ ]	28
Fig. 2.6: Places of indentation for micro-hardness test (EDMed Inconel 718 obtained at parameters setting: $(A_1B_2C_2D_2E_2)$ [OCV=50V, $I_p=5A$ , $T_{on}=200\mu s$ , $\tau=70\%$ and $F_p=0.3 bar$ ] (Average micro-hardness value $\sim 387.700 HV_{0.05}$ )	29
Fig. 2.7: Time versus temperature cure for the cryogenic treatment of the tool material adapted in the present work	31
Fig. 2.8: Setup for cryogenic treatment of the tool electrode	31
Fig. 2.9: EDMed Inconel 825 specimens along with (a) NTT and, (b) CTT	33
Fig. 2.10: EDMed surface of (a) NTW of Inconel 825 and, (b) CTW of Inconel 825 along with tool electrode	36
Fig. 2.11: EDMed work surfaces of A2 Tool Steel (304SS), Inconel 601 and Ti-6Al-4V alloy	39
Fig. 2.12: (a) Setting of workpiece and electrode tool, and (b) A snapshot of EDM in progress	40
Fig. 2.13: EDM setup with graphite tool electrode	44
Fig. 2.14: Graphite tool electrode and EDMed Inconel specimens of different grades	47
Fig. 3.1: SEM micrographs of Inconel 718 work surfaces: (a) 'as received', and (b) EDMed at parameters setting: [ $V_g=50V$ , $I_p=3A$ , $T_{on}=100\mu s$ , $\tau=65\%$ , $F_p=0.2bar$ ] i.e. Run No. 01	52
Fig. 3.2(a): Morphology of the EDMed Inconel 718 work surface obtained at parametric setting [ $V_g=50V$ ; $I_p=9A$ ; $T_{on}=400\mu s$ ; $\tau=80\%$ ; $F_p=0.5bar$ ]	53
Fig. 3.2(b): Morphology of the EDMed Inconel 718 work surface obtained at parametric setting [ $V_g=80V$ ; $I_p=11A$ ; $T_{on}=300\mu s$ ; $\tau=65\%$ ; $F_p=0.5bar$ ]	53
Fig. 3.3: SEM micrograph revealing existence of white layer and HAZ as observed in EDMed Inconel 718 at [ $V_g=70V$ ; $I_p=5A$ ; $T_{on}=400\mu s$ ; $\tau=65\%$ ; $F_p=0.4bar$ ] (Run No. 12)	54
Fig. 3.4(a): Existence of crack (Type 1) as observed in EDMed Inconel 718 specimen obtained at parametric setting [ $V_g=70V$ ; $I_p=7A$ ; $T_{on}=500\mu s$ ; $\tau=70\%$ ; $F_p=0.5bar$ ] (Run No. 13)	55
Fig. 3.4(b): Existence of crack (Type 3) as observed on EDMed Inconel 718 work surface obtained at parametric setting [ $V_g=80V$ ; $I_p=11A$ ; $T_{on}=300\mu s$ ; $\tau=65\%$ ; $F_p=0.5bar$ ] (Run No. 20)	55
Fig. 3.5(a): Chemical composition of 'as received' Inconel 718 as retrieved from EDS analysis	57
Fig. 3.5(b): Chemical composition of the EDMed Inconel 718 work surface as retrieved from EDS analysis obtained at parameters setting [ $V_g=50V$ ; $I_p=3A$ ; $T_{on}=100\mu s$ ; $\tau=65\%$ ; $F_p=0.2bar$ ] (Run No. 1)	58
Fig. 3.5(c): Chemical composition of the EDMed Inconel 718 work surface as retrieved from EDS analysis obtained at parameters setting [ $V_g=90V$ ; $I_p=11A$ ; $T_{on}=400\mu s$ ; $\tau=75\%$ ; $F_p=0.3bar$ ] (Run No. 25)	58
Fig. 3.6: XRD spectra of 'as received' Inconel 718, and EDMed work surface of Inconel 718 obtained at Run No. 1 i.e. at parameters setting:	59

[ $V_g=50V$ ; $I_p=3A$ ; $T_{on}=100\mu s$ ; $\tau=65\%$ ; $F_p=0.2bar$ ]	
Fig. 3.7: Effect of peak current (B) on $R_a$	62
Fig. 3.8: Effect of pulse-on time (C) on $R_a$	63
Fig. 3.9: Effect of flushing pressure (E) on $R_a$	64
Fig. 3.10: Effect of peak current (B) on SCD	65
Fig. 3.11: Effect of pulse-on time (C) on SCD	66
Fig. 3.12: Effect of duty factor (D) on SCD	67
Fig. 3.13: Effect of flushing pressure (E) on SCD	68
Fig. 3.14: Effect of pulse-on time (C) on WLT	70
Fig. 3.15: Effect of duty factor (D) on WLT	71
Fig. 3.16: Effect of flushing pressure (E) on WLT	71
Fig. 3.17: Mean S/N ratio (of overall utility degree) plot: Predicted optimal setting = $A_4B_1C_1D_5E_3$ i.e. [ $V_g=80V$ ; $I_p=3A$ ; $T_{on}=100\mu s$ ; $\tau=85\%$ ; $F_p=0.4bar$ ]	75
Fig. 4.1.1: XRD spectra of NTT material	82
Fig. 4.1.2: XRD spectra of CTT material	82
Fig. 4.2: SEM micrographs revealing surface irregularities of the EDMed Inconel 825 specimens obtained at parameters setting [ $I_p=10A$ ; $T_{on}=300\mu s$ ; $\tau=75\%$ ] using (a) NTT and, (b) CTT	84
Fig. 4.3.1: SEM micrographs revealing existence of surface cracks on the machined Inconel 825 work surface obtained through EDM using (a) NTT (SCD $\sim 0.0155\mu m/\mu m^2$ ), and (b) CTT (SCD $\sim 0.0042\mu m/\mu m^2$ ) for a constant parameters setting i.e. [ $I_p=10A$ ; $T_{on}=100\mu s$ ; $\tau=85\%$ ]	85
Fig. 4.3.2: SEM micrographs comparing the severity of crack formation (crack opening width, $C_w$ ) at the machined Inconel 825 work surface obtained through EDM using (a) NTT and (b) CTT, for a constant parameters setting i.e. [ $I_p=10A$ ; $T_{on}=300\mu s$ ; $\tau=85\%$ ]	86
Fig. 4.4: SEM micrographs revealing existence of white layer on the machined Inconel 825 work surface obtained through EDM using (a) NTT (WLT $\sim 14.14\mu m$ ), and (b) CTT (WLT $\sim 17.812\mu m$ ) for a constant parameters setting i.e. [ $I_p=6A$ ; $T_{on}=300\mu s$ ; $\tau=85\%$ ]	87
Fig. 4.5.1: EDS elemental spectra revealing chemical composition of 'as received' Inconel 825	88
Fig. 4.5.2: EDS elemental spectra revealing chemical composition of the EDMed Inconel 825 work surface obtained using NTT at parameters setting: [ $I_p=10A$ ; $T_{on}=300\mu s$ ; $\tau=85\%$ ]	88
Fig. 4.5.3: EDS elemental spectra revealing chemical composition of the EDMed Inconel 825 work surface obtained using CTT at parameters setting: [ $I_p=10A$ ; $T_{on}=300\mu s$ ; $\tau=85\%$ ]	88
Fig. 4.6.1: XRD spectra of 'as received' Inconel 825 work material	91
Fig. 4.6.2: XRD spectra of the EDMed Inconel 825 work surface obtained using NTT at parameters setting: [ $I_p=10A$ ; $T_{on}=300\mu s$ ; $\tau=85\%$ ]	91
Fig. 4.6.3: XRD spectra of the EDMed Inconel 825 work surface obtained using CTT at parameters setting: [ $I_p=10A$ ; $T_{on}=300\mu s$ ; $\tau=85\%$ ]	91
Fig. 4.7: Macroscopic view of the edge of (a) NTT (average thickness of deposited layer $C_w = 0.4871mm$ ), and (b) CTT (average thickness of deposited layer $C_w = 0.1203mm$ ) after EDM operation on Inconel 825 specimen	95
Fig. 4.8: EDS elemental spectra revealing chemical composition at the bottom surface of tool electrode: (a) NTT, and (b) CTT after EDM operation on Inconel 825 specimen	95
Fig. 5.1.1: SEM micrographs revealing existence of surface cracks on the machined Inconel 825 surface obtained through EDM using (a) NTT (SCD $\sim 0.0155\mu m/\mu m^2$ ), and (b) CTW (SCD $\sim 0.0080\mu m/\mu m^2$ ), for a constant parameters setting i.e. [ $I_p=10A$ ; $T_{on}=100\mu s$ ; $\tau=85\%$ ]	102
Fig. 5.1.2: SEM micrographs comparing the severity of crack formation (crack opening	103

width, $C_w$ ) at EDMed Inconel 825 work surface obtained by using (a) NTW, and (b) CTW at parameters setting: [ $I_p=10A$ ; $T_{on}=300\mu s$ ; $\tau=85\%$ ]	
Fig. 5.2: SEM micrographs revealing existence of white layer on the machined Inconel 825 surface obtained through EDM using (a) NTW (WLT~14.14 $\mu m$ ), and (b) CTW (WLT~21.692 $\mu m$ ) for a constant parameters setting i.e. [ $I_p=6A$ ; $T_{on}=300\mu s$ ; $\tau=85\%$ ]	104
Fig. 5.3.1: EDS elemental spectra revealing chemical composition of ‘as received’ Inconel 825	105
Fig. 5.3.2: EDS elemental spectra revealing chemical composition of the EDMed Inconel 825 work surface obtained using NTW at parameters setting: [ $I_p=10A$ ; $T_{on}=300\mu s$ ; $\tau=85\%$ ]	105
Fig. 5.3.3: EDS elemental spectra revealing chemical composition of the EDMed Inconel 825 work surface obtained using CTW at parameters setting: [ $I_p=10A$ ; $T_{on}=300\mu s$ ; $\tau=85\%$ ]	105
Fig. 5.4.1: XRD spectra of ‘as received’ Inconel 825	109
Fig. 5.4.2: XRD spectra of the EDMed surface of Inconel 825 obtained at parameters setting: [ $I_p=10A$ ; $T_{on}=300\mu s$ ; $\tau=85\%$ ] using NTW	109
Fig. 5.4.3: XRD spectra of the EDMed surface of Inconel 825 obtained at parameters setting: [ $I_p=10A$ ; $T_{on}=300\mu s$ ; $\tau=85\%$ ] using CTW	109
Fig. 5.5: Variation of crystallite size ( $L$ ) with respect to dislocation density ( $\delta$ ) for ‘As received’ Inconel 825, the EDMed work surface of Inconel 825 obtained by using NTW, and the EDMed work surface of Inconel 825 obtained by using CTW	113
Fig. 5.6: EDS elemental spectra revealing chemical composition of the EDMed Inconel 825 surface obtained using CTW (ramp down rate during cryogenic treatment = 0.5 $^{\circ}C/min$ ) at parameters setting: [ $I_p=10A$ ; $T_{on}=300\mu s$ ; $\tau=85\%$ ]	114
Fig. 5.7: XRD spectra of the EDMed surface of Inconel 825 obtained at parameters setting: [ $I_p=10A$ ; $T_{on}=300\mu s$ ; $\tau=85\%$ ] using CTW for (a) fast cooling rate (1 $^{\circ}C/min$ ) and (b) slow cooling rate (0.5 $^{\circ}C/min$ )	115
Fig. 5.8.1: Influence of cooling rate (ramp down rate during cryogenic treatment) on SCD on the top surface of the EDMed Inconel 825 obtained by using CTW at parameters setting: [ $I_p=10A$ ; $T_{on}=300\mu s$ ; $\tau=85\%$ ] (a) Fast cooling (at 1 $^{\circ}C/min$ ): SCD~0.0144 $\mu m/\mu m^2$ , and (b) Slow Cooling (at 0.5 $^{\circ}C/min$ ): SCD~0.0031 $\mu m/\mu m^2$	117
Fig. 5.8.2: SEM micrographs comparing the severity of crack formation (crack opening width, $C_w$ ) at the EDMed Inconel 825 work surface obtained by using CTW at parameters setting: [ $I_p=10A$ ; $T_{on}=300\mu s$ ; $\tau=85\%$ ] (a) Fast cooling (at 1 $^{\circ}C/min$ ), and (b) Slow Cooling (at 0.5 $^{\circ}C/min$ )	118
Fig. 5.9: Influence of cooling rate (ramp down rate during cryogenic treatment) on WLT on the top surface of the EDMed Inconel 825 obtained by using CTW at parameters setting: [ $I_p=10A$ ; $T_{on}=300\mu s$ ; $\tau=85\%$ ] (a) Fast cooling (at 1 $^{\circ}C/min$ ): WLT~11.462 $\mu m$ , and (b) Slow Cooling (at 0.5 $^{\circ}C/min$ ): WLT~22.222 $\mu m$	118
Fig. 6.1: XRD spectrum of 304SS (a) ‘As received’, and (b) the EDMed work surface obtained by using peak discharge current $I_p=10A$	128
Fig. 6.2: XRD spectrum of Inconel 601 (a) ‘As received’, (b) the EDMed work surface obtained by using peak discharge current $I_p=10A$	129
Fig. 6.3: XRD spectrum of Ti-6Al-4V (a) ‘As received’, (b) the EDMed work surface obtained by using peak discharge current $I_p=10A$	130
Fig. 6.4.1: EDS elemental spectra revealing chemical composition of work surface for (a) ‘As received’ 304SS, and (b) the EDMed 304SS at $I_p=10A$	131
Fig. 6.4.2: EDS elemental spectra revealing chemical composition of work surface for (a) ‘As received’ Inconel 601, and (b) the EDMed Inconel 601 at $I_p=10A$	132
Fig. 6.4.3: EDS elemental spectra revealing chemical composition of work surface for (a) ‘As received’ Ti-6Al-4V, and (b) the EDMed Ti-6Al-4V at $I_p=10A$	132
Fig. 6.5: SEM micrographs showing inferior surface integrity of the EDMed work surface of (a) 304SS, (b) Inconel 601, and (c) Ti-6Al-4V obtained at $I_p=10A$	133

Fig. 6.6.1: SEM micrographs revealing existence of surface cracks on the EDMed <b>304SS</b> work surface (a) (SCD~0.004 $\mu\text{m}/\mu\text{m}^2$ ) at $I_p=6\text{A}$ , and (b) (SCD~0.015 $\mu\text{m}/\mu\text{m}^2$ ) at $I_p=8\text{A}$ , and (c) (SCD~0.0135/ $\mu\text{m}^2$ ) at $I_p=10\text{A}$	134
Fig. 6.6.2: SEM micrographs revealing existence of surface cracks on the EDMed <b>Inconel 601</b> work surface (a) (SCD~0.0064 $\mu\text{m}/\mu\text{m}^2$ ) at $I_p=6\text{A}$ , and (b) (SCD~0.0086 $\mu\text{m}/\mu\text{m}^2$ ) at $I_p=8\text{A}$ , and (c) (SCD~0.012 $\mu\text{m}/\mu\text{m}^2$ ) at $I_p=10\text{A}$	134
Fig. 6.6.3: SEM micrographs revealing existence of surface cracks on the EDMed <b>Ti-6Al-4V</b> work surface (a) (SCD~0.0062 $\mu\text{m}/\mu\text{m}^2$ ) at $I_p=6\text{A}$ , and (b) (SCD~0.0115 $\mu\text{m}/\mu\text{m}^2$ ) at $I_p=8\text{A}$ , and (c) (SCD~0.012 $\mu\text{m}/\mu\text{m}^2$ ) at $I_p=10\text{A}$	134
Fig. 6.7: Severity of surface cracking observed on the TiC layer deposited on the EDMed Ti-6Al-4V work surface (at $I_p=10\text{A}$ )	136
Fig. 6.8.1: SEM micrographs revealing existence of white layer on the EDMed <b>304SS</b> work surface (a) (WLT~21.875 $\mu\text{m}$ ) at $I_p=6\text{A}$ , and (b) (WLT~25.625 $\mu\text{m}$ ) at $I_p=8\text{A}$ , and (c) (WLT~32.362 $\mu\text{m}$ ) at $I_p=10\text{A}$	136
Fig. 6.8.2: SEM micrographs revealing existence of white layer on the EDMed <b>Inconel 601</b> work surface (a) (WLT~21.732 $\mu\text{m}$ ) at $I_p=6\text{A}$ , and (b) (WLT~25.635 $\mu\text{m}$ ) at $I_p=8\text{A}$ , and (c) (WLT~26.72 $\mu\text{m}$ ) at $I_p=10\text{A}$	137
Fig. 6.8.3: SEM micrographs revealing existence of white layer on the EDMed <b>Ti-6Al-4V</b> work surface (a) (WLT~10.317 $\mu\text{m}$ ) at $I_p=6\text{A}$ , and (b) (WLT~14.286 $\mu\text{m}$ ) at $I_p=8\text{A}$ , and (c) (WLT~19.524 $\mu\text{m}$ ) at $I_p=10\text{A}$	137
Fig. 6.9: Non-uniform deposition of the molten material (forming while layer) observed on the EDMed Ti-6Al-4V work surface (at $I_p=8\text{A}$ )	137
Fig. 7.1: General shape of the satisfaction function	143
Fig. 7.2.1: Degree of satisfaction chart for a characteristic where the minimum value provides the best satisfaction (Lower-is-Better; LB)	144
Fig. 7.2.2: Degree of satisfaction chart for a characteristic where the maximum value provides the best satisfaction (Higher-is-Better; HB)	144
Fig. 7.3: Prediction of optimal setting ( $A_4B_5C_1D_5E_3$ ) by optimizing (minimizing) $d_T$	151
Fig. 7.4: Prediction of optimal setting ( $A_4B_5C_1D_5E_3$ ) by optimizing (minimizing) CQL	153
Fig. 7.5: Characteristics of EDMed work surface of Inconel 718 obtained at parameters setting [OCV=50V, $I_p=11\text{A}$ , $T_{on}=500\mu\text{s}$ , $\tau=85\%$ and $F_p=0.6\text{bar}$ ]	153
Fig. 7.6: SEM micrographs of Inconel 718 before and after machining: (a) 'As received' Inconel 718, and (b) EDMed work surface obtained at parameters setting ( $A_1B_1C_1D_1E_1$ ) i.e. [OCV=50V, $I_p=3\text{A}$ , $T_{on}=100\mu\text{s}$ , $\tau=60\%$ and $F_p=0.2\text{bar}$ ]	154
Fig. 7.7: Comparison on SCD of EDMed work surface of Inconel 718 obtained at parameters setting (a) $A_2B_3C_4D_5E_1$ [OCV=60V, $I_p=7\text{A}$ , $T_{on}=400\mu\text{s}$ , $\tau=85\%$ and $F_p=0.2\text{bar}$ ], and (b) $A_4B_5C_1D_5E_3$ i.e. Optimal Setting [OCV=80V, $I_p=11\text{A}$ , $T_{on}=100\mu\text{s}$ , $\tau=85\%$ and $F_p=0.4\text{bar}$ ]	155
Fig. 7.8: Comparison on WLT obtained onto the top surface EDMed Inconel 718 obtained at parameters setting (a) $A_2B_3C_4D_5E_1$ [OCV=60V, $I_p=7\text{A}$ , $T_{on}=400\mu\text{s}$ , $\tau=85\%$ and $F_p=0.2\text{bar}$ ], and (b) and $A_4B_5C_1D_5E_3$ i.e. Optimal Setting [OCV=80V, $I_p=11\text{A}$ , $T_{on}=100\mu\text{s}$ , $\tau=85\%$ and $F_p=0.4\text{bar}$ ]	156
Fig. 8.1: FIS architecture	164
Fig. 8.2.1: Taguchi's loss function of Target-the-Best (TB) type	165
Fig. 8.2.2: Taguchi's loss function of Lower-is-Better (LB) type	166
Fig. 8.2.3: Taguchi's loss function of Higher-is-Better (HB) type	166
Fig. 8.3: Flowchart of the proposed optimization route	168
Fig. 8.4: Proposed FIS architecture	172
Fig. 8.5.1: Membership Functions (MFs) for $S_{MRR}$	173
Fig. 8.5.2: Membership Functions (MFs) for $S_{EWR}$	173
Fig. 8.5.3: Membership Functions (MFs) for $S_{R_a}$	174
Fig. 8.5.4: Membership Functions (MFs) for $S_{SCD}$	174

Fig. 8.6: Membership Functions (MFs) for $S_c$	175
Fig. 8.7: Fuzzy (linguistic) rule base	177
Fig. 8.8.1: S/N ratio plot: Evaluation of optimal setting (Optimization of $S_c$ ) [Optimal setting: $A_4B_1C_1D_1E_4$ ] (Inconel 625)	178
Fig. 8.8.2: S/N ratio plot: Evaluation of optimal setting (Optimization of $S_c$ ) [Optimal setting: $A_4B_1C_1D_4E_2$ ] (Inconel 718)	178
Fig. 8.8.3: S/N ratio plot: Evaluation of optimal setting (Optimization of $S_c$ ) [Optimal setting: $A_3B_2C_4D_3E_1$ ] (Inconel 601)	179
Fig. 8.8.4: S/N ratio plot: Evaluation of optimal setting (Optimization of $S_c$ ) [Optimal setting: $A_3B_1C_2D_4E_2$ ] (Inconel 825)	179
Fig. 8.9: SEM micrographs revealing surface structure of ‘as received’ (a) Inconel 625, (b) Inconel 728, (c) Inconel 601, and (d) Inconel 825	186
Fig. 8.10: SEM micrographs revealing surface structure of the EDMed specimens of (a) Inconel 625, (b) Inconel 718, (c) Inconel 601, and (d) Inconel 825 obtained at parameters setting: [OCV=60V, $I_p$ =5A, $T_{on}$ =200 $\mu$ s, $\tau$ =70%, $F_p$ =0.3bar]	187
Fig. 8.11.1: SEM micrograph revealing White Layer Thickness (WLT~32.016 $\mu$ m) of EDMed Inconel 601 obtained at Run No. 16 i.e. [OCV=90V, $I_p$ =11A, $T_{on}$ =200 $\mu$ s, $\tau$ =80%, $F_p$ =04 bar]	188
Fig. 8.11.2: SEM micrograph revealing White Layer Thickness (WLT~28.189 $\mu$ m) of EDMed Inconel 625 obtained at Run No. 16 i.e. [OCV=90V, $I_p$ =11A, $T_{on}$ =200 $\mu$ s, $\tau$ =80%, $F_p$ =04 bar]	188
Fig. 8.11.3: SEM micrograph revealing White Layer Thickness (WLT~25.426 $\mu$ m) of EDMed Inconel 718 obtained at Run No. 16 i.e. [OCV=90V, $I_p$ =11A, $T_{on}$ =200 $\mu$ s, $\tau$ =80%, $F_p$ =04 bar]	189
Fig. 8.11.4: SEM micrograph revealing White Layer Thickness (WLT~30.692 $\mu$ m) of EDMed Inconel 825 obtained at Run No. 16 i.e. [OCV=90V, $I_p$ =11A, $T_{on}$ =200 $\mu$ s, $\tau$ =80%, $F_p$ =04 bar]	189



# List of Tables

Table No./ Table Caption	Page No.
Table 2.1(a): Chemical composition of Inconel 718 [Source: <a href="#">Newton et al., 2009</a> ]	21
Table 2.1(b): Mechanical properties of Inconel 718 [Source: <a href="#">Newton et al., 2009</a> ]	22
Table 2.2: Specification of die-sinking EDM machine at NIT Rourkela	22
Table 2.3: Fixed/constant parameters	22
Table 2.4: Machining control parameters: Domain of variation	24
Table 2.5: Design of experiment ( $L_{25}$ OA) and collected experimental data	24
Table 2.6.1: Chemical composition of Inconel 825 ( <a href="#">Prabhu and Vinayagam, 2011</a> )	30
Table 2.6.2: Mechanical properties of Inconel 825 ( <a href="#">Rajyalakshmi and Ramaiah, 2013</a> )	30
Table 2.7: Specification of the EDM setup at CTTC, Bhubaneswar	32
Table 2.8: Domain of experiments: Level values of process control parameters	32
Table 2.9: Chemical composition of (a) 304SS, (b) Inconel 601, and (c) Ti-6Al-4V	37
Table 2.10: Mechanical properties of (a) 304SS, (b) Inconel 601, and (c) Ti-6Al-4V	38
Table 2.11: Parameters kept at constant values	39
Table 2.12: Design of experiment ( $L_{25}$ OA) and collected experimental data	41
Table 2.13: Chemical composition of Inconel 625 [Source: <a href="#">Goyal, 2017</a> ]	43
Table 2.14: Mechanical properties of Inconel 625 [Source: <a href="http://www.specialmetals.com">www.specialmetals.com</a> ]	43
Table 2.15: Domain of experiments: Machining control parameters	44
Table 2.16: Design of experiment ( $L_{16}$ OA) and collected experimental data	45
Table 3.1: Utility values of individual responses: Computed values of overall utility degree and corresponding S/N ratio	74
Table 3.2: Mean response (S/N ratio of overall utility degree) table: Prediction of optimal setting by optimizing $U_o$	75
Table 4.1: The variation of crystallite size ( $L$ ), and dislocation density ( $\delta$ ) for (1) NTT material, and (2) CTT material before executing EDM operations	82
Table 4.2: The variation of crystallite size ( $L$ ), and dislocation density ( $\delta$ ) for (1) 'As received' Inconel 825, (2) EDMed work surface of Inconel 825 obtained by using NTT, and (3) EDMed work surface of Inconel 825 obtained by using CTT	93
Table 5.1: The variation of crystallite size ( $L$ ), and dislocation density ( $\delta$ ) for (1) 'as received' Inconel 825, (2) Cryogenically treated Inconel 825 prior to EDM, (3) EDMed work surface of Inconel 825 obtained by using NTW, and (4) EDMed work surface of Inconel 825 obtained by using CTW	111
Table 5.2: Effects of cooling rate on crystallite size ( $L$ ), and dislocation density ( $\delta$ ) for (1) the EDMed work surface of Inconel 825 obtained by using CTW (fast cooling $\sim 1^\circ\text{C}/\text{min}$ during CT cycle), and (2) the EDMed work surface of Inconel 825 obtained by using CTW (Slow cooling $\sim 0.5^\circ\text{C}/\text{min}$ during CT cycle)	116
Table 6.1: Results of micro-hardness test	133
Table 7.1: Normalized data	146
Table 7.2: Check for response correlation	147
Table 7.3: Results of PCA	147
Table 7.4: Computed major Principal Components (PCs)	148
Table 7.5: Computed Quality Loss (QL) estimates	149
Table 7.6: Computed satisfaction values	150
Table 7.7: Mean response (S/N ratio of $d_T$ ) table: Prediction of optimal setting by optimizing $d_T$	151
Table 7.8: Mean response (S/N ratio of CQL) table: Prediction of optimal setting by optimizing CQL	152

Table 7.9: Results of confirmatory test	154
Table 8.1.1: Satisfaction values (corresponding to each response) for all experimental runs: Computed combined satisfaction score ( $S_c$ ) [Inconel 625]	170
Table 8.1.2: Satisfaction values (corresponding to each response) for all experimental runs: Computed combined satisfaction score ( $S_c$ ) [Inconel 718]	171
Table 8.1.3: Satisfaction values (corresponding to each response) for all experimental runs: Computed combined satisfaction score ( $S_c$ ) [Inconel 601]	171
Table 8.1.4: Satisfaction values (corresponding to each response) for all experimental runs: Computed combined satisfaction score ( $S_c$ ) [Inconel 825]	172
Table 8.2: Fuzzy rule matrix	175
Table 8.3.1: Mean response table of MRR (for Inconel 625)	181
Table 8.3.2: Mean response table of EWR (for Inconel 625)	181
Table 8.3.3: Mean response table of $R_a$ (for Inconel 625)	181
Table 8.3.4: Mean response table of SCD (for Inconel 625)	181
Table 8.4.1: Mean response table of MRR (for Inconel 718)	182
Table 8.4.2: Mean response table of EWR (for Inconel 718)	182
Table 8.4.3: Mean response table of $R_a$ (for Inconel 718)	182
Table 8.4.4: Mean response table of SCD (for Inconel 718)	182
Table 8.5.1: Mean response table of MRR (for Inconel 601)	183
Table 8.5.2: Mean response table of EWR (for Inconel 601)	183
Table 8.5.3: Mean response table of $R_a$ (for Inconel 601)	183
Table 8.5.4: Mean response table of SCD (for Inconel 601)	183
Table 8.6.1: Mean response table of MRR (for Inconel 825)	184
Table 8.6.2: Mean response table of EWR (for Inconel 825)	184
Table 8.6.3: Mean response table of $R_a$ (for Inconel 825)	184
Table 8.6.4: Mean response table of SCD (for Inconel 825)	184

# Abbreviations

AECG	Abrasive Electro-Chemical Grinding
AEDM	Additive Mixed Electro-Discharge Machining
ANN	Artificial Neural Network
ANOVA	Analysis of Variance
BUE	Built-Up-Edge
CNC	Computerized Numerical Control
CPC	Composite Principal Component
CQL	Combined Quality Loss
CT	Cryogenic Treatment
CTT	Cryogenically Treated Tool
CTW	Cryogenically Treated Workpiece
DASR	Depth Average Surface Roughness
DCT	Deep Cryogenic Treatment
DM	Decision-Maker
ECM	Electro-Chemical Machining
EDD	Electro-Discharge Drilling
EDM	Electro-Discharge Machining
EDS	Energy Dispersive X-Ray Spectroscopy
EWR	Electrode Wear Rate
FCC	Face Centered Cubic
FESEM	Field Emission Scanning Electron Microscopy
FIS	Fuzzy Inference System
FLM	Fuzzy Logic Model
GA	Genetic Algorithm
GRA	Grey Relational Analysis
HAZ	Heat Affected Zone
HB	Higher-is-Better
HSS	High Speed Steel
LB	Lower-is-Better
MEDM	Micro-Electro-Discharge Machining
MEMS	Micro-Electro-Mechanical System
MH	Micro-indentation hardness
MIMO	Multi Input Multi Output
MISO	Multi Input Signal Output
MOPSO	Multi-Objective Particle Swarm Optimization
MRR	Material Removal Rate
NB	Nominal-the-Best
NTT	Non-Treated Tool
NTW	Non-Treated Workpiece
OA	Orthogonal Array
OC	Over Cut
OCV	Open Circuit Voltage
PC	Principal Component
PCA	Principal Component Analysis
PFE	Plasma Flushing Efficiency



PMEDM	Powder Mixed Electro-Discharge Machining
PSS	Porous Stainless Steel
QL	Quality Loss
RA	Roughness Average
RSM	Response Surface Methodology
S/N	Signal-to-Noise ratio
SCD	Surface Crack Density
SCT	Shallow Cryogenic Treatment
SEM	Scanning Electron Microscope
SR	Surface Roughness
TB	Target-the-Best
TEM	Transmission Electron Microscopy
TOPSIS	Technique For Order Preference By Similarity To Ideal Solution
TWR	Tool Wear Ratio
USM	Ultrasonic Machining
VMRR	Volumetric Material Removal Rate
WEDM	Wire Electro-Discharge Machining
WG	Working Gap
WL	White Layer
WLT	White Layer Thickness
WPCA	Weighted Principal Component Analysis
XRD	X-Ray Diffraction

## **Chapter 1**

# **Introduction**

### **1.1 Super Alloy Inconel**

Inconel is a family of austenite Nickel-Chromium based super alloys. These alloys are basically oxidation and corrosion resistant materials appropriate for service in extreme environments subjected to pressure and heat. Whilst heated, Inconel develops a thick, stable, passivating oxide layer protecting the surface from further attack. Inconel retains its strength over a wide range of temperature; suitable for high temperature applications.

Difficulty is faced in machining and forming of Inconel super alloys using traditional techniques due to rapid work hardening. In case of machining, after the first pass, work hardening tends to plastically deform either the workpiece or the tool on subsequent passes. Therefore, age-hardened Inconel alloys are machined using an aggressive but slow-cut with a hard tool with minimum number of passes.

#### **∞ Inconel 601**

Inconel 601 is widely used for applications that require resistance to corrosion and heat. This alloy stands out due to its resistance to high temperature oxidation. Inconel 601 develops a tightly adherent oxide scale which resists spalling even under conditions of severe thermal cycling. This alloy exhibits good high temperature strength, and retains its ductility after long service exposure. It has good resistance to aqueous corrosion, high mechanical strength, and shows easiness of readily forming, machining and welding. However, alloy 601 is not recommended for use in strongly reducing, Sulphur bearing environments. Inconel 601 is used in chemical processing, aerospace, heat treating industry, power generation, heat treating muffles and retorts, radiant tubes, catalyst support grids in nitric acid production and steam super heater tube supports.

## **∞ Inconel 625**

Inconel 625 is a corrosion and oxidation resistant Nickel alloy that is used both for its high strength and outstanding aqueous corrosion resistance. Its outstanding strength and toughness is due to the addition of Niobium which acts with the Molybdenum to stiffen the alloy's matrix. Inconel 625 exhibits excellent fatigue strength and stress-corrosion cracking resistance to chloride ions. This alloy has excellent weldability. It can resist pitting and crevice corrosion. It remains almost unaffected in alkaline, salt water, fresh water, neutral salts, and in the air. The Nickel and Chromium provide resistance to oxidizing environments. Nickel and Molybdenum provide for resistance to non-oxidizing atmospheres. Pitting and crevice corrosion are prevented due to the presence of Molybdenum. Niobium stabilizes the alloy against sensitization during welding. Inconel 625 also exhibits excellent chloride stress-corrosion cracking resistance. This alloy is capable of resisting scaling and oxidation at high temperatures.

Inconel 625 shows excellent forming and welding characteristics. Ideally, in order to control grain size, finish hot working operations are preferred at the lower end of the temperature range. Because of its good ductility, Inconel 625 is also readily formed by cold working. However, the alloy does work-harden rapidly; intermediate annealing treatments may be required for pursuing complex component forming operations. In order to restore the best balance of properties, all hot or cold worked component parts should be annealed and rapidly cooled. This alloy can be welded by both manual and automatic welding methods, including gas tungsten arc, gas metal arc, electron beam and resistance welding. It exhibits good welding characteristics. Applications of Inconel 625 include: aircraft ducting systems, aerospace, jet engine exhaust systems, engine thrust-reverser systems, specialized seawater equipment, chemical process equipment etc.

## **∞ Inconel 718**

Inconel 718 is designed to resist a wide range of severely corrosive environments like pitting and crevice corrosion. It also displays exceptionally high yield, tensile, and creep-rupture properties at high temperatures. This nickel alloy is used from cryogenic temperatures up to long term service at 1200°F. One of the distinguishing features of Inconel 718's composition is the addition of Niobium to permit age hardening which allows annealing and welding without spontaneous hardening during heating and cooling. The addition of Niobium acts with the Molybdenum to stiffen the alloy's matrix and to

provide high strength without a strengthening heat treatment. This alloy can readily be fabricated and may be welded in either the annealed or precipitation (age) hardened condition. Salient characteristics of Inconel 718 include:

- ⇒ Good mechanical properties – tensile, fatigue and creep-rupture.
- ⇒ Yield tensile strength, creep, and rupture strength properties are exceedingly high.
- ⇒ Highly resistant to chloride and sulphide stress corrosion cracking.
- ⇒ Resistant to aqueous corrosion and chloride ion stress corrosion cracking.
- ⇒ High temperature resistant.
- ⇒ Age-hardenable with a unique property of slow aging response that permits heating and cooling during annealing without the danger of cracking.
- ⇒ Excellent welding characteristics, resistant to post weld age cracking.

Inconel 718 is used in a wide variety of industries such as chemical processing, aerospace, liquid fuel rocket motor components, pollution-control equipment, nuclear reactors, cryogenic storage tanks, valves, fasteners, springs, mandrels, tubing hangers, gas turbine engine parts etc.

## ∞ Inconel 825

Inconel 825 alloy's chemical composition is designed to provide exceptional resistance at many corrosive environments (sulphuric and phosphoric acids and sea water). It exhibits excellent resistance to both reducing and oxidizing acids, to stress-corrosion cracking, and to localized attack such as pitting and crevice corrosion. This alloy is used for applications in chemical processing, pollution control, oil and gas well piping, nuclear fuel reprocessing, components in pickling equipment like heating coils, tanks, baskets and chains, acid production etc.

## 1.2 Machining Difficulties of Inconel

In order to satisfy stringent design requirements, machining and shaping of Inconel super alloys become very difficult and expensive by conventional processes such as turning, milling, grinding, etc. Problems that are frequently experienced in machining of super

alloys by conventional techniques are rapid tool wear and excessive heat generation at the tool-work interfaces; thereby resulting subsequent alteration of work material characteristics. As a result, manufacturers and design engineers are forced to opt for modern machining processes. The properties of these super alloys, such as high temperature strength, high hardness, low thermal diffusivity, presence of highly abrasive carbide particles and high tendency to weld onto the tool forming Built-Up Edge (BUE) etc. are responsible for inviting various machining difficulties. Their ability to maintain their mechanical properties at high temperatures severely affects the machinability of these alloys. Its poor thermal diffusivity generates high temperature at the tool tip as well as high thermal gradients in the cutting tool, affecting the tool life adversely. Whilst machining, these alloys tend to be work hardened rapidly, generate enormous heat during cutting, exhibit tendency to weld on the cutting tool surface, and offer high resistance towards metal removal because of their high shear strengths. Loss of surface integrity of the machined part component is due to excessive work hardening, rapid tool wear due to uneven strong stress field by thermo-mechanical coupling. Owing to aforesaid problems, it seems indeed a great challenge to machine Inconel super alloys by conventional machining processes and that too by conventionally used cutting tool materials (Hewidy et al., 2005; Rao et al., 2013; Ashtiani and Zarandooz, 2016; Shankar et al., 2001; Ramanujam et al., 2014; Thirumalai and Senthilkumaar, 2013; Aggarwal et al., 2015; Prihandana et al., 2014; Rajyalakshmi and Ramaiah, 2013). Therefore, non-traditional machining of Inconel super alloys has really become an important research agenda in the present context.

## **1.3 Literature Review**

### **1.3.1 State of Art on Non-Traditional Machining of Inconel**

Hewidy et al. (2005) developed mathematical models for correlating the inter-relationships of various Wire Electro-Discharge Machining (WEDM) machining parameters of Inconel 601 material such as: peak current, duty factor, wire tension and water pressure on the metal removal rate, wear ratio and surface roughness.

Ramakrishnan and Karunamoorthy (2008) predicted the best cutting parameters of WEDM process for machining of Inconel 718 work material. The responses (viz. material

removal rate and surface roughness) were optimized concurrently using multi-response Signal-to-Noise (S/N) ratio in addition to Taguchi's parametric design approach. Analysis of Variance (ANOVA) was employed to identify the level of importance of the machining parameters on the multiple performance characteristics. [Imran et al. \(2008\)](#) examined the feasibility of deep-hole micro-drilling on Nickel-based super alloy. In this work, the effect of processing parameters such as drill feed rate, spindle speed, and peck depth were evaluated. Additionally, the tool wear mechanism was also investigated. The authors highlighted that micro-drilling route was found technically feasible offering good hole dimension and potentially competitive lead times.

[Newton et al. \(2009\)](#) performed an experimental investigation to determine the main Electro-Discharge Machining (EDM) parameters which contributed to recast layer formation for Inconel 718 work material. It was found that average recast layer thickness increased primarily with energy per spark, peak discharge current, and current pulse duration. The recast layer was found to possess in-plane tensile residual stress, lower hardness and lower elastic modulus than the bulk material. [Rajesh et al. \(2010\)](#) carried out EDM experiments on Inconel 718 workpiece using 99.9% pure Copper electrode with tubular cross section. The effects of process parameters (viz. pulse current, duty factor, sensitivity, gap control and dielectric flushing pressure) on the formation of recast layer, heat affected zone and spattered EDM surface were analyzed. It was observed that the process parameters, base material properties and white layer composition had significant influence on crack formation. In addition to that, crack propagation was observed varying significantly with pulse current as well as duty factor.

[Kumar et al. \(2011\)](#) studied the influence of process input parameters on machining characteristics of Inconel 718 in aluminum Additive Mixed Electro-Discharge Machining (AEDM) with Copper tool electrode. The effectiveness of AEDM process on Inconel 718 was evaluated in terms of material removal rate, surface roughness, and electrode wear ratio. It was found that particle concentration and particle size significantly affected machining efficiency. [Manikandan and Venkatesan \(2012\)](#) applied Taguchi method to analyze the effect of EDM parameters on the machining characteristics (viz. metal removal rate, overcut, and tool wear ratio etc.) for Inconel 718 work material and to predict the optimal choice for each EDM parameters including discharge current, pulse-on time, and pulse-off time. It was found that these parameters had a significant influence on the machining characteristics. [Rajesh et al. \(2012\)](#) performed an experimental study considering EDM on Inconel 718 work material using

Response Surface Methodology (RSM). In this work, the effects of five major process parameters: pulse current, duty factor, sensitivity control, gap control, and flushing pressure on the following process responses: Material Removal Rate (MRR) and Surface Roughness (SR) were discussed. Analysis showed significant interaction effect of pulse current and duty factor on MRR yielding a wide range from 14.4~22.6 mm<sup>3</sup>/min; while pulse current remained the most contributing factor with approximate changes in the MRR and SR of 48% and 37%, respectively, corresponding to the extreme values considered. Moreover, the thickness of the sputtered layer and the crack length were found to be functions of pulse current.

[Lin et al. \(2013\)](#) applied grey-Taguchi method towards optimizing micro-milling electrical discharge machining process parameters of Inconel 718 super alloy in order to achieve multiple performance characteristics such as low electrode wear, high material removal rate and low working gap. In this work, the influences of peak current, pulse-on time, pulse-off time and spark gap on electrode wear, material removal rate, and working gap were analyzed. [Sengottuvel et al. \(2013\)](#) investigated effects of various EDM input parameters as well as the influence of different tool geometry on material removal rate, tool wear rate, and surface roughness for machining of Inconel 718 work material by using Copper electrode. Five EDM parameters, namely pulse-on time, pulse-off time, peak current, flushing pressure, and electrode tool geometry (circular, square, rectangular, and triangular cross sections) were considered in this work. The parameters were optimized using multi-objective optimization technique called desirability function approach. The significance of each parameter was analyzed by ANOVA. In addition, Fuzzy Logic Model (FLM) was used to infer the functional relationship between input and output responses. Overall, the rectangular tool geometry emerged successful.

[Rajyalakshmi and Ramaiah \(2013\)](#) applied Taguchi based grey relational analysis to the experimental results of WEDM on Inconel 825 work material with consideration of multiple response measures. The authors aimed at obtaining improved material removal rate, surface roughness, and spark gap. [Ay et al. \(2013\)](#) used grey relational analysis to optimize micro-electrical discharge machining (drilling) process of Inconel 718 super alloy in consideration with multi-performance characteristics (viz. hole taper ratio, and hole dilation). The pulse current was found to be more efficient on performance characteristics than pulse duration.

[Wang et al. \(2013\)](#) proposed a high current density electrical discharge milling for machining of Inconel 718 super alloy. In this research, the effects of peak current and

injection flushing pressure on the MRR and EWR were investigated. It was observed that the micro-cracks within the recast layer penetrated into the base material and propagated along the grain boundary of the EDMed work surface. [Li et al. \(2014\)](#) focused on surface integrity and machining efficiency of WEDM in machining of Inconel 718 by one rough cut (RC) mode followed by three trim cut (TC) modes. In this study, material removal efficiency, surface roughness, surface topography, surface alloying, and micro-hardness were characterized. Results showed that Six-sigma distribution of  $R_a$  in RC mode was different from that of TC modes. The high toughness of Inconel 718 was found to be the major contributing factor towards suppressing micro-cracks in the TC modes.

[Yadav and Yadava \(2014\)](#) analyzed the impact of tool rotation in Electro-Discharge Drilling (EDD) of aerospace Nickel alloys. Experimental results confirmed that tool rotation had substantive effect on surface roughness and average circularity of the hole made by EDD process. [Manohar et al. \(2014\)](#) observed that the bottom surface profile of the electrode influenced significantly on material removal rate, electrode wear rate, surface roughness and surface integrity of the EDMed Inconel 718 specimen. In this work, electrodes of different bottom profiles (Convex, Concave and Flat profile at their bottom surface) were used; and the machined surfaces were analyzed in terms of recast layer, surface topology, form tolerance and MRR. It was concluded that the adverse effects caused due to the erosion of flat profile electrodes on the machined surfaces could be overcome by employing convex profile electrodes; concave profile electrodes almost simulated the condition of eroded flat-profile electrode; convex profile electrodes produced machined surfaces of better quality in terms of higher surface finish, thinner recast layer and closer geometry, in addition to higher MRR as compared to flat profile or concave profile electrodes.

[Muthukumar et al. \(2014\)](#) applied response surface methodology for prediction of radial overcut in die sinking electrical discharge machining process for Incoloy 800 super alloy with Copper electrode. The study considered current, pulse-on time, pulse-off time, and voltage as input process parameters. It was found that current and voltage had significant effect on the radial overcut. [Mohanty et al. \(2014a\)](#) studied the influence of different EDM process variables peak current, duty factor, and pulse-on duration on various performance characteristics such as material removal rate, surface roughness, radial overcut, and surface crack density. The most influencing factor for responses viz. MRR, SR, and Radial Overcut (ROC) was found to be the peak discharge current. Finally, Grey



Relational Analysis (GRA) was utilized to optimize process parameters during EDM of Inconel 825.

[Dhanabalan et al. \(2014\)](#) presented an experimental work on electro-discharge machining of Inconel 718 and 625 super alloys. In this work, the significance of input parameters namely peak current, pulse-on time, and pulse-off time on the form tolerances were investigated. [Prihandana et al. \(2014\)](#) investigated the influence of Molybdenum Disulfide ( $\text{MoS}_2$ ) powder suspended in dielectric fluid on the performance of micro-EDM of Inconel 718. It was observed that  $\text{MoS}_2$  powder suspension with 50nm of size and 5g/l of concentration could produce better quality micro-holes on Inconel 718 work material. Moreover, 50nm  $\text{MoS}_2$  powder was found as the best powder size to achieve the highest material removal rate. [Li et al. \(2015\)](#) focused on machining characteristics of Inconel 718 by Wire-EDM and Sinking-EDM with Cu-SiC electrode, respectively. Material removal efficiency, surface roughness, surface topography, surface alloying, and electrode wear were characterized herein. It was found that the fabricated Cu-SiC electrode for Sinking-EDM exhibited better performance in terms of material removal rate, surface roughness, and electrode wear. It was inferred that the higher melting temperature and fine microstructure of SiC contributed towards minimizing electrode wear of the fabricated Cu-SiC electrode as compared to the traditional Cu electrode.

[Sharma et al. \(2015\)](#) examined WEDM performance on Inconel 706 super alloy in purview of material removal rate, surface roughness, recast surface, topography, micro-hardness, micro-structural and metallurgical changes of the machined components. The experimental results revealed that servo voltage, pulse-on time, and pulse-off time greatly influenced MRR, and SR. As such no micro-cracks were observed on the machined surface of Inconel 706 due to its high toughness. But, propensity of thick recast layer formation was noticed at high pulse-on time and low servo voltage. [Aggarwal et al. \(2015\)](#) attempted empirical modeling of process parameters of the WEDM for Inconel 718 super alloys by using response surface methodology. In this work, the parameters such as pulse-on time, pulse-off time, peak current, spark gap voltage, wire feed rate, and wire tension were considered as input variables. The performance was measured in terms of cutting rate and surface roughness.

[Torres et al. \(2016\)](#) studied the influence of EDM parameters and graphite electrode for Inconel 600 super alloy considering positive and negative polarity both. In this work, the machining performances were evaluated in terms of material removal rate, electrode wear, and surface roughness. It was found that that the use of negative polarity lead to

higher material removal rate; whereas, positive polarity was found suitable for ensuring low values of electrode wear and good surface roughness. It was highlighted that graphite electrode and negative polarity were the most economical choice.

### **1.3.2 Cryogenic Treatment (CT) of Material**

Cryogenic Treatment (CT) is the process of treating material to cryogenic temperatures in order to seek enhanced stress relief and stabilization, and thereby improved wear resistance. The scientific community generally defines cryogenic temperatures as temperatures below  $-150^{\circ}\text{C}$ . However, this is, admittedly, an artificial upper limit; temperatures used presently in cryogenic treatment are generally  $-185^{\circ}\text{C}$ . CT of tool material appears favorable since cryogenically treated material corresponds to longer part life, improved fatigue life (less failure due to cracking), improved thermal properties (increase in thermal conductivity), better electrical properties including less electrical resistance (increase in electrical conductivity), reduced coefficient of friction, less creep and walk, improved flatness, and easiness of machining.

Generally, the parts can be cryogenically treated either by (i) Shallow Cryogenic Treatment (SCT) or by (ii) Deep Cryogenic Treatment (DCT) ([Kumar et al., 2014](#)). During cryogenic treatment, the part component is immersed into the liquid Nitrogen ( $\text{LN}_2$ ) for specified time duration ([Patil and Tated, 2012](#)).

During DCT, the temperature is gradually reduced to  $-185^{\circ}\text{C}$  at a cooling rate of  $1^{\circ}\text{C}/\text{min}$  and the part component is kept in the cryogenic processor container for about 24h durations. The temperature is then gradually raised to the room temperature again. The parts are then tempered under similar conditions to incur stress relief. By conducting the cool-down cycle in gaseous Nitrogen, temperature can be controlled accurately, and thermal shocks to the material are avoided. Cryogenic treatment can also be performed without tempering process; as reported by ([Kumar et al., 2015](#)). The benefits of cryogenic treatment of tool material (conventional cutting tools) could be well retrieved from the reporting by ([Seah et al., 2003](#); [Firouzdor et al., 2008](#); [Reddy et al., 2009](#); [Gill and Singh, 2010](#); [Kalsi et al., 2010](#); [Sundaram et al., 2009](#); [Abdulkareem et al., 2009](#); [Nadig et al., 2011](#)).

⇒ Imparts high resistance to abrasive wear. In Carbon tool steels, CT modifies its Carbon structure through precipitation of ‘eta-carbides’ which in turn improves

hardness, increases resistance to wear and also warrants better tool life (in case of cutting tools).

- ⇒ Improves the microstructure (more consistent grain structure) of the material (not just the surface) being cryogenically treated. This is because, CT promotes in eliminating voids or imperfections present within the parent material. This in turn improves durability of the work material.
- ⇒ Cryogenically treated parts may be subsequently reground or machined without affecting the benefits imparted by the cryogenic treatment.
- ⇒ In general, CT results in decrease in residual stress, while increasing toughness (i.e. resistance to impact) and dimensional stability.
- ⇒ This technology is eco-friendly as well as nontoxic; can be executed without imposing environmental harm.

### **1.3.3 Use of Cryogenically Treated Tool/Workpiece during Execution of EDM/WEDM Processes**

Cryogenic Treatment (CT) is basically the process of deep-freezing materials at cryogenic temperatures in order to enrich mechanical and physical properties of materials. The execution of cryogenic processing on tool materials is expected to improve wear resistance, hardness, and dimensional stability; reduce tool consumption and down time for the setup, thus incurring substantial cost reduction. Additionally, CT of work material prior to EDM may be proved beneficial in terms of remarkable improvement in the material properties as it may relieve residual stresses, promote grain refinement, and improve electrical as well as thermal properties. Therefore, application potential of cryogenically treated tool/workpiece in the context of electro-discharge machining specially on '*difficult-to-cut*' materials has been reported in literature.

Gill and Singh (2010) investigated the effect of Deep Cryogenic Treatment (DCT) on machinability of Ti 6246 alloy in electric discharge drilling with electrolytic Copper tool. The authors attempted to compare the production accuracy of holes drilled in deep cryogenically treated Ti 6246 (DCT Ti 6246) alloy and non-treated Ti 6246 alloy in terms of surface roughness and overcut. Improved material removal rate and wear ratio, lower tool wear rate were observed in case of EDD of DCT Ti 6246 alloy workpiece as compared with non-treated work material. Also, superior production accuracy of holes

was reported while EDD of DCT workpiece. [Srivastava and Pandey \(2012a, b\)](#) performed parametric study on EDM process using ultrasonic assisted cryogenically cooled Copper electrode during electro-discharge machining of M2 grade high speed steel. In this work, electrode wear ratio, material removal rate, and surface roughness were analyzed. Discharge current, pulse-on time, duty cycle and gap voltage were considered as the controllable process variables. The MRR, Electro Wear Rate (EWR) and SR obtained in EDM process with normal electrode, cryogenically cooled electrode and ultrasonic assisted cryogenically cooled electrode were compared. Thus, in the present work the aforesaid process route was recommended superior in performances than conventional EDM process due to better tool life, satisfactory tool shape retention ability and better surface integrity.

[Kapoor et al. \(2012\)](#) investigated the effect of deep cryogenic treatment on the brass wire electrode used in wire electrical discharge machining on EN31 work material. In this work, the microstructure and crystalline phase of deep and non-treated brass wire electrodes was observed. More refined structure was observed in case of deep cryogenic treatment. Improved electrical conductivity was obtained for the deep cryogenically treated tool electrode. The effect of deep cryogenic treatment on the brass wire electrode was also investigated for the performance of wire electrical discharge machining. Taguchi experimental design was applied to investigate the optimal parameters for maximum material removal rate. The ANOVA analysis indicated that type of wire, pulse width, time between two pulses and wire tension were the significant factors to achieve maximum material removal rate. [Jafferson and Hariharan \(2013\)](#) reported a comparative study on machining performance of both cryogenically treated and untreated micro electrodes in micro-EDM along with electrical resistivity, crystallite size, micro-hardness and microscopic analysis. From the study, significant reduction of 58% in tool wear rate was observed for Tungsten electrode followed by brass and Cu electrodes with 51% and 35%, respectively.

[Khanna and Singh \(2016\)](#) presented a comparison for normal and cryogenically treated high Carbon high Chromium cold alloy tool (D-3) steel for execution of WEDM process. The response variables namely cutting rate, metal removal rate, and surface roughness were considered, and six input process parameters like pulse width, time between two pulses, servo reference mean voltage, short pulse time, maximum feed rate, and wire mechanical tension were used for evaluating overall machining performance. [Sharma et al. \(2014\)](#) investigated the effect of process control parameters (viz. pulse-on time, pulse-

off time, servo voltage, and peak current) on surface roughness of the WEDMed D-2 tool steel specimens. In order to increase the wear resistance, the cryogenically treated workpiece was used herein. The Mathematical modeling of the process was carried with the help of response surface methodology. It was observed that pulse-on time imposed the maximum effect on surface roughness.

[Srivastava and Pandey \(2014\)](#) studied the effect of discharge current, pulse-on time, duty cycle, and gap voltage on electrode wear ratio, material removal rate, and surface roughness for EDM of M2 grade High Speed Steel (HSS) workpiece using cryogenically cooled electrode. The analysis revealed that discharge current, pulse-on time, and duty cycle significantly affected EWR and MRR. Discharge current and pulse-on time were found to be the most influential factors in affecting SR. [Dhobe et al. \(2014\)](#) studied the effect of WEDM parameters on surface finish of cryogenically treated AISI D2 tool steel. [Kumar et al. \(2015\)](#) attempted an experimental investigation towards machining of three grades of Titanium alloy TITAN 15, TITAN 21, and TITAN 31 using powder mixed electro-discharge machining in order to study the effect of cryogenic treatment of tool/work material and its effect on tool wear rate.

[Kumar et al. \(2016a\)](#) investigated the effect of cryogenic treatment on the machining performance of Ti-5Al-2.5Sn alpha Titanium alloy during electric discharge machining. Untreated, shallow cryogenically treated ( $-110^{\circ}\text{C}$ ), and deep cryogenically treated ( $-184^{\circ}\text{C}$ ) Titanium alloys were machined by varying current and pulse-on time. The machining performance was evaluated in terms of higher material removal rate, higher micro-hardness, lesser tool wear rate, and lesser surface roughness. The results showed significant improvement in the machining performance with deep cryogenically treated alloy when compared with shallow and untreated alloy. [Hui et al. \(2016\)](#) investigated discharge characteristics and discharge gap whilst machining of Ti-6Al-4V alloy by cryogenically cooled tool electrode during electro-discharge machining in distilled water using the monopulse discharge method. The influence of the cryogenically cooled tool electrode on the discharge gap and the initial maintaining voltage between the electrode and workpiece were analyzed under various temperatures. A comparative experiment of machining Ti-6Al-4V alloy was carried out by using cryogenically cooled tool electrode EDM and conventional EDM. Lower electrode wear, higher material removal rate, and higher corner size machining accuracy were obtained by using cryogenically cooled tool electrode EDM.

[Gaikwad and Jatti \(2016\)](#) focused on optimization of electro-discharge machining process parameters for maximization of material removal rate while machining of cryogenically treated NiTi alloy. In this study, gap current, pulse-on time, pulse-off time, workpiece electrical conductivity, and tool conductivity were considered as process variables. It was found that work electrical conductivity, gap current and pulse-on time were the significant parameters that affected the material removal rate. [Kumar et al. \(2016b\)](#) investigated on improvement in EDMed work surface properties of cryogenically treated Titanium alloy after Powder-Mixed Electro-Discharge Machining (PMEDM) process. In this work, peak current was observed as the highly influential parameter that affected the micro-hardness as well as surface quality of the machined surface.

## **1.4 Motivation and Objectives**

Literature has depicted that substantial volume of work has been carried out by pioneers to understand machining and machinability aspects of Inconel super alloys (especially grade 718) during EDM, WEDM, micro-Electro-Discharge Drilling (micro-EDD) etc. Influence of process parameters on different performance attributes has been experimentally investigated and analyzed through mathematical modeling. Effort has also been made to optimize process responses (performance indicators/ process outputs) towards determining the most favorable process environment (parameters setting) for machining of Inconel super alloys. From literature survey, it has been understood clearly that the process parameters do interact in a complicated manner; thereby, influencing machining performance characteristics.

However, majority of the past reporting has considered only a particular grade of Inconel alloy (i.e. Inconel 718). Literature has been found sparse to deliver a consolidated database comparing machinability of different Inconel grades (viz. Inconel 601, Inconel 625, Inconel 825 etc.) whilst executing electro-discharge machining operation. It is felt that the ease of machining (i.e. the extent of machinability) is likely to vary with variation of Inconel grades due to variation in their chemical composition, physical and mechanical properties etc. To address this issue, present work has aimed to perform an in depth experimental study to compare machining behavior of different grades of Inconel in course of EDM operation.

It has also been noticed that most of the past studies have considered MRR, EWR, SR etc. as the indicators of machining performance. Aspects of surface cracking, formation of white layer onto the EDMed work surface, and their quantification (in terms of surface crack density, crack opening width, white layer thickness etc.) have rarely been addressed. Moreover, limited effort has been put by previous researchers on investigating surface integrity (viz. surface roughness, surface morphology, hardness, residual stress, recast or white layer formation, severity of cracks etc.) in detail along with metallurgical characteristics of the EDMed work surface with reference to ‘as received’ (unaffected) parent material. It is felt indeed a necessity to interpret the thermo-mechanical phenomena incurred during execution of EDM operation on influencing phase transformation, carbide precipitation, extent of grain refinement, change in crystallite size and dislocation density for the EDMed work surface of Inconel super alloys in comparison with unaffected parent material.

Optimization of EDM responses for machining of Inconel work material has been attempted in literature; however, emphasis has been made to maximize MRR, minimize  $R_a$  (roughness average of the EDMed work surface) as well as EWR. EDMed surface topographical measures like Surface Crack Density (SCD) and White Layer Thickness (WLT) etc. have not been considered yet as objective functions for such a multi-response optimization problem that has aimed to predict the most suitable EDM process environment (optimal parameters setting).

In view of the machining difficulties of low-conductive materials, prior to EDM, cryogenic treatment of tool/workpiece has been recommended in literature. It has been reported that in the context of EDM, CT of tool/work material substantially improves MRR, SR and ensures reduced tool wear. However, aspects of electro-discharge machining using cryogenically treated tool electrode and/or workpiece have rarely been addressed in literature in the context of machining of Inconel super alloys. Moreover, from extensive literature survey, it has been found that rare attempt has been made to compare machinability of Inconel and other super alloys (like Ti-6Al-4V) with respect to conventional metals/alloys (like 304SS). Motivated by the scope of research as described above, the objectives of the present dissertation have been planned accordingly. The specific objectives of the current research have been pointed out below.

- ⇒ To analyze surface characteristics (i.e. surface integrity in terms of surface morphology and topography) of the EDMed Inconel 718 specimen.
- ⇒ To examine electro-discharge machining performance on Inconel 825 work material using deep cryogenically treated Copper tool electrode. Emphasis is made on assessing surface integrity and metallurgical characteristics of the EDMed work surface.
- ⇒ To study ease of electro-discharge machining of deep cryogenically treated Inconel 825 workpiece (as compared to untreated work material) using normal Copper tool electrode.
- ⇒ To compare machinability (in view of surface integrity and metallurgical characteristics of the EDMed work surface) of A2 Tool Steel (SAE 304SS), super alloy Inconel 601 and Titanium alloy Ti-6Al-4V.
- ⇒ To predict an optimal setting of EDM process parameters (viz. gap voltage, peak discharge current, pulse-on time, duty factor, and flushing pressure) for achieving satisfactory EDM performance on Inconel 718 work material. An integrated optimization route combining satisfaction function approach coupled with Taguchi method is proposed herein.
- ⇒ To compare optimal parameters setting for EDM of Inconel 601, Inconel 625, Inconel 718, and Inconel 825 work materials, respectively, in order to ensure maximum material removal rate, minimum electrode wear and minimum surface roughness as well as minimum surface crack density for the EDMed specimens. Justification on the predicted optimal settings is provided in purview of chemical constituents and mechanical properties of the respective work materials. In order to solve such a multi-response optimization problem, an integrated module combining satisfaction function approach, Fuzzy Inference System (FIS) and Taguchi method is recommended herein.



## 1.5 Organization of the Present Dissertation

The present dissertation has been organized into eight different chapters. Brief outline of each chapter has been provided below.

### **Chapter 1 (*Introduction*):**

In this chapter, a detailed introduction on Inconel super alloys: different grades, properties, applications etc. has been delineated. Machining difficulties of Inconel super alloys as compared to traditional metals/alloys have been pointed out. An extensive literature survey has been carried out at this stage to understand state of art of past research on emphasizing machining and machinability aspects of Inconel super alloys. Scope for improvement of the EDM performance upon using cryogenically treated tool/workpiece has well been understood. Based on outcome of the past research as documented in existing literature resource, present research gaps have been identified. Following which the specific objectives of the present dissertation have been highlighted.

### **Chapter 2 (*Experimental Details*):**

Detailed experimental schema has been documented in this chapter. Materials and methods, equipment utilized, procedural steps for sample preparation as well as data collection have been elaborately described herein.

### **Chapter 3 (*Analysis on Surface Characteristics of Electro-Discharge Machined Inconel 718*):**

In this chapter, a detailed experimental study has been carried out to investigate surface characteristics of the machined Inconel 718 work material during electro-discharge machining. Surface integrity in terms of surface roughness (roughness average;  $R_a$ ), surface crack density and white layer thickness (developed onto the EDMed Inconel 718 work surface) has been studied. Effects of EDM process parameters (viz. gap voltage, peak current, pulse-on time, duty factor, and flushing pressure) on influencing topographic features of the EDMed work surface have been represented graphically. Metallurgical aspects of the EDMed work surface have also been investigated through XRD analysis. Results have been interpreted in support of EDS analysis and micro-hardness test data. Finally, utility based Taguchi approach has been applied to determine an optimal setting of process parameters to ensure satisfactory machining yield.

#### **Chapter 4 (*Electro-Discharge Machining of Inconel 825 using Cryogenically Treated Copper Electrode: Emphasis on Surface Integrity and Metallurgical Characteristics of the EDMed Part*):**

In this chapter, an attempt has been made to investigate effects of using deep cryogenically treated Copper tool electrode during execution of EDM operation on Inconel 825 work material. By considering three process parameters (viz. peak discharge current, pulse-on time, and duty factor), experiments have been conducted to study the EDM performance in terms of surface topographical features (viz. crack density, and depth of white layer) for the EDMed work surface of Inconel 825. As compared to EDM with normal tool and normal workpiece, effects of cryogenic treatment of Copper tool electrode have been discussed in purview of grain refinement and micro-hardness of the EDMed samples. Improvement in surface integrity (viz. reduced crack density, reduced crack opening width etc.) has been observed for EDM with deep cryogenically treated tool electrode. Additionally, effect of cryogenic treatment of the tool electrode has been interpreted in regards of crystallite size, dislocation density, Carbon enrichment at the work surface for the EDMed Inconel 825 specimens as compared to ‘as received’ parent material. Moreover, as compared to normal tool electrode, effects of cryogenic treatment of the tool electrode have been examined in view of thickness of the deposited Carbon layer at the bottom surface as well as the edge of tool electrode; tool shape retention capability etc. This has further been correlated with aspects of tool life.

#### **Chapter 5 (*Electro-Discharge Machining of Cryogenically Treated Inconel 825 using Cooper Tool Electrode*):**

This chapter has aimed to investigate the effects of using deep cryogenically treated Inconel 825 work material to execute electro-discharge machining with normal (untreated) Copper tool electrode. Effects of deep cryogenic treatment of the work material has been analysed focusing morphology and topographical features of the EDMed work surface of Inconel 825 in terms of surface crack density, white layer thickness, crack opening width etc. Additionally, metallurgical features of the EDMed work surfaces along with chemical composition, micro-hardness and residual stress etc. have been studied. Effects of cooling rate (applied in the cryogenic treatment cycle) for deep cryogenic treatment of the work piece have also been studied in view of overall EDM performance.

**Chapter 6 (*Surface Integrity and Metallurgical Characteristics of the EDMed Work Surfaces of A2 Tool Steel (SAE 304SS), Inconel 601 and Ti-6Al-4V: A Comparative Analysis*):**

This chapter has investigated surface integrity and metallurgical characteristics of the EDMed work surface of Inconel 601 super alloy in comparison with EDMed 304SS as well as EDMed Titanium alloy Ti-6Al-4V. Severity of surface cracking and formation of white layer depth have been studied for aforesaid three work materials machined by EDM route. Results, obtained thereof, have been interpreted with EDS, XRD analysis and micro-hardness test data.

**Chapter 7 (*Machining Performance Optimization during EDM of Inconel 718: Application of Satisfaction Function Approach Integrated with Taguchi Method*):**

This chapter has attempted to determine an optimal setting of EDM process parameters (viz. gap voltage, peak current, pulse-on time, duty factor, and flushing pressure) to ensure maximum material removal rate, minimum electrode wear rate, minimum surface roughness ( $R_a$ ), minimum crack density, minimum white layer thickness, and minimum micro-hardness (at a location approximately at the mid-depth of the white layer measured from the top surface of EDMed specimen) for EDMed Inconel 718 specimen. An integrated methodology combining satisfaction function approach and Taguchi method has been introduced herein to solve such a multi-response optimization problem. Result, obtained thereof, has been compared to that of obtained by exploring Principal Component Analysis (PCA), Combined Quality Loss (CQL) concept integrated with Taguchi's optimization philosophy.

**Chapter 8 (*Machining Performance Optimization during Electro-Discharge Machining of Inconel 601, 625, 718 and 825 Super Alloys*):**

In this chapter, effort has been made to determine an optimal parametric setting for achieving satisfactory machining performance for sound execution of EDM operation on Inconel 601, 625, 718 and 825 work materials, respectively. An integrated optimization route combining satisfaction function approach, fuzzy inference system and Taguchi method has been proposed herein. Optimal parameters setting for different work materials thus obtained, has been interpreted along with scientific justification in purview of their chemical constituents and mechanical properties.

**Chapter 9 (*Summary and Contribution*):**

This chapter has provided executive summary of the entire work carried out in this dissertation and has highlighted specific contributions to the extent body of past research in the context of electro-discharge machining of Inconel super alloys. Limitations of the present work have also been pointed out with reference to the scope for future work.



## Chapter 2

# Experimental Details

### 2.1 Experiment (Phase I): Material and Methods

Inconel 718 plates of dimension  $(50 \times 50 \times 5) \text{ mm}^3$  have been used as work material. The chemical composition and mechanical properties of Inconel 718 have been depicted in [Table 2.1.a](#) and [Table 2.1.b](#), respectively. A (99.9%) pure Copper rod of circular cross section ( $\phi 20$ ) has been used as tool electrode ([Fig. 2.1](#)).

The experiments have been carried out on die sinking EDM setup (Make: Electronica ElektraPlusPS 50ZNC; Country: India), available in NIT Rourkela. The specifications of the setup have been presented in [Table 2.2](#). Commercial grade EDM oil (with specific gravity of 0.763 and flushing point  $94^\circ\text{C}$ ) has been used as dielectric fluid. Polarity has been kept positive (i.e. workpiece positive). The other parameters such as gap servo sensitivity (SEN), anti-arcing sensitivity (ASEN), working time (Tw), and lift time (T") have been kept at constant values (refer to [Table 2.3](#)) throughout experimentation.

[Table 2.1\(a\)](#): Chemical composition of Inconel 718 [Source: [Newton et al., 2009](#)]

Element	Range (% wt.)
Ni	50.50
Fe	20.24
Cr	18.16
Nb	5.02
Mo	2.91
Ti	1.05
Al	0.62
Co	0.15
Si	0.08
Mn	0.07
Cu	0.06
C	0.05
P	0.008
Ta	0.003
B	0.003

**Table 2.1(b):** Mechanical properties of Inconel 718 [Source: Newton et al., 2009]

Property	Value
Density	8.19 g/cc
Thermal conductivity	11.2 W/m-K
Electrical resistivity	127 $\mu \Omega$ cm
Elastic modulus	200 GPa
Yield strength	434 MPa
Tensile strength	855 MPa
Hardness	89 HR <sub>B</sub>

**Table 2.2:** Specification of die-sinking EDM machine at NIT Rourkela

Machine tool	PS50 ZNS
Work table dimensions	550*350 mm
Transverse (X,Y,Z)	300*200*350 mm
Maximum electrode weight	100 gram
Maximum job height on table	250 mm
Position measuring system (X,Y,Z)	Incremental linear scale
Pulse generator	S50 ZNS
Pulse generator type	MOSFET
Current range ( $I_p$ )	0-50 A
Pulse on time range, ( $T_{on}$ )	0.5-4000 $\mu$ s
Duty factor range, ( $\tau$ )	50-93%
Open circuit voltage, (OCV)	40-60
Connected load	6KVA included PF unit

**Table 2.3:** Fixed/constant parameters

<b>SEN</b>	<b>ASEN</b>	<b>Tw (s)</b>	<b>T↑ (s)</b>	<b>Pol</b>
6	3	0.3	0.2	+ve



**Fig. 2.1:** Copper tool electrode

In the present work, five controllable process variables (parameters) have been selected based on literature survey. The selected process parameters have been OCV (also called gap voltage;  $V_g$ ), peak current ( $I_p$ ), pulse-on time ( $T_{on}$ ), duty factor ( $\tau$ ) and flushing

pressure ( $F_p$ ). In the experimental layout, each process parameter under consideration has been varied at five discrete levels (Table 2.4), as per provision of parametric setting (adjustment) available with the setup. The definitions of the process parameters (considered in this study) have been provided below.

**(a) Peak discharge current (also called peak current):** During execution of EDM operation, MRR and TWR both increase with increase in peak discharge current. This is due to the fact that an increase in peak discharge current eventually causes an increase in the pulse energy that leads to an increase in heat input rate onto the workpiece and thereby increased rate of melting as well as evaporation.

**(b) Pulse-on time (spark-on time or pulse duration):** The duration (per cycle) in which the current is allowed to flow through the discharge gap. The energy input is directly proportional to the pulse-on duration; hence, an increase in pulse duration results in increased material removal rate.

**(c) Gap voltage (also called OCV):** It is the potential difference applied between two electrodes (tool and workpiece). Gap voltage is also directly related to the energy input supplied onto the workpiece. Therefore, increase in gap voltage results in increased heat input and hence increased volumetric material removal rate.

**(d) Duty cycle (may be expressed as duty factor):** It is a percentage of the pulse-on time relative to the total cycle time.

$$\tau = \frac{T_{on}}{T_{on} + T_{off}} \quad (2.1)$$

**(e) Flushing pressure:** Flushing is a process of removing the burr and other materials from the machining area. Pressurized electrolyte is passed through the gap between tool and work piece to reach the working zone. The flushing pressure is supplied by the pump in the dielectric circulation system during EDM operation.

The design of experiment has been selected based on 5-level-5-factor  $L_{25}$  Orthogonal Array (OA) as shown in Table 2.5.



Table 2.4: Machining control parameters: Domain of variation

Parameters	Unit	Notation	Levels of variation				
			1	2	3	4	5
Gap voltage ( $V_g$ )	[V]	A	50	60	70	80	90
Peak current ( $I_p$ )	[A]	B	3	5	7	9	11
Pulse-on Time ( $T_{on}$ )	[ $\mu$ s]	C	100	200	300	400	500
Duty Factor ( $\tau$ )	[%]	D	65	70	75	80	85
Flushing Pressure ( $F_p$ )	[bar]	E	0.2	0.3	0.4	0.5	0.6

Table 2.5: Design of experiment ( $L_{25}$  OA) and collected experimental data

Sl. No.	L <sub>25</sub> OA (factors are in coded form)					Experimental data			
						Response variables to be optimized simultaneously			MH [HV <sub>0.05</sub> ]
	A	B	C	D	E	R <sub>a</sub> [μm]	SCD [μm/μm <sup>2</sup> ]	WLT [μm]	
1	1	1	1	1	1	3.800	0.0158	19.261	439.3333
2	1	2	2	2	2	6.333	0.0166	19.577	387.7000
3	1	3	3	3	3	9.133	0.0151	16.954	441.1333
4	1	4	4	4	4	9.867	0.0136	18.596	463.7000
5	1	5	5	5	5	7.600	0.0141	17.667	389.5667
6	2	1	2	3	4	3.733	0.0154	19.074	391.4333
7	2	2	3	4	5	4.400	0.0152	17.065	518.0667
8	2	3	4	5	1	8.067	0.0152	17.523	388.9667
9	2	4	5	1	2	7.667	0.0156	20.308	373.8667
10	2	5	1	2	3	9.600	0.0056	17.742	392.4333
11	3	1	3	5	2	2.967	0.0189	19.861	394.5000
12	3	2	4	1	3	5.533	0.0163	20.090	390.0000
13	3	3	5	2	4	7.267	0.0168	20.100	406.4333
14	3	4	1	3	5	8.533	0.0093	19.445	405.9667
15	3	5	2	4	1	9.733	0.0125	19.086	390.3000
16	4	1	4	2	5	4.267	0.0172	18.310	384.1333
17	4	2	5	3	1	5.267	0.0157	18.067	352.6000
18	4	3	1	4	2	7.200	0.0108	18.137	385.6333
19	4	4	2	5	3	5.667	0.0084	18.673	390.6333
20	4	5	3	1	4	9.867	0.0110	18.835	410.7333
21	5	1	5	4	3	2.133	0.0156	17.602	378.2000
22	5	2	1	5	4	5.667	0.0117	16.646	372.9000
23	5	3	2	1	5	7.333	0.0136	17.707	375.8000
24	5	4	3	2	1	9.200	0.0116	19.752	399.1000
25	5	5	4	3	2	10.333	0.0100	19.077	431.8667

Experiments have been conducted as per 25 factorial settings; the EDM of Inconel 718 plates have been carried out with copper electrode. Both workpiece and tool have been immersed in dielectric fluid. The machining duration has been kept constant (10 minutes) for each experimental run. After performing experiments, in order to analyze surface characteristics of the EDMed Inconel 718 specimen, the responses studied herein have been Roughness average ( $R_a$ ), Surface Crack Density (SCD), and White Layer Thickness (WLT).

In addition to that, the micro-hardness values for all EDMed specimens have been determined by Vicker's micro-hardness tester (Make: LECO; Modal No. LM810; Country: USA). Hardness measurements have been carried out with test load of 50gf and at a constant indenter dwell time of 10s. All indentation tests have been performed under ambient laboratory conditions.

In order to determine the elements and phases present on the surface of 'as received' Inconel 718 as well as EDMed Inconel 718 specimen, EDS (energy dispersive spectrograph) and XRD (X-ray diffraction) have been carried out. In this work, the chemical composition of Inconel 718 samples (before and after machining) have also been detected by Energy Dispersive X-ray Spectroscopy (EDS) under Scanning Electron Microscope (Model No. SU3500), and EDS (Model No. 51\_ADD0034), manufactured by Hitachi, Japan.



Fig. 2.2: EDMed workpiece

The phases present on the EDMed work surface of Inconel 718 along with residual stress induced within the part component have been determined by XRD microscopy (Model No: D8 ADVANCE with DAVINCI design; Make: BRUKER; Country: Germany). Apart from 'as received' Inconel 718, residual stress induced within the EDMed specimen produced at Run No. 1 i.e. [parameters setting:  $V_g=50V$ ;  $I_p=3A$ ;  $T_{on}=100\mu s$ ;  $\tau=65\%$ ;  $F_p=0.2bar$ ] has been measured and compared with each other. In addition to these, XRD spectra for 'as received' Inconel 718 as well as EDMed Inconel 718 work surface (obtained at Run No. 1) have been analyzed to identify various phases present therein and

to collect the information in relation to grain refinement, alloying effect, formation of new phase etc. as the consequences of EDM operations. These have been described in Chapter 3. The experimental results in relation to process responses like  $R_a$ , SCD and WLT have been depicted in [Table 2.5](#). The snapshot of EDM machined work pieces has been provided in [Fig. 2.2](#). Definitions of aforesaid response measures in the context of the present work have also been provided below.

**Surface Roughness:** Arithmetic average roughness, or  $R_a$ , is the arithmetic average of the heights of surface irregularities (consisting of peak heights and valleys) with respect to the mean line, measured within the sampling length. The measurement of surface roughness ( $R_a$  value) of the EDMed surface has been carried out with portable stylus type profilometer, Talysurf (Model: Taylor Hobson, Surtronic 3+), with cut-off length ( $L_c$ ) of 0.8 mm, sample length ( $L_n$ ) of 4 mm, and filter CR ISO.

**Surface Crack Density (SCD):** It is well known that generation of surface crack is detrimental since it results inferior surface finish. It seems very difficult to quantify the phenomenon of cracking in terms of width, length, or depth of the crack or even by the extent of cracking; therefore, in the present work, surface crack density has been measured and analysed to evaluate the severity of cracking. As mentioned by ([Bhattacharyya et al., 2007](#)), surface crack density is defined as the total length of cracks ( $\mu\text{m}$ ) per unit surface area ( $\mu\text{m}^2$ ).

In course of the present work, to measure surface crack density, the top surface morphology of the EDMed Inconel 718 specimen has been studied using scanning electron microscope. For a particular sample, SEM images have been captured in three distinct locations and corresponding surface crack densities have been collected. The average of these three has been considered as the representative measure of SCD for that particular specimen. For a particular sample area, the total crack length has been measured using *PDF-XChange Viewer* Software ([Fig. 2.3](#)). The total crack length divided by the specimen area provided the measure of SCD.

It is worth of mentioning that SCD value may increase when the SEM images are captured at higher magnification; therefore, the word ‘surface crack density’ should be understood as ‘relative surface crack density’ throughout the dissertation ([Upadhyay et al., 2016](#)).

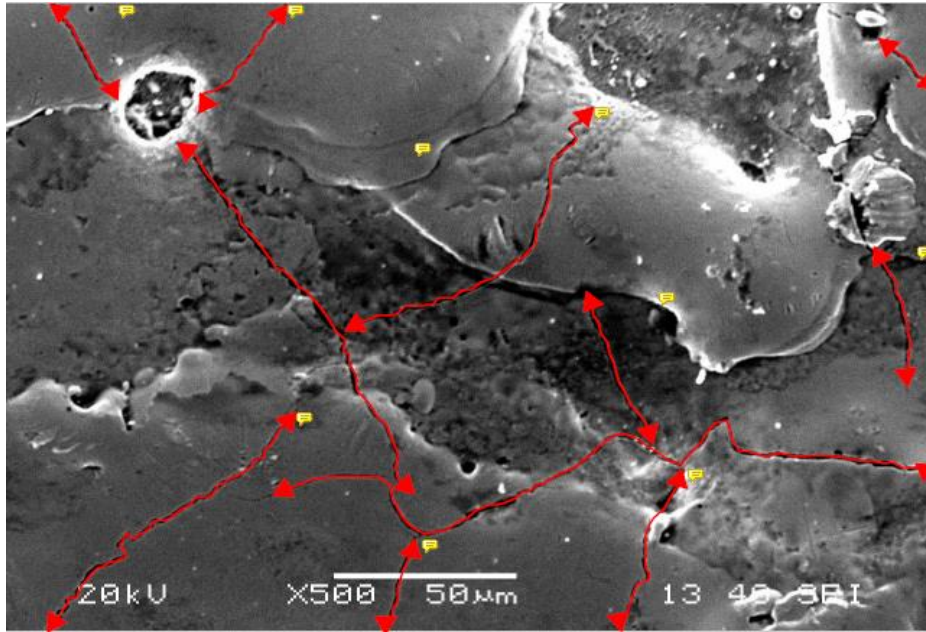


**Fig. 2.3:** Measurement of Surface Crack Density (SCD) of the EDMed work surface obtained at parameters setting  $A_2B_1C_2D_3E_4$  i.e. [OCV=60V,  $I_p=3A$ ,  $T_{on}=200\mu s$ ,  $\tau=75\%$  and  $F_p=0.5bar$ ]

#### **White Layer Thickness (WLT):**

In order to measure white layer thickness, each specimen has been sectioned in appropriate dimension and cold mounted by using cold mounting compound resin bed revealing the edge of the workpiece to go for grinding and subsequent polishing operation. For cold mounting of specimens, Geosyn cold mounting compound powder and liquid have been used. Fig. 2.4 depicts snapshot of a cold mounted specimen.



**Fig. 2.4:** Cold mounted specimen

The cold mounted specimens have been ground successively on water-proof SiC papers with grit sizes 120, 320, 400, 600, 800, 1200 and 1500, respectively. Grinding has been performed for 60-120 seconds at 240-300 RPM speed of the grinding wheel. Finally, the specimen surface has been polished with SELVYT Cloth (made in England) and diamond paste of 1 $\mu$ m size. The surface has then been subsequently electro-polished with slurry of HIFIN Fluid with ‘OS’ type diamond compound. Next, the polished surface has been etched in Kalling’s Reagent solution (5g CuCl<sub>2</sub> + 100 ml conc. HCl + 100 ml pure ethanol) for 20s immersion. This has been felt necessary in order to expose white layer and corresponding distinct boundary line separating HAZ and/or base material. The specimen has then been viewed under SEM (Model: Joel JSM-6480LV; Country: Japan) to capture the image of the white layer formed. The thickness of the white layer has been measured by *ImageJ* Software at five different locations across each cross-sectioned specimen (Fig. 2.5); and an average value has been considered for further analysis. Hence, the notation WLT should be understood as ‘relative/average’ WLT throughout the dissertation.

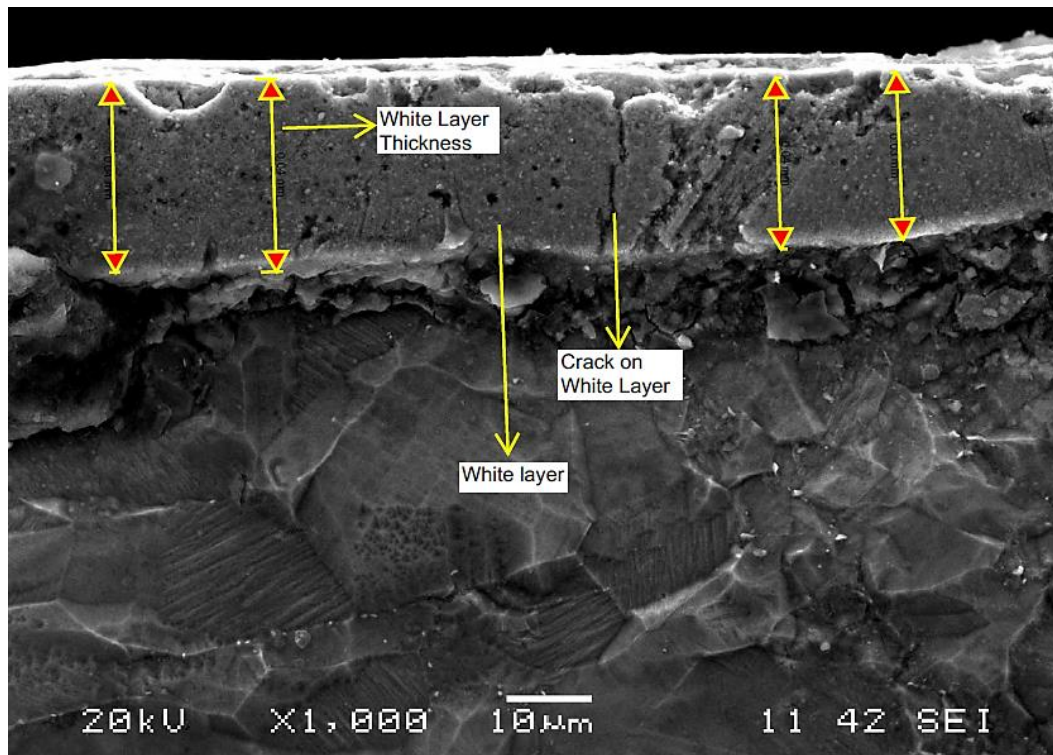
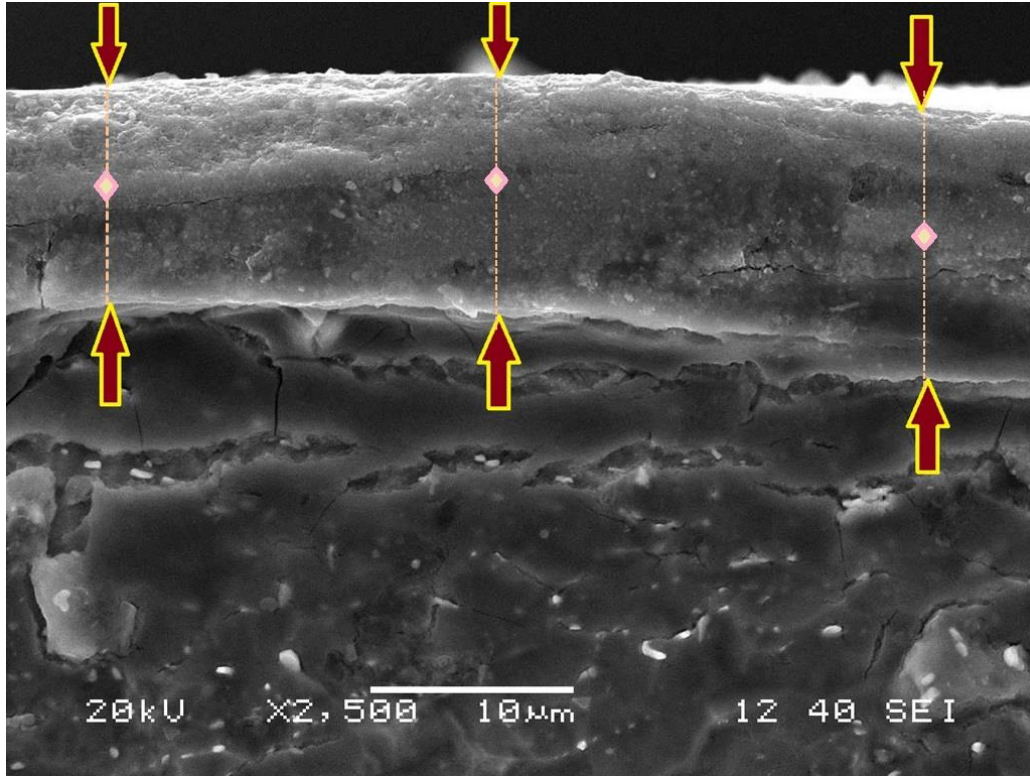


Fig. 2.5: Measurement of White Layer Thickness (WLT) for the EDMed Inconel 718 specimen obtained at parameters setting A<sub>5</sub>B<sub>1</sub>C<sub>5</sub>D<sub>4</sub>E<sub>3</sub> i.e. [OCV=90V, I<sub>p</sub>=3A, T<sub>on</sub>=500 $\mu$ s,  $\tau$ =80% and F<sub>p</sub>=0.4 bar]





**Fig. 2.6:** Places of indentation for micro-hardness test (EDMed Inconel 718 obtained at parameters setting: ( $A_1B_2C_2D_2E_2$ ) [OCV=50V,  $I_p$ =5A,  $T_{on}$ =200 $\mu$ s,  $\tau$ =70% and  $F_p$ =0.3 bar] (Average micro-hardness value ~ 387.700 HV<sub>0.05</sub>)

During micro-hardness tests, the points of indentations followed at three distinct locations (approximately at the middle position along the thickness of white layer) for a particular sample (transverse cut section of the EDMed workpiece through WEDM route); have been depicted in Fig. 2.6. The average of the micro-hardness values obtained at three distinct locations has been treated as the relative (or average) micro-hardness for that particular specimen.

## 2.2 Experiment (Phase II): Material and Methods

In Phase II of the experimental schema, Inconel 825 square shaped flat plates of dimension  $(50 \times 50 \times 5)mm^3$  have been used as workpiece. The chemical composition and mechanical properties Inconel grade 825 have been shown in Table 2.6.1-2.6.2, respectively.

Table 2.6.1: Chemical composition of Inconel 825 (Prabhu and Vinayagam, 2011)

Element	Weight (%)
Ni	38-46
Fe	22
Cr	19.5-23.5
Mo	2.5-3.5
Cu	1.5-3.0
Ti	0.0-1.2
C	0.05
Si	0.5
Mn	1.0
Al	0.2
S	0.03

Table 2.6.2: Mechanical properties of Inconel 825 (Rajyalakshmi and Ramaiah, 2013)

Properties	Values
Density	8.14 g/cm <sup>3</sup>
Melting point	1400 °C
Coefficient of expansion	14.0 m/m/°C (20-100°C)
Modulus of rigidity	75.9 N/mm <sup>2</sup>
Modulus of elasticity	196 kN/mm <sup>2</sup>
Thermal conductivity	12.3 W/m.°C at 100°C

Before conducting EDM experiments, the tool electrode have been cryogenically treated in order to improve their properties. For DCT, the workpiece and tool have been cooled down (ramp-down) to approximately -185°C at cooling rate 1°C/min, and held for 24h and then gradually heated back at the same rate i.e. at cooling rate 1°C/min to the ambient temperature (ramp-up). The DCT cycle adapted herein has been depicted in Fig 2.7. The snapshot of the set up used for cryogenic treatment of tool electrode has also been presented in Fig. 2.8.

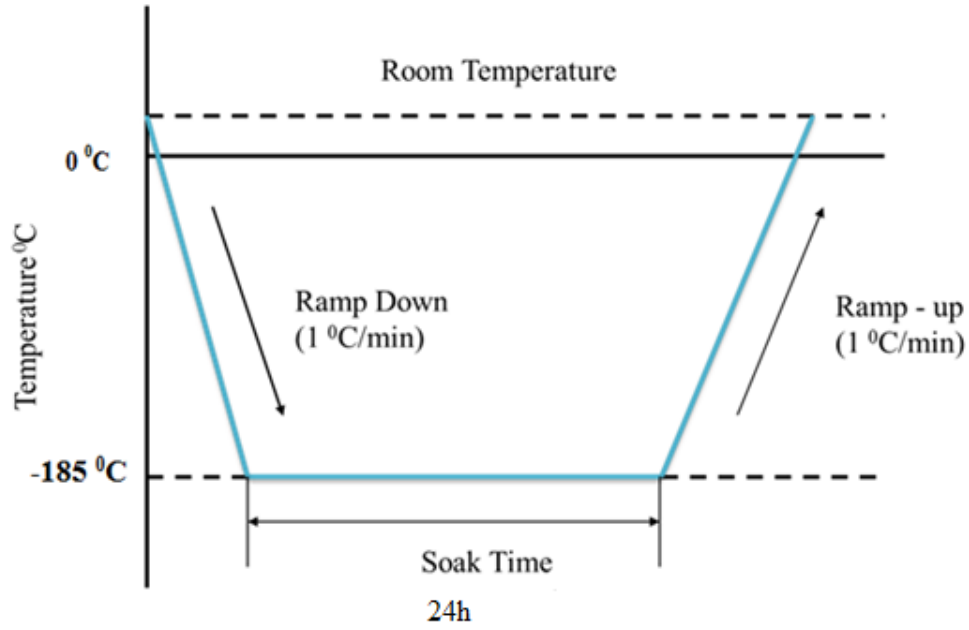


Fig. 2.7: Time versus temperature cure for the cryogenic treatment of the tool material adapted in the present work

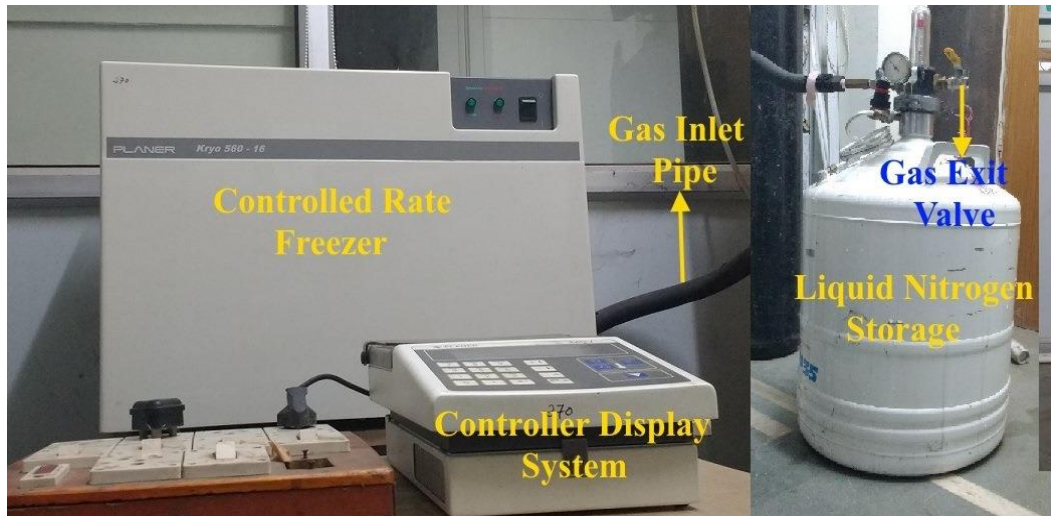


Fig. 2.8: Setup for cryogenic treatment of the tool electrode

EDM experiments have been carried out on Die Sinking EDM (Make: Electronica, Model ELEKTRA EMS-5535; Pune, India) setup, available in CTTC, Bhubaneswar. (Specifications of the setup have been furnished in Table 2.7). A (99.9%) pure Copper [thermal conductivity 401 W/ (m·°C) at 20° C; melting point 1082.78° C; boiling point: 2567° C] rod of circular cross section ( $\phi 20$ ) has been used as a tool electrode. Commercially available grade Rustlick™ EDM-30 oil of ITW Professional Brand



(Specific Gravity: 0.80 @ 25° F; Viscosity: 36 SSU @ 100°F (38°C); Flash Point: 200° F; Dielectric Strength: 45KV) has been used as dielectric medium. Polarity has been kept positive (i.e. workpiece positive) throughout experimentation.

**Table 2.7:** Specification of the EDM setup at CTTC, Bhubaneswar

Item(s)	Value/ Range
Mounting surface (Length× Width)	550×350 mm
Maximum workpiece height	250 mm
Maximum job weight	300 kg
X-Axis travel	300 mm
Y- Axis travel	200 mm
Transverse (X,Y, Z)	300, 200, 200 mm
Least count of hand wheel with Vernier scale	0.02 mm
Maximum table quill distance	515 mm
Minimum table quill distance	265 mm
Width of the work tank	820 mm
Depth of the work tank	490 mm
Height of the work tank	325 mm
Pulse generator	50 ampere
Current range ( $I_p$ )	0 -10 A
Pulse-on time range ( $T_{on}$ )	0.5 - 3000 $\mu$ s
Duty factor range ( $\tau$ )	8 -100%
Open circuit voltage range ( $V_g$ )	0 - 30 V

**Table 2.8:** Domain of experiments: Level values of process control parameters

Parameters	Unit	Notation	Levels of variation		
			1	2	3
Peak current ( $I_p$ )	[A]	A	6	8	10
Pulse-on Time ( $T_{on}$ )	[ $\mu$ s]	B	100	200	300
Duty Factor ( $\tau$ )	[%]	C	65	75	85

Experiments have been carried out using three controllable process parameters: peak discharge current ( $I_p$ ), pulse-on-time ( $T_{on}$ ), and duty factor ( $\tau$ ); each varied at three discrete levels as per availability of factorial setting in the particular EDM setup used herein. The domain of experiment as selected for the present work has been shown in [Table 2.8](#). Apart from aforesaid three electrical parameters; there have been few parameters whose values have been kept constant throughout experiments. The constant parameters and corresponding values have been: gap voltage ( $V_g$ ) =25V; flashing pressure=2.1bar; spark gap distance=50 $\mu$ m. EDM experiments have been performed on

few selected parametric settings (viz.  $A_1B_3C_3$ ,  $A_2B_3C_3$ ,  $A_3B_3C_3$ ,  $A_3B_1C_3$ ,  $A_3B_2C_3$ ,  $A_3B_3C_1$ ,  $A_3B_3C_2$ ) in multiple trials using (i) Non-Treated Tool (NTT) (here, the term ‘non-treated’ represents ‘un-cryogenically treated’), and (ii) Cryogenically Treated Tool (CTT).

The machining duration has been kept constant (10 minutes) for each of the experimental runs. A snapshot of EDMed Inconel 825 specimens has been provided in Fig 2.9. After EDM operations, topographical measures of the EDMed work surface viz. Surface Crack Density (SCD) and White Layer Thickness (WLT) have been measured for each of the experimental schema.



Fig. 2.9: EDMed Inconel 825 specimens along with (a) NTT and, (b) CTT

In addition to that, residual stress and micro-hardness tests have been carried out on few selected specimens using XRD Texture Measurement Machine [Model No: D8 ADVANCE with DAVINCI design, Make: BRUKER, Country: Germany] and Vicker’s Micro-hardness tester [Model No. LECO LM 810; with Load 25gf and dwell time 10s], respectively.

#### ⇒ **Determination of Crystallite Size and Dislocation Density**

Additionally, XRD peak patterns have been analyzed further to investigate the effects of cryogenic treatment of the work material on quantitative metallurgical information like Crystallite Size ( $L$ ) and Dislocation density ( $\delta$ ) of the test specimens. The extent of grain refinement and the effect imposed thereof on crystal/grain structure of the work surface (obtained under different conditions of EDM) has been interpreted mathematically with relevance to the computed data. While quantifying various measurement indices to describe specimens’ grain structure; the following information needs to be well acknowledged.

### ▲ Crystallite Size ( $L$ )

The crystallite size ( $L$ ) for each of the specimens ('as received'/ cryogenically treated workpiece/ EDMed work surface) has been calculated from X-ray diffraction profiles of strong reflections with intensity % by measuring the Full-Width-Half-Maximum (FWHM).

The *Scherrer* equation for computing the crystallite size is given by (Eq. 2.2).

$$L = \frac{K\lambda}{\beta_L \cos \theta} \quad (2.2)$$

In this expression,  $L$  relates the crystallite size corresponding to the broadening  $\beta_L$  of its diffraction peaks (ignoring other effects such as broadening due to instrument and broadening due to strain),  $\theta$  is the usual Bragg angle,  $\lambda$  is the radiation wavelength ( $\lambda_{Co} = 1.7906 \text{ \AA}$  for  $CoK_\alpha$ ), and  $K$  is a constant (*Scherrer* constant = 0.9).

It is to be noted that  $\beta_L$  is approximately equal to the FWHM of the sharp (high intensity) peaks on the XRD spectra. Thus, it is seen that  $\beta_L$  and  $L$  are reciprocally related. This implies that: the greater the broadening the smaller the crystallite size and vice-versa (Subbaiah et al., 2006; Singh et al. 2008; Vinila et al., 2014).

### ▲ Calculation of $d$ spacing

The value of  $d$  i.e. the inter planner spacing between the atoms, is computed using the *Braggs's Law*:

$$2d \sin \theta = n\lambda \quad (2.3)$$

i.e.  $d = \frac{\lambda}{2 \sin \theta}$ ,  $n = 1$ . (Wavelength of X-ray =  $1.7906 \text{ \AA}$  for  $CoK_\alpha$ )

### ▲ XRD-Dislocation Density ( $\delta$ )

The dislocation density is defined as the length of dislocation lines per unit volume of the crystal. Theoretically a dislocation is a crystallographic irregularity or a defect formed within the crystal. The properties of the crystal formed are strongly influenced by the defects inside the crystal (Subbaiah et al., 2006; Singh et al., 2008; Vinila et al., 2014; Jacob et al., 2015). Shift or movement of a dislocation is impeded by other dislocations present within the specimen. Jacob et al. (2015) inferred that the dislocation density

increases while grain size decreases with increasing strain and ultimately these parameters reach saturation values. The dislocation density ( $\delta$ ) can be computed as:

$$\delta = \frac{15\beta_L \cos \theta}{4aL} \quad (2.4)$$

$\beta_L$  = FWHM measured in radians

$\theta$  = Diffracting angle

$a$  = The cell parameter (Lattice constant measured from XRD data)

Also  $a = d\sqrt{(h^2 + k^2 + l^2)}$ , and

$L$  = Crystallite size in nm

Also the notations  $h, k, l$  denote *Miller* indices representing a particular crystallographic direction.

## 2.3 Experiment (Phase III): Material and Methods

In Phase III, Inconel 825 square shaped flat plates of dimension  $(50 \times 50 \times 5) \text{ mm}^3$  have been used as workpiece. The chemical composition and mechanical properties Inconel grade 825 have already been provided in [Table 2.6.1-2.6.2](#) (in Phase II), respectively.

Before conducting EDM experiments, the work material has been cryogenically treated in order to improve its properties. For DCT, the workpiece has been cooled down (ramp-down) to approximately  $-185^\circ\text{C}$  at cooling rate  $1^\circ\text{C}/\text{min}$ , and held for 24h, and then gradually heated back at the same rate (i.e.  $1^\circ\text{C}/\text{min}$ ) to the ambient temperature (ramp-up). The deep cryogenic treatment cycle adapted herein has been depicted in [Fig 2.7](#) (refer to Phase II).

Using same experimental setup as used in Phase II and also considering the similar domain of experiment ([Table 2.8](#)); EDM operations have been carried out on few selected parametric settings (viz.  $A_1B_3C_3$ ,  $A_2B_3C_3$ ,  $A_3B_3C_3$ ,  $A_3B_1C_3$ ,  $A_3B_2C_3$ ,  $A_3B_3C_1$ ,  $A_3B_3C_2$ ) in multiple trials using (i) Non-Treated Workpiece (NTW), and (ii) Cryogenically Treated Workpiece (CTW).

In addition to that, another set of experiment on EDM using CTW has been carried out for a selected parameters setting (i.e.  $A_3B_3C_3$ ), in which the workpiece has been cryogenically treated with a cooling rate (as well as ramp-up) of  $0.5^\circ\text{C}/\text{min}$  and the

soaking time of 24h. This has been planned to investigate the effect of cooling rate on the machining performance of EDM on CTW of Inconel 825.

The machining duration has been kept constant (10 minutes) for each of the experimental runs. A snapshot of EDMed Inconel 825 specimens has been provided in Fig 2.10. After EDM operations, the parameters of the EDMed work surface topography in terms of Surface Crack Density (SCD) and White Layer Thickness (WLT) have been measured for each of the experimental schema. In addition to that, residual stress and micro-hardness tests have been carried out on few selected specimens. Details of such data collection have already been described in Phase II.



Fig. 2.10: EDMed surface of (a) NTW of Inconel 825 and, (b) CTW of Inconel 825 along with tool electrode

## 2.4 Experiment (Phase IV): Material and Methods

In Phase IV, 304SS, Inconel 601 and Ti-6Al-4V plates with dimension  $(50 \times 50 \times 50) \text{ mm}^3$  have been used as workpiece material. The mechanical properties of 304SS, Inconel 601 and Ti-6Al-4V have been furnished in Table 2.9. Additionally, chemical compositions of aforementioned three work materials have been provided in Table 2.10. A 99.9% pure Copper [thermal conductivity  $401 \text{ W/(m} \cdot ^\circ\text{C)}$  at  $20^\circ\text{C}$ ; melting point  $1082.78^\circ\text{C}$ ; boiling point:  $2567^\circ\text{C}$ ] rod (of circular cross section) has been used as tool electrode.

Table 2.9: Chemical composition of (a) 304SS, (b) Inconel 601, and (c) Ti-6Al-4V

(a) 304SS [Source: <a href="#">Xavior and Adithan, 2009</a> ]	
Element	Range (% wt.)
C	0.05487
Si	0.64
Mn	1.66
Cr	18.2
Ni	9.11
Mo	0.092
Cu	0.14
Ti	0.006
V	0.046
W	0.48
Co	0.40
Nb	0.013
Pb	0.015
Fe	69.7

(b) Inconel 601 [Source: <a href="#">Sidhu et al., 2006</a> ]	
Element	% Weight
C	0.025
Si	0.37
Cu	0.1
Mn	0.1
Cr	23.05
Ni	62.6
Al	1.4
Fe	12.355

(c) Ti-6Al-4V [Source: <a href="#">Hasçalık and Çaydaş, 2007a, b</a> ]	
Element	Range (% wt.)
Ti	89.464
Al	6.08
V	4.02
Fe	0.22
O	0.18
C	0.02
N	0.01
H	0.0053

**Table 2.10:** Mechanical properties of (a) 304SS, (b) Inconel 601, and (c) Ti-6Al-4V

(a) Mechanical properties of 304SS [Source: <a href="#">Xavior and Adithan, 2009</a> ]	Unit	Value
Density	kg/m <sup>3</sup>	8000
Elastic modulus	GPa	193
Poisson's ratio	-	0.30
Coefficient of thermal expansion	Mmm <sup>-1</sup> °C <sup>-1</sup>	17.8
Thermal conductivity	W/mK	16.2
Specific heat capacity	J/kgK	500

(b) Mechanical properties of Inconel 601 [Source: <a href="http://www.specialmetals.com">www.specialmetals.com</a> ]	Value
Density	8.11 g/cm <sup>3</sup>
Thermal conductivity	12.7 W/m- °C (20 - 100°C)
Electrical resistivity	1.192 μ Ω m (20 - 100°C)
Modulus of elasticity (Tension)	206 GPa (at 20 °C)
Yield strength	205-310 MPa
Tensile strength	550-690 MPa
Hardness	60-75 R <sub>b</sub>
Melting Point	1360 – 1411 °C
Elongation	65-45%

(c) Mechanical properties of Ti-6Al-4V [Source: <a href="#">Hasçalık and Çaydaş, 2007a, b</a> ]	Value
Hardness (HV <sub>20</sub> )	600
Melting point (°C)	1660
Ultimate tensile strength (MPa)	832
Yield strength (MPa)	745
Impact-toughness (J)	34
Elastic modulus (GPa)	117
Thermal conductivity (W/m.°C at 20°C)	7.2

From the ‘as received’ commercially available Copper rod, the required tool dimension (20mm diameter) has been obtained. Here, Copper has been selected as electrode material because of its high thermal and electrical conductivity as well as corrosion resistance.

The electrode has been given into the required shape through Computer Numeric Controlled (CNC) machining. The CNC machining operation may develop micro-cracks and the cutting forces which may create thermal stresses. The combination of all may deteriorate surface integrity of the tool material. This may affect EDM performance adversely. To elicit such happenings, very low feed rate and coolant have been used during execution of CNC turning operation. Moreover, after machining, electrode tool has



been polished in wet condition by 220 grade emery paper. This has further helped to improve surface quality of the tool electrode. Hence, it has been assumed that surface integrity of tool electrode has imposed negligible effect on EDM performance.

EDM experiments have been carried out on the EDM setup, available in CTTC, Bhubaneswar (as mentioned in Phase II). In this experiment, commercially available Rustlick™ EDM-30 oil has been used as dielectric fluid.

During execution of EDM experiments, straight polarity (i.e. tool as cathode and workpiece as anode) has been maintained. The peak discharge current has been chosen as the process variable with three distinct level values (viz. 6A, 8A, and 10A, respectively). The remaining parameters such as pulse-on time, gap voltage, duty factor, flushing pressure, spark gap and machining time have been kept constant throughout experimentation (Table 2.11). A snapshot of the EDMed end product of 304SS, Inconel 601 and Ti-6Al-4V has been provided in Fig. 2.11.

Table 2.11: Parameters kept at constant values

Parameters	Unit	Value
Gap voltage ( $V_g$ )	[V]	25
Pulse-on-Time ( $T_{on}$ )	[ $\mu s$ ]	300
Duty Factor ( $\tau$ )	[%]	85
Flushing pressure	[bar]	2.1
Polarity	-	Positive
Spark gap	[ $\mu m$ ]	50

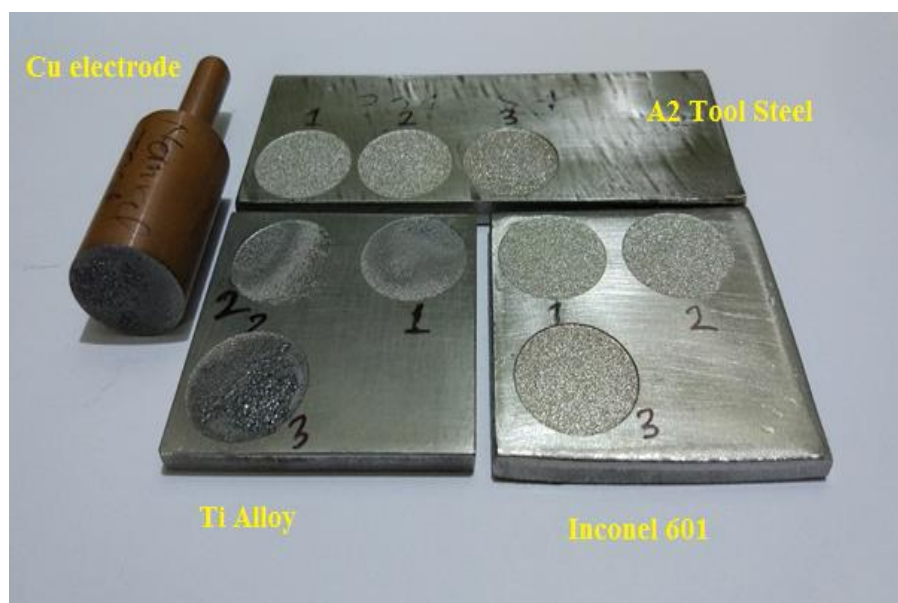


Fig. 2.11: EDMed work surfaces of A2 Tool Steel (304SS), Inconel 601 and Ti-6Al-4V alloy



The responses studied have been surface roughness ( $R_a$  value), Surface Crack Density (SCD) as well as White Layer Thickness (WLT) observed onto the machined surface. Additionally, Micro-hardness (MH) has been measured at a position approximately at mid-depth of the white layer (measured from the top surface) for each of the EDMed specimens.

Metallurgical analyses of the EDMed specimen surfaces (as compared to ‘as received’ work materials) have been carried out by using X-ray Diffraction Microscopy. In addition to that, EDS and micro-hardness tests have been carried out on few selected specimens using Scanning Electron Microscope and Vicker’s Micro-hardness tester, respectively. Details of such experimental data collection have already been provided in Phase II.

## 2.5 Experiment (Phase V): Material and Methods

Phase V is basically extension of the experimental part as highlighted in Phase I. Apart from  $R_a$ , SCD, WLT and MH; two other performance features have also been collected for further analysis. These responses are: Material Removal Rate (MRR) and Electrode Wear Rate (EWR). The experimental domain (Table 2.4) and design of experiment (Table 2.5) as utilized in Phase I have also been followed herein. Fig. 2.12a, b depicts snapshots of experimentation. The experimental results (consolidated data in relation to all the response features) have been depicted in Table 2.12. The definitions of the following response measures: MRR as well as EWR as considered herein have been provided below along with their computational formulae. The definitions of remaining responses have already been provided in Phase I.

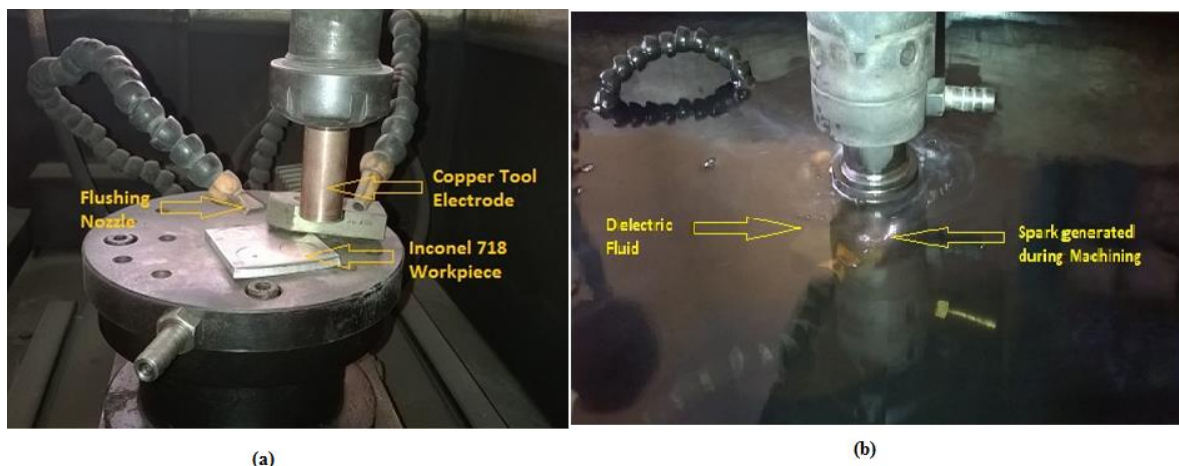


Fig. 2.12: (a) Setting of workpiece and electrode tool, and (b) A snapshot of EDM in progress

Table 2.12: Design of experiment (L<sub>25</sub> OA) and collected experimental data

Sl. No.	L <sub>25</sub> OA (DOE)					Experimental data					
	A	B	C	D	E	MRR [mm <sup>3</sup> /min]	EWR [mm <sup>3</sup> /min]	R <sub>a</sub> [μm]	SCD [μm/μm <sup>2</sup> ]	WLT [μm]	MH [HV <sub>0.05</sub> ]
1	1	1	1	1	1	8.926014	0.111982	3.800	0.0158	19.261	439.3333
2	1	2	2	2	2	14.10501	0.022396	6.333	0.0166	19.577	387.7000
3	1	3	3	3	3	38.40095	0.022396	9.133	0.0151	16.954	441.1333
4	1	4	4	4	4	48.49642	0.078387	9.867	0.0136	18.596	463.7000
5	1	5	5	5	5	88.21002	0.111982	7.600	0.0141	17.667	389.5667
6	2	1	2	3	4	4.892601	0.156775	3.733	0.0154	19.074	391.4333
7	2	2	3	4	5	15.179	0.134378	4.400	0.0152	17.065	518.0667
8	2	3	4	5	1	26.92124	0.044793	8.067	0.0152	17.523	388.9667
9	2	4	5	1	2	38.78282	0.055991	7.667	0.0156	20.308	373.8667
10	2	5	1	2	3	89.16468	0.145577	9.600	0.0056	17.742	392.4333
11	3	1	3	5	2	5.298329	0.011198	2.967	0.0189	19.861	394.5000
12	3	2	4	1	3	10.04773	0.011198	5.533	0.0163	20.090	390.0000
13	3	3	5	2	4	18.30549	0.011198	7.267	0.0168	20.100	406.4333
14	3	4	1	3	5	49.21241	0.022396	8.533	0.0093	19.445	405.9667
15	3	5	2	4	1	79.57041	0.067189	9.733	0.0125	19.086	390.3000
16	4	1	4	2	5	2.362768	0.011198	4.267	0.0172	18.310	384.1333
17	4	2	5	3	1	4.868735	0.022396	5.267	0.0157	18.067	352.6000
18	4	3	1	4	2	22.52983	0.022396	7.200	0.0108	18.137	385.6333
19	4	4	2	5	3	44.8926	0.022396	5.667	0.0084	18.673	390.6333
20	4	5	3	1	4	49.06921	0.011198	9.867	0.0110	18.835	410.7333
21	5	1	5	4	3	1.312649	0.011198	2.133	0.0156	17.602	378.2000
22	5	2	1	5	4	7.207637	0.011198	5.667	0.0117	16.646	372.9000
23	5	3	2	1	5	18.61575	0.033595	7.333	0.0136	17.707	375.8000
24	5	4	3	2	1	25.1074	0.044793	9.200	0.0116	19.752	399.1000
25	5	5	4	3	2	48.01909	0.022396	10.333	0.0100	19.077	431.8667

**Material Removal Rate (MRR):** MRR can be defined as the rate at which loss of material takes place from the workpiece. The MRR is determined by weight loss of the workpiece and can be calculated using the following equation.

$$MRR = \frac{(W_i - W_f)}{(t \times \rho)} \left[ \frac{mm^3}{min} \right] \quad (2.5)$$

Here  $W_i$  and  $W_f$  are initial and final weights (kg) of the workpiece, respectively;  $t$  is the machining time (in minutes) and  $\rho$  represents density of the work material (in g/cc). (Density of Inconel 718: 8.19 g/cm<sup>3</sup>)

**Electrode Wear Rate (EWR):** EWR can be defined as the rate at which loss of material takes place from the electrode. This can be computed using the following equation.

$$EWR = \frac{(E_i - E_f)}{(t \times \rho_E)} \left[ \frac{mm^3}{min} \right] \quad (2.6)$$

Here  $E_i$  and  $E_f$  are initial and final weights of the tool electrode (in kg), respectively;  $t$  is the machining time (in minutes) and  $\rho_E$  represents density of the electrode material (in g/cc). (Density of pure Copper: 8.93 g/cm<sup>3</sup>)

In this experimentation, weight loss of work and tool material have been measured by electronic weighing balance (Model: DJ 300S; Make: Shinko Denshi Co. Ltd; Country: Japan; Accuracy: 0.001g).

The melting and re-solidification of the material causes formation of white layer onto the top of the machined surface. The formation of WL and HAZ adversely affect surface integrity (which is characterized by high surface roughness i.e.  $R_a$  value), development of induced residual stress, altered composition of the surface, reduced corrosion resistance etc. (Rao et al., 2014). Therefore, formation of while layer and HAZ needs to be controlled. However, in the present case, HAZ has not been clearly demarcated from the unaffected parent material from the SEM micrographs.

In the present work, micro-hardness (MH) of the white layer has been considered as one of the machining performance features with an aim to minimize it (i.e. MH correspond to Lower-is-Better (LB) criteria). The justification is as follows. Formation while layer is evident in EDM; but by proper controlling of process variables, it is possible to minimize WLT. Formation of white layer enhances possibility of occurrence of surface cracks, surface irregularities and rough surface finish. If the end product (EDMed component) is subjected to further machining operation, additional difficulties may arise due to existence of while layer onto the top of the machined surface. Inconel 718 itself is a hard material (*difficult-to-cut*); and hence, it is indeed a necessity to minimize the hardness of the while layer (since hardness of white layer has appeared more as compared to base metal) though it exists to a minimum (optimized) extent.

## 2.6 Experiment (Phase VI): Material and Methods

The work pieces (used in Phase VI) for the experiment have been Inconel of different grades viz. Inconel 601, 625, 718, and 825 of square shaped plate (50×50×5)mm<sup>3</sup>. The chemical compositions of Inconel 718, 825, 601 have already been provided in Table 2.1a, Table 2.6.1, and Table 2.9b, respectively. The chemical composition of Inconel 625 has been furnished in Table 2.13.

**Table 2.13:** Chemical composition of Inconel 625 [Source: [Goyal, 2017](#)]

Element	Range (% wt.)
Ni	58 (min)
Cr	20-23
Fe	5
Co	1
Mo	8-10
Nb	3.2-4.2
Ti	0.4
Al	0.4
C	0.1
Mn	0.5
Si	0.5

Mechanical properties of Inconel 625 have also been provided in [Table 2.14](#). The mechanical properties of Inconel 718, Inconel 825 and Inconel 601 have already been provided in [Table 2.1b](#), [Table 2.6.2](#), and [Table 2.10b](#)), respectively. The experiments have been carried out on die sinking EDM setup (as mentioned in Phase I). Graphite rod of cylindrical shape( $\phi 12$ ) has been used as a tool electrode ([Fig. 2.13](#)). Commercially available grade EDM oil with specific gravity of 0.763 has been used as dielectric fluid. Polarity has been kept positive (i.e., workpiece positive). The other parameters such as gap servo sensitivity (SEN), anti-arcing sensitivity (ASEN), working time (Tw), and lift time (T'') have been held at constant values (same as used in Phase I).

**Table 2.14:** Mechanical properties of Inconel 625 [Source: [www.specialmetals.com](http://www.specialmetals.com)]

Property	Value
Density	8.44 g/cm <sup>3</sup>
Elastic modulus	207.5 GPa ( at 21 °C)
Thermal conductivity	10.8 W/m °C ( 20-100 °C)
Electrical Resistivity	132 $\mu\Omega$ -cm ( 20-100 °C)
Yield strength	414-655 MPa
Tensile strength	827-1034 MPa
Hardness	145-220 HB
Melting Point	1290 – 1350 °C
Elongation	60-40 %



Fig. 2.13: EDM setup with graphite tool electrode

Experiments have been carried out using five controllable process parameters each varied at four discrete levels as per availability of factorial setting in the EDM setup. The selected process variables have been considered as: gap voltage (OCV), peak current ( $I_p$ ), pulse-on time ( $T_{on}$ ), duty factor ( $\tau$ ), and flushing pressure ( $F_p$ ). The domain of experiment has been presented in Table 2.15.

Table 2.15: Domain of experiments: Machining control parameters

Parameters	Unit	Notation	Levels of variation			
			1	2	3	4
OCV (V)	[V]	A	60	70	80	90
Peak current ( $I_p$ )	[A]	B	5	7	9	11
Pulse-on-Time ( $T_{on}$ )	[ $\mu$ s]	C	200	300	400	500
Duty Factor ( $\tau$ )	[%]	D	70	75	80	85
Flushing Pressure ( $F_p$ )	[bar]	E	0.3	0.4	0.5	0.6

Table 2.16: Design of experiment (L<sub>16</sub> OA) and collected experimental data

Run No.	L <sub>16</sub> OA					Experimental data			
	A	B	C	D	E	<b>Inconel 625</b>			
						MRR [mm <sup>3</sup> /min]	EWR [mm <sup>3</sup> /min]	Roughness average (R <sub>a</sub> ) [μm]	SCD [μm/μm <sup>2</sup> ]
1	1	1	1	1	1	4.7038	0.0441	7.6333	0.0281
2	1	2	2	2	2	2.9739	0.0882	8.2333	0.0157
3	1	3	3	3	3	4.1943	0.1764	9.8667	0.0152
4	1	4	4	4	4	9.0403	0.1764	10.7333	0.0169
5	2	1	2	3	4	2.7725	0.0882	4.8667	0.0180
6	2	2	1	4	3	13.3531	0.1323	8.7000	0.0177
7	2	3	4	1	2	7.6066	0.1764	7.6000	0.0238
8	2	4	3	2	1	17.2512	0.2206	8.9667	0.0148
9	3	1	3	4	2	1.5640	0.0882	6.5333	0.0169
10	3	2	4	3	1	2.3104	0.0441	7.0000	0.0171
11	3	3	1	2	4	16.1493	0.0882	9.4667	0.0158
12	3	4	2	1	3	13.5545	0.1764	10.5000	0.0186
13	4	1	4	2	3	1.3389	0.0441	4.7000	0.0164
14	4	2	3	1	4	2.9028	0.0882	7.6333	0.0216
15	4	3	2	4	1	9.4905	0.1323	9.2000	0.0190
16	4	4	1	3	2	29.3128	0.1323	11.5333	0.0233

Table 2.16 (Continued)

Run No.	L <sub>16</sub> OA					Experimental data			
	A	B	C	D	E	<b>Inconel 718</b>			
						MRR [mm <sup>3</sup> /min]	EWR [mm <sup>3</sup> /min]	Roughness average (R <sub>a</sub> ) [μm]	SCD [μm/μm <sup>2</sup> ]
1	1	1	1	1	1	2.5885	0.0441	6.9000	0.0201
2	1	2	2	2	2	5.9707	0.0882	9.5000	0.0180
3	1	3	3	3	3	3.4432	0.0882	10.0000	0.0151
4	1	4	4	4	4	15.9951	0.1323	10.2667	0.0186
5	2	1	2	3	4	2.1734	0.0441	7.9000	0.0136
6	2	2	1	4	3	6.9109	0.0882	9.7000	0.0137
7	2	3	4	1	2	10.4274	0.0882	6.8667	0.0164
8	2	4	3	2	1	14.7863	0.1323	11.9000	0.0145
9	3	1	3	4	2	1.1844	0.0441	4.9333	0.0193
10	3	2	4	3	1	3.0647	0.0441	6.8333	0.0143
11	3	3	1	2	4	17.4481	0.0882	12.2667	0.0122
12	3	4	2	1	3	20.7204	0.1323	12.3667	0.0145
13	4	1	4	2	3	1.7705	0.0441	6.0000	0.0187
14	4	2	3	1	4	7.1429	0.0882	8.2667	0.0122
15	4	3	2	4	1	15.0305	0.0882	8.9000	0.0199
16	4	4	1	3	2	31.5995	0.1323	12.1000	0.0153

Table 2.16 (Continued)

Run No.	L <sub>16</sub> OA					Experimental data			
	A	B	C	D	E	Inconel 601			
						MRR [mm <sup>3</sup> /min]	EWR [mm <sup>3</sup> /min]	Roughness average (R <sub>a</sub> ) [μm]	SCD [μm/μm <sup>2</sup> ]
1	1	1	1	1	1	7.5709	0.0441	8.1333	0.0211
2	1	2	2	2	2	9.3958	0.0882	10.2333	0.0158
3	1	3	3	3	3	6.8681	0.0882	10.8000	0.0141
4	1	4	4	4	4	9.3835	0.1323	11.6000	0.0167
5	2	1	2	3	4	3.8718	0.0882	8.3000	0.0189
6	2	2	1	4	3	13.6375	0.0882	12.0667	0.0170
7	2	3	4	1	2	6.6461	0.0882	12.2667	0.0193
8	2	4	3	2	1	12.3674	0.1323	10.8667	0.0164
9	3	1	3	4	2	1.8249	0.0441	7.8333	0.0219
10	3	2	4	3	1	2.6880	0.0441	9.3667	0.0182
11	3	3	1	2	4	17.6572	0.0882	12.1667	0.0216
12	3	4	2	1	3	27.6942	0.1323	11.7000	0.0202
13	4	1	4	2	3	2.5524	0.0441	4.9667	0.0209
14	4	2	3	1	4	9.3465	0.0882	6.5333	0.0200
15	4	3	2	4	1	20.8878	0.1323	14.0000	0.0179
16	4	4	1	3	2	36.3132	0.1764	12.4667	0.0179

Table 2.16 (Continued)

Run No.	L <sub>16</sub> OA					Experimental data			
	A	B	C	D	E	Inconel 825			
						MRR [mm <sup>3</sup> /min]	EWR [mm <sup>3</sup> /min]	Roughness average (R <sub>a</sub> ) [μm]	SCD [μm/μm <sup>2</sup> ]
1	1	1	1	1	1	5.8108	0.0882	8.7333	0.0170
2	1	2	2	2	2	5.2826	0.1323	8.5333	0.0257
3	1	3	3	3	3	1.9533	0.1323	10.2333	0.0148
4	1	4	4	4	4	6.7322	0.1764	11.5333	0.0233
5	2	1	2	3	4	1.5233	0.0441	6.0667	0.0190
6	2	2	1	4	3	11.0811	0.1323	8.3333	0.0253
7	2	3	4	1	2	3.4889	0.1323	9.7667	0.0148
8	2	4	3	2	1	5.0860	0.1764	13.2000	0.0187
9	3	1	3	4	2	1.2654	0.0441	6.5333	0.0201
10	3	2	4	3	1	3.1818	0.0882	8.8667	0.0180
11	3	3	1	2	4	21.4005	0.1764	10.6333	0.0242
12	3	4	2	1	3	24.7052	0.2206	10.1333	0.0170
13	4	1	4	2	3	2.2973	0.0882	3.7333	0.0200
14	4	2	3	1	4	5.9582	0.0882	5.5333	0.0191
15	4	3	2	4	1	14.4963	0.1323	9.0000	0.0202
16	4	4	1	3	2	25.9459	0.1764	11.3333	0.0201



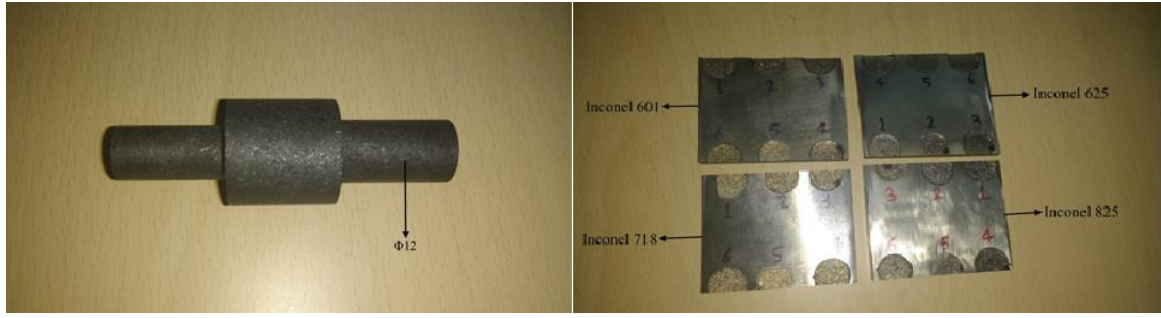


Fig. 2.14: Graphite tool electrode and EDMed Inconel specimens of different grades

The design of experiment has been planned as per 5-factor-4-level  $L_{16}$  orthogonal array (Table 2.16). The array has consisted of sixteen experimental runs in relation to different combination of machining parameters. After proper selection of machining parameters and finalizing the design of experiment, EDM operations have been carried out on different Inconel grades, separately. The machining duration for each experimental run has been kept constant (10 minutes). For each experimental run, machinability of different Inconel grades has been investigated by considering the following machining response features viz. Material Removal Rate (MRR), Electrode Wear Rate (EWR), Roughness average ( $R_a$ ) and Surface Crack Density (SCD). The experimental results have been depicted in Table 2.16. Fig. 2.14 has exhibited the snapshot of machined Inconel specimens of different grades. For computing volumetric material removal rate, the following density values have been used.

Density of Inconel 601 =  $8.11 \text{ g/cm}^3$

Density of Inconel 625 =  $8.44 \text{ g/cm}^3$

Density of Inconel 718 =  $8.19 \text{ g/cm}^3$

Density of Inconel 825 =  $8.14 \text{ g/cm}^3$

For computing electrode wear rate, the density of graphite  $2.267 \text{ g/cm}^3$  has been used.





## **Chapter 3**

# **Analysis on Surface Characteristics of Electro-Discharge Machined Inconel 718**

### **3.1 Coverage**

An experimental investigation has been carried out on electro-discharge machining of Inconel 718 using Copper tool electrode. Based on  $L_{25}$  Orthogonal Array, experiments have been conducted by considering controllable process parameters (viz. gap voltage, peak current, pulse-on time, duty factor and flushing pressure), each varied at five discrete levels, within selected parametric domain. The following responses in relation to surface characteristics of the EDMed Inconel 718 specimen viz. Roughness average ( $R_a$ ), Surface Crack Density (SCD) and White Layer Thickness (WLT) have been investigated. SEM micrographs revealing surface irregularities associated with surface morphology of the EDMed Inconel 718 have been analyzed in detail and correlated with the information obtained through EDS, XRD and micro-hardness tests of the machined surface. Presence of different types of cracks within the EDMed work surface has also been identified. Effects of significant process parameters on surface topography in terms of roughness average, surface crack density, white layer thickness etc. have been graphically presented. Finally, Utility theory in conjugation with Taguchi's optimization philosophy has been attempted to select the most favorable process environment (parameters setting) to satisfy optimal  $R_a$ , SCD and WLT; thereby, ensuring high product quality along with its specified functional requirements in appropriate application domain.

### **3.2 Scope of the Work**

Owing to the widespread application of Inconel 718 especially over automotive, aerospace and defense industries; machining and machinability aspects of this super alloy

has become an important research agenda today. However, machining of Inconel 718 appear to be a challenge since several difficulties are likely to arise due to their high strength, high temperature resistance, work-hardening tendency, affinity to form built-up-edge etc.. These restrict sound processing of Inconel 718 through conventional machining operations. On the contrary, non-conventional machining processes like EDM, ECM, wire-EDM routes etc. have been recommended by part researchers to improve machining performance on Inconel 718 and consequently to achieve satisfactory product quality up to the desired extent. In this context, an attempt has been made to investigate different aspects of electro-discharge machining of Inconel 718 using Cu tool electrode.

EDM process is controlled by several input parameters: gap voltage, peak discharge current, pulse-on duration, pulse-off duration, duty factor, flushing pressure etc. Peak current can be defined as the maximum value of discharge current intensity applied between tool electrode and the workpiece to be machined by EDM. As described by (Jabbaripour et al., 2012), pulse-on time is the period in which the current is allowed to flow per cycle. Open Circuit Voltage (OCV) is the potential difference between tool and workpiece before pulse generation. The duty factor is the ratio of pulse-on time relative to the total cycle time. The flushing pressure is the pressure at which flushing is done by forcing the dielectric fluid through the inter electrode gap so that debris can be transported easily away from the machining zone. Otherwise, EDM debris (or chip) tends to be re-machined again and again, obstructing the machining process to progress effectively. Literature depicts that EDM input parameters interact in a complex manner; thereby, affecting process performance characteristics (for example, material removal rate, tool wear ratio, roughness average, surface crack density, white layer thickness etc.). Critical analysis is indeed required to control EDM response features before the part component is subjected to service. In this context, in-depth understanding on formation of surface cracks as well as white layer is highly essential to suppress the occurrence of those and to minimize detrimental effects imposed by them.

Crack formation in EDMed component is incurred due to presence of induced thermal stress and tensile stress within the machined surface. As explained by (Guu and Hou; 2007), thermal stress is evolved due to drastic heating and subsequent cooling of the machined zone and the consequence of uneven temperature distribution. Tensile residual stress within the specimen is generated because dielectric is incapable of washing out the debris completely from the machined zone. (Yan et al., 2005; 2007; Ekmekci et al., 2006; Ekmekci, 2007) explained that due to the ingress of carbon particles either from electrode

or from pyrolysis of dielectric fluid (hydrocarbon), the molten material contracts to a greater extent as compared to the unaffected parent part during the cooling process; and, when the stress in the surface rises above the material's ultimate tensile strength, cracks are formed.

During EDM operations, existence of white layer (also called recast layer) is highly undesirable, but its formation is inevitable. Hence, as pointed out by (Yildiz et al., 2015), the mechanism behind white layer formation needs to be clearly understood and its thickness should be accurately determined to efficiently perform post-treatment operations for removing the white layer resulted by the EDM process.

At the end of each discharge, depending on the Plasma Flushing Efficiency (PFE) (i.e. the ability of plasma channel in removing molten material from the molten material crater), collapsing of plasma channel causes violent suction and severe bulk boiling of some molten material and removal of them from the molten crater. The material remained in the crater re-solidifies, which is called the 'white layer' or 'recast layer'. An annealed Heat Affected Zone (HAZ) lay directly below the recast layer. The micro-cracks created in the white layer can penetrate into the HAZ. Additionally, this layer appears softer than the underlying base material. This annealed zone is prematurely weak; and cause fracture that can lead to minor malfunctioning of the part and finally catastrophic failure.

The melting and re-solidification of the material causes formation of White Layer (WL) onto the top of the machined surface. (Rao et al., 2014) described that the formation of WL and HAZ adversely affect surface integrity (which is characterized by high surface roughness i.e.  $R_a$  value), development of residual stress, altered composition of the work surface, reduced corrosion resistance etc. Therefore, formation of while layer and HAZ needs to be controlled.

It is understood that different response features during EDM correspond to conflicting requirements in the sense that high MRR is strongly appreciated; whereas, attention must be paid to ensure minimal tool wear, low roughness average, reduced surface crack density as well as tiny white layer. Proper control of process input parameters may achieve satisfactory machining yield. Hence, it is necessary to understand the effect of process variables on various response measures of EDM process. In literature, emphasis has been made to investigate effects of electrical parameters (mainly discharge current, pulse duration and duty factor) on various performance measures (Ramakrishnan and Karunamoorthy, 2008; Newton et al., 2009; Kumar et al., 2011; Rajesha et al., 2012; Lin et al., 2013; Ay et al., 2013; Dhanabalan et al., 2014; Prihandana et al., 2014; Li et al.,

2015; Aggarwal et al., 2015); limited attempt has been made to examine the effect of flushing pressure on aforementioned responses in the context of EDM on Inconel 718. Apart from this, literature is sparse in correlating machining responses like  $R_a$ , SCD and WLT with micro-hardness and residual stress resulted with EDMed workpiece along with its change in chemical composition and metallurgical aspects like phases present, grain orientation etc. The present study has been aimed to examine these aspects through experimentation and subsequent data analysis.

An unique attempt has also been made to optimize different performance measures in relation to surface topography of the EDMed Inconel 718 specimen viz.  $R_a$ , SCD and WLT simultaneously; thus, to determine the most favorable process environment (parameters setting). Utility-based Taguchi approach has been attempted in this part of work.

### 3.3 Results and Discussion

#### 3.3.1 Analysis of SEM Micrographs: Results of EDS, XRD and Micro-Hardness Tests

As compared to the unaffected parent material (Fig. 3.1), the EDMed work surface of Inconel 718 observed under SEM has revealed existence of various surface irregularities which have consisted of several defects including overlapping craters, globules of debris (spherical deposition), pockmarks or chimneys (Fig. 3.2a-3.2b).

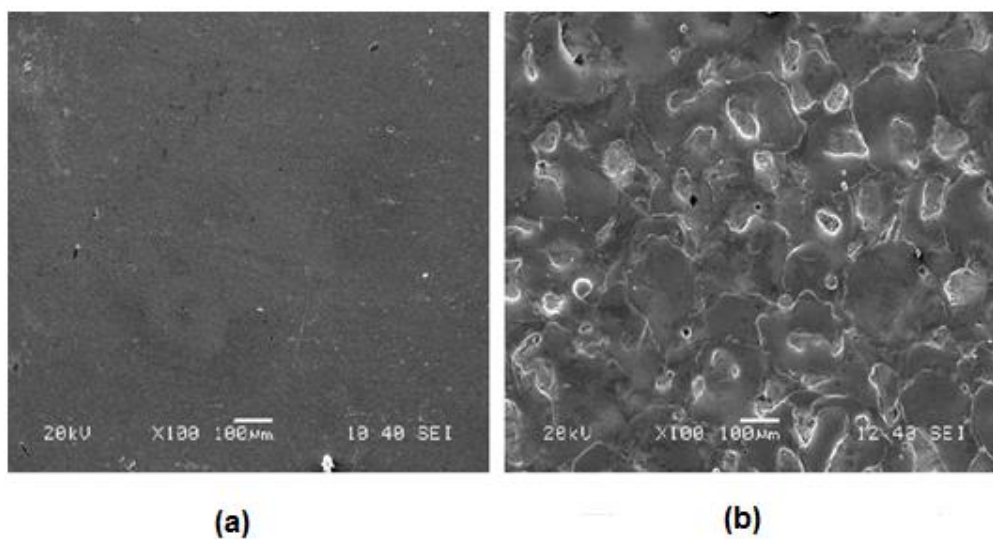


**Fig. 3.1:** SEM micrographs of Inconel 718 work surfaces: (a) ‘as received’, and (b) EDMed at parameters setting: [ $V_g=50V$ ,  $I_p=3A$ ,  $T_{on}=100\mu s$ ,  $\tau=65\%$ ,  $F_p=0.2bar$ ] i.e. Run No. 01

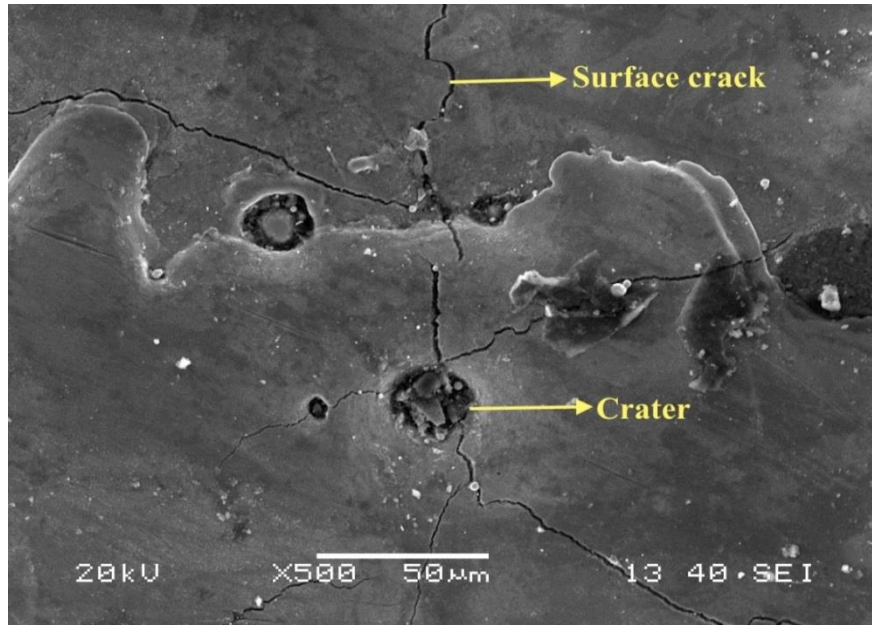


Fig. 3.2(a): Morphology of the EDMed Inconel 718 work surface obtained at parametric setting [ $V_g=50V$ ;  $I_p=9A$ ;  $T_{on}=400\mu s$ ;  $\tau=80\%$ ;  $F_p=0.5bar$ ]

Another prominent feature found on the machined surface has been the existence of micro-cracks in abundance (Fig. 3.2a-3.2b). The spherical shape of globules of debris has been resulted from the effect of surface tension. Pockmarks have been generated on the surface due to gas bubbles expelled from the molten material during solidification. The micro-cracks have been found due to the consequence of thermal stresses developed.

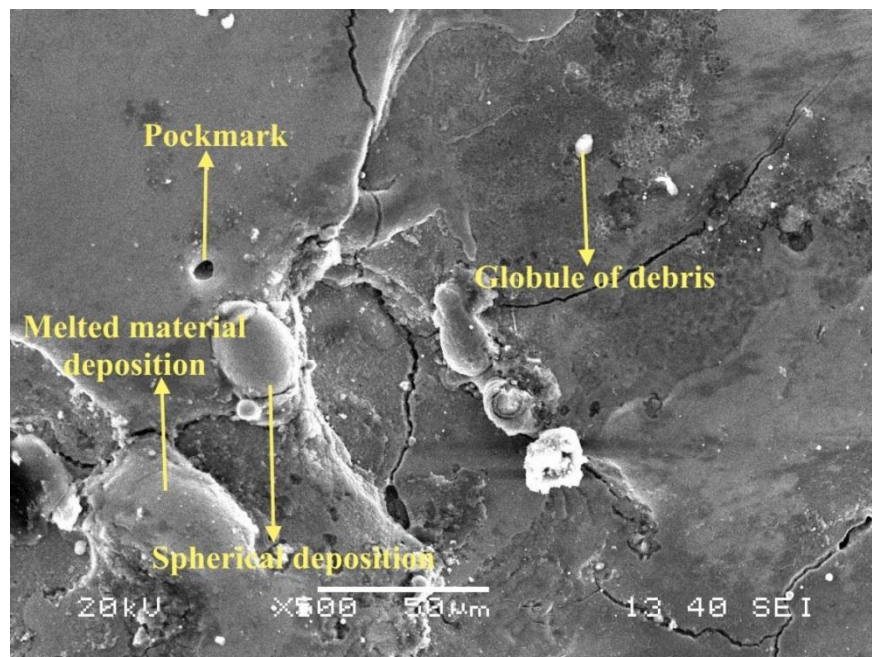


Fig. 3.2(b): Morphology of the EDMed Inconel 718 work surface obtained at parametric setting [ $V_g=80V$ ;  $I_p=11A$ ;  $T_{on}=300\mu s$ ;  $\tau=65\%$ ;  $F_p=0.5bar$ ]



Typically the transverse-cut section of the EDMed workpiece exhibits several distinct layers (refer to Fig. 3.3). On the top surface, formation of white layer is responsible for altering metallurgical structure of the workpiece.

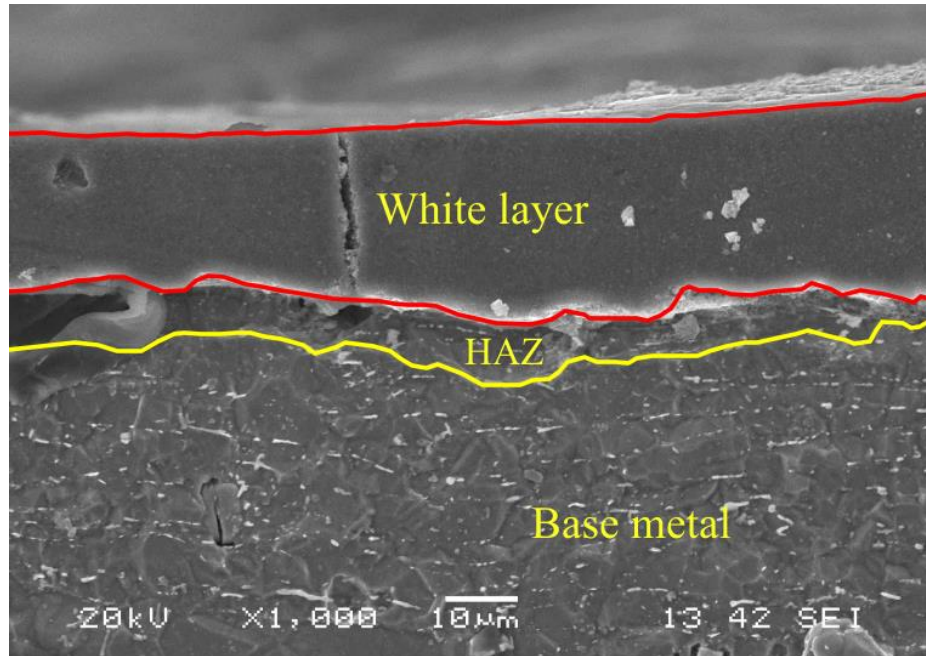


Fig. 3.3: SEM micrograph revealing existence of white layer and HAZ as observed in EDMed Inconel 718 at [ $V_g=70V$ ;  $I_p=5A$ ;  $T_{on}=400\mu s$ ;  $\tau=65\%$ ;  $F_p=0.4bar$ ] (Run No. 12)

According to (Tsai et al., 2003), it is quite hard and non-etchable. Next to white layer, heat-affected zone (or annealed layer) appears. This layer is heated during operation but not melted. This layer experiences high temperature rise to cause a quenching effect. It is also referred to as the ‘rehardened layer’. Newton et al. (2009) explained that the HAZ contains an altered microstructure, tensile stresses, micro-cracks, impurities, and other undesirable features which can lead to premature part failure whilst subjected to service.

Ekmekci (2009) reported that cracks developed on the EDMed work piece have three distinctive characteristics. The first type of micro-cracks, called surface cracks, appear in the white layer which initiates at its surface and tends to propagate perpendicularly down toward the interference zone, separating the HAZ and the white layer, and usually terminates at this interference. The second type of micro-cracks, denoted as penetrating cracks, penetrates the entire white layer thickness with a tendency to emerge into the parent material. The third type of micro-cracks can be identified to be present usually around globular or irregular-shaped attachments on crater rims. Such cracks correspond to negligible depth of penetration and are randomly distributed over the EDMed surface.

However, in the present work, analysis of SEM micrographs of the EDMed specimens could retrieve only two crack types (first and third type) distinctly (Fig. 3.4a-3.4b).

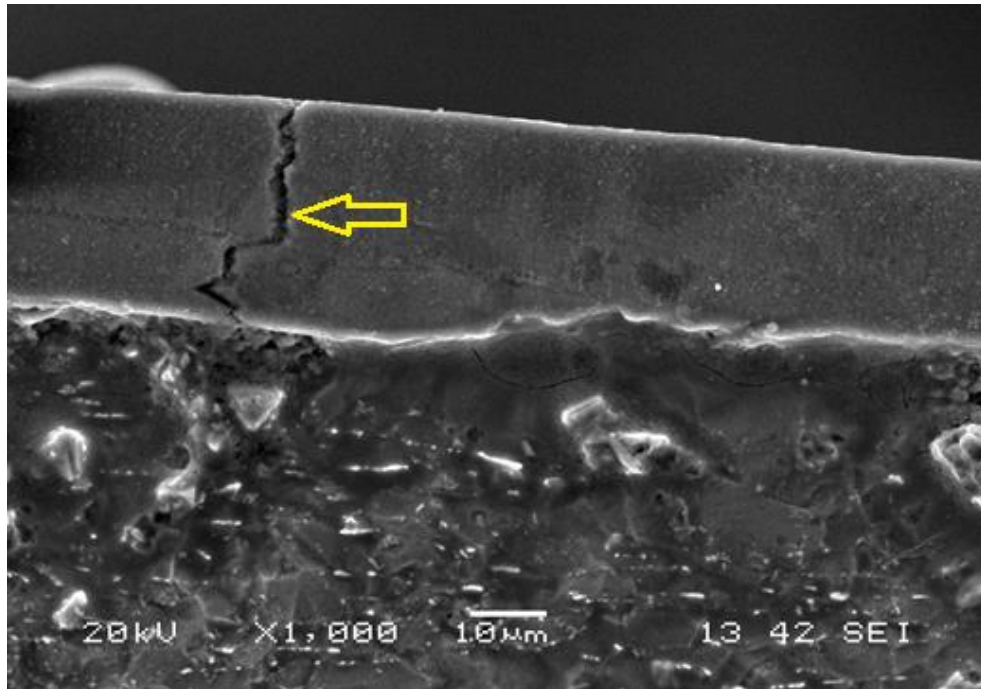


Fig. 3.4(a): Existence of crack (Type 1) as observed in EDMed Inconel 718 specimen obtained at parametric setting [ $V_g=70V$ ;  $I_p=7A$ ;  $T_{on}=500\mu s$ ;  $\tau=70\%$ ;  $F_p=0.5bar$ ] (Run No. 13)

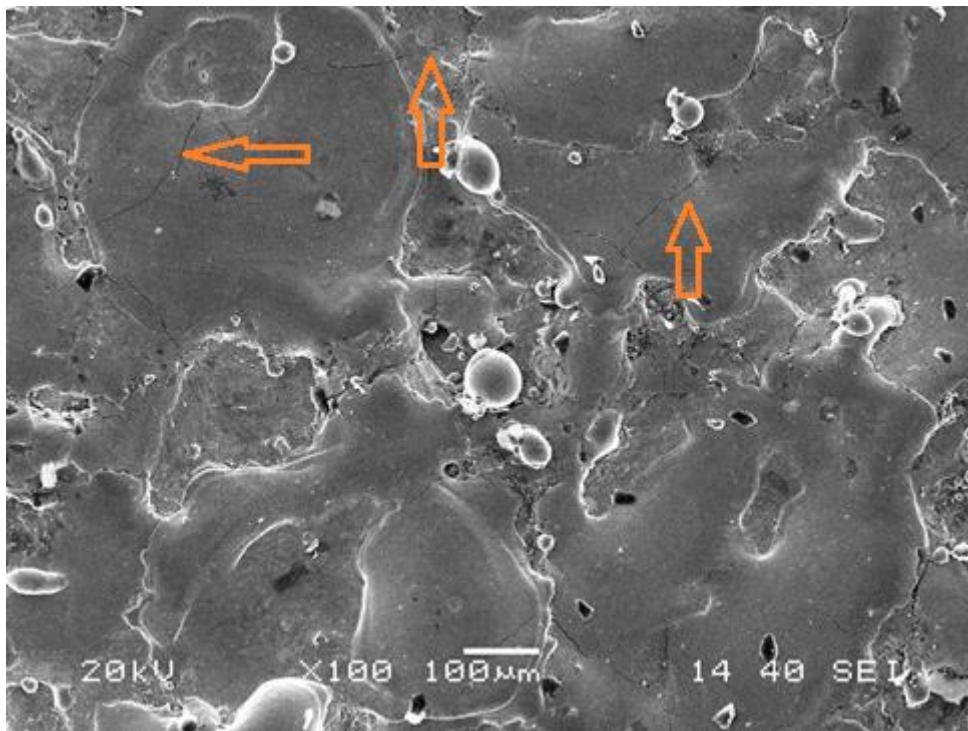


Fig. 3.4(b): Existence of crack (Type 3) as observed on EDMed Inconel 718 work surface obtained at parametric setting [ $V_g=80V$ ;  $I_p=11A$ ;  $T_{on}=300\mu s$ ;  $\tau=65\%$ ;  $F_p=0.5bar$ ] (Run No. 20)



This can be attributed by the fact that the parametric settings employed herein might not be enough to reveal development of cracks of second type. Since surface cracking is the combined effect of induced residual stress along with thermal stress developed during EDM operations; evolution of such stresses and their magnitude highly depends on the process environment (parameters setting) employed. The process parameters influence the machining performance to a varied degree (levels of significance are different); therefore, variation of parametric settings incur surface cracking with varied intensity.

According to (Opitz, 1960), white layer is generally heavily alloyed with the pyrolysis products from the cracked dielectric fluid as well as tool electrode and thus possesses high hardness values; however distribution of micro-hardness seems non-uniform with respect to EDM parameters settings. This has also been reflected by the EDS analysis of EDMed Inconel 718 specimen with respect to ‘as received’ parent material.

By comparing (Fig. 3.5b-3.5c) with respect to (Fig. 3.5a), it has been observed that Carbon content of Inconel 718 has been increased during EDM operation. It has been noted that wt% of C in Inconel 718 has been substantially increased from 0.049 wt% (for ‘as received’ Inconel 718) to 22.19wt% (for the EDMed specimen prepared at Run No. 1); and, 16.28wt% (for the EDMed specimen prepared at Run No 25). This has resulted higher micro-hardness values of the EDMed Inconel 718 work surfaces as compared to the base material. The micro-hardness values (measured approximately at the mid-depth of white layer) for the EDMed Inconel 718 samples have been obtained for all experimental runs and depicted in Table 2.5 of Chapter 2. It has been observed that it has varied from 352.600 HV<sub>0.05</sub> to 518.067 HV<sub>0.05</sub> for the EDMed specimens prepared under different parameters settings; whereas, micro-hardness of ‘as received’ Inconel 718 has corresponded to a lower hardness value i.e. 269.400 HV<sub>0.05</sub>. Increased micro-hardness of the machined surface (as compared to base material) has been resulted due to Carbon enrichment through dielectric cracking.

Literature by (Tönshoff and Brinksmeier, 1980) ascertains that investigation on micro-hardness of the EDMed surface is necessary for identifying yield strength changes, structure alterations, work hardening or softening of surface layers, etc. Crookall and Khor (1975) also reported that the hardness of white layer appeared to be substantially higher than for the parent material. Guu and Hou (2007) observed non-uniform distribution of micro-hardness in the EDMed part caused by the non-uniformity of micro-structure and chemical compositions in the machined regions. Ekmekci et al. (2005) experimentally found that the hardness values remain more or less constant within the

white layer. Remarkable decrement in micro-hardness may be observed within HAZ with a tendency to settle down to the unaffected parent material hardness.

Another important aspect of EDM process is the evolution of residual stress within the machined part. Since it plays an important role towards evaluating fatigue life of any machined component. (Ogata and Mukoyama, 1991; Kruth and Bleys, 2000) reported that the EDMed surface exhibits large in-plane tensile residual stresses. Existing literature by (Rebelo et al., 1998) depicts that as energy per spark increases, the depth of the peak tensile residual stress also increases. This may be due to the fact that presence of micro-cracks relieves the tensile stress on the surface. The evolution of residual stress can also be explained due to thermal gradients during cooling of the white layer. As white layer resolidifies and its temperature drops down to that of the bulk workpiece (unaffected parent material), its contraction is opposed by the bulk workpiece. Ekmekci et al. (2005) experimentally found that the residual stress generally increases from the bulk material to a maximum extent and then tends to decrease again near to the surface. This decrease can be logically correlated with occurrences of surface cracks since residual stress exceeds the fracture strength of the material.

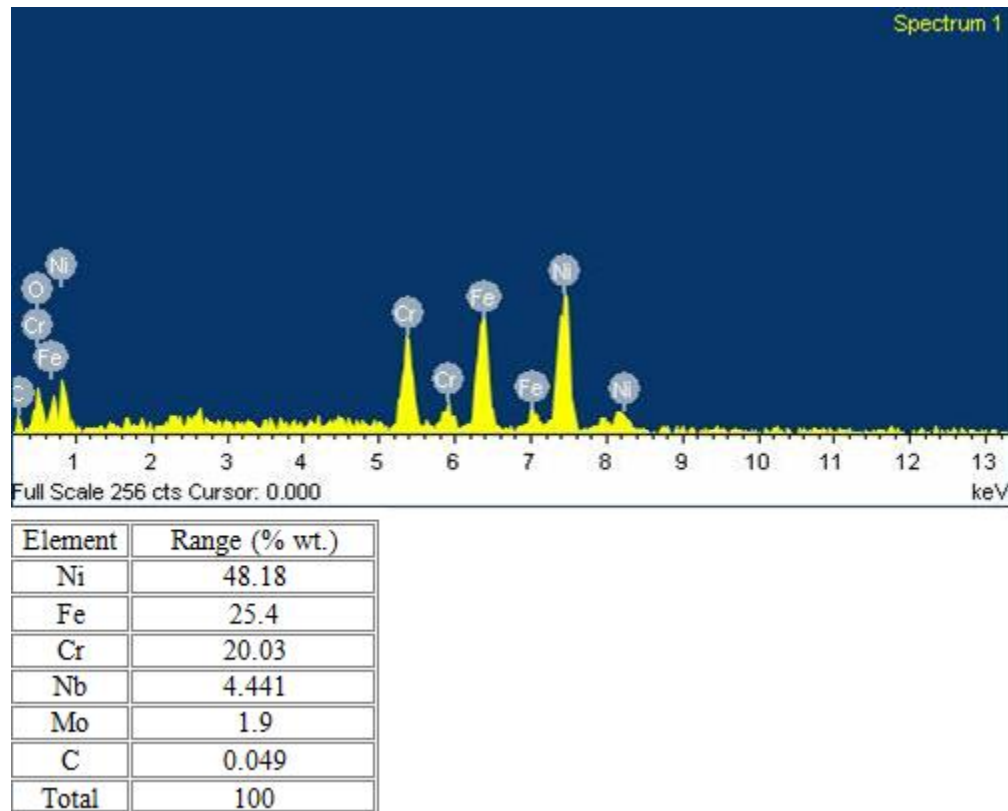


Fig. 3.5(a): Chemical composition of 'as received' Inconel 718 as retrieved from EDS analysis

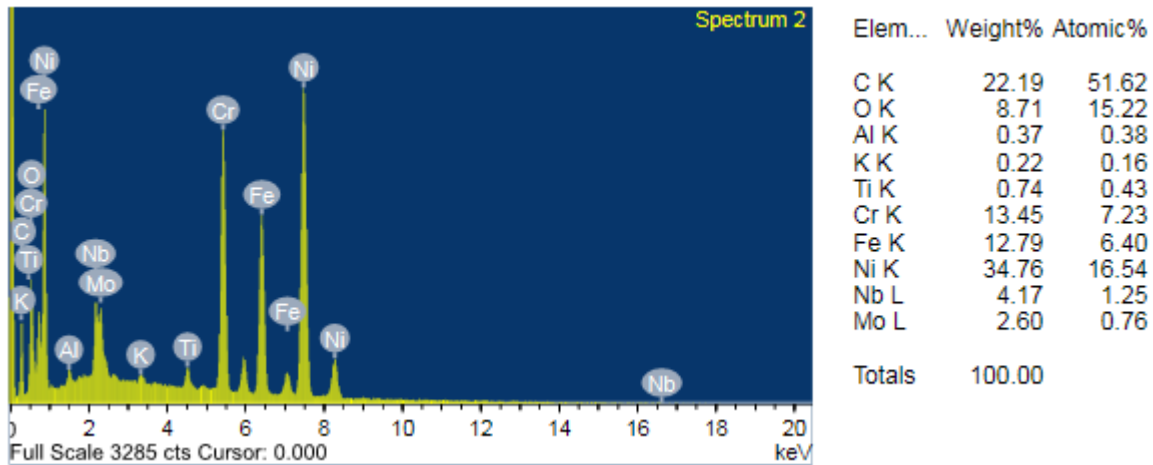


Fig. 3.5(b): Chemical composition of the EDMed Inconel 718 work surface as retrieved from EDS analysis obtained at parameters setting  $[V_g=50V; I_p=3A; T_{on}=100\mu s; \tau=65\%; F_p=0.2bar]$  (Run No. 1)

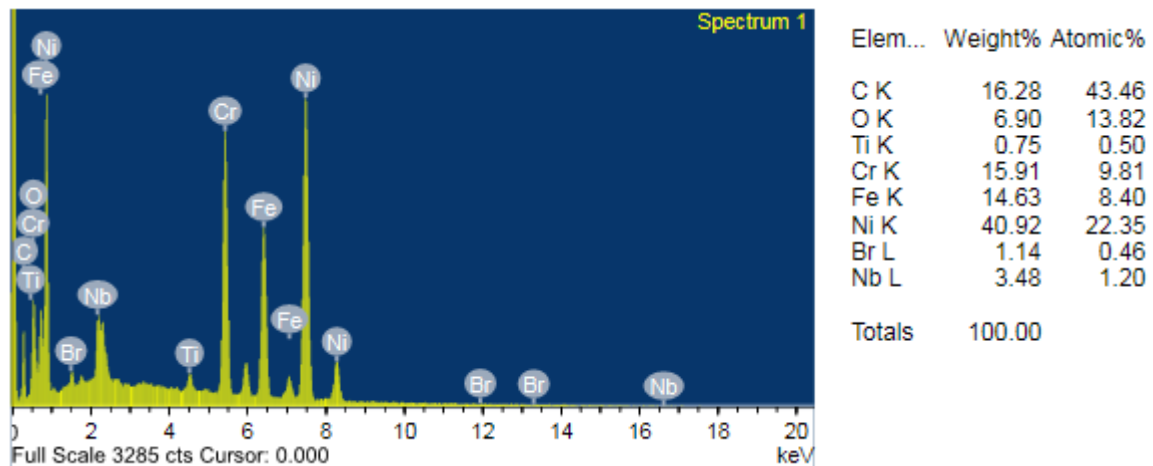


Fig. 3.5(c): Chemical composition of the EDMed Inconel 718 work surface as retrieved from EDS analysis obtained at parameters setting  $[V_g=90V; I_p=11A; T_{on}=400\mu s; \tau=75\%; F_p=0.3bar]$  (Run No. 25)

In the present work, XRD analysis has revealed induced residual stress of tensile in nature, for the EDMed Inconel 718 specimen (obtained at Run No.1), which has corresponded to a value  $1.7123 \pm 0.268$  GPa. This has been found substantially higher as compared to the residual stress within ‘as received’ Inconel 718 i.e.  $-(0.4384 \pm 0.127)$  GPa (compressive stress, in the present case).

Tönshoff and Brinksmeier (1980) described that residual stress generated during EDM process is primarily due to non-homogeneity of heat flow and metallurgical transformations or due to localized inhomogeneous plastic deformation. Moreover, static and dynamic strength, stress corrosion resistance, chemical resistance, and magnetic

properties etc. of the EDMed component are influenced by the presence of residual stress. According to (Guu and Hocheng, 2001) high value of pulse current results more frequent cracking of the dielectric, thereby, causing more melt expulsions and larger tensile residual stresses. These problems in an amplified manner incur poor surface finish and serious surface damage.

XRD analysis for ‘as received’ and EDMed work surface of Inconel 718 has been shown in Fig. 3.6. XRD has been performed to determine whether any metallurgical change has taken place (such as phase transformation or any modification in grain size along with orientation) on the machined work surface of Inconel 718 affected by the EDM operation. Crystal structure and phase change phenomenon can be understood by examining the position of the peaks; whereas, crystallite size can be determined through FWHM (full width half maxima). XRD analysis has revealed Face Centered Cubic (FCC) crystal structure of ‘as received’ Inconel 718 which is basically Ni-based solid solution having PDF index name: Chromium Cobalt Molybdenum Nickel (Ni-Cr-Co-Mo) [Reference Code: 35-1489].

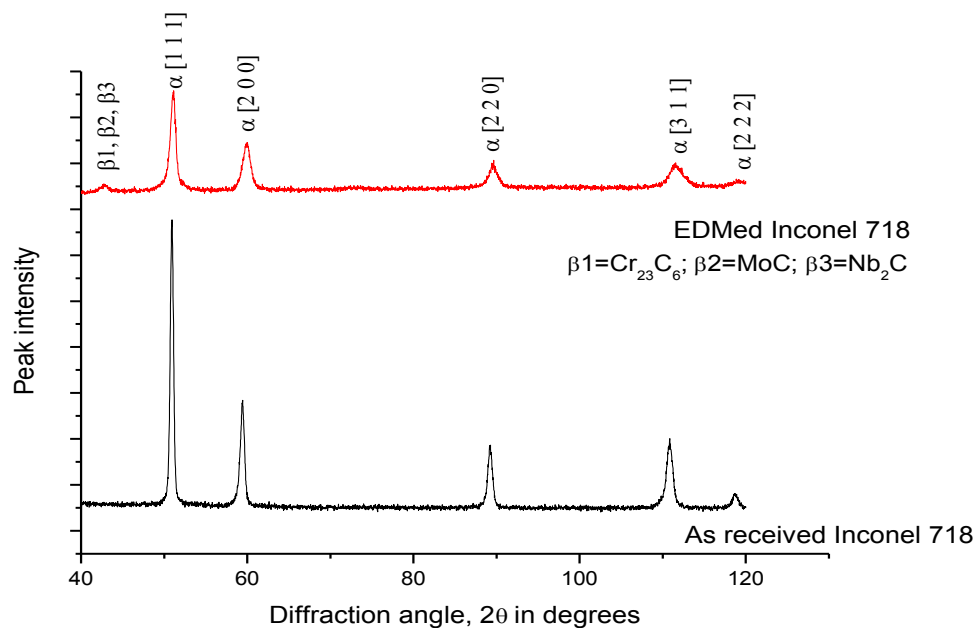


**Fig. 3.6:** XRD spectra of ‘as received’ Inconel 718, and EDMed work surface of Inconel 718 obtained at Run No. 1 i.e. at parameters setting: [ $V_g=50\text{V}$ ;  $I_p=3\text{A}$ ;  $T_{on}=100\mu\text{s}$ ;  $\tau=65\%$ ;  $F_p=0.2\text{bar}$ ]

The XRD patterns of the test sample EDMed at Run No.1 [ $V_g=50\text{V}$ ;  $I_p=3\text{A}$ ;  $T_{on}=100\mu\text{s}$ ;  $\tau=65\%$ ;  $F_p=0.2\text{bar}$ ] has shown almost similar sequence of peaks. Therefore, it can be concluded that no phase change has incurred during the EDM operation utilizing parameters setting of Run No. 1. Broadening (FWHM) of peaks on the XRD spectra

divulges the variation of the crystallite size. Comparing the XRD spectra of ‘as received’ Inconel 718 to that of the EDMed surface obtained at Run No. 1; clear difference in terms of the intensity and the width of the peaks has been retrieved. Therefore, it can be concluded that EDM process has induced grain refinement of the machined surface. The grain refinement is mainly due to the thermo-mechanical effect which in turn causes metallurgical alteration of the work surface.

XRD pattern of EDMed specimen has revealed existence of an extra peak which may be due to the precipitation of  $\text{Cr}_{23}\text{C}_6$  (Chromium Carbide), MoC (Molybdenum Carbide) and  $\text{Nb}_2\text{C}$  (Niobium Carbide) on the main matrix. This is because, EDM process results Carbon enrichment onto the machined zone during pyrolysis of dielectrics. Carbides are thus formed and precipitates on the work surface.

### 3.3.2 Study of Parametric Influence

Literature is rich in establishing and explaining relationships amongst various process parameters with respect to different EDM responses. Most of the earlier studies concentrated on understanding the influence of electrical parameters (viz. spark gap voltage, gap voltage, discharge current, pulse-on time, pulse-off time, duty factor) on different machining responses. Rare attempt has been made to reveal the effect of flushing rate on EDM performances on Inconel 718. Flushing plays an important role during EDM operations and the rate at which it takes place should be properly adjusted so as to improve overall machining yield.

[Wong et al. \(1995\)](#) stated that the dielectric fluid applied for EDM should possess high dielectric strength and ability to quick recovery after breakdown, effective quenching and flushing capability. During EDM flushing, the dielectric fluid is distributed through the spark gap in order to remove debris (eroded particles) generated during EDM and to maintain dielectric temperature well below its flash point. Hence, it seems necessary to study the effect of flushing rate on different features of machining performance during EDM of Inconel 718. Improper flushing may result in uneven tool wear, affecting machining accuracy and poor surface finish; it can also reduce material removal rate due to unstable machining environments and arcing around regions with high concentration of debris. In this part of work, research has been extended to identify effects of various electrical parameters (especially  $I_p$ ,  $T_{on}$  and  $\tau$ ) along with dielectric flushing circulation

pressure on surface roughness, surface crack density and white layer thickness of the EDMed end product.

Experimental data corresponding to  $L_{25}$  OA design have been found insufficient to reflect accurate trend of variation of output response(s) with respect to process inputs; Taguchi method has been explored to generate required number of response data with respect to all possible parametric combinations as per full factorial experimental design. Taguchi predicted response data have been plotted to exhibit the direct effect of process parameters on  $R_a$ , SCD, and WLT for the EDMed Inconel 718 specimen; trends of variations thus observed have been compared to that of reported in literature for other materials within specific domains of experiments. However, these trends shown herein have been made to somewhat approximated; because, Taguchi method assumes linear relationship of the output(s) with respect to the inputs; however, in practice, this may not be so. Hence, two successive points on the direct effect plots have been joined by means of a straight line rather than a smooth curve.

### **3.3.2.1 Parametric Influence on Surface Roughness**

According to (Lee and Yur, 2000), it is understood that the performance and service life of the EDMed end product is greatly influenced by the surface characteristics developed during surface erosion. Proper tuning of controllable process parameters may yield satisfactory machining performance in terms of surface finish. Hence, adequate knowledge about the influence of process parameters on surface roughness is of utmost important.

The effect of peak current (B) on surface roughness ( $R_a$ ) has been presented graphically in Fig. 3.7. It has been observed that surface roughness tends to increase as peak current increases, while keeping other parameters fixed at constant levels. This can be explained by the fact that as peak current increases; discharges strike the specimen surface more intensely, which in turn results enormous erosion effect; thereby, causing deterioration of the surface morphology to a remarkable extent. Rajesha et al., (2010) explained that the higher input power associated with increased pulse current causes huge distortion on the EDMed surface due to more frequent molten material expulsion. This leads to an increase in  $R_a$  value.

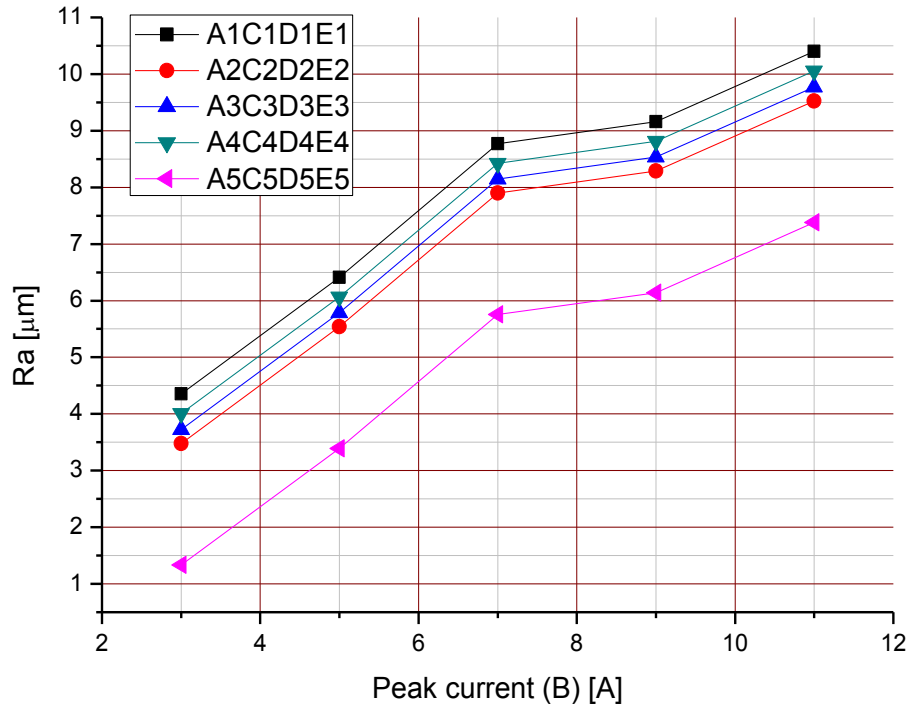


Fig. 3.7: Effect of peak current (B) on  $R_a$

(Guu et al., 2005; Ramasawmy et al., 2005; Keskin et al., 2006) found that that superior surface finish can be achieved by adjusting process control parameters at a low pulse current and a small pulse-on time. According to (Simao et al., 2003), low values of  $R_a$  can only be obtained with low levels of discharge energy. Hewidy et al. (2005) and Williams and Rajurkar (1991) reported that surface roughness increases with increased peak discharge current. Huang et al. (1999) and Haşçalýk and Çaydaş (2004) also claimed that surface roughness increases with increase in energy per spark during EDM operations.

The effect of pulse-on time (C) on  $R_a$  has been plotted in Fig. 3.8. It has been observed that while keeping other parameters fixed at constant level values; an increase in  $T_{on}$  (up to 400μs) results increase in  $R_a$ . Increase in  $T_{on}$  produces adverse effect on the workpiece by increasing surface roughness. Similar trend has also been observed by (Lee and Tai, 2003).

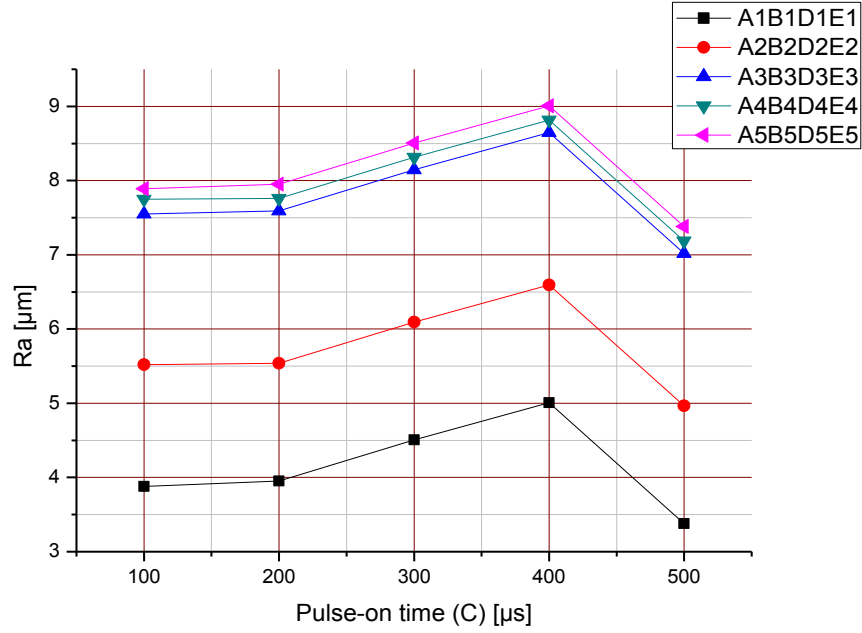


Fig. 3.8: Effect of pulse-on time (C) on  $R_a$

It may be due to the fact that for  $T_{on}$  (in between 100-400 $\mu$ s), deeper discharge craters are expected to be formed and more material is eroded per spark since spark energy is directly proportional to  $T_{on}$ . This leads to increase in  $R_a$  value. For the values of  $T_{on}$  (beyond 400 $\mu$ s) the drop in  $R_a$  can be understood by high values of pulse-off time. Since duty factor has been kept fixed at contest level, a higher  $T_{off}$  value has been allowed corresponding to a higher  $T_{on}$  value. However, no material removal is incurred during  $T_{off}$ . The  $T_{off}$  being sufficiently large the total machining time increases, which in turn decreases MRR as well as  $R_a$ . However, (Saha and Choudhury, 2009) reported that this non-cutting time does not have a significant effect on the  $R_a$  value. Huang et al. (1999) and Ramakrishnan and Karunamoorthy (2008) also experimentally examined that surface roughness increases with increased pulse duration.

Fig. 3.9 represents the effect of flushing pressure on  $R_a$ , while other electrical parameters (viz. gap voltage, peak current, pulse-on time and duty factor) have been kept constant. An approximate curve can be drawn by considering the plotted points to retrieve a trend for physically interpreting the relationship between  $R_a$  and flushing pressure. It has been inferred that with increase in flushing pressure,  $R_a$  tends to decrease.



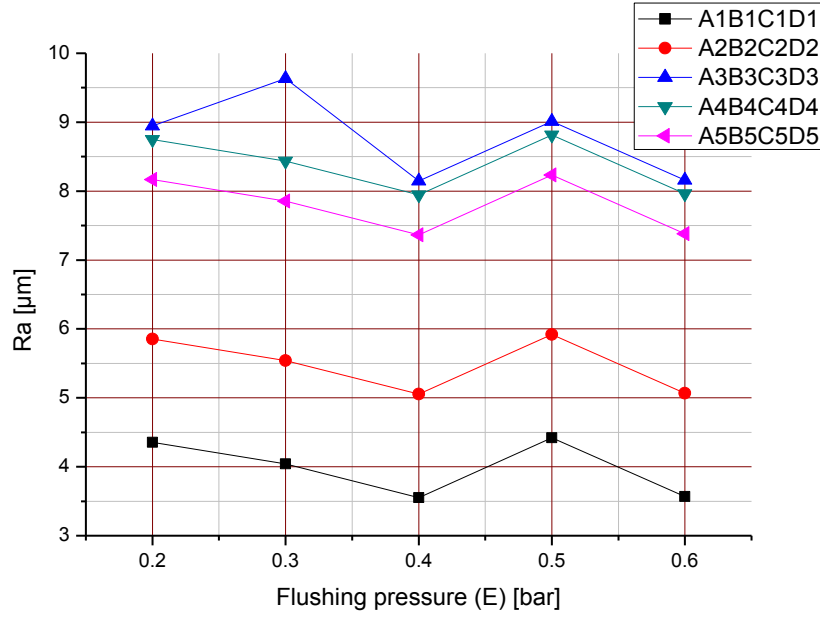


Fig. 3.9: Effect of flushing pressure (E) on  $R_a$

Flushing pressure helps to drain out gaseous and solid debris generated during EDM operation in the spark gap between workpiece and the tool electrode. As a result, increase in flushing pressure ensures efficient removal of debris by the dielectric medium, thereby, improving surface finish ( $R_a$  value decreases). Makenzi and Ikua (2008) reported that when the flushing pressure is too low, the flushing appears ineffective to wash out gaseous as well as eroded particles (or debris) completely after each discharge. However, if the pressure is excessively high, proper machining cannot be performed as the ionized plasma channel is continuously swept away. Excessive flushing pressure can also accelerate electrode wear and create turbulence in the cavity.

### 3.3.2.2 Parametric Influence on Surface Crack Density

EDMed end products, such as tools and dies, are often subjected to severe cyclic pressure and temperature loadings for specific applications. Hence, (Thomson, 1989; Zeid, 1997; Tai and Lu, 2009) reported that the surface irregularities, particularly cracks, may lead to shortened service life due to reduction in material resistance to fatigue and corrosion, especially under tensile loading conditions. Therefore, surface cracks appear a fundamental consideration whilst assessing machining yield during EDM. Hence, it is indeed a necessity to understand proper controlling of process parameters to suppress

their formation. The formation of surface cracks are rendered due to the differentials of high contraction stresses exceeding work material's ultimate tensile strength within the white layer. Hence, it is required to understand the effect of EDM parameters on different measures of surface crack.

The variation of SCD with respect to change in peak current (B) has been furnished in Fig. 3.10. For Inconel 718, trend has been observed in the manner that with increase in peak current, SCD decreases. With increase in peak current, the thickness and hence the area of white layer tends to increase, resulting decrement in SCD since the length of the cracks produced does not increase in a similar rate. Lower value of SCD can also be explained due to simultaneous release of unstable energy with increase in peak current till a critical point is accomplished.

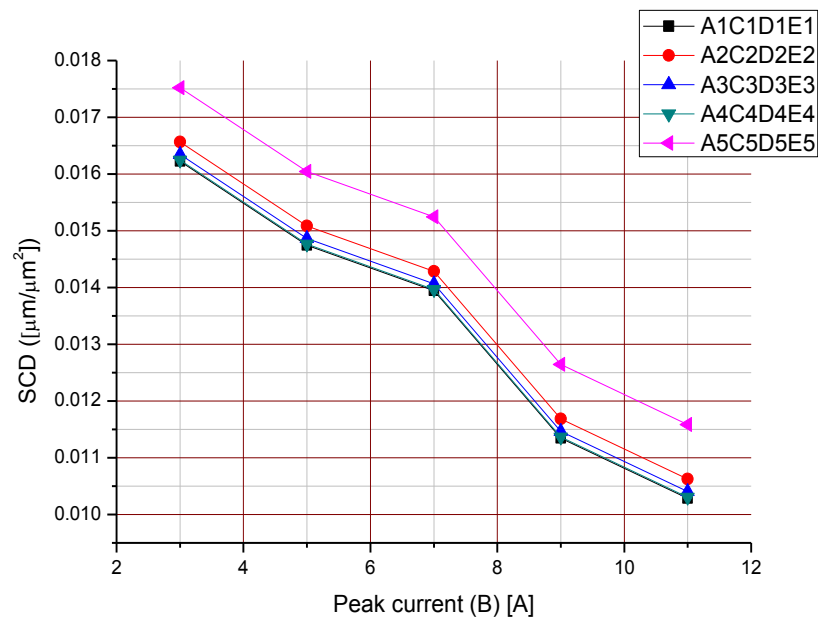


Fig. 3.10: Effect of peak current (B) on SCD

However, (Bhattacharya et al., 2007) worked on EDM of M2 Die Steel and showed that with increase in peak current, SCD decreases to some extent; assumes gradual increment afterwards. However, within present parametric domain experimental data could retrieve only the trend of decrement of SCD with respect to increase in peak current.

The effect of pulse-on time (C) on SCD has been demonstrated in Fig. 3.11. With increase in pulse-on time SCD increases while other parameters kept at constant level values. Similar trend has been observed in the work by (Lee and Tai, 2003; Guu and Hou, 2007; Kahng and Rajukar, 1977). Literature depicts that for a constant pulse current,

surface crack density assumes an increasing trend as pulse-on time increases. (Mamalis et al., 1987; Lee et al., 1988; Lee et al., 1990; Lee et al., 1992) also reported that cracking increases as pulse energy increases. The crater size increases with increase in pulse energy; similar effect is attributed for surface crack density. Furthermore, the cracks penetrate into the white layer and tend to propagate to depths that depend on the pulse energy.

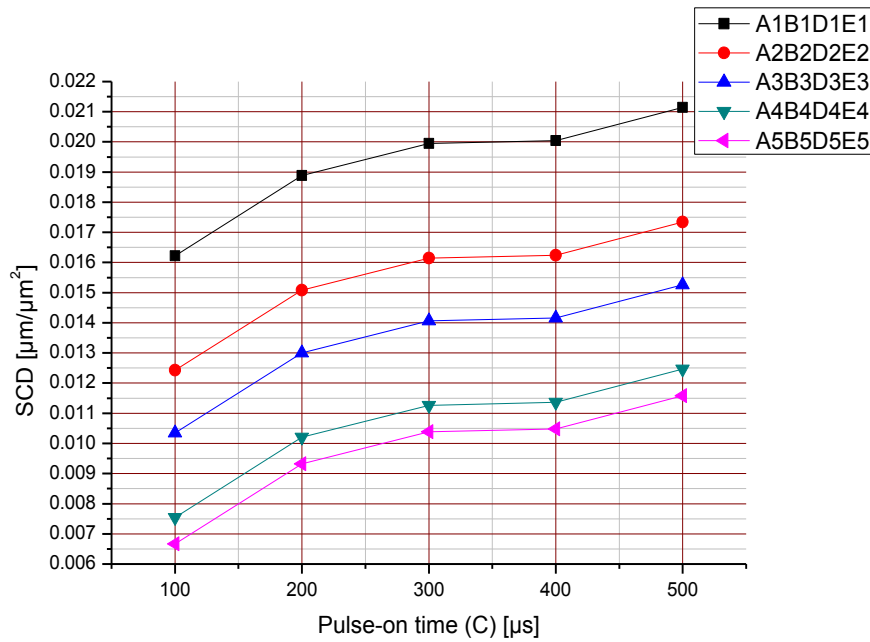


Fig. 3.11: Effect of pulse-on time (C) on SCD

Development of surface crack is strongly related to the EDM process parameters. Increased pulse-on duration amplify both average white layer thickness and induced stress. As stated by (Lee and Tai, 2003; Rajesha et al., 2010), these two conditions stimulate crack formation. Ekmekci et al. (2005) and Mamalis (1987) reported that crack density is inversely proportional to the thermal conductivity of the work material; as Carbon content within the white layer increases, surface crack intensity increases very rapidly. Jabbaripour et al. (2012) also reported that with increase in pulse-on time, density of micro-holes and pits, surface cracks and irregularities etc. increase; surface cracks in longer pulse-on time appear wider.

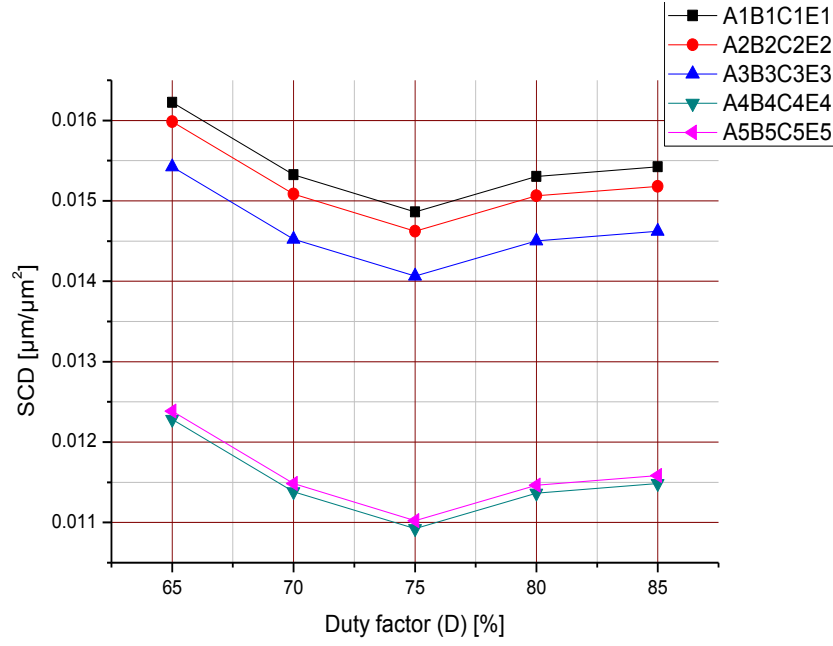


Fig. 3.12: Effect of duty factor (D) on SCD

The effect of duty factor (D) on surface crack density could be well understood from Fig. 3.12, while other parameters kept at constant level values. It has been observed that SCD gradually decreases with increase in duty factor up to certain point (duty factor 75%); then slowly assumes an increasing trend with respect to increased duty factor value. This may be explained referring to the fact that at constant gap voltage, peak-current and  $T_{on}$ , increase in duty factor results in decrease of  $T_{off}$ , which in turn reduces total cycle time (i.e.  $T_{on}+T_{off}$ ) and thereby increases discharge frequency. The reduced  $T_{off}$  seems insufficient for subsequent cooling of molten material near the machined surface; immense heat is evolved herein which causes excess evaporation of the molten material. The rate of evaporation being higher as compared to the rate of resolidification and hence, tendency to form white layer; as a consequence white layer thickness gradually reduces (Fig. 3.15). Reduction of white layer formation results in decreased surface crack density; that too, however, up to certain value of duty factor i.e. 75% (Fig. 3.12). Beyond this, rate formation of white layer assumes more or less constant; but intense heat generated at the machining zone (as  $T_{off}$  decreases) increases residual stress within the white layer. The rate of crack formation being higher; SCD gradually increases (Fig. 3.12).

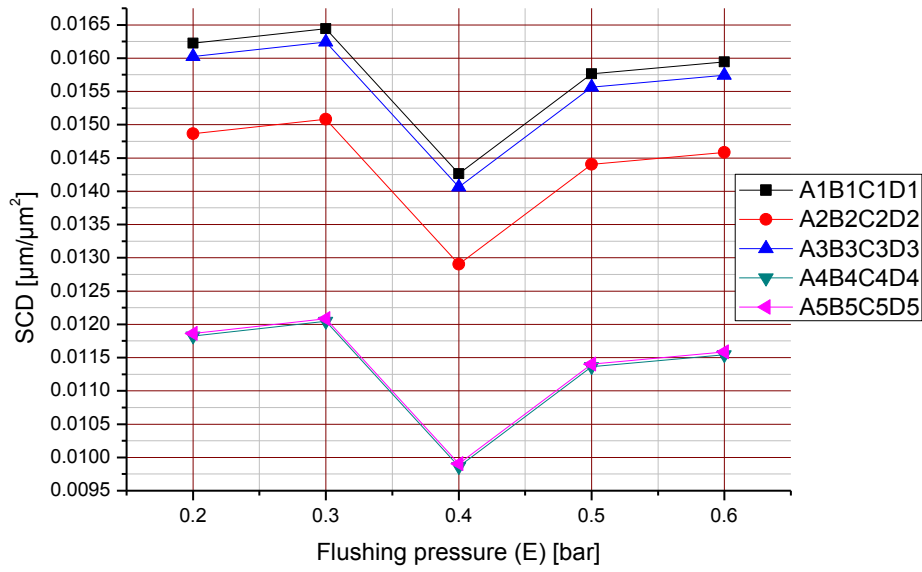


Fig. 3.13: Effect of flushing pressure (E) on SCD

Based on Fig. 3.13, the effect of flushing pressure on SCD on the EDMed work surface has been explained. The plots have been obtained by utilizing constant parameters of EDM. An optimal dielectric flushing pressure of about 0.4bar has been noticed where the crack density assumes a minimal value. The trend of variation of SCD that could be retrieved from Fig. 3.13 appears somewhat similar to that reported by (Wong et al., 1995). While flushing pressure increases from 0.2bar to 0.4bar, dielectric fluid appears increasingly effective in removing eroded particle from the inter-electrode gap; this in turn reduces the possibility of white layer formation and subsequent surface cracks. At low flushing pressure, the concentration of debris is high and this may stimulate preferential discharges or arcing in the territory of accumulated debris. Massive discharge rate in this region combined with enormous heat concentration due to inadequate flushing pressure of dielectric flow induce probability of surface cracking to a remarkable extent. While flushing pressure is increased beyond the optimal level, the quenching effect of dielectric onto the EDMed surface becomes more predominant. According to (Lee et al., 1992), as higher heat conduction through the parent material suppress the propensity of crack formation; the higher quenching rate offered by the highly pressurized dielectric flow reduces relative heat conduction rate through the parent metal resulting more cracks at the machined surface.

### 3.3.2.3 Parametric Influence on White Layer Thickness

The occurrence of spark during EDM melts and vaporizes a tiny area on the surface of tool electrode. At the end of the pulse-on time, a small amount of molten material is ejected from the surface and the remaining liquid resolidifies. As explained by (Tomlinson and Adkin, 1992), this resolidified/recast layer is typically very fine grained and possesses high hardness as compared to the base metal, and may be alloyed with Carbon from the cracked dielectric (products coming out through pyrolysis of dielectric) or with material transferred from the tool. It is also denoted as 'white layer' since it remains unaffected by etching, and appears 'white' in colour under optical microscope. As reported by (Huang et al., 2004), beneath the white layer, existence of a heat affected zone can be noticed due to the consequence of rapid heating as well as quenching cycles during EDM.

The formation of white layer is incurred under different spark erosion conditions, and it exhibits surface irregularities in the form of pock marks, globules of debris, cracks and micro-cracks, whose density is greatly influenced by the process environment employed. The white layer possesses high tensile residual stresses, which seems detrimental for the part functionality.

Along with various process parameters (such as gap voltage, discharge current, pulse-on time, duty factor etc.) the occurrence of white layer depends on initial Carbon content of the workpiece and the type of dielectric applied. Literature by (Ramasawmy et al., 2005) depicts that the thickness of white layer is directly dependent upon the magnitude of the pulse energy.

The white layer exhibits high hardness, good adherence to the bulk and good resistance to corrosion. However, as discussed by (Liao et al., 2004), white layer formed by EDM process produces inferior surface finish and decreases fatigue strength due to the presence of micro-cracks and micro-voids. Formation of white layer is inevitable but highly undesirable. Proper controlling of EDM process parameters may reduce thickness of the white layer up to certain extent. Hence, in-depth understanding of process behavior especially, the influence of various EDM parameters on white layer thickness appears very important. The thickness of the white layer needs to be precisely controlled thus facilitating subsequent lapping process. As mentioned by (Ramasawmy et al., 2005), lapping is a post-machining (post-EDM) operation to be performed to remove white layer before the end product is subjected to its prescribed application domain.

Fig. 3.14 shows that WLT and its deviation increase with increase in pulse-on time. An average trend of upward increment has been observed for WLT with respect to the increment of pulse-on time, whilst keeping other parameters fixed at constant levels. Literature also supports that average white layer thickness tends to increase with energy per spark, peak discharge current, and current pulse duration. According to (Bozkurt et al., 1996), this could be understood by the fact that the dielectric fluid can flush out a constant amount of molten material from the machining zone, not the entire material. Therefore, as immense heat is transferred into the specimen due to increased pulse-on time, the dielectric seems unable to clear away the molten material completely; it adheres on the specimen surface. During subsequent cooling this molten material resolidifies and hence simulates formation of white layer. Similar trend has also been observed in the work performed by (Jabbaripour et al., 2012).

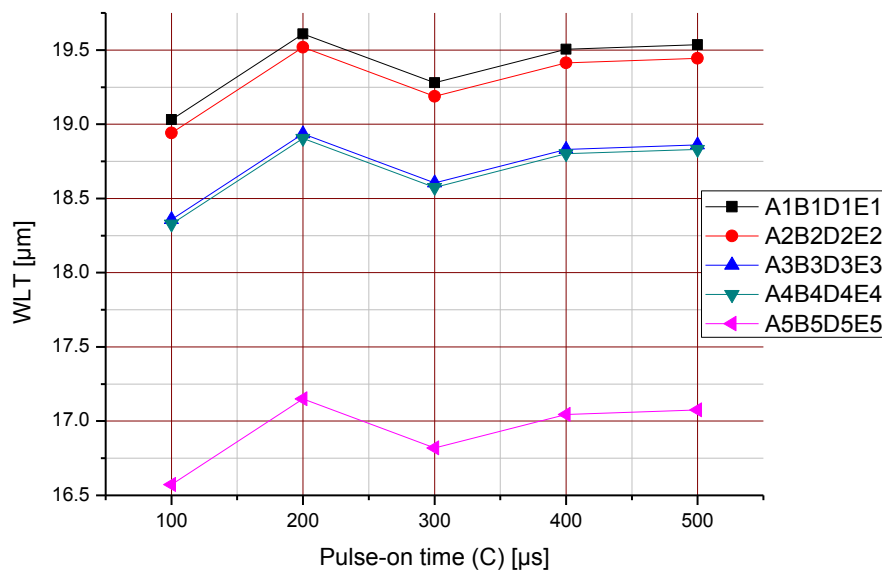


Fig. 3.14: Effect of pulse-on time (C) on WLT

The effect of flushing pressure (E) on WLT has been shown in Fig. 3.16. An average trend has been observed that WLT tends to decrease with increase in flushing pressure keeping other parameters set at constant level values. With increment of  $F_p$ , the effect of quenching property and debris removal capability of the dielectric fluid becomes predominant, thereby; chance of white layer growth diminishes.

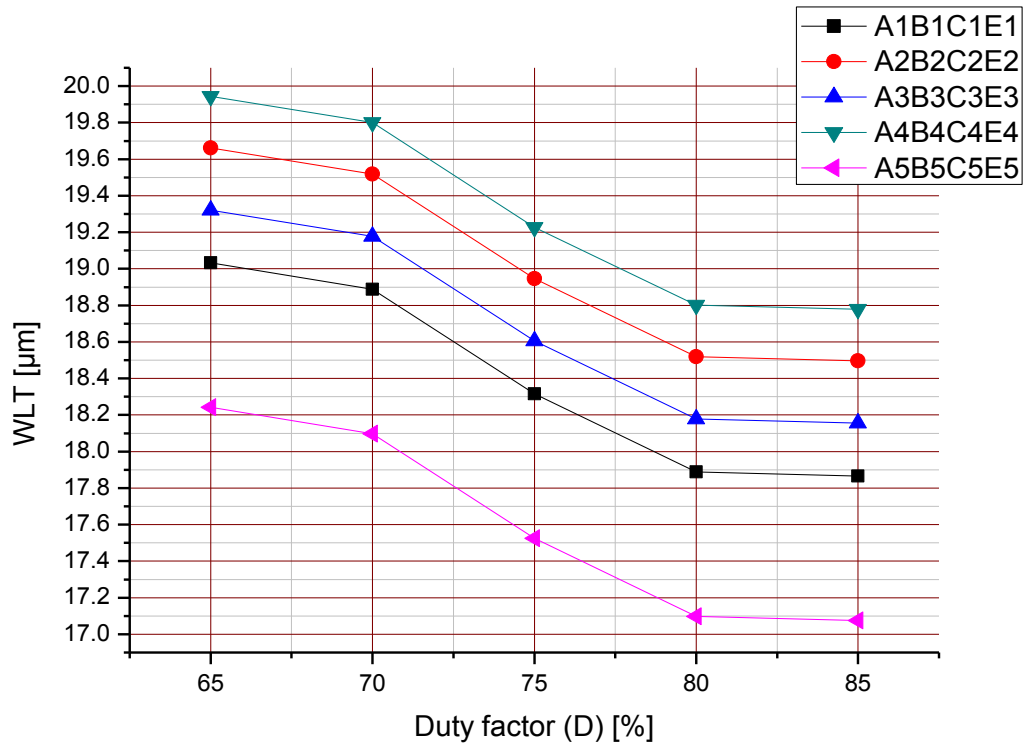


Fig. 3.15: Effect of duty factor (D) on WLT

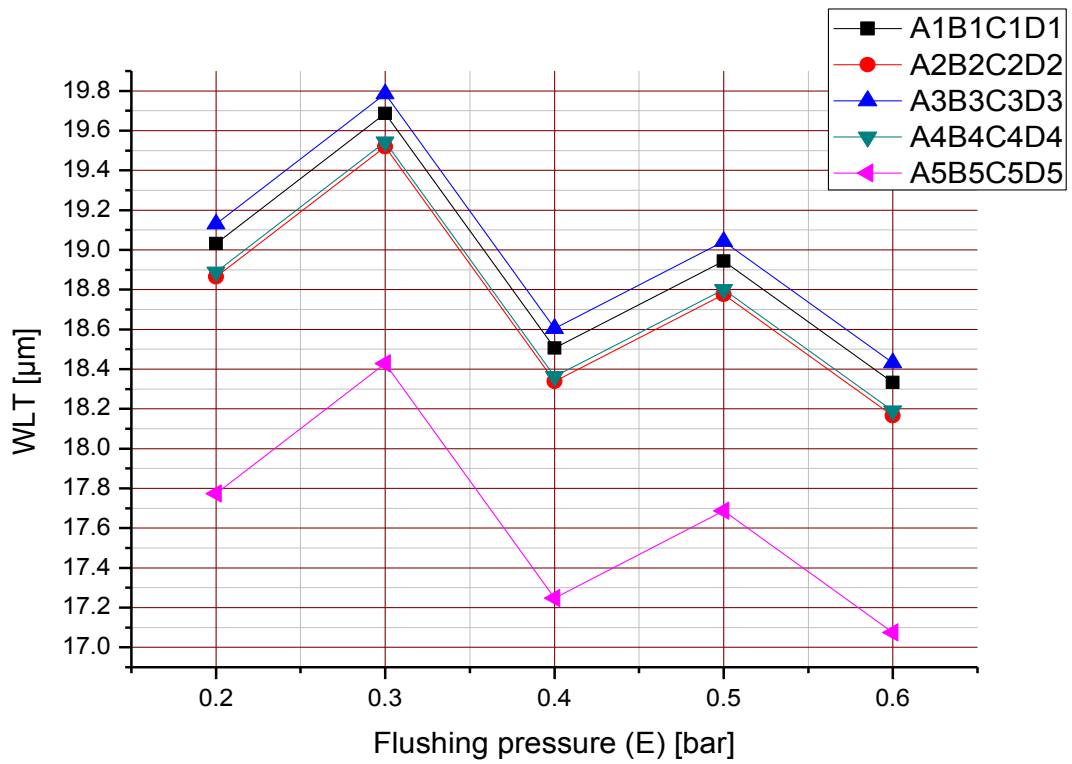


Fig. 3.16: Effect of flushing pressure (E) on WLT



## 3.4 Optimization of Machining Responses

### 3.4.1 Methodology: Utility Theory Combined with Taguchi Method

As described by (Walia et al., 2006; Singh and Kumar, 2006), utility can be defined as the usefulness of a product/process with reference to the customers' expectations. A product/process is characterized by several performance measures of conflicting requirements (ex. Higher-is-Better, HB; Lower-is-Better, LB). The advantage of utility theory is to aggregate utility of individual performances features into a unique index called overall utility degree. The best product/process should correspond to the maximum overall utility.

Therefore, the overall usefulness of a product can be assessed by overall utility degree which is the sum of individual utilities of various performance characteristics of the product/process.

Assuming an EDM process is characterized by a total  $K$  performance attributes (ex.  $K = 3$ ; i.e.  $R_a$ , SCD and WLT, in the present case); and, a total  $N$  settings (parametric combinations) are available for evaluation (ex.  $N = 25$ ; in the present case). The 25 parametric combinations of  $L_{25}$  OA are nothing but possible process environments; can be understood as candidate alternatives. Each process environment is capable of providing performance outputs. The goal of adopting utility theory is to select the best process environment to satisfy contradicting requirements of multi-performance yields simultaneously.

If  $x_i(k)$  is the measure of effectiveness (experimental data) of  $k^{th}$  attribute (or performance characteristic) in  $i^{th}$  experimental run ( $i = 1, 2, \dots, N$ ) and there exists a total of  $K$  attributes evaluating the outcome space, then the joint utility function can be expressed as:

$$U_o(x(1), x(2), \dots, x(k), \dots, x(K)) = f(U(1), U(2), \dots, U(k), \dots, U(K)) \quad (3.1)$$

A preference scale for each performance attribute is constructed for determining its utility value. Two arbitrary numerical values (preference number) 0 and 9 are assigned to the just acceptable (the worst) and the most acceptable (the best) value of the performance attribute, respectively. The preference number (also called utility value) of a particular response can be expressed on a logarithmic scale as follows.

$$U_i(k) = A \times \log \left( \frac{x_i(k)}{\bar{x}(k)} \right) \quad (3.2)$$

Here  $U_i(k)$  denotes utility value of  $k^{th}$  attribute in  $i^{th}$  setting;  $x_i(k)$  is the value of  $k^{th}$  performance attribute obtained at  $i^{th}$  setting; where,  $(k = 1, 2, \dots, K)$  and  $(i = 1, 2, \dots, N)$ .

Also,  $\bar{x}(k)$  is the just acceptable value of  $k^{th}$  performance attribute with the following condition i.e.

$\bar{x}(k) = \underset{i=1,2,\dots,N}{Min} [x_i(k)]$ , if the requirement of  $k^{th}$  performance attribute is Higher-is-Better; else,

$\bar{x}(k) = \underset{i=1,2,\dots,N}{Max} [x_i(k)]$ , if the requirement of  $k^{th}$  performance attribute is Lower-is-Better.

The value of  $A$  can be found by utilizing two boundary conditions that

if  $x_i(k) = \bar{x}(k) \Rightarrow U_i(k) = 0$

and if  $x_i(k) = x^*(k) \Rightarrow U_i(k) = 9$ .

Here,

$x^*(k) = \underset{i=1,2,\dots,N}{Max} [x_i(k)]$ , if the requirement of  $k^{th}$  performance attribute is Higher-is-Better;

else,

$x^*(k) = \underset{i=1,2,\dots,N}{Min} [x_i(k)]$ , if the requirement of  $k^{th}$  performance attribute is Lower-is-Better;

$x^*(k)$  being the most acceptable value for  $k^{th}$  performance attribute.

$$\text{Therefore, } A = \frac{9}{\log\left(\frac{x^*(k)}{\bar{x}(k)}\right)} \quad (3.3)$$

The overall utility degree  $U_i^O$  for  $i^{th}$  process environment can be calculated as follows. (assuming equal priority weight of individual attributes).

$$U_i^O = \frac{1}{K} \sum_{k=1}^K U_i(k); (i = 1, 2, \dots, N; k = 1, 2, \dots, K) \quad (3.4)$$

Based on  $U_i^O$ , the superiority of performance can be well articulated for the setting which corresponds to maximum  $U_i^O$ ; and, this setting can be treated as optimal setting. However, in the present work, the most favorable setting (with maximum  $U_i^O$ ) can easily be identified from amongst 25 settings experimented as per  $L_{25}$  OA. But this setting cannot be treated as optimal because there may be a possibility that the maximum  $U_i^O$  may be obtained at a different setting beyond  $L_{25}$  OA since full factorial designed experimentation is not performed. Therefore, overall utility thus obtained from  $L_{25}$  OA

experimentation needs to be extrapolated. This can be done by Taguchi method. Hence, the advantage of exploring utility theory can be well understood by the fact that utility theory provides a basis for logical aggregation of multi-performance features into a single performance index thus providing scope for applying Taguchi method for optimization; because, traditional Taguchi method fails to solve multi-response optimization problem. Utility theory eliminates dimensional effect and criteria conflict and combines utility values of individual responses into overall utility which corresponds to Higher-is-Better (HB) requirement.

**Table 3.1:** Utility values of individual responses: Computed values of overall utility degree and corresponding S/N ratio

Sl. No.	Experimental data			Individual utility degree			Overall utility Degree, $U_o$	Correspo nding S/N ratio [dB]	Predicted S/N ratio at optimal setting [dB]
	Response variables to be optimized simultaneously			$U_{Ra}$	$U_{SCD}$	$U_{WLT}$			
	$R_a$ [ $\mu m$ ]	SCD [ $\mu m/\mu m^2$ ]	WLT [ $\mu m$ ]						
1	3.800	0.0158	19.261	5.706	1.326	2.396	3.1393	9.9367	19.7934
2	6.333	0.0166	19.577	2.793	0.960	1.659	1.8022	5.1161	
3	9.133	0.0151	16.954	0.704	1.661	8.170	3.5082	10.9017	
4	9.867	0.0136	18.596	0.263	2.435	3.986	2.2259	6.9501	
5	7.600	0.0141	17.667	1.752	2.168	6.306	3.4052	10.6429	
6	3.733	0.0154	19.074	5.808	1.515	2.837	3.3833	10.5868	
7	4.400	0.0152	17.065	4.870	1.612	7.875	4.7808	13.5900	
8	8.067	0.0152	17.523	1.412	1.612	6.676	3.2302	10.1846	
9	7.667	0.0156	20.308	1.702	1.420	0.000	1.0396	0.3373	
10	9.600	0.0056	17.742	0.420	9.000	6.114	5.1728	14.2745	
11	2.967	0.0189	19.861	7.118	0.000	1.007	2.7056	8.6453	
12	5.533	0.0163	20.090	3.563	1.095	0.488	1.7137	4.6787	
13	7.267	0.0168	20.100	2.008	0.871	0.466	1.1140	0.9377	
14	8.533	0.0093	19.445	1.092	5.247	1.965	2.7653	8.8348	
15	9.733	0.0125	19.086	0.341	3.059	2.809	2.0676	6.3093	
16	4.267	0.0172	18.310	5.045	0.697	4.688	3.4731	10.8143	
17	5.267	0.0157	18.067	3.844	1.373	5.292	3.4994	10.8799	
18	7.200	0.0108	18.137	2.061	4.141	5.117	3.7691	11.5248	
19	5.667	0.0084	18.673	3.426	6.000	3.799	4.4041	12.8771	
20	9.867	0.0110	18.835	0.263	4.005	3.408	2.5562	8.1519	
21	2.133	0.0156	17.602	9.000	1.420	6.472	5.6251	15.0026	
22	5.667	0.0117	16.646	3.426	3.548	9.000	5.3196	14.5176	
23	7.333	0.0136	17.707	1.956	2.435	6.203	3.5280	10.9506	
24	9.200	0.0116	19.752	0.662	3.612	1.256	1.8418	5.3048	
25	10.333	0.0100	19.077	0.000	4.710	2.830	2.5109	7.9966	

### 3.4.2 Evaluation of Optimal Parameters Setting

Experimentally obtained response data (as shown in Table 3.1) have been utilized to compute utility values of individual responses ( $R_a$ , SCD and WLT). In this computation, utility degrees of individual responses have been computed based on Lower-is-Better (LB) criterion (Eq. 3.2) and shown in Table 3.1. Assuming equal priority weight of the responses, overall utility index ( $U_i^o$ ) has been computed (using Eq. 3.4) for all experimental runs; values have been provided in Table 3.1. The overall utility has been treated as single objective function and finally optimized (maximized) by Taguchi method. Table 3.2 exhibits mean response (S/N ratio of overall utility) values for different factorial settings; the same has been plotted in Fig. 3.17.

**Table 3.2:** Mean response (S/N ratio of overall utility degree) table:  
Prediction of optimal setting by optimizing  $U_o$

Level	Mean S/N ratio values at different factorial levels				
	A	B	C	D	E
1	8.709	10.997	11.818	6.811	8.523
2	9.795	9.756	9.168	7.289	6.724
3	5.881	8.900	9.319	9.840	11.547
4	10.850	6.861	8.125	10.675	8.229
5	10.754	9.475	7.560	11.373	10.967
Delta	4.968	4.136	4.258	4.562	4.823
Rank	1 <sup>#</sup>	5	4	3	2

<sup>#</sup>The most influential parameter is A (Rank 1)

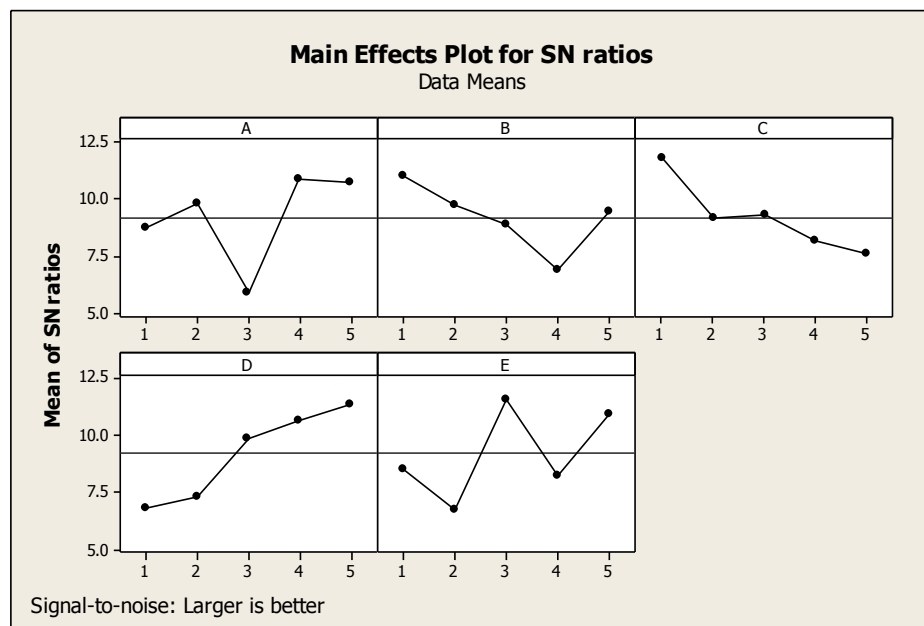


**Fig. 3.17:** Mean S/N ratio (of overall utility degree) plot:  
Predicted optimal setting =  $A_4B_1C_1D_5E_3$  i.e. [ $V_g=80V$ ;  $I_p=3A$ ;  $T_{on}=100 \mu s$ ;  $\tau=85\%$ ;  $F_p=0.4bar$ ]

The optimal setting appears as  $A_4B_1C_1D_5E_3$  i.e. [ $V_g=80V$ ;  $I_p=3A$ ;  $T_{on}=100\mu s$ ;  $\tau=85\%$ ;  $F_p=0.4bar$ ]. The predicted S/N ratio value of  $U^o$  at optimal setting corresponds to a value of 19.7934 dB which seems more as compared to the S/N ratios of  $U^o$  obtained in all 25 experimental runs (Table 3.1). As S/N ratio dictates its requirement of Higher-is-Better (HB) type; the highest S/N ratio of  $U^o$  at optimal setting confirms Taguchi's prediction to a reliable extent. This has further been verified by confirmatory test.

### 3.5 Conclusions

The following conclusions have been drawn from the aforesaid research.

- ▲ Alteration of chemical composition due to pyrolysis of dielectric fluid has been observed for the the EDMed work surface of Inconel 718. Increased Carbon content at the machined surface has resulted increased micro-hardness value for the EDMed work surface as compared to the unaffected base material. However, micro-hardness of the white layer has been found to vary from 352.600 HV<sub>0.05</sub> to 269.400 HV<sub>0.05</sub> depending on the parameters setting used during EDM operation.
- ▲ Surface morphology of the EDMed work surface Inconel 718 has been characterized by the presence of surface cracks, cracker, globule of debris, pockmarks etc. whose intensity has been found to vary depending on the parameters settings used. Two different types of cracks have been identified for the EDMed specimens of Inconel 718.
- ▲ It has been observed that thermo-mechanical effect of the EDM process has induced residual stress within the test specimen. The residual stress induced within the EDMed specimen has appeared relatively high as compared to the 'as received' parent material. Evolution of residual stress during machining tends to promote crack formation and subsequent propagation.
- ▲ XRD analysis of the EDMed work surface of Inconel 718 has exhibited a surface structure of Cubic FCC matrix consisting of Ni-based solid solution with precipitates of Cr<sub>23</sub>C<sub>6</sub> (Chromium Carbide), MoC (Molybdenum Carbide) and Nb<sub>2</sub>C (Niobium Carbide). Grain refinement has also been experienced during EDM of Inconel 718 super alloys.
- ▲ In relation of the setup utilized in this research and within selected experimental domain, the most favourable (optimal) process environment has been predicted as:

[ $V_g=80V$ ;  $I_p=3A$ ;  $T_{on}=100\mu s$ ;  $\tau=85\%$ ;  $F_p=0.4bar$ ] in order to satisfy requirements of multi-responses, simultaneously. Confirmatory test has depicted that predicted optimal parameters setting has been found capable of minimizing roughness average, surface crack density and white layer thickness, simultaneously, up to the maximum possible extent. Aforesaid work has also highlighted application of utility theory integrated with Taguchi method for solving such a multi-response optimization problem.



## Chapter 4

# Electro-Discharge Machining of Inconel 825 using Cryogenically Treated Copper Electrode: Emphasis on Surface Integrity and Metallurgical Characteristics of the EDMed Part

### 4.1 Coverage

In the present work, analysis of surface integrity and metallurgical characteristics of the machined Inconel 825 work surface has been carried out in relation to electro-discharge machining using Cryogenically Treated Tool (CTT) in comparison with Non-Treated Tool (NTT). Degree of severity of surface cracking as well as formation of white layer onto the EDMed Inconel 825 work surface has been investigated herein. The process physics of EDM using CTT has been explained with scientific relevance to EDS, XRD, residual stress as well as micro-hardness test data of the test samples. For a constant setting of process parameters [Peak current ( $I_p$ )=10A; Pulse-on time ( $T_{on}$ )=100 $\mu$ s; Duty factor ( $\tau$ )=85%], surface crack density has been found relatively less (~73%) for the EDMed Inconel 825 work surface obtained by using CTT, as compared to the case of NTT. However, relatively thick white layer (~26%) has been found attributed to the EDMed Inconel 825 specimen obtained by using CTT, as compared to the case of NTT (for a common parameters setting:  $I_p$ =6A;  $T_{on}$ =300 $\mu$ s;  $\tau$ =85%). Additionally, effects of cryogenic treatment of tool electrode have also been discussed emphasizing aspects of tool life, extent of Carbon deposition at the bottom as well as the edge of the electrode, and tool shape retention capability. As compared to NTT, Carbon (possibly carbide) layer (deposited at the edge of the tool electrode) of relatively low thickness value (~75%) has been observed for CTT.



## 4.2 Scope of the Work

Extensive literature review has been carried out to retrieve potential benefits of cryogenic processing of tool materials in order to improve thermal and electrical properties, wear resistance etc. to a remarkable extent, thus to achieve satisfactory machining performance in perspectives of product quality as well as productivity. Literature survey has depicted considerable effort put by past researchers to study aspects of machinability of Inconel super alloys during electro-discharge machining ([Newton et al., 2009](#); [Ay et al., 2013](#); [Lin et al., 2013](#); [Aggarwal et al., 2015](#); [Li et al., 2015](#); [Rajyalakshmi and Ramaiah, 2003](#)); however, application potential of cryogenically treated tool electrode has been found an unexplored area of research.

Inconel 825 is a Nickel (Ni)-Iron (Fe)-Chromium (Cr) based super alloy with additions of Molybdenum (Mo) and Copper (Cu). As compared to Inconel 825, Inconel 718 contains Niobium (Nb) which imparts strength and high temperature resistance. The Mo and Cu in Inconel 825 provide substantially improved corrosion resistance in reducing environments (when compared to conventional austenitic stainless steels). Inconel 825 thus finds its application in chemical processing, pollution-control equipment, oil and gas well piping, nuclear fuel reprocessing, acid production, and pickling equipment.

It is well understood that machinability characteristics of Inconel (different grades) super alloys are almost similar; thus, these alloys are included in the category of ‘*difficult-to-cut*’ materials. However, depending on their chemical composition; their property, application, performance of the machined surface may differ. Since, work has already been reported to a remarkable extent on machining of Inconel 718; aspects of machining and machinability of Inconel 825 has not been sufficiently addressed in exiting literature resource. Hence, this study has considered Inconel 825 as work material.

In addition to that, it has been noticed that most of the past research have considered material removal rate, electrode wear rate, and surface roughness etc. (of the EDMed Inconel end product) as the major focus towards evaluating machining performance ([Sundaram et al., 2009](#) [Yildiz et al., 2011](#)); aspects of surface cracking and white layer formation (and their quantification) have not been emphasized intensively.

Cryogenic processing of tool material has been reported to examine improvements in MRR, EWR etc.; whilst it is felt that effect of the same on Surface Crack Density (SCD), White Layer Thickness (WLT), and chemical composition of the EDMed work surface, metallurgical characteristics of the machined surface, residual stress and micro-hardness

etc. need to be investigated in detail. To this context, the specific objectives of the present work have been delineated herein.

1. To study application potential of using CTT whilst performing EDM on Inconel 825 as compared to the case of EDM using NTT.
2. To study the effects of cryogenic treatment of electrode material on crystallize size, dislocation density, extent of grain refinement etc. (as compared to ‘non-treated’ electrode material).
3. To study surface integrity (morphology and topography) of the EDMed Inconel 825 work surface obtained by using CTT as compared to NTT. Topographic measures of the EDMed work surface viz. Surface Crack Density (SCD), crack opening width, and White Layer Thickness (WLT) etc. are indented to be studied in detail to articulate potential benefits of using cryogenically treated tool electrode.
4. To examine chemical constituents, metallurgical aspects (phases present: matrix and precipitates, degree of grain refinement, crystallize size, dislocation density etc.), residual stress and micro-hardness of the EDMed Inconel 825 specimen obtained by using CTT as compared to NTT.
5. To investigate the effect of cryogenic treatment of the electrode material on (a) tool shape retention capability, (b) aspects of tool wear, and (c) extent of Carbon deposition at the bottom surface/edge of the tool during execution of EDM operation on Inconel 825.
6. Finally, to investigate whether cryogenic processing of electrode material proves beneficial to improve ease of electro-discharge machining of Inconel 825.

## **4.3 Results and Discussion**

### **4.3.1 Effects of Cryogenic Treatment of Tool Electrode**

Effect of cryogenic treatment of Copper electrode has been studied in perspectives of metallurgical information obtained from XRD analysis, residual stress, and micro-hardness test data. XRD spectra of ‘non-treated’ Copper has revealed existence of cubic crystal system (Fig. 4.1.1); peak patterns have been found almost exactly matching to that of Cu with impurities from 0.001-0.01%, Ag, Al, Bi, Fe, Si, and Zn (Reference Code: 04-0836). It has also been observed that no significant phase change has been attributed due to cryogenic treatment of Copper (Fig. 4.1.1-4.1.2).

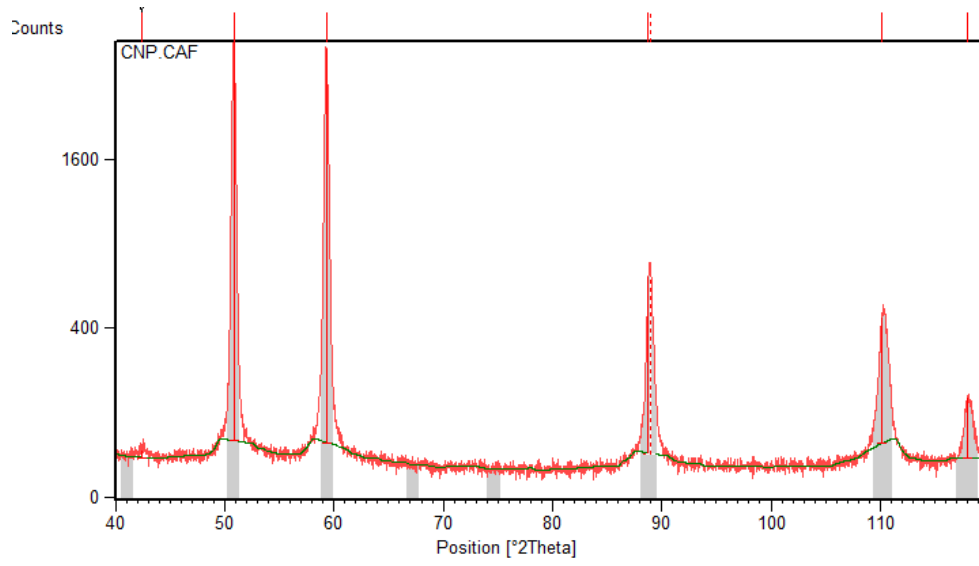


Fig. 4.1.1: XRD spectra of NTT material

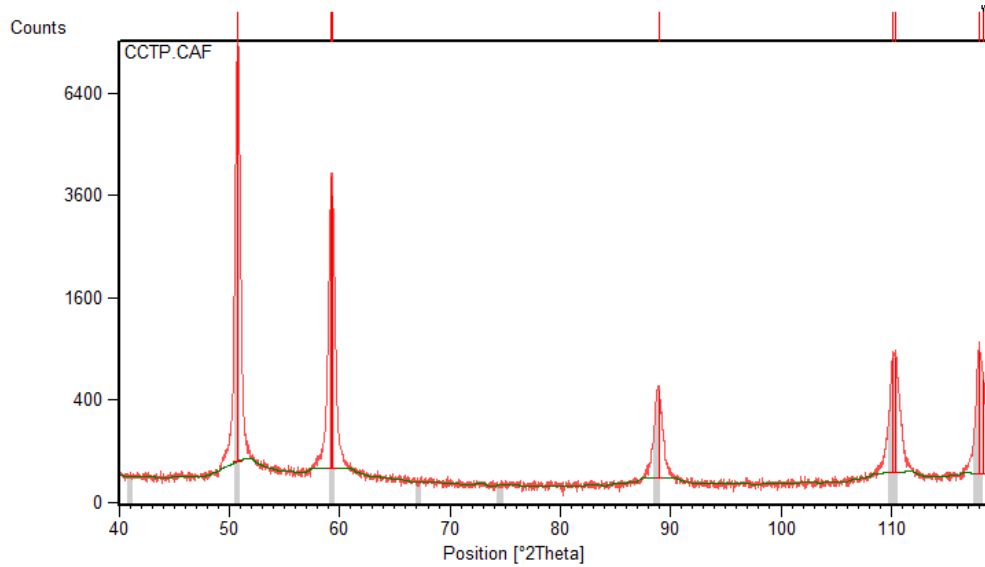


Fig. 4.1.2: XRD spectra of CTT material

Table 4.1: The variation of crystallite size ( $L$ ), and dislocation density ( $\delta$ ) for (1) NTT material, and (2) CTT material before executing EDM operations

Sl. No.	Data of high intensity peaks of XRD for different specimens	$2\theta$ ( $^{\circ}$ )	FWHM ( $\beta_L$ ) [rad]	Crystallite size ( $L$ ) [nm]
(1)	NTT	50.8560	$5.166 \times 10^{-3}$	34.54
(2)	CTT	50.7254	$5.856 \times 10^{-3}$	30.45

Table 4.1 (Continued)

Sl. No.	Data of high intensity peaks of XRD for different specimens	Miller indices $[h, k, l]$	Inter planner spacing between the atoms ( $d$ ) [ $\text{\AA}$ ] (Obtained from <i>X'pert HighScore Plus Software</i> )	Lattice constant ( $a$ ) [ $\text{\AA}$ ]	Dislocation density ( $\delta$ ) $\times 10^4$
(1)	NTT	[2 0 0]	2.08477	4.16954	12.148
(2)	CTT	[2 0 0]	2.08979	4.17958	15.592

As compared to ‘non-treated’ electrode material, deep cryogenic treatment has resulted substantial grain refinement; which has attributed to smaller crystallite size and higher dislocation density (Table 4.1). The computation of crystallite size has been carried out using *Debye Scherrer's* formulation. The theoretical basis and formulations for computing dislocation density could be found in the reporting by (Subbaiah et al., 2006; Singh et al., 2008; Vinila et al., 2014; Jacob et al., 2015). Analysis has depicted that NTT has corresponded to the crystallite size 34.54nm; whilst, CTT has exhibited reduced crystallite size ( $L \sim 30.45\text{nm}$ ). Reduction of crystallite size has resulted increase in dislocation density i.e.  $\delta \sim 12.148 \times 10^{-4}$  for NTT; whilst  $\delta \sim 15.592 \times 10^{-4}$  has been observed for CTT.

This has been found in good agreement with the micro-hardness test data. Experiment has revealed that cryogenically treated Copper specimen has shown relatively high micro-hardness value (Range  $\sim 114.2\text{HV}$  to  $119.8\text{HV}$ ) as compared to that of ‘non-treated’ tool material (Range  $\sim 94.1\text{HV}$  to  $99.3\text{HV}$ ). Effect of cryogenic treatment has thus been interpreted in view of reduced degree of crystal imperfections, voids as well as dislocations; and consequently, evolution of residual stress of lesser magnitude  $[(-79.4 \pm 37.3) \text{MPa}]$  as compared to that of ‘non-treated’ tool material  $[(-181.2 \pm 114.7) \text{MPa}]$ .

(Barron, 1985; Hands, 1986) claimed that CT of tool material contributes favourably by reducing barriers of heat conduction (dislocations, residual stresses and strains) and thereby improving thermal conductivity of the metal. Trucks (1983) also claimed that the cryogenic process increases the homogeneity of the crystal structure, dissolving gaps and dislocations, and thereby reducing electrical resistivity. The enhanced structural compactness and uniformity in turn improves electrical conductivity. Increases in

electrical conductivities of materials also cause increase in thermal conductivities as per *Wiedemann-Franz-Lorenz Law* (Isaak and Reitz, 2008).

Kalsi et al. (2010) reported that increase in thermal conductivity due to CT increases heat dissipation capacity of cutting tool materials and thus helps in decreasing the tool-tip temperature and ultimately improved tool life.

Therefore, in the present case, it has been assumed that CT must have improved electrical as well as thermal conductivities of the tool material; thus improving ease of electro-discharge machining of Inconel 825 work material. Moreover, it has been observed that cryogenic treatment of the tool electrode has resulted reduced tool material consumption (lesser tool wear) as compared to NTT. These have been explained in later sections.

### 4.3.2 Effects of using CTT during EDM on Inconel 825

#### 4.3.2.1 Surface Integrity: Emphasis on Surface Cracking and Formation of White Layer

As compared to ‘normal’ Inconel 825, the EDMed work surface of Inconel 825 has exhibited poor surface integrity (in purview of morphology and topography) whilst executing EDM using NTT as well as CTT. The inferior surface morphology has resulted formation of crater marks, globules of debris, melted metal deposition, pockmarks or chimneys, surface cracks and white layer. However, the intensity of such surface irregularities has been found different for the case of EDM on Inconel 825 using cryogenically treated Copper tool as compared to that of normal tool electrode (Fig. 4.2).

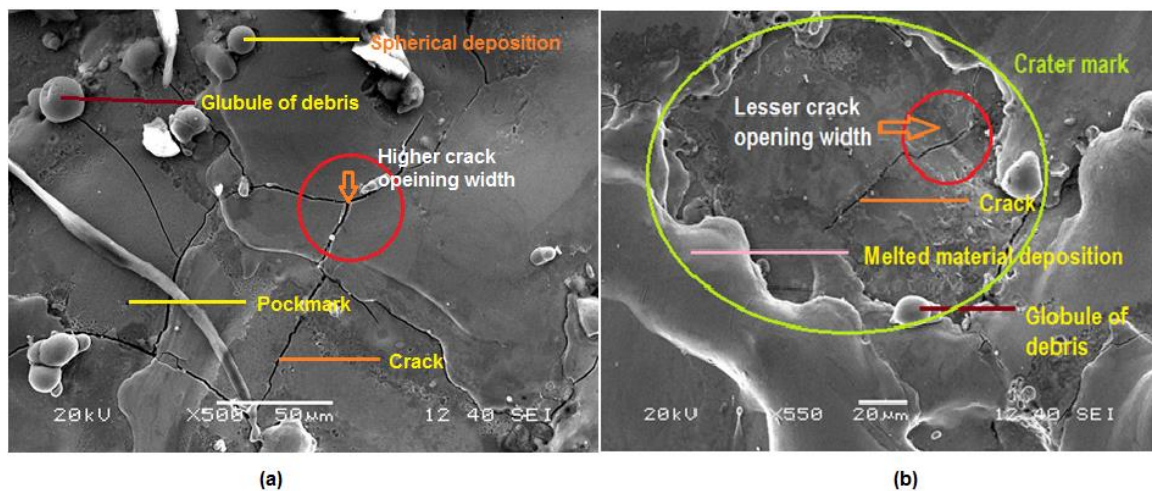
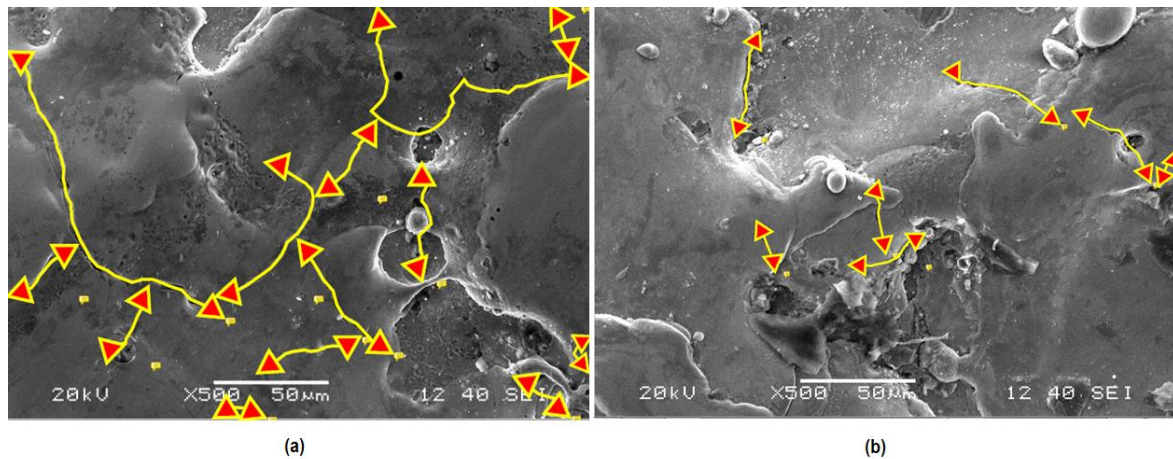


Fig. 4.2: SEM micrographs revealing surface irregularities of the EDMed Inconel 825 specimens obtained at parameters setting [ $I_p=10A$ ;  $T_{on}=300\mu s$ ;  $\tau=75\%$ ] using (a) NTT and, (b) CTT

During spark discharge, particles are eroded from the work surface thus forming crater. Due to enormous heat generated in the spark gap during EDM operation, eroded particles melt and these are carried away by the dielectric fluid. However, flashing pressure being inadequate to remove all the molten material away from the spark gap. During pulse-off duration (i.e. during  $T_{off}$ ), a part of the molten material resolidifies adhering on the work surface, thus forming resolidified layer (also called recast layer or white layer). Globules of debris are formed due to the effect of surface tension; whereas, pockmarks are developed while entrapped gases are released during resolidification of part of molten material pool. EDM process develops huge thermal stress (appears as tensile residual stress) within the work specimen; which stimulates generation of surface cracks and its propagation towards entire white layer depth, HAZ and finally to the unaffected parent material. However, intensity of aforesaid surface irregularities largely depends on the EDM process parameters setting involved and the condition of the tool electrode used (i.e. CTT or NTT, in the present case).

SEM micrographs revealing existence of surface cracks on the machined Inconel 825 work surface obtained through EDM using (a) NTT, and (b) CTT, for a constant parameters setting i.e. [ $I_p=10A$ ;  $T_{on}=100\mu s$ ;  $\tau=85\%$ ] have been depicted in Fig. 4.3.1-4.3.2.



**Fig. 4.3.1:** SEM micrographs revealing existence of surface cracks on the machined Inconel 825 work surface obtained through EDM using (a) NTT ( $SCD \sim 0.0155 \mu m / \mu m^2$ ), and (b) CTT ( $SCD \sim 0.0042 \mu m / \mu m^2$ ) for a constant parameters setting i.e. [ $I_p=10A$ ;  $T_{on}=100\mu s$ ;  $\tau=85\%$ ]



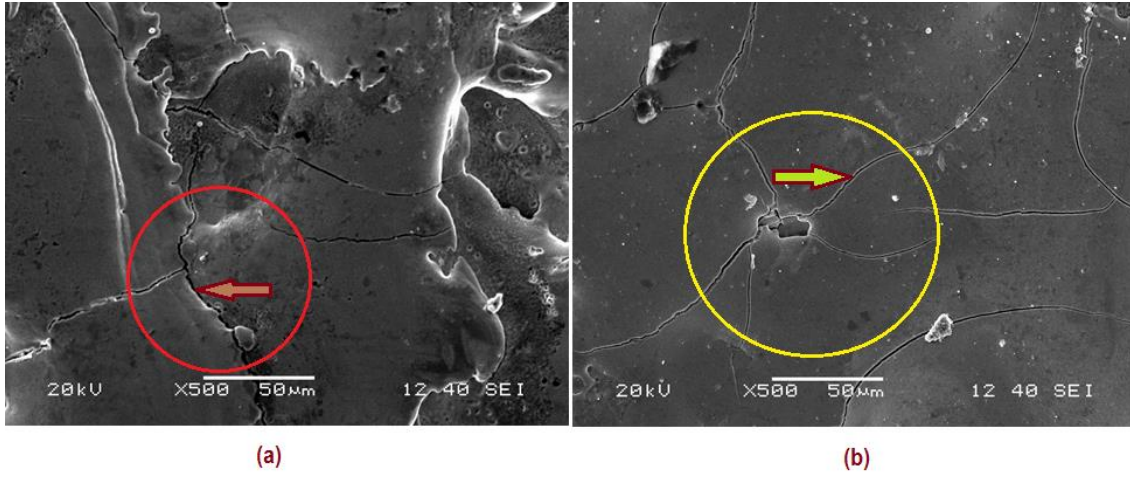


**Fig. 4.3.2:** SEM micrographs comparing the severity of crack formation (crack opening width,  $C_w$ ) at the machined Inconel 825 work surface obtained through EDM using (a) NTT and (b) CTT, for a constant parameters setting i.e. [ $I_p=10A$ ;  $T_{on}=300\mu s$ ;  $\tau=85\%$ ]

It has clearly been understood that use of CTT has been noticed fruitful since intensity of surface cracks developed on the machined surface of Inconel 825 has been found relatively less as compared to the case of NTT. Surface cracks are highly undesirable whilst the EDMed part component is subjected to practical application field; reduced crack density thus supports application potential of cryogenic treatment of the tool material in the context of EDM on Inconel 825. The explanation for reduced crack density has been explained well by (Hui et al., 2016). According to (Hui et al., 2016), cryogenic treatment enhances thermal conductivity of the electrode tool; thus, facilitating improved rate of heat transfer through bulk of the electrode material. The occurrence of which leads to (i) decrease the length of the discharge gap, and (ii) decrease in energy density of the discharge channel; which in turn results in smooth deposition of the melted material on the surface of the workpiece. This in turn suppresses severity of surface cracking.

SEM micrographs revealing existence of white layer on the EDMed Inconel 825 work surface obtained using NTT as well as CTT, for a constant parameters setting [ $I_p=6A$ ;  $T_{on}=300\mu s$ ;  $\tau=85\%$ ] have also been depicted in Fig. 4.4. It has been noticed that white layer thickness has assumed higher values for the case of EDM using CTT as compared to the case of NTT. This may be due to the enhancement of heat dissipation capacity of the electrode material (after cryogenic treatment) which results in increased heat transfer rate through the bulk of the electrode material. Due to increased rate of heat transfer, molten material gets uniformed cooled at a faster rate and deposited smoothly onto the top surface of the machined zone. Hassle-free deposition of the molten material

(resolidification) in turn increases the thickness of the white layer. Uniform deposition of the molten material also results in evolution of lesser residual stress and thus reduces probability of formation of surface cracks to some extent.

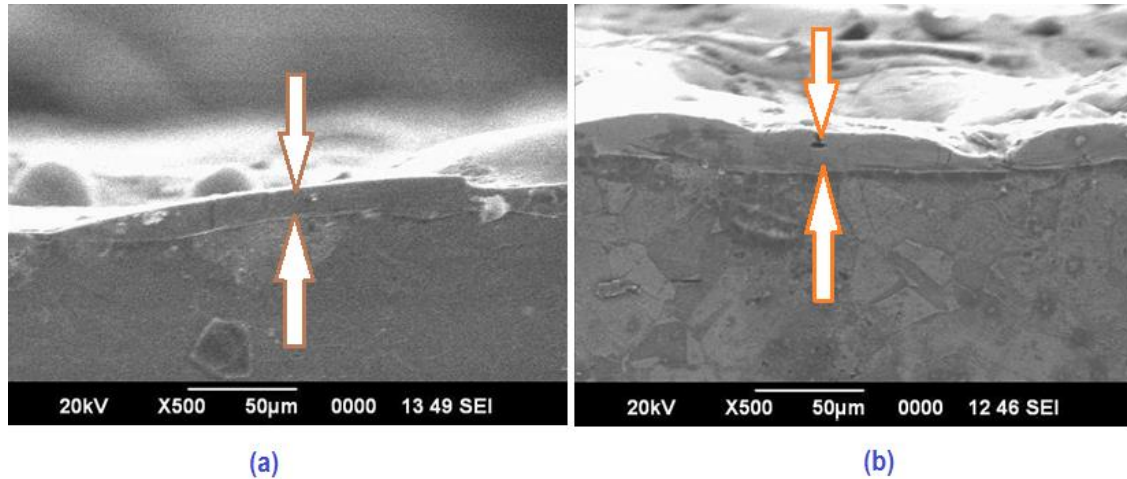


**Fig. 4.4:** SEM micrographs revealing existence of white layer on the machined Inconel 825 work surface obtained through EDM using (a) NTT (WLT~14.14μm), and (b) CTT (WLT~17.812μm) for a constant parameters setting i.e. [ $I_p=6A$ ;  $T_{on}=300\mu s$ ;  $\tau=85\%$ ]

#### 4.3.2.2 Analysis of EDS and Micro-Hardness Test Data

Energy Dispersive X-Ray Spectroscopy (EDS) elemental spectra revealing chemical composition (wt%) of ‘normal’ Inconel 825, EDMed work surfaces of Inconel 825 obtained through using NTT, and CTT (for a constant setting of EDM parameters i.e.  $I_p=10A$ ,  $T_{on}=300\mu s$ ,  $\tau=85\%$ ) have been shown in Fig. 4.5.1-4.5.3, respectively. It has been observed that Carbon content has been increased during EDM due to Carbon enrichment onto the machined zone while dielectric cracking has been incurred. The EDM oil (used as dielectric medium) being a hydrocarbon; during spark discharge, pyrolysis of dielectric fluid has taken place. Thus, Carbon got deposited on the machined zone leading to increase in Carbon content of the EDMed work surface as compared to the unaffected (normal) parent material.



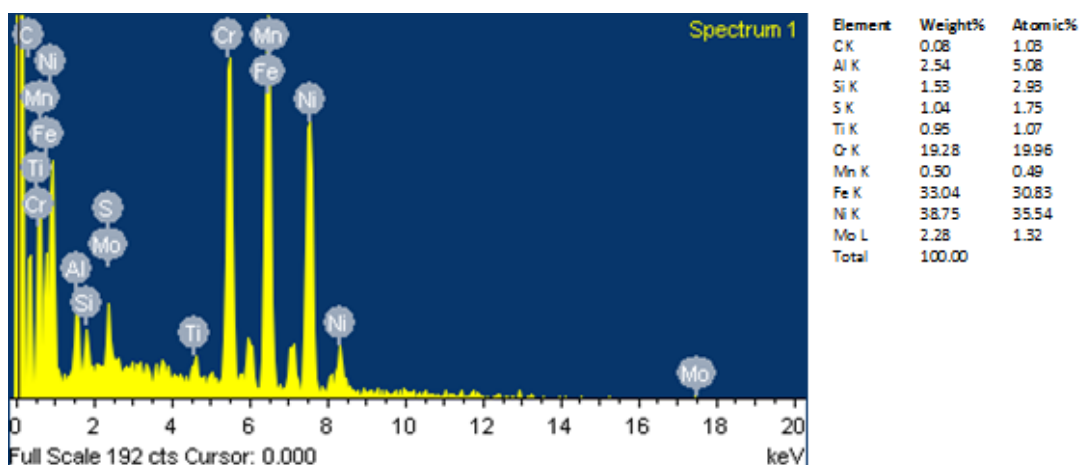


Fig. 4.5.1: EDS elemental spectra revealing chemical composition of 'as received' Inconel 825

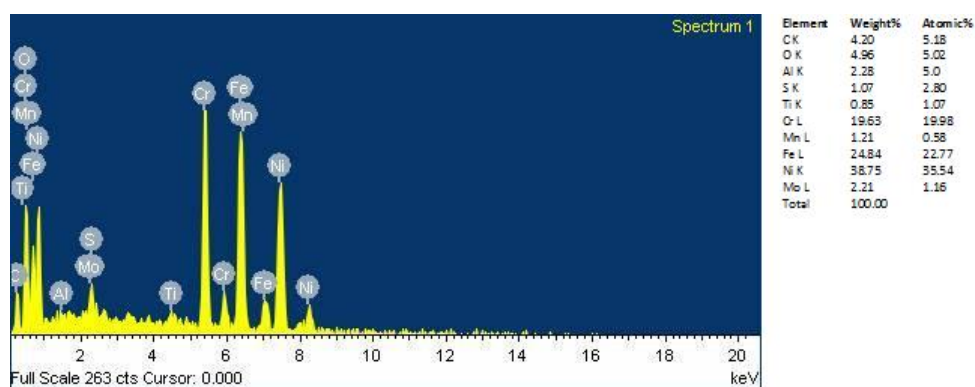


Fig. 4.5.2: EDS elemental spectra revealing chemical composition of the EDMed Inconel 825 work surface obtained using NTT at parameters setting: [ $I_p=10A$ ;  $T_{on}=300\mu s$ ;  $\tau=85\%$ ]

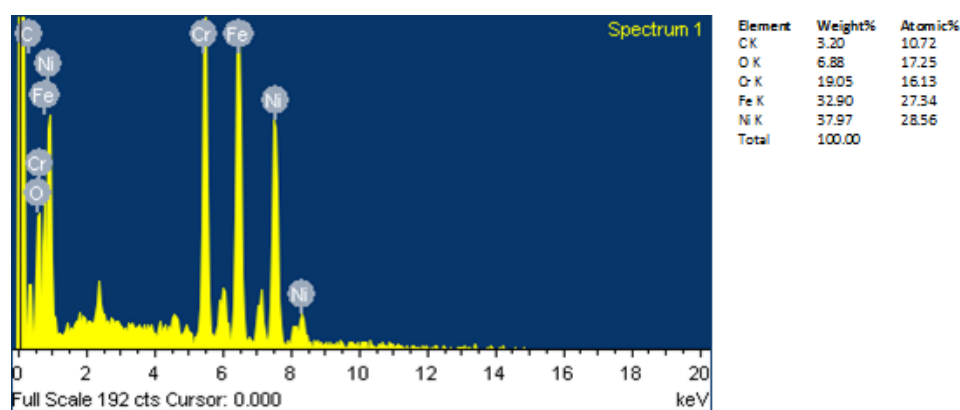


Fig. 4.5.3: EDS elemental spectra revealing chemical composition of the EDMed Inconel 825 work surface obtained using CTT at parameters setting: [ $I_p=10A$ ;  $T_{on}=300\mu s$ ;  $\tau=85\%$ ]

EDS analysis has exhibited that as compared to 'normal' Inconel 825 (0.08 wt% C), Carbon content of the EDMed Inconel 825 work surface has been increased to 4.2% (for the case of EDM using NTT), and 3.2% (for the case of EDM using CTT). It has been observed that as compared to EDM with NTT; use of CTT has caused lesser extent of Carbon enrichment onto the machined zone which has been understood beneficial.

Since, the topmost layer of the EDMed surface is detrimental for the service life of the part component when subjected to fatigue loading. This is because surface cracks do initiate at this surface. Lesser Carbon content of this layer should correspond to lower hardness value; thus, imparts relatively more resistance to surface cracking.

The decrement of Carbon content onto the top surface of the EDMed Inconel 825 (obtained by using CTT), as compared to NTT, can be explained by the fact that cryogenic processing of electrode tool substantially improves electrical as well as thermal properties of the tool material. Hence, during EDM using CTT, the increased rate of heat dissipation through the tool electrode in turn decreases energy density at the spark gap. This may suppress the tendency of carbide precipitation on the machined zone. Thus, EDMed Inconel 825 work surface obtained by using CTT has exhibited relatively less Carbon content.

For micro-hardness tests, indentations have been made at three distinct locations (approximately at the middle position along the thickness of white layer measured from the top surface) for a particular sample (transverse cut section of EDMed workpiece through WEDM route). As compared to 'normal' Inconel 825 (micro-hardness in the range ~ from 235.0 HV to 242.1 HV), the EDMed Inconel 825 specimen (obtained at parameters setting:  $I_p=10A$ ,  $T_{on}=300\mu s$ ,  $\tau=85\%$ ) has exhibited higher hardness values falling in the range ~ (from 568.0 HV to 632.8 HV), (from 827.6 HV to 863.0 HV), for the following two cases of EDM using NTT, and CTT, respectively.

In this context, it may be noted that EDS analysis has been made on the work surface of the EDMed Inconel 825; whilst, micro-hardness has been measured (for the transverse-cut section of EDMed specimen) approximately at the mid-depth (from the top surface) of the white layer thickness. Moreover, from XRD test, it has been observed that EDMed work surface of Inconel 825 using CTT has corresponded to relatively less crystallite size (more refined grain structure) as compared to the case of EDM using NTT. Hence, as compared to NTT, more micro-hardness value that has been obtained in case of EDM using CTT could be well justified.

#### 4.3.2.3 Analysis of Residual Stress

Literature has claimed that CT of material removes crystal imperfections (voids, dislocations, stress lines etc.) to a major extent and thereby provides a more refined grain structure. As a consequence, chance of fatigue failure is substantially reduced (Akincioglu et al., 2015).

Residual stress generated within the EDMed work surface is basically the effect of non-homogeneity of heat flow and metallurgical transformations or the localized inhomogeneous plastic deformation that occurs during EDM operation (Ekmekci, 2007). It is well known that the residual stress resulted by rapid cooling and phase changes in the white layer induce surface cracking. Literature reported that such residual stress is of tensile in nature whose magnitude appears to be the highest at the surface. It was also reported that the residual stress increases with increase in pulse energy (Crookall and Khor, 1972). Such residual stress is indeed harmful since its magnitude stimulates surface cracking. Lee et al. (2004) reported that the formation of surface crack is basically due to the differentials of high contraction stresses exceeding the work material's ultimate tensile stress within the white layer depth.

In the present work, it has been observed that 'normal' Inconel 825 has corresponded to the compressive residual stress (-413.0 to -261.4 MPa). The residual stress of tensile nature has been attributed to the EDMed specimen of Inconel 825 (obtained at constant parameters setting:  $I_p=10A$ ,  $T_{on}=300\mu s$ ,  $\tau=85\%$ ) for the case of EDM using NTT (868.7 to 1492.3 MPa), and CTT (712.2 to 958.0 MPa), respectively. Thus, the EDMed Inconel 825 specimen obtained by using CTT has exhibited lesser residual stress as compared to the case of NTT. Evolution of relatively less residual stress is indeed beneficial since it reduces severity of surface cracking. This helps in improving fatigue life of the EDMed end product.

#### 4.3.2.4 XRD Tests: Metallurgical Analyses of the EDMed Inconel 825 Work Surface

##### ⇒ Phase Analysis

X-Ray Diffraction (XRD) spectra inferring metallurgical aspects of 'normal' Inconel 825, and EDMed work surface of Inconel 825 obtained by using NTT, and CTT (for a constant setting of EDM parameters i.e.  $I_p=10A$ ,  $T_{on}=300\mu s$ ,  $\tau=85\%$ ) have been provided in Fig. 4.6.1-4.6.3, respectively.

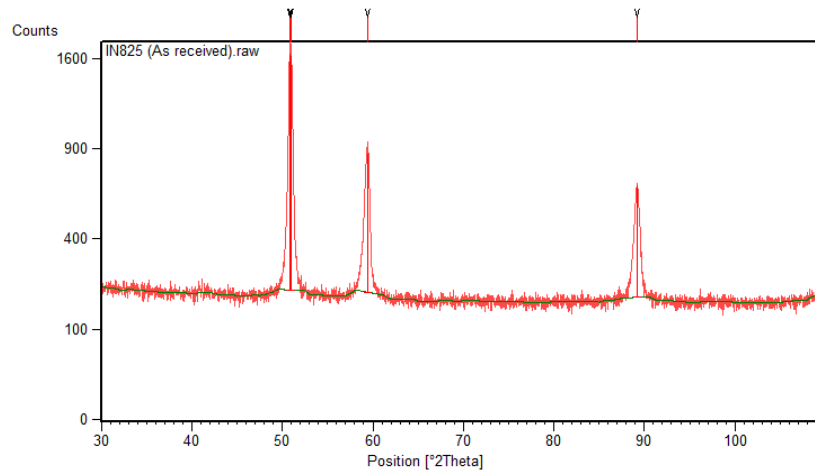


Fig. 4.6.1: XRD spectra of 'as received' Inconel 825 work material

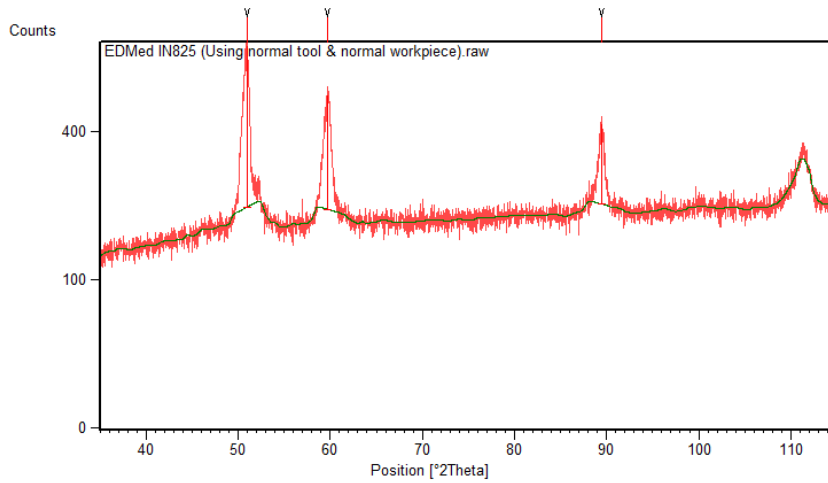


Fig. 4.6.2: XRD spectra of the EDMed Inconel 825 work surface obtained using NTT at parameters setting: [ $I_p=10A$ ;  $T_{on}=300\mu s$ ;  $\tau=85\%$ ]

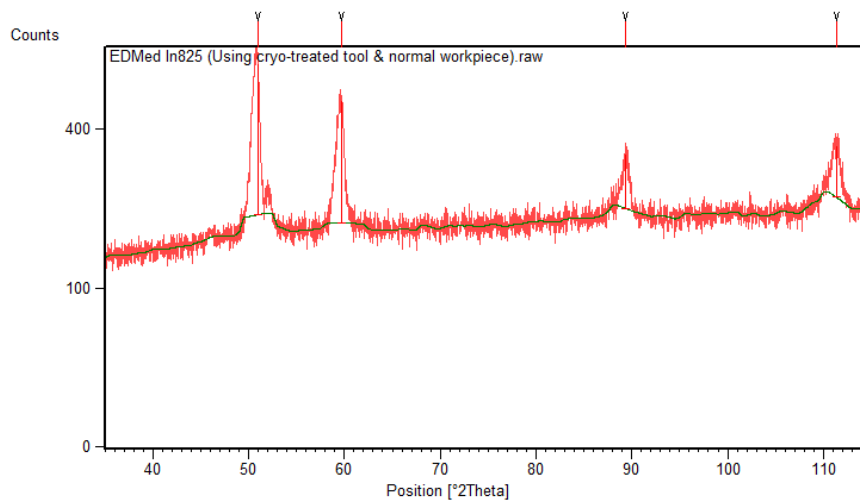


Fig. 4.6.3: XRD spectra of the EDMed Inconel 825 work surface obtained using CTT at parameters setting: [ $I_p=10A$ ;  $T_{on}=300\mu s$ ;  $\tau=85\%$ ]

In this work, XRD measurements have been performed using a Panalytical X'Pert PRO diffractometer with  $\text{CoK}_\alpha$  radiation ( $\lambda = 1.7906 \text{ \AA}$ ). The XRD patterns have been indexed with *X'Pert HighScore Plus* software containing PDF-2 files database.

As compared to unaffected (normal) Inconel 825 (Fig. 4.6.1), the peak pattern has appeared almost similar (approximately at similar positions; slightly sifted rightward along the  $2\theta$  axis) for the surface of the EDMed Inconel 825 specimen obtained by using NTT, and CTT (Fig. 4.6.2-4.6.3, respectively). Considering Full-Width-Half-Maximum (FWHM) of the peaks, it has been observed that grain refinement has taken place during EDM operation for the Inconel 825 work surface as compared to the 'normal' Inconel 825 parent material and that too irrespective of the condition of the tool material used (viz. NTT and CTT) during execution of EDM operation. Occurrence of peaks at similar positions has affirmed that no remarkable phase alteration has taken place as a result of EDM.

XRD analysis has revealed that 'normal' Inconel 825 basically has consisted of Iron-Nickel and Chromium based cubic solid solution matrix with precipitates of Copper Nickel [Reference Code: 47-1406 and Chemical Formula:  $\text{Cu}_{0.81}\text{Ni}_{0.19}$ ]. However, the peak pattern of unaffected Inconel 825 has exactly matched to that of Iron Nickel [Reference Code: 47-1405 and Chemical Formula:  $\text{Fe}_{0.64}\text{Ni}_{0.36}$ ] and also Iron Nickel [Reference Code: 18-0646 and Chemical Formula:  $\text{FeNi}$ ].

The XRD analysis from (Fig. 4.6.2) of the EDMed Inconel 825 work surface obtained by using NTT (at parameters setting:  $I_p=10\text{A}$ ,  $T_{\text{on}}=300\mu\text{s}$ ,  $\tau=85\%$ ) has identified presence of matrix of Iron Nickel [Reference Code: 47-1405 and Chemical Formula:  $\text{Fe}_{0.64}\text{Ni}_{0.36}$ ] with precipitates of Copper Nickel [Reference Code: 47-1406 and Chemical Formula:  $\text{Cu}_{0.81}\text{Ni}_{0.19}$ ] and Nickel Aluminum Titanium Carbide [Reference Code: 19-0035 and Chemical Formula:  $\text{Ni}_3(\text{Al, Ti})\text{C}$ ]. Such carbides are expected to be deposited along the grain boundaries of the specimen. Carbide formation can be attributed due to Carbon enrichment onto the machined zone during pyrolysis of the dielectric medium. Similar information has been retrieved from the XRD spectra of the EDMed Inconel 825 work surface obtained by using CTT (at parameters setting:  $I_p=10\text{A}$ ,  $T_{\text{on}}=300\mu\text{s}$ ,  $\tau=85\%$ ) as shown in Fig. 4.6.3.

**Table 4.2:** The variation of crystallite size ( $L$ ), and dislocation density ( $\delta$ ) for (1) ‘As received’ Inconel 825, (2) EDMed work surface of Inconel 825 obtained by using NTT, and (3) EDMed work surface of Inconel 825 obtained by using CTT

Sl. No.	Data of the highest intensity peak of XRD for different specimens	$2\theta (^{\circ})$	FWHM ( $\beta_L$ ) [rad]	Crystallite size ( $L$ ) [nm]
(1)	‘As received’ Inconel 825	50.8245	0.00294	60.686
(2)	EDMed work surface of Inconel 825 obtained by using NTT	50.9457	0.004134	43.1854
(3)	EDMed work surface of Inconel 825 obtained by using CTT	50.9736	0.013776	12.9593

**Table 4.2 (Continued)**

Sl. No.	Data of the highest intensity peak of XRD for different specimens	Miller indices [ $h, k, l$ ]	Inter planner spacing between the atoms ( $d$ ) [ $\text{\AA}$ ] (Obtained from <i>X'pert HighScore Plus Software</i> )	Lattice constant ( $a$ ) [ $\text{\AA}$ ]	Dislocation density ( $\delta$ ) $\times 10^4$
(1)	‘As received’ Inconel 825	[2 0 0]	2.08632	4.1726	3.9327
(2)	EDMed work surface of Inconel 825 obtained by using NTT	[2 0 0]	2.08135	4.1627	7.7853
(3)	EDMed work surface of Inconel 825 obtained by using CTT	[2 0 0]	2.08029	4.16058	86.4878

N.B:  $1\text{\AA} = 0.1\text{nm}$ ;  $1^{\circ} = 0.0175\text{rad}$

### ⇒ Computation of Crystallite Size, and Dislocation Density

The variation of crystallite size ( $L$ ), and dislocation density ( $\delta$ ) for (1) ‘as received’ Inconel 825, (2) EDMed work surface of Inconel 825 obtained by using NTT, and (3) EDMed work surface of Inconel 825 obtained by using CTT has been depicted in [Table 4.2](#). Considering a particular crystallographic plane in the direction [2 0 0] corresponding to the highest intensity peak selected from the peak pattern of XRD spectra, it has been observed that as compared to (1) ‘as received’ Inconel 825 (which has corresponded to

$L \sim 60.686\text{nm}$  and  $\delta \sim 3.9327 \times 10^{-4}$ ), (2) EDMed work surface of Inconel 825 obtained by using NTT and at parameters setting:  $I_p=10\text{A}$ ;  $T_{on}=300\mu\text{s}$ ;  $\tau=85\%$ , and (3) EDMed work surface of Inconel 825 obtained by using CTT and at similar parametric setting have exhibited sufficient grain refinement followed by decrease in crystallite size and consequently, increase in dislocation density. However, the degree of grain refinement has been found relatively high for the case of (3) EDMed Inconel 825 work surface obtained by using CTT ( $L \sim 12.9593\text{nm}$ ;  $\delta \sim 86.4878 \times 10^{-4}$ ) as compared to the case of (2) EDMed Inconel 825 work surface obtained by using NTT ( $L \sim 43.1854\text{nm}$ ;  $\delta \sim 7.7853 \times 10^{-4}$ ).

#### **4.3.3 Effects of Using CTT during EDM: Tool Wear and Tool Shape Retention Capability**

While comparing micro-hardness of the cryogenically treated Copper tool to that of normal tool electrode; it has been found that cryogenic treatment has improved hardness of the tool material due to substantial grain refinement and internal stress relief (refer to Table 4.1). Results have indicated that ‘normal’ Copper has shown micro-hardness values falling in the range  $\sim$  from 94.1 HV to 99.3 HV; whilst cryogenically treated Copper electrode has exhibited micro-hardness values falling in the range  $\sim$  from 114.2 HV to 119.8 HV. This has been found in good agreement of the comment made by (Lal et al., 2001; Leskovsek et al., 2006; Molinari et al., 2001) that CT of metals/alloys improves their hardness and consequently the wear resistance. Thus, tool wear of lesser extent is expected for the case of EDM using cryogenically treated tool.

Macroscopic view of the edge of the tool electrode (NTT and CTT, both) after EDM operations on Inconel 825 has been depicted in Fig. 4.7. Carbon deposition has been observed at the bottom surface as well as around the edge of the tool electrode during EDM operation.

This can be explained by the fact that during electrical discharge, pyrolysis of the dielectric medium takes place. Due to the pyrolysis of dielectric fluid (also called dielectric cracking), Carbon atoms come out and get deposited onto the bottom/edge of the tool (and also on the work surface) forming a blackish layer. However, as compared to normal tool, cryogenically treated tool electrode has exhibited presence of very thin layer of the deposited Carbon. As observed under optical microscope [Model No: OM-19;



Make: Radical Instruments; Country: India], the thickness of the deposited layer (after EDM experiments using NTT) has appeared as  $\sim 0.4871\text{mm}$  (Fig. 4.8a); whilst the deposited layer has been found to be very tiny ( $\sim 0.1203\text{ mm}$ ) after EDM operations with CTT (Fig. 4.8b).

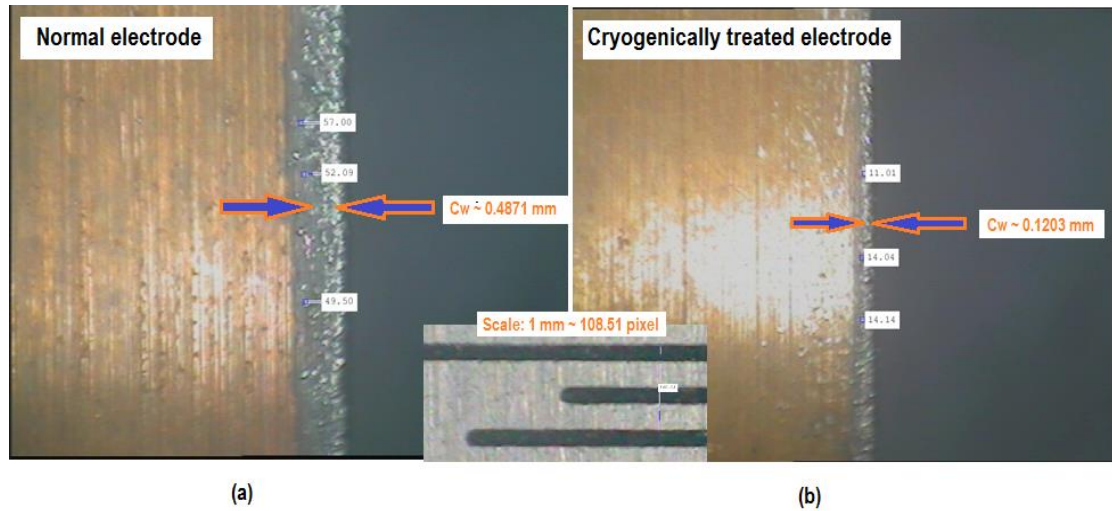


Fig. 4.7: Macroscopic view of the edge of (a) NTT (average thickness of deposited layer  $C_w = 0.4871\text{mm}$ ), and (b) CTT (average thickness of deposited layer  $C_w = 0.1203\text{mm}$ ) after EDM operation on Inconel 825 specimen

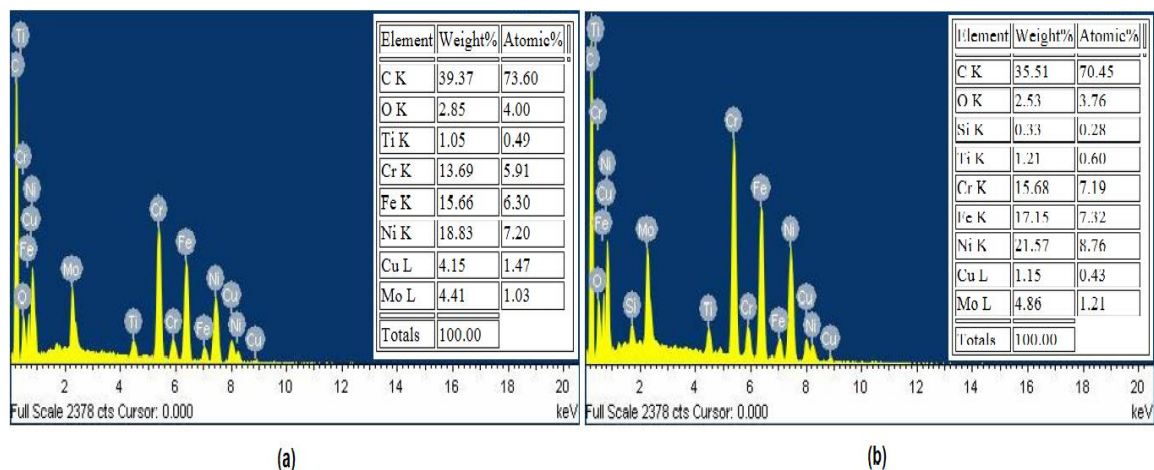


Fig. 4.8: EDS elemental spectra revealing chemical composition at the bottom surface of tool electrode: (a) NTT, and (b) CTT after EDM operation on Inconel 825 specimen

Cryogenic treatment of tool electrode has thus found advantageous due to less Carbon deposition (may be deposited material is in the form of Copper Carbide) at the bottom surface as well as along the edge of the electrode. This may be due to the fact that through cryogenic treatment, the electrical and thermal properties of tool material are substantially improved (Amini et al., 2012). Hence, electrode material can dissipate heat at a faster



case (than in the case of normal electrode) which in turn suppresses the tendency of the Carbon atoms to be deposited and thus restricts the formation of carbides. The improved thermal and electrical conductivity of the tool material is expected to improve tool life and thus to reduce electrode wear. Moreover, lesser extent of deposited Carbon layer along the electrode edge has been found favorable from the viewpoint of shape retention capability of the tool electrode. On the contrary, relatively thick Carbon layer has been found set down both at the bottom surface and also along the edge of NTT after EDM. Formation of such layer creates a barrier for the heat to be transmitted through the electrode material and thus more heat is required to execute the same for the progress of EDM operation. It imposes untoward effect on the tool electrode with excessive tool wear and reduced tool life. Shape retention capability of the tool electrode is also adversely affected. The phenomenon of formation of thin carbon layer at the bottom surface and edge of the cryogenically treated tool electrode has also been supported by the information (wt% of C) obtained from the EDS elemental spectra of the bottom surface of the tool electrodes (Fig. 4.8). It has clearly been noticed that as compared to NTT which has corresponded to 39.37 wt% Carbon at the bottom surface; the bottom surface of the CTT has corresponded to lesser extent of carbon content (35.51 wt%) owing to the formation of very thin deposited layer of Carbon (or possibly carbides).

## 4.4 Conclusions

The conclusions drawn from the aforesaid research have been summarized below.

- ▲ Deep cryogenic treatment of Copper tool electrode has attributed decrease in crystallite size resulting relatively more refined grain structure as compared to that of ‘non-treated’ Copper. Cryogenic treatment of the electrode material has resulted reduced (~12%) crystallite size and increased (~28%) dislocation density as compared to NTT material. Moreover, cryogenic treatment has resulted reduced residual stress and crystal imperfections; thus ensuring improved tool life and improved tool shape retention capability; and also reduced tool wear.
- ▲ Top surface morphology of the EDMed work surface of Inconel 825 has exhibited presence of crater mark, globules of debris, spherical deposition, pock marks (or chimneys), and surface cracks. However, the intensity of aforesaid surface irregularities has been found relatively less for the case of EDM with CTT as compared to the case NTT. Reduced crack density (and also the crack opening width)

for the case of EDM using CTT could be found beneficial for the fatigue life of the EDMed part component whilst subjected to service. For a constant setting of process parameters: [ $I_p=10A$ ;  $T_{on}=100\mu s$ ;  $\tau=85\%$ ], surface crack density has been found relatively less (~73%) for the EDMed Inconel 825 work surface obtained by using CTT, as compared to the case of NTT.

- ▲ The white layer has been found relatively thick onto the top surface of the EDMed Inconel 825 specimen obtained by using CTT. Increased heat conduction rate and thereby reduced tool wear has resulted decrease in energy density at the discharge gap. Due to smooth deposition of molten material, thicker white layer has been formed. Results have indicated that relatively thick white layer (~26%) has been attributed to the EDMed Inconel 825 specimen obtained by using CTT, as compared to the case of NTT for a common parameters setting: [ $I_p=6A$ ;  $T_{on}=300\mu s$ ;  $\tau=85\%$ ].
- ▲ As compared to 'normal' Inconel 825 parent material, EDS elemental spectra of EDMed work surface has exhibited higher Carbon content (wt%). This has been attributed due to the Carbon enrichment onto the work surface during pyrolysis of dielectric fluid. However, for the case of EDM using CTT, Carbon enrichment on the work surface has been found relatively less as compared to the case of EDM using NTT.
- ▲ As compared to 'normal' Inconel 825 work material, the average micro-hardness (obtained at the transverse-cut section of the EDMed specimen; approximately at the mid-depth of the thickness of white layer measured from the top surface) has been found more for EDM using NTT and CTT both. This may be explained due to thermo-electrical effect of EDM process which has resulted considerable grain refinement (decrease in crystallite size) within the work material. However, for the case of the EDMed specimen obtained using CTT, average micro-hardness has been found the highest. As compared to the EDMed work surface of Inconel 825 obtained by using NTT (at parameters setting:  $I_p=10A$ ;  $T_{on}=300\mu s$ ;  $\tau=85\%$ ), the EDMed Inconel 825 work surface obtained by CTT has exhibited relatively less crystallite size (~70% reduced) due to the formation of more refined grain structure. Hence, the EDMed Inconel 825 specimen obtained by using CTT has exhibited higher hardness values as compared to the case of NTT.
- ▲ As compared to 'normal' Inconel 825 work material, the residual stress has been found more for the EDMed specimen obtained using NTT and CTT both. However, for the case of EDM with CTT, evolution of residual stress within the EDMed

specimen has been found relatively less in magnitude as compared to the case of EDM using NTT.

- ▲ XRD spectra of EDMed Inconel 825 work surfaces have identified presence of Nickel-Iron solid solution with precipitates of carbides of varied extent. As compared to the EDMed surface obtained by using NTT; use of CTT has caused relatively more grain refinement. This has further been found in good agreement to the decrease in crystallite size and consequently the increase in dislocation density.
- ▲ In comparison with NTT, use of CTT has resulted relatively tiny layer of deposited Carbon at the bottom as well as edge of the tool electrode. This in turn has facilitated increased rate of heat transfer through the bulk of the electrode material. This is expected to cause reduction of tool wear, and hence, substantial improvements of tool shape retention capability. As compared to NTT, deposited Carbon (possibly carbides) layer of relatively less thickness (~75%) has been observed at the edge of the tool electrode for CTT, after execution of EDM operation.
- ▲ During electro-discharge machining operations, stresses are induced within the work material resulting in internal stresses, strains, voids and dislocations. The combined effect of those creates a barrier (resistance) to heat transfer through the bulk of the work material. This in turn, results in decreased rate of heat transfer through the work material; as a result, EDM performance is adversely affected. During cryogenic treatment of the work material, internal stresses and strains are substantially reduced with refinement of the grain structure. These effects are expected to favourably improve thermal conductivity of the work material thereby improving performance of the EDM process.

## **Chapter 5**

# **Electro-Discharge Machining of Cryogenically Treated Inconel 825 Using Copper Tool Electrode**

### **5.1 Coverage**

In the present work, an attempt is made to compare performance of electro-discharge machining (using Copper tool electrode) on deep cryogenically treated Inconel 825 workpiece to that of achieved on ‘as received’ work material. Effects of using Cryogenically Treated Workpiece (CTW) during EDM have been evaluated in terms of surface topographical features viz. Surface Crack Density (SCD) and White Layer Thickness (WLT) developed onto the top surface of the EDMed end product. It has been observed that as compared to EDM on Non-Treated Workpiece (NTW), use of CTW of Inconel 825 has ensured lesser extent of surface cracking and formation of relatively thick white layer. Experimental results have been interpreted with scientific relevance to the data obtained from EDS, XRD, residual stress, and micro-hardness tests. Effects of cryogenic treatment as well as thermo-electric effects imposed by the EDM operation on Inconel 825 work material have been analyzed from perspectives of metallurgical information like crystallite size, and dislocation density present within the EDMed test specimens as compared to ‘as received’ Inconel 825. Moreover, effects of cooling rate (used in cryogenic treatment of the workpiece) have also been investigated on influencing overall EDM performance on CTW of Inconel 825.

## 5.2 Scope of the Work

Extensive literature survey has been made to retrieve potential benefits of cryogenic treatment of hard and high temperature resistant work materials in order to improve thermal and electrical properties thus providing additional advantages during execution of the machining operation (Bensely et al., 2006; Das et al., 2007; Das et al., 2008; Akhbarizadeh et al., 2009; Gill and Singh, 2010; Patil and Tated, 2012; Kumar et al., 2014; Kumar et al., 2015; Khanna and Singh, 2016; Kumar et al., 2016a). Super alloy Inconel 825 being ‘*difficult-to-cut*’; it is expected that cryogenic processing (cryogenic treatment) of the work material may yield satisfactory EDM performance in terms of higher material removal rate, reduced tool wear, lower surface crack density, improved corner size machining accuracy etc. Literature provided substantial evidence of past research pursued by pioneers on emphasizing machinability of Inconel super alloys for electro-discharge machining; however, feasibility on using cryogenically treated Inconel workpiece (as compared to normal or non-treated workpiece) during EDM has rarely been studied.

Moreover, majority of the existing literature have considered MRR, Tool Wear Rate (TWR), and surface roughness (of the EDMed Inconel end product) as EDM performance features; the phenomenon of surface cracking and the formation white layer formation (followed by their quantitative measures like SCD and WLT) have not been extensively reported so far.

Cryogenic processing of work material (for example, Titanium alloy, D3 Steel etc.) has been reported in the literature to examine improvements in MRR, TWR etc. (Gill and Singh, 2010; Khanna and Singh, 2016); whilst it is felt that effect of the same on SCD, WLT, chemical composition of the machined surface, metallurgy of the machined zone, residual stress and micro-hardness of EDMed end product need to be investigated in detail, especially for EDM of cryogenically treated Inconel 825 work material. To this context, the objectives of the present work have been pointed out below.

1. To study the effects of cryogenic treatment of Inconel 825 work material on its electrical and thermal conductivities, aspects of surface metallurgy viz. phases present, crystallize size, dislocation density, extent of grain refinement etc. (as compared to ‘as received’ Inconel 825) that are expected to improve machinability of Inconel 825 during EDM operation. It is worth of investigating how use of

Cryogenically Treated Workpiece (CTW) facilitates EDM operation as compared to the case of EDM executed on Non-Treated Workpiece (NTW).

2. To study surface morphology of the EDMed Inconel 825 specimens (obtained through using NTW, and CTW both) as compared to that of ‘as received’ Inconel 825 specimen.
3. To examine chemical constituents, metallurgical aspects (phases present: matrix and precipitates, degree of grain refinement, crystallize size, dislocation density etc.), residual stress and micro-hardness of the EDMed Inconel 825 end product (obtained through using NTW as well as CTW) as compared to that of ‘as received’ Inconel 825.
4. To investigate effects of cooling rate (applied in the cryogenic processing cycle for CT of the work material) on machining performance during EDM on CTW, for a particular (constant) setting of process parameters.
5. Finally, to infer whether use of CTW of Inconel 825 proves beneficial to facilitate EDM operation and thereby, to improve overall machinability of Inconel 825.

## **5.3 Results and Discussion**

### **5.3.1 Effects of Cryogenic Treatment of Inconel 825 Work Material**

In this section, effects of deep cryogenic treatment on Inconel 825 work material have been analyzed in perspectives of residual stress and micro-hardness test data. It has been expected that remarkable grain refinement taking place due to cryogenic treatment of the workpiece resulting reduced crystallite size and consequently higher dislocation density. Such grain refinement has been expected to help in removing crystal imperfections, stress lines, voids and dislocations. These in turn have been expected to contribute towards improving thermal as well as electrical conductivities of Inconel 825 work material.

As compared to ‘as received’ Inconel 825 (i.e. NTW) which has corresponded to compressive residual stress (-413.0 to -261.4 MPa) and micro-hardness (in the range ~ 235.6 HV to 242.1 HV); deep cryogenically treated Inconel 825 (CTW) has exhibited presence of residual stress (tensile in nature) falling in the range ~ (297.4 to 494.6 MPa) and has shown higher micro-hardness value (range~ 265.5HV to 275.0 HV). This has been found in support of the claim that during cryogenic treatment of the work material significant grain refinement taking place through relief of internal stresses inherently present within the ‘as received’ work material of Inconel 825.

### 5.3.2 Effects of using Cryogenically Treated Workpiece (as Compared to Normal Workpiece) during EDM on Inconel 825

#### 5.3.2.1 Surface Topography: Emphasis on Surface Cracking and Formation of White Layer

As compared to Inconel 825 ‘as received’, the EDMed work surface of Inconel 825 specimen has exhibited poor surface integrity in terms of surface morphology depending on the condition of the workpiece (i.e. NTW, and CTW) employed. SEM micrographs taken at the top surface of the EDMed Inconel 825 specimens have exhibited presence of crater marks, globules of debris, pockmarks or chimneys, surface cracks as well as white layer. However, intensity of such surface irregularities has been found largely dependent on the condition of the work material used i.e. NTW/CTW.

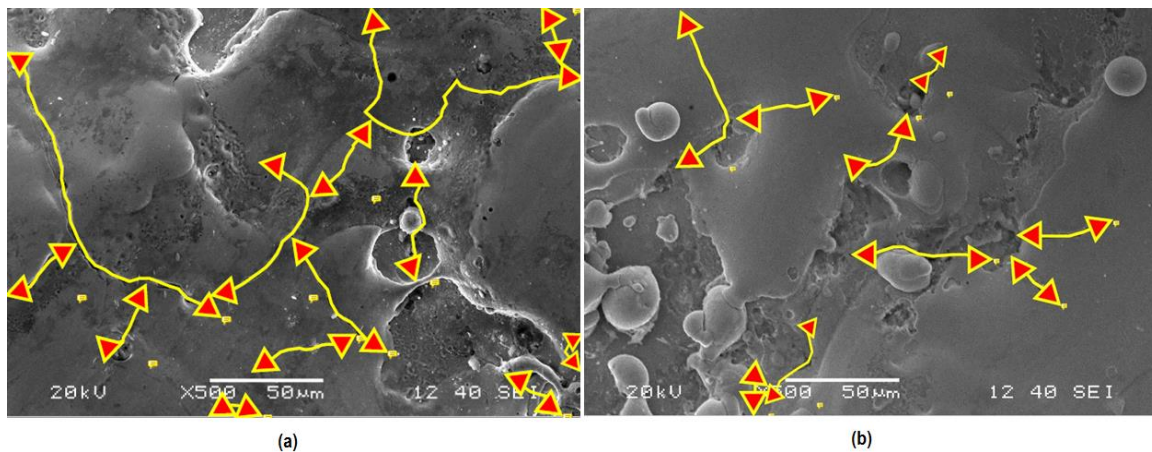


**Fig. 5.1.1:** SEM micrographs revealing existence of surface cracks on the machined Inconel 825 surface obtained through EDM using (a) NTW ( $SCD \sim 0.0155 \mu\text{m}/\mu\text{m}^2$ ), and (b) CTW ( $SCD \sim 0.0080 \mu\text{m}/\mu\text{m}^2$ ), for a constant parameters setting i.e. [ $I_p=10\text{A}$ ;  $T_{on}=100\mu\text{s}$ ;  $\tau=85\%$ ]

SEM micrographs revealing existence of surface cracks on the machined Inconel 825 work surface obtained through EDM using (a) NTW, and (b) CTW, for a constant parameters setting i.e. [ $I_p=10\text{A}$ ;  $T_{on}=100\mu\text{s}$ ;  $\tau=85\%$ ] have been depicted in Fig. 5.1.1-5.1.2. It has clearly been understood that cryogenic treatment of the work material has appeared beneficial since intensity of surface cracks developed on the EDMed work surface of Inconel 825 has been found lesser as compared to that obtained through EDM using NTW. Since presence of surface cracks is highly unappealing from the perspective of the product’s fatigue life whilst subjected to practical application field; reduced crack density thus obtained, strongly motivates application of cryogenic treatment of the workpiece in the context of EDM on Inconel 825 work material.

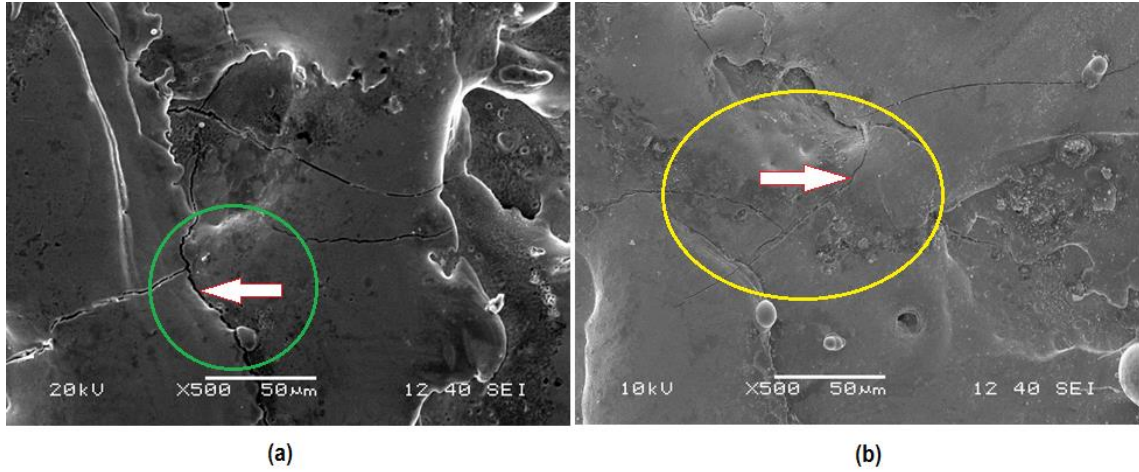


**Fig. 5.1.2:** SEM micrographs comparing the severity of crack formation (crack opening width,  $C_w$ ) at EDMed Inconel 825 work surface obtained by using (a) NTW, and (b) CTW at parameters setting: [ $I_p=10A$ ;  $T_{on}=300\mu s$ ;  $\tau=85\%$ ]

Literature depicts that cryogenic treatment improves electrical as well as thermal conductivity of the work material (as per *Wiedemann-Franz-Lorenz Law*, shown in Eq. 5.1) which in turn facilitates increased rate of heat transfer through the bulk of the work material as compared to the case of EDM with NTW. This results evolution of thermal stress (of relatively less magnitude) within the specimen; and, hence severity of cracking gets suppressed.

The *Wiedemann-Franz-Lorenz Law* states that for all metals at not too low temperature, the ratio of the thermal conductivity  $K$  to the electrical conductivity  $\sigma$  is directly proportional to the temperature  $T$  along with the constant of proportionality  $L$ , whose value is independent of the particular metal (Isaak and Reitz, 2008).

$$\frac{K}{\sigma} = LT \quad (5.1)$$

Theoretically, the proportionality constant, known as the *Lorenz Number*, is equal to:

$$L = \frac{K}{\sigma T} = 2.44 \times 10^{-8} \text{ W}\Omega\text{K}^{-2}$$

SEM micrographs revealing existence of white layer developed onto the top surface of the machined Inconel 825 obtained through EDM using (a) NTW, and (b) CTW, for a constant parameters setting [ $I_p=6A$ ;  $T_{on}=300\mu s$ ;  $\tau=85\%$ ] have also been depicted in Fig. 5.2.



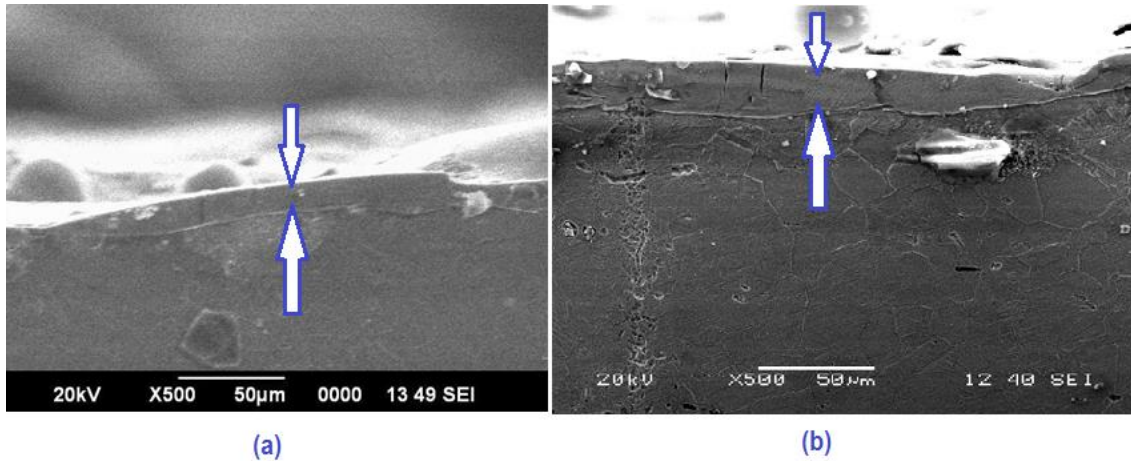


**Fig. 5.2:** SEM micrographs revealing existence of white layer on the machined Inconel 825 surface obtained through EDM using (a) NTW (WLT~14.14 $\mu$ m), and (b) CTW (WLT~21.692 $\mu$ m) for a constant parameters setting i.e. [ $I_p$ =6A;  $T_{on}$ =300 $\mu$ s;  $\tau$ =85%]

It has been noticed that relatively thick white layer has been attributed for the EDMed specimens using CTW as compared to the EDMed samples obtained by using NTW. This may be due to the enhancement of heat dissipation capacity of the work material during cryogenic treatment which results in increased heat transfer rate through the bulk of the parent material. Due to increased rate of heat transfer, molten material gets smoothly cooled (at faster rate) and uniformly deposited onto the top surface of the machined zone. The occurrence of which, in turn, increases thickness of the deposited layer as compared to the case of EDM using NTW. Smooth deposition of the molten material also results in evolution of residual stress of lesser extent and thus reduces the likelihood of occurrence of surface cracks to some extent.

Next to white layer, usually a zone is expected to appear in which no melting takes place but it is greatly affected by the heat energy generated during the EDM process. This zone corresponds to micro-structural alternation (as compared to the machined zone as well as base material) is denoted as heat affected zone. HAZ may consist of several layers; however, they are not prominently distinguishable. The transition between white layer and HAZ may clearly be visualized under SEM; whereas, it is very difficult to identify the demarcation line between the HAZ and the base material. In the present study, HAZ has not been clearly visualized from the SEM micrographs shown herein.

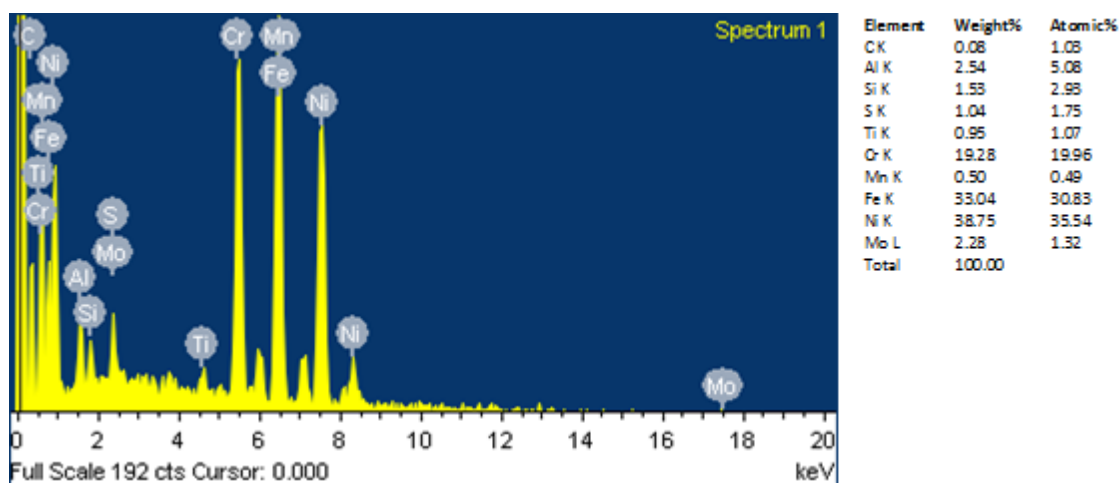


Fig. 5.3.1: EDS elemental spectra revealing chemical composition of 'as received' Inconel 825

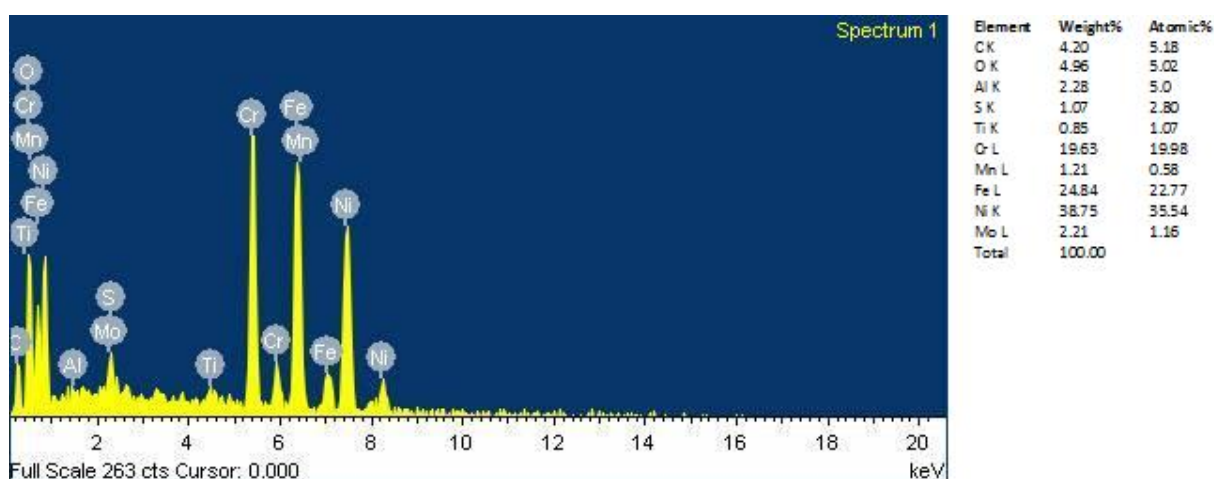


Fig. 5.3.2: EDS elemental spectra revealing chemical composition of the EDMed Inconel 825 work surface obtained using NTW at parameters setting: [ $I_p=10A$ ;  $T_{on}=300\mu s$ ;  $\tau=85\%$ ]

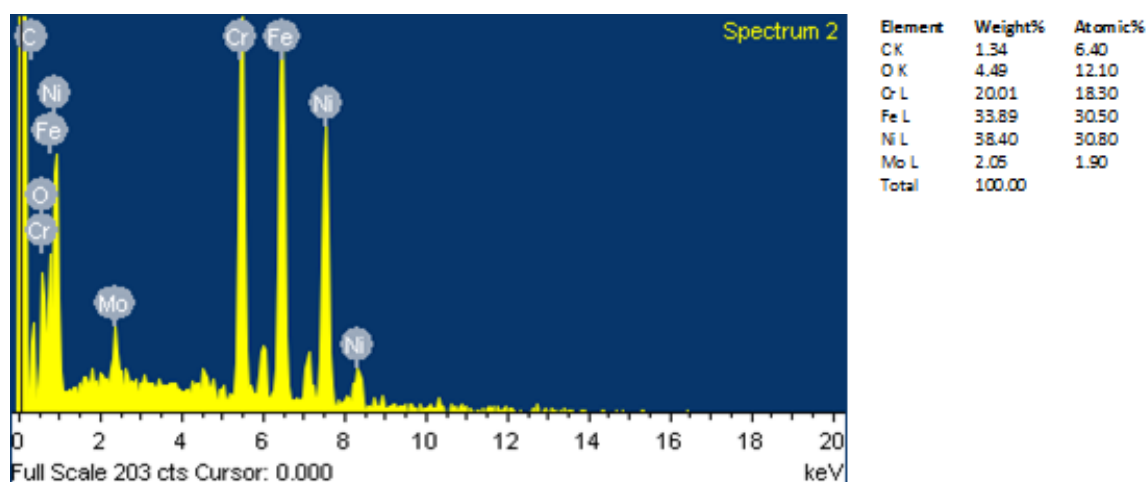


Fig. 5.3.3: EDS elemental spectra revealing chemical composition of the EDMed Inconel 825 work surface obtained using CTW at parameters setting: [ $I_p=10A$ ;  $T_{on}=300\mu s$ ;  $\tau=85\%$ ]

### 5.3.2.2 EDS Analysis and Micro-Hardness Test

Energy Dispersive X-Ray Spectroscopy (EDS) elemental spectra revealing chemical composition (wt%) of (1) 'as received' Inconel 825, the EDMed work surfaces of Inconel 825 obtained through using (2) NTW, and (3) CTW (for a constant setting of EDM parameters i.e.  $I_p=10A$ ,  $T_{on}=300\mu s$ ,  $\tau=85\%$ ) have been shown in [Fig. 5.3.1-5.3.3](#), respectively. It has been observed that Carbon content has been increased during EDM due to Carbon enrichment onto the machined zone while dielectric cracking has been incurred. The EDM oil (used as dielectric medium) being a hydrocarbon; during spark discharge pyrolysis of dielectric takes place. Thus, carbon gets deposited on the machined zone leading to increase in Carbon content of the EDMed work surface as compared to the 'as received' parent material. EDS analysis has exhibited that as compared to 'as received' Inconel 825 (0.08 wt% C), Carbon content of the EDMed Inconel 825 work surface (obtained at parameters setting:  $I_p=10A$ ,  $T_{on}=300\mu s$ ,  $\tau=85\%$ ) has been increased to 4.2% (for the case of EDM using NTW), and 1.54% (for the case of EDM using CTW).

It has been observed that as compared to EDM with NTW, use of cryogenically treated workpiece (i.e. CTW) has resulted in lesser extent of Carbon enrichment onto the machined zone which has been found beneficial. Since the topmost layer of the EDMed work surface is detrimental for the service life of the part component when subjected to fatigue loading. Surface cracks do initiate at this surface. Thus, post machining operation is indeed a necessity to remove such unwanted layer. Lesser Carbon content of this layer corresponds to lower hardness values; thus, facilitating easy and economic removal of the same. The decrement of Carbon content onto the top surface of the EDMed Inconel 825 (obtained through using CTW) as compared to that obtained by NTW can be attributed to the fact that cryogenic processing improves electrical and thermal properties of the work material. Hence, as compared to normal EDM, large crater is formed resulting high volumetric material removal rate. The rate of material removal being more than that of Carbon enrichment (deposition) onto the machined zone (due to dielectric cracking), wt% of Carbon tends to decrease.

The reduced Carbon content of the EDMed work surface of Inconel 825 (obtained by using CTW) may be due to refined microstructure of the work material, which restricts the penetration of Carbon atoms into the surface being machined; thus suppressing the tendency to carbide formation and its precipitation over the machined zone. The results of EDS analysis has been found in good agreement of the micro-hardness test data.

As compared to ‘as received’ Inconel 825 (micro-hardness in the range of ~ 235.0 HV to 242.1 HV) and CTW of Inconel 825 (micro-hardness in the range of ~ 265.5 HV to 275.0 HV), the EDMed work surface (obtained at parameters setting:  $I_p=10A$ ,  $T_{on}=300\mu s$ ,  $\tau=85\%$ ) has exhibited higher hardness values falling in the range of ~ (568.0 HV to 632.8 HV), and ~ (739.2 HV to 800.6 HV) for two different cases of EDM using viz. NTW, and CTW, respectively.

### **5.3.2.3 Analysis of Residual Stress**

Cryogenic treatment of work material imposes beneficial effects mainly due to relief of internal stresses. ‘As received’ material is subjected to internal residual stresses inherently attributed during phase transformation. When molten material is transformed from liquid phase to solid phase, solidification starts from the surfaces as well as edges of the mould cavity at a faster rate than the interior part of the mould. This is because these areas are cooled down quickly. During solidification, dendritic (and columnar shaped) crystals first appear at the surface and edges; then, they grow in size gradually towards inner part of the mould. When, growth of a dendrite is restricted by another one, a stress line is generated which results in occurrence of dislocations, voids, crystal imperfections, slip, twinning etc. Moreover, when the solidified cast product (in the form of billet, plat etc.) is subjected to heat treatment (to normalize its mechanical properties like tensile strength, hardness, impact strength etc.) and subsequent rolling, forging, machining operations, additional stress is evolved within the material. The aggregated effect of such residual stresses appears detrimental in perspectives of fatigue life of the part component as residual stress is the prime cause for development of cracks. Cryogenic treatment of workpiece reduces induced residual stresses by removing dislocations, voids, and other defects; thus, providing a more refined grain structure. Such grain refinement is expected to increase hardness of the cryogenically treated material and remarkably improves wear resistance.

Therefore, it is well understood that EDM process parameters along with particular workpiece (viz. NTW, and CTW, considered in the present case) should carefully be selected to suppress possible detrimental effect of the induced residual stress of high magnitude. It has been observed that ‘as received’ Inconel 825 has corresponded to the compressive residual stress (-413.0 to -261.4 MPa). The residual stress of tensile nature has been attributed to the EDMed specimen of Inconel 825 (obtained at constant parameters setting:  $I_p=10A$ ,  $T_{on}=300\mu s$ ,  $\tau=85\%$ ) for the case of EDM using NTW

(Range~868.7 to 1492.3 MPa), and CTW (Range~609.4 to 970.8 MPa). As cryogenic treatment of the work material results in refinement of grain structure (due to stress relief); the EDMed Inconel 825 obtained by using CTW has exhibited presence of less residual stress as compared to that using NTW.

#### **5.3.2.4 XRD Tests: Metallurgical Analyses (Phase Information, Crystallite Size, and Dislocation Density of the EDMed work surface of Inconel 825)**

##### **⇒ Phase Analysis**

X-Ray Diffraction (XRD) spectra inferring metallurgical aspects of ‘as received’ Inconel 825, and the EDMed surface of Inconel 825 obtained by using NTW, and CTW (for a constant setting of EDM parameters i.e.  $I_p=10A$ ,  $T_{on}=300\mu s$ ,  $\tau=85\%$ ) have been provided in Fig. 5.4.1-5.4.3, respectively. Identification of different phases along with relevant metallurgical information has been retrieved from the analysis of these XRD patterns through *X’Pert High Score* software.

As compared to the ‘as received’ parent material (Fig. 5.4.1), peak patterns have appeared almost similar (approximately at similar positions; slightly sifted rightward along the  $2\theta$  axis) for the EDMed Inconel 825 work surfaces obtained by using NTW, and CTW (Fig. 5.4.2-5.4.3, respectively). Considering Full-Width-Half-Maximum (FWHM) of the peaks, it has been observed that grain refinement has taken place during EDM operation for the EDMed work surface as compared to the ‘as received’ Inconel 825; and that too, irrespective of the workpiece condition used (viz. NTW and CTW). Occurrence of peaks at similar positions has affirmed that no remarkable phase alteration has taken place as a result of EDM.

XRD analysis has revealed that ‘as received’ Inconel 825 basically has consisted of Iron-Nickel and Chromium based Cubic solid solution matrix with precipitates of Copper Nickel [Reference Code: 47-1406 and Chemical Formula:  $Cu_{0.81}Ni_{0.19}$ ]. However, the peak pattern of unaffected Inconel 825 almost has exactly matched to that of Iron Nickel [Reference Code: 47-1405 and Chemical Formula:  $Fe_{0.64}Ni_{0.36}$ ] and also Iron Nickel [Reference Code: 18-0646 and Chemical Formula:  $FeNi$ ].

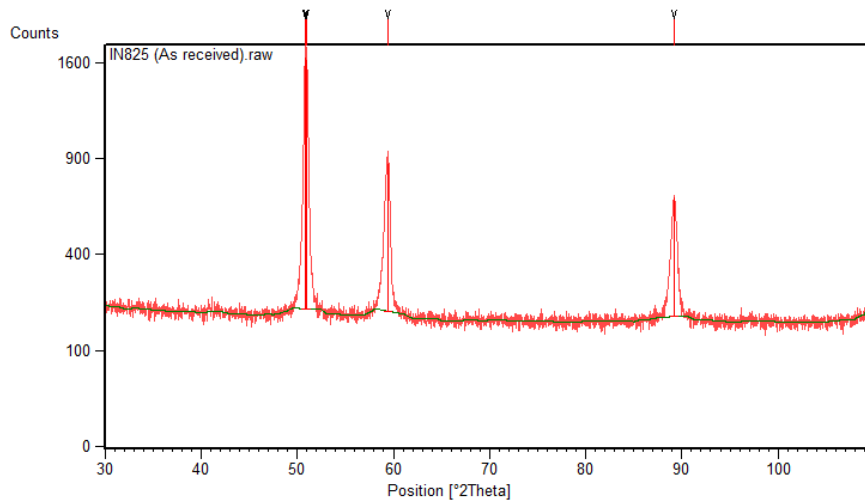


Fig. 5.4.1: XRD spectra of 'as received' Inconel 825

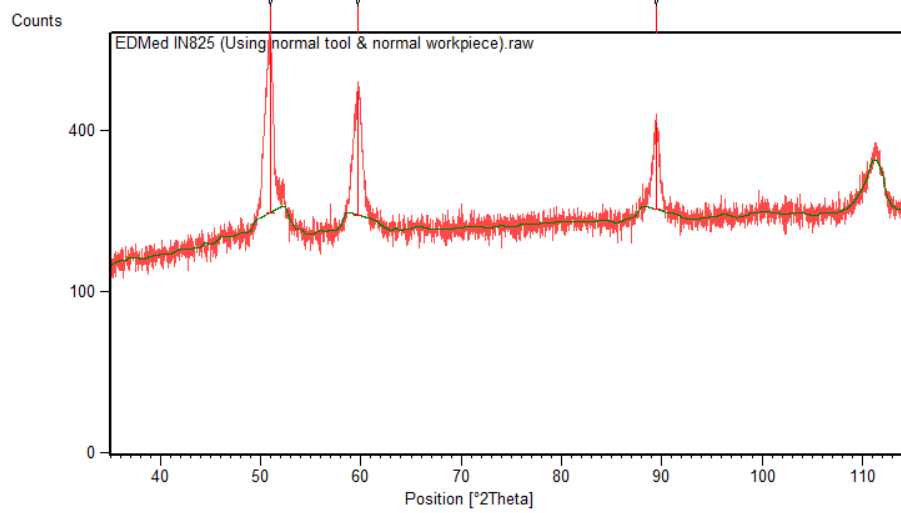


Fig. 5.4.2: XRD spectra of the EDMed surface of Inconel 825 obtained at parameters setting:  $[I_p=10A; T_{on}=300\mu s; \tau=85\%]$  using NTW

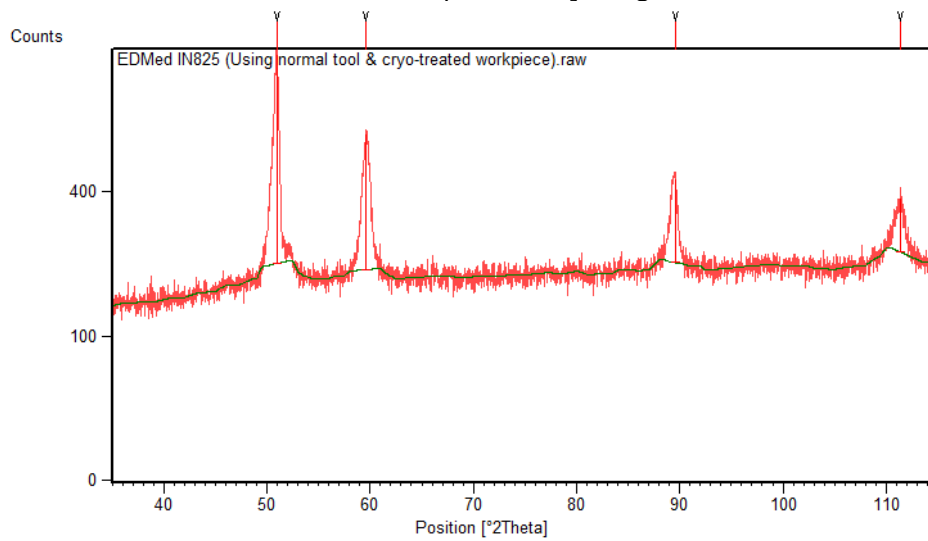


Fig. 5.4.3: XRD spectra of the EDMed surface of Inconel 825 obtained at parameters setting:  $[I_p=10A; T_{on}=300\mu s; \tau=85\%]$  using CTW

The XRD analysis from [Fig. 5.4.2](#) of the EDMed Inconel 825 work surface obtained by using NTW (at parameters setting:  $I_p=10A$ ,  $T_{on}=300\mu s$ ,  $\tau=85\%$ ) has identified presence of matrix of Iron Nickel [Reference Code: 47-1405 and Chemical Formula:  $Fe_{0.64}Ni_{0.36}$ ] with precipitates of Copper Nickel [Reference Code: 47-1406 and Chemical Formula:  $Cu_{0.81}Ni_{0.19}$ ] and Nickel Aluminum Titanium Carbide [Reference Code: 19-0035 and Chemical Formula:  $Ni_3(Al, Ti)C$ ]. Such carbides have been expected to be deposited along the grain boundaries of the specimen. Carbide formation can be attributed due to Carbon enrichment onto the machined zone during pyrolysis of the dielectric medium. Similar information has been retrieved from the XRD spectra of the Inconel 825 work surface obtained (at parameters setting:  $I_p=10A$ ,  $T_{on}=300\mu s$ ,  $\tau=85\%$ ) by using CTW ([Fig. 5.4.3](#)). However, in case of EDM using CTW (at parameters setting:  $I_p=10A$ ,  $T_{on}=300\mu s$ ,  $\tau=85\%$ ), precipitates of Copper Nickel [Reference Code: 09-0205 and Chemical Formula:  $Cu_{3.8}Ni$ ] has also been observed.

Additionally, XRD peak patterns have been analyzed further to investigate the effects of cryogenic treatment of the work material on quantitative metallurgical information like Crystallite Size ( $L$ ) and Dislocation density ( $\delta$ ) of the test specimens. The extent of grain refinement and the effect imposed thereof on crystal/grain structure of the work surface (obtained under different conditions of EDM) has been interpreted mathematically with relevance to the computed data.

The crystallite size ( $L$ ) for each of the specimens viz. (1) ‘as received’ Inconel 825, (2) cryogenically treated Inconel 825, the EDMed Inconel 825 work surface obtained by using (3) NTW, and (4) CTW at parametric combination: [ $I_p=10A$ ;  $T_{on}=300\mu s$ ;  $\tau=85\%$ ] has been calculated from X-ray diffraction profiles of strong reflections with intensity % by measuring the Full-Width-Half-Maximum (FWHM). The *Scherrer* equation has been applied for computing the crystallite size; similarly, dislocation density has been computed using. A sample computation has been given in the [APPENDIX](#).

The variation of crystallite size ( $L$ ), and dislocation density ( $\delta$ ) for (1) ‘as received’ Inconel 825, (2) Cryogenically treated Inconel 825 (before machining), (3) the EDMed work surface of Inconel 825 obtained by using, and (4) the EDMed work surface of Inconel 825 obtained by using CTW has been depicted in [Table 5.1](#).



**Table 5.1:** The variation of crystallite size ( $L$ ), and dislocation density ( $\delta$ ) for (1) ‘as received’ Inconel 825, (2) Cryogenically treated Inconel 825 prior to EDM, (3) EDMed work surface of Inconel 825 obtained by using NTW, and (4) EDMed work surface of Inconel 825 obtained by using CTW

Sl. No.	Data of the highest intensity peak of XRD for different specimens	$2\theta (^{\circ})$	FWHM ( $\beta_L$ ) [rad]	Crystallite size ( $L$ ) [nm]
(1)	‘As received’ Inconel 825	50.8245	0.00294	60.686
(2)	‘Cryogenically treated’ Inconel 825 (before machining) (Refer to Fig. 4.11a)	50.9423	0.0041335	43.169
(3)	EDMed work surface of Inconel 825 obtained by using NTW	50.9457	0.004134	43.1854
(4)	EDMed work surface of Inconel 825 obtained by using CTW	50.9653	0.004821	37.0276

**Table 5.1 (Continued)**

Sl. No.	Data of the highest intensity peak of XRD for different specimens	Miller indices [ $h, k, l$ ]	Inter planner spacing between the atoms ( $d$ ) [ $\text{\AA}$ ] (Obtained from <i>X'pert HighScore Software</i> )	Lattice constant ( $a$ ) [ $\text{\AA}$ ]	Dislocation density ( $\delta$ ) $\times 10^4$
(1)	‘As received’ Inconel 825	[2 0 0]	2.08632	4.1726	3.9327
(2)	‘Cryogenically treated’ Inconel 825 (before machining)	[2 0 0]	2.08148	4.16296	7.78695
(3)	EDMed work surface of Inconel 825 obtained by using NTW	[2 0 0]	2.08135	4.1627	7.7853
(4)	EDMed work surface of Inconel 825 obtained by using CTW	[2 0 0]	2.08060	4.1612	10.5919

While comparing data of the highest intensity peaks of the XRD spectra (Table 5.1) for (1) ‘as received’ Inconel 825, and (2) Cryogenically treated Inconel 825, it has been found that grain refinement has taken place resulting reduced crystallite size ( $L \sim 43.169\text{nm}$ ) for the cryogenically treated work surface than that of ‘as received’ Inconel 825 ( $L \sim 60.686\text{nm}$ ) at a particular crystallographic plane in the direction [2 0 0]. Such grain refinement has been attributed to the increase in dislocation density



$(\delta \sim 7.78695 \times 10^{-4})$  for the EDMed specimen surface as compared to the case of ‘as received’ Inconel 825 corresponding to the value of dislocation density  $(\delta \sim 3.9327 \times 10^{-4})$ .

While comparing data of the highest intensity peaks of the XRD spectra (Table 5.1) for (1) ‘as received’ Inconel 825, and (3) the EDMed work surface of Inconel 825 obtained by using NTW (at parameters setting:  $I_p=10A$ ;  $T_{on}=300\mu s$ ;  $\tau=85\%$ ), it has been found that grain refinement has taken place during EDM operation which has resulted reduced crystallite size ( $L \sim 43.1854 \text{ nm}$ ) for the EDMed work surface than that of ‘as received’ Inconel 825 ( $L \sim 60.686 \text{ nm}$ ) at a particular crystallographic plane in the direction  $[2\ 0\ 0]$ . Such grain refinement has been attributed to the increase in dislocation density  $(\delta \sim 7.7853 \times 10^{-4})$  for the EDMed specimen surface as compared to the case of ‘as received’ Inconel 825 corresponding to the value of dislocation density  $(\delta \sim 3.9327 \times 10^{-4})$ .

Similar observation has been made whilst comparing the highest intensity peak pattern of XRD spectra of (1) ‘as received’ Inconel 825, and (4) the EDMed work surface of Inconel 825 obtained by using CTW (at parameters setting:  $I_p=10A$ ;  $T_{on}=300\mu s$ ;  $\tau=85\%$ ), (refer to Table 5.1). Significant grain refinement has been found taking place for the EDMed work surface of cryogenically treated Inconel 825 (corresponding to lower crystallite size i.e.  $L \sim 37.0276 \text{ nm}$  and consequently higher dislocation density i.e.  $\delta \sim 10.5919 \times 10^{-4}$ ) for the particular crystallographic plane in the direction  $[2\ 0\ 0]$ . Also, for the crystallographic plane in the direction  $[2\ 0\ 0]$ , extent of grain refinement has been found much more for the EDMed work surface of cryogenically treated Inconel 825 (obtained through EDM by using CTW) with respect to the case of EDMed work surface of Inconel 825 obtained through NTW. It has also been found clear that decrease in crystallite size has appeared as the strong indication of occurrence of grain refinement followed by the increased dislocation density. The variation of crystallite size ( $L$ ) with respect to different dislocation density ( $\delta$ ) has been graphically presented in Fig. 5.5.

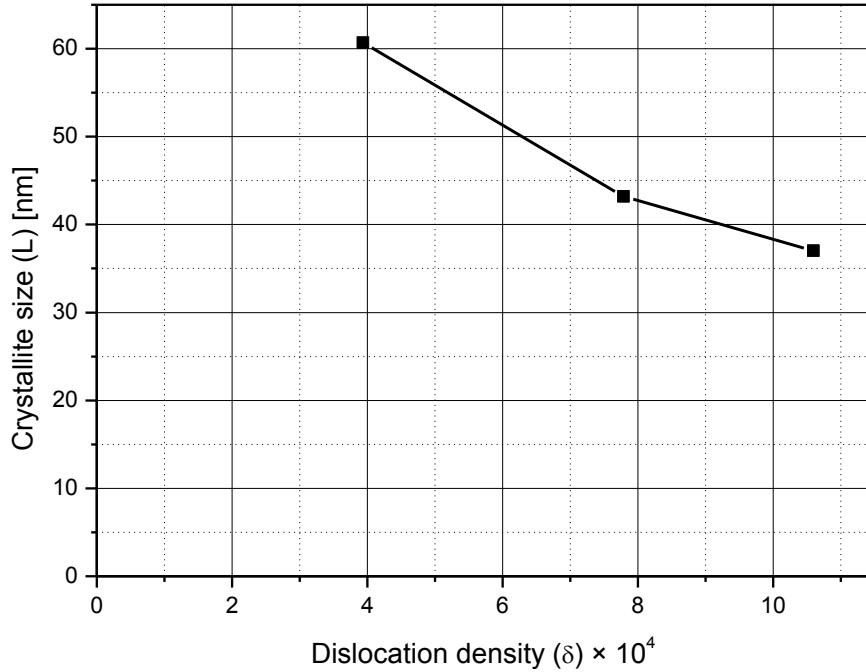


**Fig. 5.5:** Variation of crystallite size ( $L$ ) with respect to dislocation density ( $\delta$ ) for ‘As received’ Inconel 825, the EDMed work surface of Inconel 825 obtained by using NTW, and the EDMed work surface of Inconel 825 obtained by using CTW

#### 5.3.2.5 Effects of Cooling Rate (During DCT of workpiece) on EDMed surface of Inconel 825

Effects of cooling rate (ramp-down and same also for ramp-up) during cryogenic treatment of the work material has been investigated on influencing the extent of Carbon enrichment onto the machined surface of Inconel 825 during EDM using NTCTW. It has already been stated that EDM experiments as discussed in Chapter 2 (Phase II, Fig. 2.7), have been conducted considering cryogenically treated workpiece; where, cryogenic treatment has been performed at a cooling rate  $1^{\circ}\text{C}/\text{min}$ .

An additional experiment has been performed later for EDM of Inconel 825 using CTW in which cooling rate of  $0.5^{\circ}\text{C}/\text{min}$  has been set in the cryogenic treatment cycle executed for the workpiece. It has been observed that decrease in cooling rate in turn has reduced Carbon content of the EDMed work surface of Inconel 825. The weight percentage of Carbon has been observed as 1.34% (Fig. 5.3.3) for the EDMed surface obtained at parameters setting: [ $I_p=10\text{A}$ ;  $T_{on}=300\mu\text{s}$ ;  $\tau=85\%$ ] by using CTW; in this case the cooling rate of  $1^{\circ}\text{C}/\text{min}$  has been set during cryogenic treatment of the workpiece. On the

contrary, 1.29% (by weight) Carbon content has been found in the EDS elemental spectra of the EDMed Inconel 825 work surface obtained at the similar parametric condition of [ $I_p=10A$ ;  $T_{on}=300\mu s$ ;  $\tau=85\%$ ] whilst using CTW that too obtained by setting  $0.5^\circ C/min$  cooling rate in the cryogenic treatment cycle of the workpiece (Fig. 5.6).

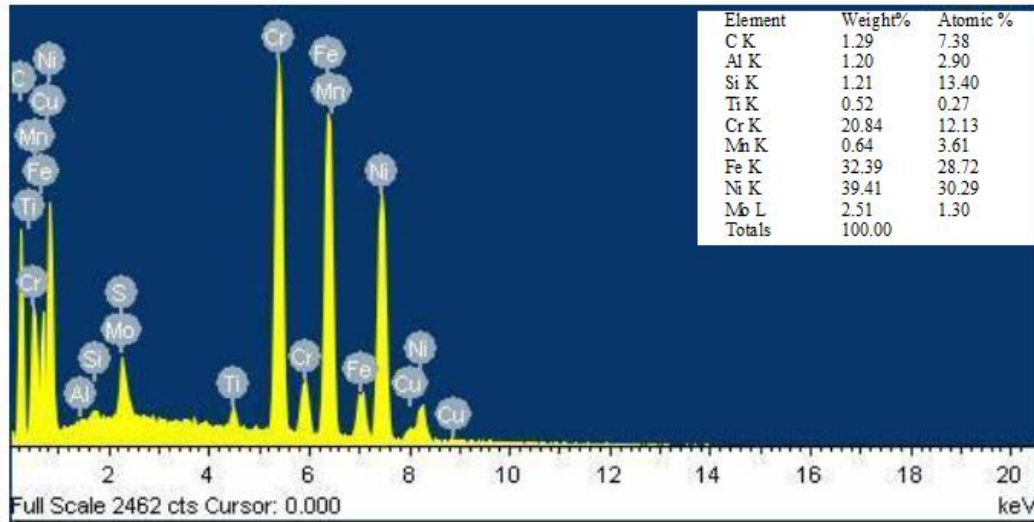
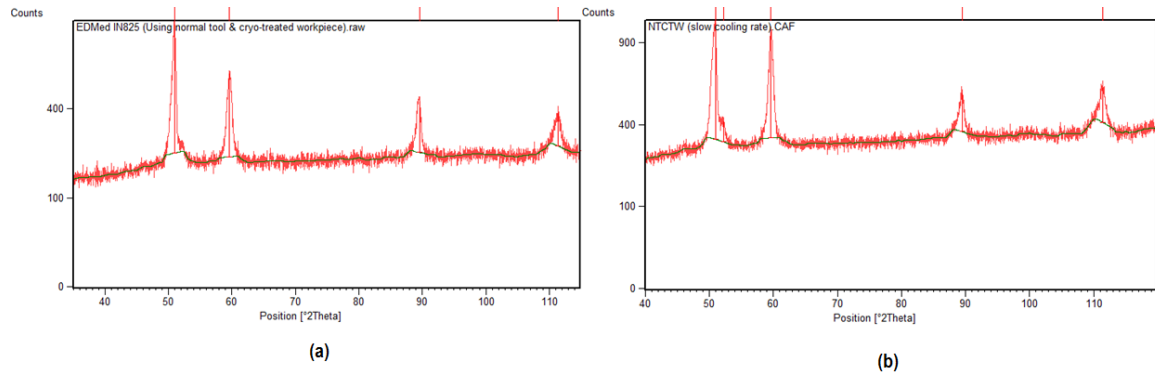


Fig. 5.6: EDS elemental spectra revealing chemical composition of the EDMed Inconel 825 surface obtained using CTW (ramp down rate during cryogenic treatment =  $0.5^\circ C/min$ ) at parameters setting: [ $I_p=10A$ ;  $T_{on}=300\mu s$ ;  $\tau=85\%$ ]

XRD spectra providing metallurgical information of the EDMed work surface of Inconel 825 obtained at parameters setting: [ $I_p=10A$ ;  $T_{on}=300\mu s$ ;  $\tau=85\%$ ] using CTW has been shown herein; in which (a) fast cooling rate ( $1^\circ C/min$ ) and (b) slow cooling rate ( $0.5^\circ C/min$ ) has been applied during cryogenic treatment cycle of the work material (Fig. 5.7a-5.7b). As compared to the EDMed workpiece using CTW (considering CT at  $1^\circ C/min$  cooling rate) (Fig. 5.7a), peak patterns have appeared almost similar for the surface of the EDMed Inconel 825 obtained by using CTW, considering slow cooling rate of  $0.5^\circ C/min$  in the CT cycle (Fig. 5.7b). Occurrence of peaks approximately at similar positions has confirmed that no significant phase alteration has taken place as a result of variation of cooling rate during CT of the workpiece prior to conducting EDM operations.



**Fig. 5.7:** XRD spectra of the EDMed surface of Inconel 825 obtained at parameters setting: [ $I_p=10A$ ;  $T_{on}=300\mu s$ ;  $\tau=85\%$ ] using CTW for (a) fast cooling rate ( $1^\circ C/min$ ) and (b) slow cooling rate ( $0.5^\circ C/min$ )

However, the XRD spectra for EDMed work surface of cryogenically treated Inconel 825 (for slow cooling in the CT cycle) has exhibited occurrence of an extra peak (of very less intensity) at  $52.2188^\circ$  at  $2\theta(^{\circ})$  axis. This may be due to precipitation of (i) Manganese Carbide Silicon (Reference Code: 71-0000 and Chemical formula:  $Mn_{2.26}Si_{5.4}C_4$ ), (ii) Manganese Silicon Carbide (Reference Code: 71-0029 and Chemical formula:  $Mn_{7.53}Si_{1.8}C_{1.33}$ ), and Aluminum Nickel Carbide (Reference Code: 29-0058 and Chemical formula:  $AlNi_3C_{0.5}$ ) of very less magnitude. This phenomenon may be attributed due to the cryogenic treatment (with slow cooling) of the work material combined with the effect of EDM, similar to the case of precipitation of micro-fine ‘eta carbides’ in case of cryogenic treatment of tool steels.

Considering Full-Width-Half-Maxima (FWHM) of the peaks, it has been observed that grain refinement of greater extent has taken place for the case of EDM using CTW with slow cooling rate. During CT of workpiece with slow cooling rate, the effect of grain refinement has become predominant as compared to the case of fast cooling. Additional grain refinement has been found attributed to the workpiece due the thermal effect of the EDM process itself. Hence, it has been viewed that for a common setting of process parameters i.e. [ $I_p=10A$ ,  $T_{on}=300\mu s$ ,  $\tau=85\%$ ], EDMed Inconel 825 obtained using CTW (with slow cooling rate) has exhibited relatively less residual stress  $\sim$  (608.7 to 930.1 MPa) and relatively low micro-hardness (range $\sim$  577.6 HV to 637.3 HV) as compared to the case of fast cooling in CT cycle executed during cryogenic treatment of the work material; which has corresponded to residual stress value falling in the range $\sim$  (609.4 to 970.8 MPa) and micro-hardness in the range  $\sim$  (739.2 HV to 800.6 HV).

**Table 5.2:** Effects of cooling rate on crystallite size ( $L$ ), and dislocation density ( $\delta$ ) for (1) the EDMed work surface of Inconel 825 obtained by using CTW (fast cooling  $\sim 1^{\circ}\text{C}/\text{min}$  during CT cycle), and (2) the EDMed work surface of Inconel 825 obtained by using CTW (Slow cooling  $\sim 0.5^{\circ}\text{C}/\text{min}$  during CT cycle)

Sl. No.	Data of the highest intensity peak of XRD for different specimens	$2\theta (^{\circ})$	FWHM ( $\beta_L$ ) [rad]	Crystallite size ( $L$ ) [nm]
(1)	EDMed work surface of Inconel 825 obtained by using CTW (Fast cooling $\sim 1^{\circ}\text{C}/\text{min}$ during CT cycle)	50.9653	0.004821	37.0276
(2)	EDMed work surface of Inconel 825 obtained by using CTW (Slow cooling $\sim 0.05^{\circ}\text{C}/\text{min}$ during CT cycle)	50.9680	0.0061985	28.801

**Table 5.2 (Continued)**

Sl. No.	Data of the highest intensity peak of XRD for different specimens	Miller indices [ $h, k, l$ ]	Inter planner spacing between the atoms ( $d$ ) [ $\text{\AA}$ ] (Obtained from <i>X'pert HighScore Software</i> )	Lattice constant ( $a$ ) [ $\text{\AA}$ ]	Dislocation density ( $\delta$ ) $\times 10^4$
(1)	EDMed work surface of Inconel 825 obtained by using CTW (Fast cooling $\sim 1^{\circ}\text{C}/\text{min}$ during CT cycle)	[2 0 0]	2.08060	4.1612	10.5919
(2)	EDMed work surface of Inconel 825 obtained by using CTW (Slow cooling $\sim 0.05^{\circ}\text{C}/\text{min}$ during CT cycle)	[2 0 0]	2.08050	4.1610	17.5089

N.B:  $1\text{\AA} = 0.1\text{nm}$ ;  $1^{\circ} = 0.0175\text{rad}$

In addition to that, data for the highest intensity peaks from the XRD spectra of test specimens has been interpreted to understand effects of cooling rate (for the CT cycle) on crystallite size ( $L$ ), and dislocation density ( $\delta$ ) for (1) the EDMed work surface of Inconel 825 obtained by using CTW (fast cooling  $\sim 1^{\circ}\text{C}/\text{min}$  during CT cycle), and (2) the EDMed work surface of Inconel 825 obtained by using CTW (slow cooling  $\sim 0.5^{\circ}\text{C}/\text{min}$  during CT cycle) as presented in Table 5.2.

Significant grain refinement has been attributed for the EDMed work surface of cryogenically treated (using slow cooling) Inconel 825 specimen as compared to the case of fast cooling, for a particular crystallographic plane in the direction  $[2\ 0\ 0]$ . This has resulted in lower crystallite size ( $L \sim 28.801\text{nm}$ ) and consequently higher dislocation density ( $\delta \sim 17.5089 \times 10^{-4}$ ) for the EDMed work surface of slow-cooled-cryogenically treated Inconel 825 in comparison to that obtained in the EDMed work surface of fast-cooled-cryogenically treated Inconel 825 which has shown ( $L \sim 37.0276\text{nm}$ ) and ( $\delta \sim 10.5919 \times 10^{-4}$ )

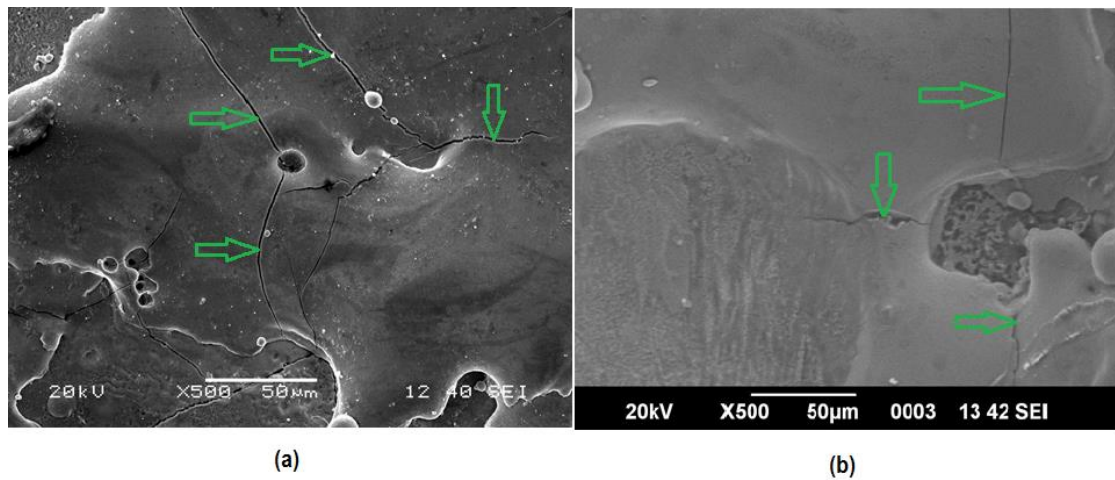


**Fig. 5.8.1:** Influence of cooling rate (ramp down rate during cryogenic treatment) on SCD on the top surface of the EDMed Inconel 825 obtained by using CTW at parameters setting: [ $I_p=10\text{A}$ ;  $T_{on}=300\mu\text{s}$ ;  $\tau=85\%$ ] (a) Fast cooling (at  $1^{\circ}\text{C}/\text{min}$ ):  $\text{SCD} \sim 0.0144\ \mu\text{m}/\mu\text{m}^2$ , and (b) Slow Cooling (at  $0.5^{\circ}\text{C}/\text{min}$ ):  $\text{SCD} \sim 0.0031\ \mu\text{m}/\mu\text{m}^2$

Influence of cooling rate (ramp down rate during cryogenic treatment) on surface crack density developed onto the top surface of the EDMed Inconel 825 specimen obtained by using CTW at parameters setting: [ $I_p=10\text{A}$ ;  $T_{on}=300\mu\text{s}$ ;  $\tau=85\%$ ] has been depicted in Fig. 5.8.1-5.8.2. From the micrographs shown in Fig. 5.8.1-5.8.2, it has clearly been understood that slow cooling rate has promoted relatively less surface cracking onto the work surface during EDM operation with CTW. This can be explained as follows: during



cryogenic treatment of the work material, slow cooling rate results larger extent of grain refinement as compared to the case of fast cooling. Moreover, grain refinement causes sufficient relief of internal stresses (compressive residual stress) present within the work material. Above all, cryogenic treatment of the workpiece at a slow cooling rate incurs improvement in its thermo-electrical properties (as compared to fast cooling). This favorably influences in heat dissipation at a faster rate (than the case of fast cooling) and thereby reduces magnitude of tensile residual stress developed within the EDMed specimen. These in turn reduces tendency of surface cracking.

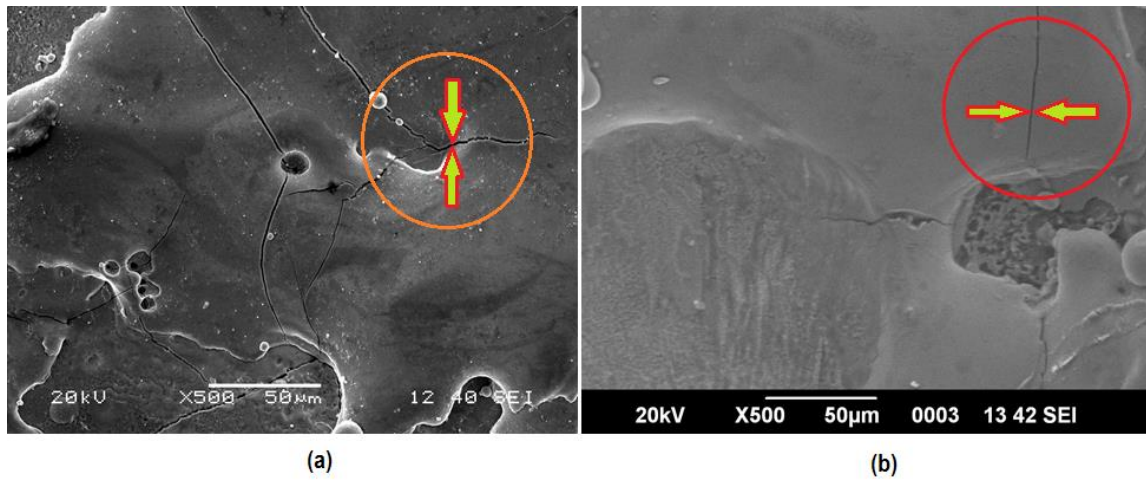


**Fig. 5.8.2:** SEM micrographs comparing the severity of crack formation (crack opening width,  $C_w$ ) at the EDMed Inconel 825 work surface obtained by using CTW at parameters setting: [ $I_p=10A$ ;  $T_{on}=300\mu s$ ;  $\tau=85\%$ ] (a) Fast cooling (at  $1^{\circ}C/min$ ), and (b) Slow Cooling (at  $0.5^{\circ}C/min$ )

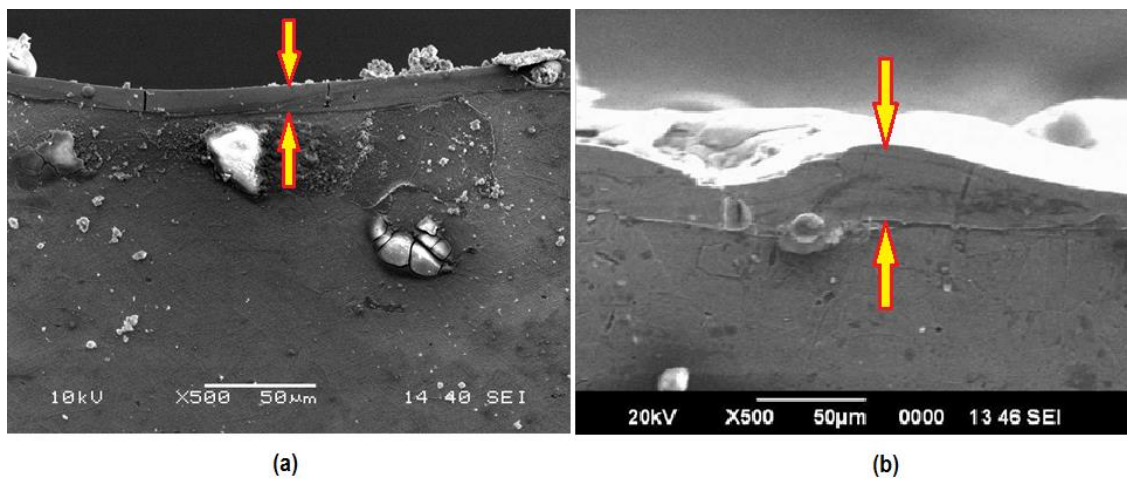


**Fig. 5.9:** Influence of cooling rate (ramp down rate during cryogenic treatment) on WLT on the top surface of the EDMed Inconel 825 obtained by using CTW at parameters setting: [ $I_p=10A$ ;  $T_{on}=300\mu s$ ;  $\tau=85\%$ ] (a) Fast cooling (at  $1^{\circ}C/min$ ): WLT~11.462  $\mu m$ , and (b) Slow Cooling (at  $0.5^{\circ}C/min$ ): WLT~22.222  $\mu m$

Increased heat transfer rate as experienced during EDM operations performed on cryogenically treated workpiece (corresponding to slow cooling rate), has resulted in smooth deposition of the molten material promoting formation of thicker white layer in contrast to the case of fast cooling during cryogenic treatment of the work material (Fig. 5.9).

## 5.4 Conclusions

The conclusions drawn from the aforesaid research have been summarized below.

- ▲ Deep cryogenic treatment is expected to improve electrical and thermal conductivities of Inconel 825 work material. These have been attributed due to the decrease in crystallite size resulting relatively more refined grain structure for the cryogenically treated work material as compared to that of ‘as received’ Inconel 825. Such grain refinement has resulted decrease in crystallite size and also increase in dislocation density. Moreover, cryogenic treatment reduces residual stress and crystal imperfections; thus increases the rate of heat transfer. This in turn reduces energy density at the spark discharge gap (during execution of EDM operation) and facilitates formation of large crater of relatively wider dimension. As a consequence, volumetric material removal rate is expected to be increased.
- ▲ Top surface morphology of the EDMed work surfaces of Inconel 825 (NTW and CTW both) has exhibited presence of crater mark, globules of debris, spherical deposition, pock marks (or chimneys), and surface cracks. However, the amount of such surface irregularities has been found relatively less for the case of EDM on CTW as compared to the case of EDM on NTW of Inconel 825. Reduced crack density (and also the crack opening width) has appeared beneficial for the fatigue life of the EDMed part component whilst subjected to service.
- ▲ The white layer of relatively thick has been found developed onto the top surface of the EDMed specimen obtained on cryogenically treated work material. Increased heat conduction rate as attributed during cryogenic treatment of the workpiece has resulted decrease in energy density at the discharge gap. A uniform spark discharge has thus been taken place resulting higher volumetric material removal rate. Due to smooth deposition of molten material, thicker white layer has been formed.
- ▲ It has been observed that, as compared to ‘as received’ Inconel 825, Carbon content (wt%) onto the top surface of the EDMed Inconel 825 specimen has been increased



due to effect of Carbon enrichment during pyrolysis of the dielectric medium. This has resulted in increase of micro-hardness of the EDMed specimen (three trials taken at the transverse-cut section of the specimen within 20 $\mu$ m depth from the top surface) as compared to the 'as received' parent material. Amongst all EDMed specimens (obtained using NTW, and CTW) analysed through EDS, the minimum extent of Carbon enrichment (on the top surface of machined zone) has been attributed for the case of EDM using CTW.

- ▲ The average micro-hardness has been found relatively high for the EDMed work surface of cryogenically treated Inconel 825 as compared to the EDMed specimen obtained by using NTW. This may be due to precipitation of fine carbides along with boundaries of refined grains attributed due to the combined effect of cryogenic treatment as well as electro-discharge machining.
- ▲ As compared to 'as received' Inconel 825, it has been observed that irrespective of the workpiece condition (i.e. normal/cryogenically treated) used during EDM operations (NTW and CTW); residual stress of tensile nature has been developed within the specimens of EDMed Inconel 825. Amongst the EDMed samples (as produced by NTW and CTW), induced tensile residual stress of lesser magnitude has been attributed to the EDMed Inconel 825 prepared by using CTW. Evolution of residual stress of relatively less magnitude in turn reduces severity of surface cracking.
- ▲ During EDM on CTW, Carbon enrichment onto the machined zone has been found less (and hence, less micro-hardness) in case of slow cooling (during cryogenic treatment of work material) as compared to fast cooling. Similarly, tensile residual stress of relatively less magnitude has been attributed within the EDMed sample of 'slow cooled-cryogenically treated' Inconel 815 (resulted due to larger extent of grain refinement; and thus decrease in crystallite size and increase in dislocation density) as compared to the EDMed surface of NTW of Inconel 825.
- ▲ During EDM on CTW, severity of surface cracking (in terms of surface crack density and crack opening width) has been found relatively less in case of 'slow cooled-cryogenically treated' workpiece. However, relatively wide white layer has been developed onto the EDMed surface of 'slow cooled-cryogenically treated' Inconel 825 as compared to that of 'fast cooled-cryogenically treated' work material.

## APPENDIX

### *Sample calculation for determining crystallite size and dislocation density:*

With reference to Table 5.1; the crystallite size and dislocation density of the ‘as received’ Inconel 825 work material have been computed.

$$L = \frac{K\lambda}{\beta_L \cos \theta}$$

$$K = 0.9 \text{ (Scherrer constant)}$$

$$\lambda = \text{radiation wavelength (} \lambda_{Co} = 1.7906 \text{Å}^0 \text{ for } CoK_{\alpha} \text{)}$$

$$\beta_L (FWHM) = 0.00294 \text{ rad}$$

$$\text{Crystallite size: } L = \frac{0.9 \times 1.7906 \times 0.1}{0.00294 \cos\left(\frac{50.8245}{2}\right)^0} = 60.686 \text{nm}$$

$$\text{N.B: } 1\text{Å}^0 = 0.1 \text{nm}; 1^0 = 0.0175 \text{rad}$$

$$\delta = \frac{15\beta_L \cos \theta}{4aL}$$

$$a = \text{Lattice constant}$$

$$a = d\sqrt{(h^2 + k^2 + l^2)} = 2.08632 \times \sqrt{(2^2 + 0^2 + 0^2)} = 4.1726 \text{Å}^0$$

The notations  $h, k, l$  denote *Miller* indices representing a particular crystallographic direction.

$$\text{Dislocation density: } \delta = \frac{15 \times 0.00294 \times \cos\left(\frac{50.8245}{2}\right)^0}{4 \times 4.1726 \times 0.1 \times 60.686} = 3.9327 \times 10^{-4} \text{nm}^{-2}$$



## **Chapter 6**

# **Surface Integrity and Metallurgical Characteristics of the EDMed Work Surfaces of A2 Tool Steel (SAE 304SS), Inconel 601 and Ti-6Al-4V: A Comparative Analysis**

### **6.1 Coverage**

In the present work, a comparative analysis on surface integrity and metallurgical characteristics of the machined surface A2 tool steel (304SS), Inconel 601 super alloy and Titanium alloy (Ti-6Al-4V) has been attempted during execution of electro-discharge machining. Experiments have been conducted at different values of peak discharge current to study morphology as well as topographical features of the EDMed work surface in terms of Surface Crack Density (SCD) as well as White Layer Thickness (WLT). XRD analysis has also been carried out to understand metallurgy of the EDMed work surface. Results have been interpreted with relevance to EDS and micro-hardness test data. Effects of peak discharge current on the EDMed work surface topography have also been examined.

### **6.2 Properties and Applications of 304SS, Super Alloy Inconel 601 and Ti-6Al-4V**

SAE 304 Stainless Steel (also known as A2 Stainless Steel or Staybrite 18/8 Stainless Steel) contains both Chromium (~18%) and Nickel (~8%) metals as the main non-iron constituents. It is basically an austenite steel. SAE 304SS is not very electrically or

thermally conductive and exhibits non-magnetic character. It offers high corrosion resistance than regular steel and finds huge application because of the ease of forming/machining to transform into various shapes. It generally contains 17.5–20% Chromium, 8–11% Nickel, and less than 0.08% Carbon, 2% Manganese, 1% silicon, 0.045% Phosphorus, and 0.03% Sulfur. 304SS has excellent resistance to a wide range of atmospheric environments and many corrosive media; therefore, it is used for a variety of household (viz. kitchen and food applications) and industrial applications such as screws, machinery parts, car headers, and food-handling equipment, and also in the architectural field for exterior accents such as water and fire features.

Aspects of machinability of variety of steels (mild steel, stainless steel, and tool steel) have been studied in (Guu et al., 2003; Pradhan and Biswas, 2010; Lingadurai et al., 2012; D’Urso et al., 2014; Natarajan and Suresh, 2015; Wang et al., 2016; Nayak et al., 2016).

Nickel-based high temperature super alloys (i.e. Inconel 601, in the present case) are often found in aerospace engine and power generation turbine components, as well as in petrochemical, food processing, nuclear reactor, and pollution control equipment. Inconel exhibits poor machinability. The unique feature that provides superior high temperature strength makes them ‘*difficult-to-cut*’. Additionally, reduced speeds of the cutting tool can hamper productivity. The common problems that arise during machining of Inconel include:

- ⇒ Evolution of high cutting temperatures; generation of enormous heat at the tool-tip, heavily concentrated in the cutting edge area (as compared to conventional alloy steel machining); limitation in cutting speed capability.
- ⇒ Low thermal conductivity of Inconel results more heat to be absorbed by the tool (as compared to the workpiece); which in turn causes high temperature at the tool-tip as well as excessive tool wear. This tends to limit cutting speeds and reduce useful tool life.
- ⇒ The hard, abrasive intermetallic compounds and carbides present on the Ni-based solid solution matrix of Inconel causes severe abrasive wear (crater wear and severe plastic deformation) at the tool-tip. This affects tool geometry adversely leading to catastrophic failure of the cutting tool.

- ⇒ Tendency of work hardening causes depth-of-cut notching on the tool, which can lead to formation of burr, BUE and coating delamination on the workpiece. Hence, surface integrity of the finished part may be disappointing.
- ⇒ The chips produced whilst machining of Inconel appear tough as well as continuous, and hence require superior chip breaker geometry.
- ⇒ Heat generated during machining can remarkably alter the alloy microstructure; induces residual stress/surface cracks that can further deteriorate fatigue life of the end product.

Aspects of machinability of super alloy Inconel have been studied in ([Hewidy et al., 2005](#); [Ramakrishnan and Karunamoorthy, 2008](#); [Newton et al., 2009](#); [Ay et al., 2013](#); [Lin et al., 2013](#); [Mohanty et al., 2014a](#); [Dhanabalan et al., 2014](#); [Aggarwal et al., 2015](#); [Torres et al., 2016](#)).

Inconel 601 is considered as a general-purpose engineering material that exhibits excellent resistance to high-temperature oxidation. The alloy also has good resistance to aqueous corrosion, possesses high mechanical strength.

The alloy's Nickel based solid solution matrix, in conjunction with substantial Chromium content, provides resistance towards many corrosive media and high-temperature environments. Oxidation resistance is further enhanced by the Aluminum content. Inconel 601 is widely used in many fields viz. thermal processing, chemical processing, pollution control, aerospace, and power generation.

Nowadays, Titanium (Ti) alloys are widely used in the area of aerospace (such as jet engine and airframe components), spacecraft, military applications, automotive (connecting rods on expensive sports cars and some premium sports equipment) and biomedicine (ex. dentistry) due to their excellent mechanical properties (viz. extraordinary corrosion resistance, a high strength–weight ratio, and high temperature strength) and biocompatibility ([Josef et al., 2011](#); [Petr et al., 2012](#)). The excellent strength-to-weight ratio of Ti-alloys results in reduction of aircraft weight and causes minimum fuel consumption and emission. Therefore, Titanium alloys are increasingly replacing Aluminum (and its alloys) in various domains of engineering applications ([Lütjering and Williams, 2007](#)).

Ti-6Al-4V (Ti-alloy Grade 5) has a chemical composition of 6% Aluminum, 4% Vanadium, 0.25% (maximum) iron, 0.2% (maximum) Oxygen, and the remainder Titanium. It is significantly stronger than commercially available pure Titanium; while

having the same stiffness and thermal properties (excluding thermal conductivity, which is about 60% lower in Grade 5 than in commercially pure Ti). Ti-6Al-4V is also called  $\alpha$  and  $\beta$  alloys, which are metastable and generally include some combination of both  $\alpha$  and  $\beta$  stabilizers; it can also be heat treated. Ti-6Al-4V is known as the ‘workhorse’ of the Titanium industry because it accounts for more than 50% of total Titanium usage.

However, the utilization is somewhat restricted by high cost and processing difficulties due to its poor machinability (Ezugwu and Wang, 1997). The common challenges being encountered while machining of Ti-alloys are very low thermal conductivity, chemical-reactivity (tendency to chemically react with the Cobalt binder which exists in most of the tool materials and low elastic modulus (Kibri et al. 2010). Therefore, Ti-alloys are recognized as ‘difficult-to-cut’ materials mainly because of their susceptibility to work hardening during execution of machining operations. Additionally, other obstacles during conventional machining of Ti-alloys are due to cutting speed limitation, chipping, and premature failure of the cutting tools. Thus, traditional machining operations are found inefficient to achieve satisfactory machining performance on Ti-alloys in regards of surface integrity, dimensional accuracy of the part component as well as tool life.

In order to overcome technical difficulties in conventional machining processes, non-conventional machining processes like electro-discharge machining and micro-EDM (drilling, milling etc.) are increasingly being attempted for the machining of Ti-alloys. These non-traditional routes are basically electro-thermal process of removing materials regardless of hardness of the work material; where, the force between the workpiece and the tool electrode is negligible (Tsai and Masuzawa, 2004). Moreover, the phenomenon of tool deformation due to cutting force action is almost zero. Problems associated with chatters, mechanical stress, and vibration during machining operation are basically nil; as there is no direct contact between the electrode and the workpiece (Ho and Newman, 2003). Aspects of machinability of Ti alloys as studied by previous researchers have been well documented in (Chen et al., 1999; Hascalik and Caydas, 2007a; Hascalik and Caydas, 2007b; Lin et al., 2000; Alias et al., 2012; Sivaprakasam et al., 2014; Kolli and Kumar, 2015; Khan et al., 2015; Kao et al., 2010; Tiwary et al., 2015; Altug et al., 2015; Amorim et al., 2014; Yadav and Yadava, 2015).

## 6.3 Scope of the Work

Owing to the widespread engineering applications of Nickel as well as Titanium based super alloys (viz. Inconel 601 and Titanium alloy: Ti-6Al-4V, respectively, in the present case), machining and machinability aspects of these materials have become an important research agenda today. Since, conventional machining operations are inappropriate for those materials; non-conventional machining routes viz. EDM, WEDM, EDD etc. are being adapted by the manufacturing companies to obtain desired shape and contour of the machined end product with intricate geometry and dimensions that are really difficult to achieve through traditional machining operations. However, low material removal and inferior surface finish seem to be a challenge.

Inconel 601 as well as Titanium alloy Ti-6Al-4V possess very low thermal conductivity that results in poor heat dissipation through the work material whilst subjected to machining. Moreover, Titanium alloy is highly chemically reactive exhibiting the tendency of producing galling, welding and smearing along with rapid destruction of the cutting tool.

Since, EDM is the most commonly used non-traditional machining route in which material is removed from the workpiece due to occurrence of spark; and, hence erosion of the work material takes place by high velocity electrons in the spark gap between two electrodes (tool and workpiece). Therefore, EDM performance is greatly influenced by the thermal conductivity of the work material as well as the tool electrode.

As Inconel 601 and Ti-6Al-4V do possess very low thermal conductivity as compared to conventional metal and alloys (for example 304SS); the EDM performance is expected to be adversely affected while these low conductive super alloys are being machined. Therefore, extent of machinability of these super alloys during EDM is required to be investigated in detail. In this context, the present study has aimed at examining machinability of super alloys (Inconel 601 and Titanium alloys) as compared to A2 Steel (SAE 304SS) during EDM operation.

Morphology of the EDMed work surface of Inconel 601 and Ti-6Al-4V has been compared to that of 304SS. In this experimental study, the EDM performance has been evaluated in terms of EDMed surface topography which includes surface crack density as well as white layer thickness. Metallurgical observations have also been carried out through XRD. Results have been interpreted physically in support of EDS analysis and micro-hardness test data. Additionally, effects of peak discharge current on influencing



various process-performance features have also been studied. In short, a comparative study has been made to understand the machinability of Inconel 601 as well as Ti-6Al-4V as compared to 304SS during electro-discharge machining.

## 6.4 Results and Discussion

### 6.4.1 XRD Analysis (Metallurgical Observations)

X-ray diffraction (XRD) measurements have been performed on the specimens for phase identification, using a Panalytical X'Pert PRO diffractometer with  $\text{CoK}_\alpha$  radiation ( $\lambda = 1.7906 \text{ \AA}$ ). The XRD patterns have been indexed with *X'Pert HighScore Plus* software containing PDF-2 files database.

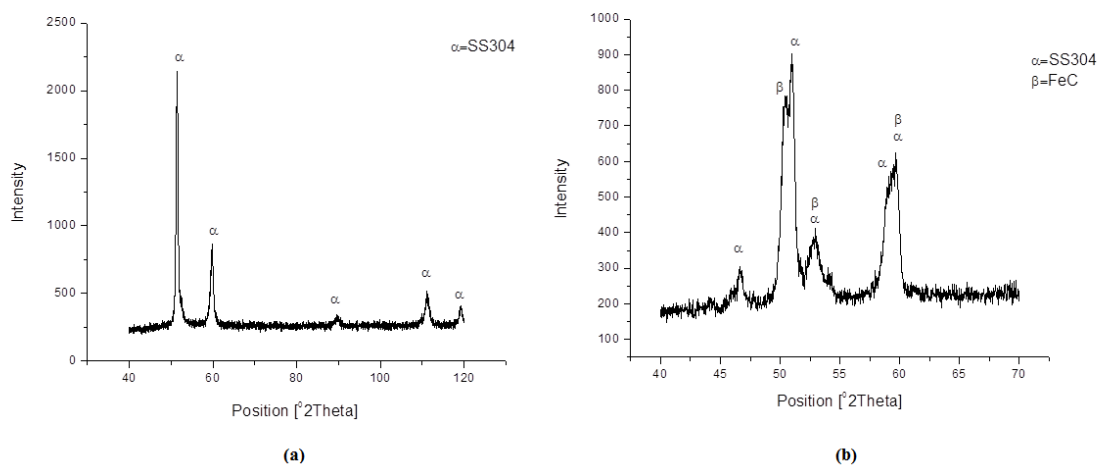


**Fig. 6.1:** XRD spectrum of 304SS (a) 'As received', and (b) the EDMed work surface obtained by using peak discharge current  $I_p = 10 \text{ A}$

XRD elemental spectra for 'as received' 304SS has exhibited five different peaks of varied intensity at positions  $51.5193^\circ$ ,  $59.8688^\circ$ ,  $89.7170^\circ$ ,  $111.1182^\circ$  and  $119.3202^\circ$  along the  $2\theta$  axis (with  $2\theta$  limit  $40^\circ$ - $120^\circ$ ) (Fig. 6.1). The corresponding directions of the crystallographic planes have been identified as:  $[1\ 1\ 1]$ ,  $[2\ 0\ 0]$ ,  $[2\ 2\ 0]$ ,  $[3\ 1\ 1]$ , and  $[2\ 2\ 2]$ . The peak pattern for 'as received' 304SS has exactly matched with that of  $\text{Cr}_{0.19}\text{Fe}_{0.7}\text{Ni}_{0.11}$  (Reference Code: 33-0397). As compared to 'as received' 304SS, the peak pattern for the EDMed work surface of 304SS (obtained by using highest discharge energy i.e. highest level of peak discharge current; 10A) has exhibited slight alteration in peak positions along the  $2\theta$  axis. Moreover, few extra peaks have been detected herein due to formation of FeC (PDF Index Name: Iron Carbide; Reference Code: 06-0686). The

formation of FeC is attributed due to pyrolysis of dielectric fluid during spark discharge (Fig. 6.1).

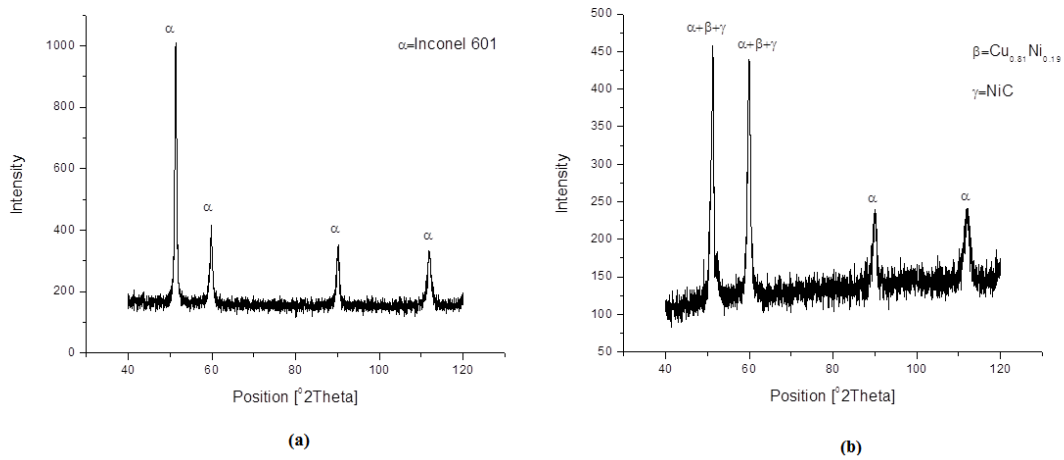
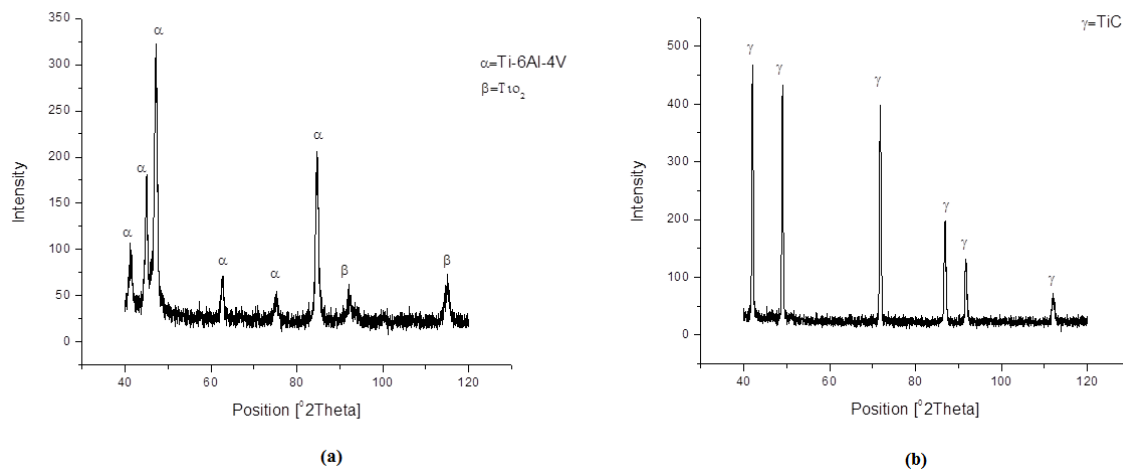


Fig. 6.2: XRD spectrum of Inconel 601 (a) ‘As received’, (b) the EDMed work surface obtained by using peak discharge current  $I_p = 10A$

XRD elemental spectra for ‘as received’ Inconel 601 has indicated peaks of varied intensity that have been observed at crystallographic planes in directions [1 1 1], [2 0 0], [2 2 0] and [3 1 1], respectively corresponding to positions  $51.2757^\circ$ ,  $59.8182^\circ$ ,  $90.1449^\circ$  and  $111.6793^\circ$  along the  $2\theta$  axis (Fig. 6.2). It has corresponded to a Nickel-Iron-Chromium based cubic solid solution matrix in which highest intensity peak has been observed at crystallographic plane in the direction [1 1 1].

It has been also found that with increase in peak discharge current (and consequently energy input); peak broadening has taken place at the same crystallographic plane direction. Considering Full-Width-Half-Maximum (FWHM) of the peaks (at direction of the crystallographic plane [1 1 1]; approximately at  $(\sim 51^\circ)$  position along the  $2\theta$  axis) for the EDMed Inconel 601 work surfaces obtained at different energy input; it has been inferred that grain refinement of increasing magnitude has incurred with increase in peak discharge current. However, as compared to ‘as received’ Inconel 601, formation of  $Cu_{0.81}Ni_{0.19}$  (PDF Index Name: Copper-Nickel; Reference Code: 47-1406) and NiC (PDF Index Name: Nickel Carbide; Reference Code: 14-0020) have been found at crystallographic planes in directions: [1 1 1] and [2 0 0] (Fig. 6.2). This has been caused due to thermo-electrical effect of EDM process. Formation of Copper-Nickel is attributed due to wear of Copper tool during EDM operation. Formation of carbide is due to pyrolysis of dielectric fluid during spark discharge.



**Fig. 6.3:** XRD spectrum of Ti-6Al-4V (a) ‘As received’, (b) the EDMed work surface obtained by using peak discharge current  $I_p = 10A$

XRD elemental spectra of ‘as received’ Titanium alloy (Ti-6Al-4V) has exhibited a peak pattern almost similar to Ti (PDF Index Name: Titanium; Reference Code: 44-1294). Peaks of different intensities have been observed at crystallographic planes in directions viz. [1 0 0], [0 0 2], [1 0 1], [1 0 2], [1 1 0], and [1 0 3] corresponding to the positions  $41.3801^\circ$ ,  $44.9771^\circ$ ,  $47.1546^\circ$ ,  $62.7153^\circ$ ,  $75.1316^\circ$ , and  $84.7021^\circ$ , respectively, along the  $2\theta$  axis (Fig. 6.3). In addition, two peaks at positions  $92.2074^\circ$  and  $115.1413^\circ$  have also been observed herein which may be due to presence of Titanium oxides on the surface of Ti-6Al-4V.

However, on analysis of XRD patterns of the EDMed Ti-6Al-4V work surface with different discharge energy; it has been observed that in comparison with ‘as received’ Ti-6Al-4V, the machined surface of has undergone remarkable alteration (in peak pattern) irrespective of the peak current supplied. All EDMed Ti-6Al-4V work surfaces have exhibited highly intense peak of TiC (PDF Index Name: Titanium Carbide; Reference Code: 03-1213) at crystallographic planes in directions: [1 1 1], [2 0 0], [2 2 0], [3 1 1], [2 2 2], and [4 0 0], respectively (Fig. 6.3).

Additionally, it has also been found that the amount of carbide precipitation has been found increased with increasing spark energy input. Carbide formation may be attributed due to the phenomenon of dielectric cracking during electric discharge. The dielectric fluid being a hydrocarbon, Carbon atoms are generated during pyrolysis of the same. These carbon atoms react with Titanium forming a Carbide layer onto the top of the machined surface. The formation of such carbide layer over the machined surface is

experienced as highly detrimental as it obstructs smooth machining operation to be executed.

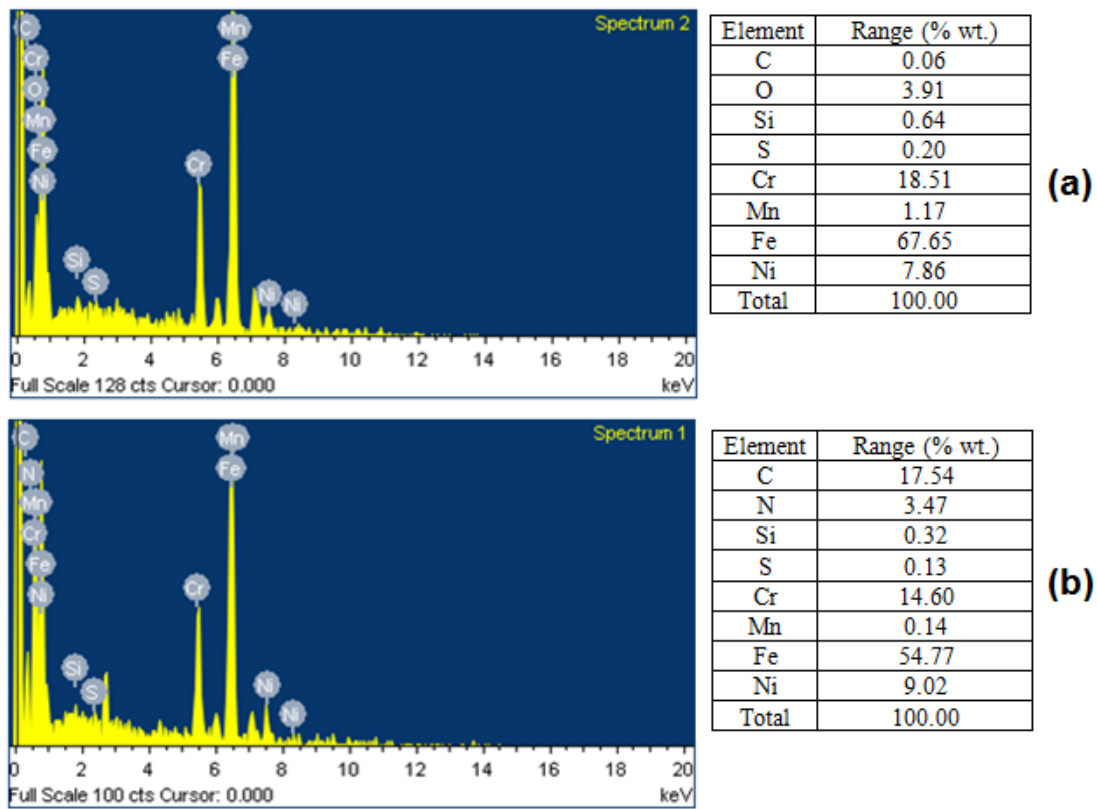


Fig. 6.4.1: EDS elemental spectra revealing chemical composition of work surface for (a) 'As received' 304SS, and (b) the EDMed 304SS at  $I_p=10A$

EDS analysis has exhibited significant Carbon enrichment onto the machined surface of 304SS, Inconel 601 as well as Ti-6Al-4V; this has resulted in increase of Carbon percentage (wt%) at the EDMed work surface as compared to the unaffected parent material (Fig. 6.4.1-6.4.3). It has been found that as compared to 'as received' 304SS (wt% of ~0.06%), the EDMed work surface of 304SS has exhibited more Carbon content (wt% of ~17.54%) as shown in Fig. 6.4.1. Similar conclusion has been made for the EDMed work surface of Inconel 601 which has shown significant Carbon enrichment (wt% of C~35.99%) as compared to unaffected parent material (wt% of C~0.028%) as indicated in Fig. 6.4.2. A representative figure of EDS elemental spectra showing Carbon enrichment has been provided for the EDMed work surface of Ti-6Al-4V (wt% of C~1.08%) while compared with 'as received' Ti-6Al-4V (wt% of C~0.04%) work material (Fig. 6.4.3). Such carbon enrichment has resulted formation of carbides onto the top surface of EDMed specimen leading to increase in micro-hardness value (Table 6.1).

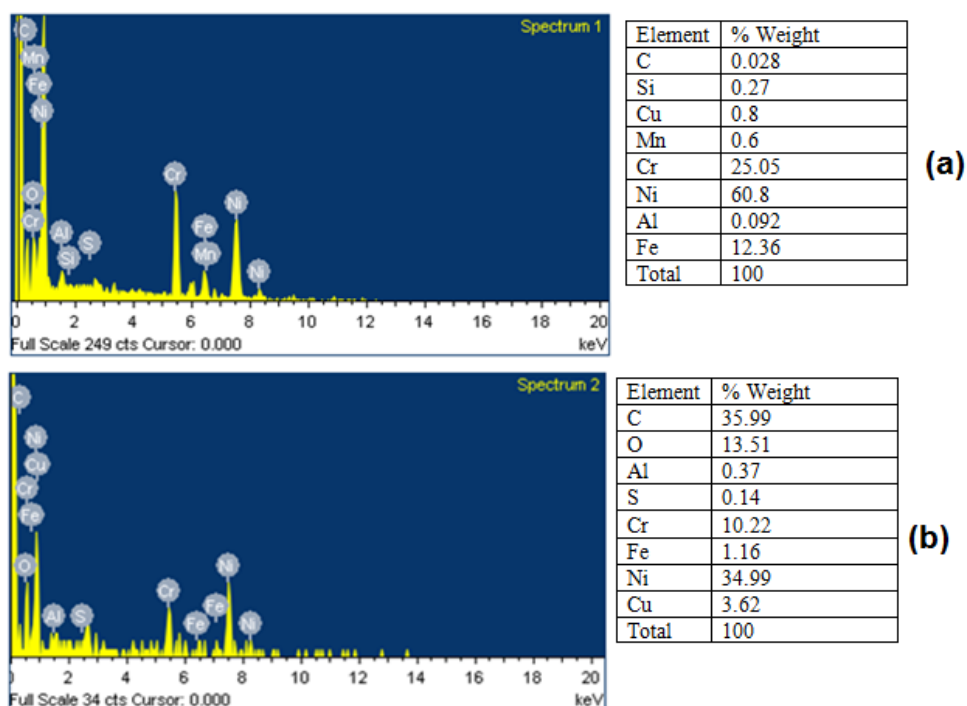


Fig. 6.4.2: EDS elemental spectra revealing chemical composition of work surface for (a) 'As received' Inconel 601, and (b) the EDMed Inconel 601 at  $I_p=10A$

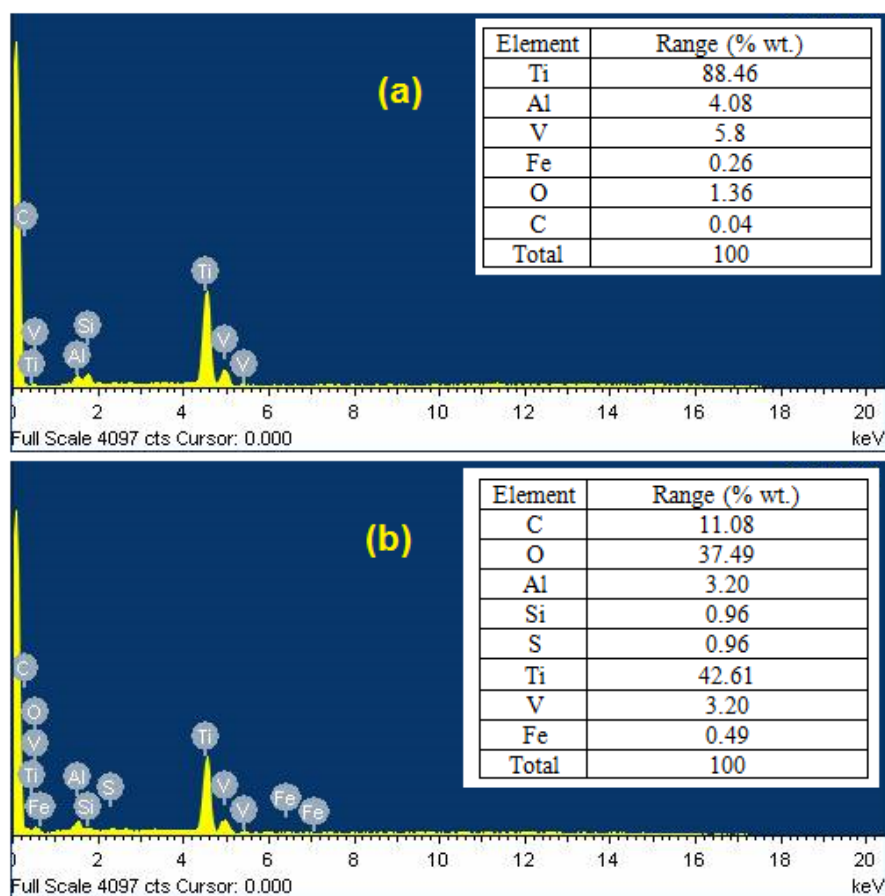


Fig. 6.4.3: EDS elemental spectra revealing chemical composition of work surface for (a) 'As received' Ti-6Al-4V, and (b) the EDMed Ti-6Al-4V at  $I_p=10A$

## 6.4.2 Effects of Peak Discharge Current

SEM micrographs revealing surface integrity of EDMed 304SS, Inconel 601 and Ti-6Al-4V specimens have exhibited poor surface morphology in terms of crater marks, globules of debris, melted material deposition, spherical deposition, pockmark (or chimney), large surface cracks, micro-cracks and white layer (Fig. 6.5). However, it is expected that intensity of aforesaid surface irregularities may vary with variation of work material as well as spark energy input.

Table 6.1: Results of micro-hardness test

Specimen	Micro-hardness [HV <sub>0.025</sub> ]			
	Trial 1	Trial 2	Trial 3	Average
‘As received’ 304SS	295.8	292.1	281.9	289.9
EDMed 304SS at I <sub>p</sub> =10A	397.5	486.8	383.2	422.5
‘As received’ Inconel 601	278.4	255.7	248.1	260.7
EDMed Inconel 601 at I <sub>p</sub> =10A	432.4	375	439.2	415.5
‘As received’ Ti-6Al-4V	328.8	308.5	310.5	315.9
EDMed Ti-6Al-4V at I <sub>p</sub> =10A	409.2	483.8	437.1	443.4

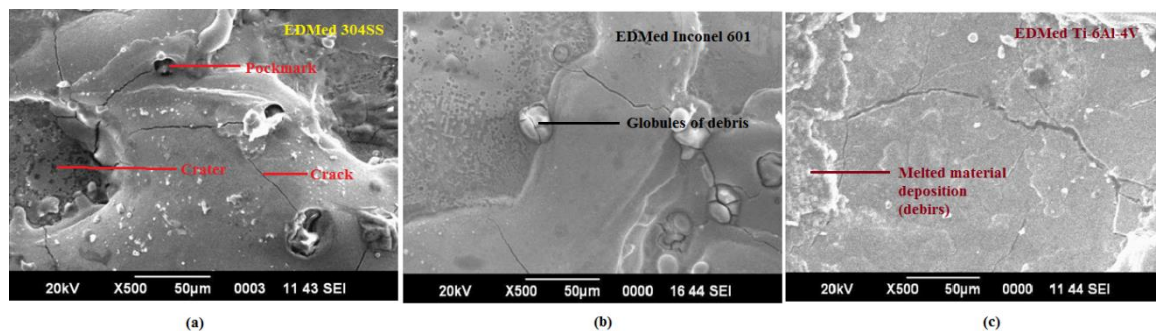


Fig. 6.5: SEM micrographs showing inferior surface integrity of the EDMed work surface of (a) 304SS, (b) Inconel 601, and (c) Ti-6Al-4V obtained at I<sub>p</sub>=10A

According to (Ekmekci, 2007), residual stress generated within the EDMed specimen is the effect of non-homogeneity of heat flow and metallurgical transformations or the localized inhomogeneous plastic deformation that occurs during EDM operation. It is well known that the residual stress resulted by rapid cooling and phase changes in the white layer, induce surface cracking. Literature on the residual stress of the EDMed part component reported that the residual stress is of tensile in nature whose magnitude appears to be the highest at the surface. It was also reported that the residual stress increases with increase in pulse energy. Such residual stress is harmful since its magnitude stimulates surface cracking.



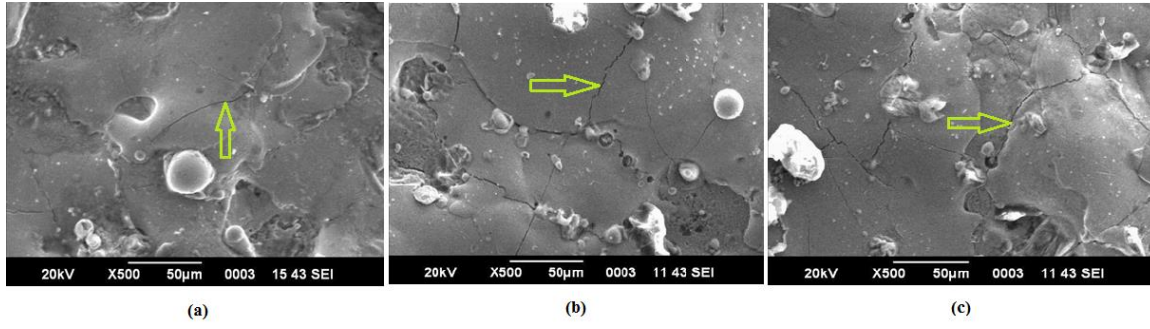


Fig. 6.6.1: SEM micrographs revealing existence of surface cracks on the EDMed **304SS** work surface (a) ( $SCD \sim 0.004 \mu\text{m}/\mu\text{m}^2$ ) at  $I_p=6\text{A}$ , and (b) ( $SCD \sim 0.015 \mu\text{m}/\mu\text{m}^2$ ) at  $I_p=8\text{A}$ , and (c) ( $SCD \sim 0.0135/\mu\text{m}^2$ ) at  $I_p=10\text{A}$

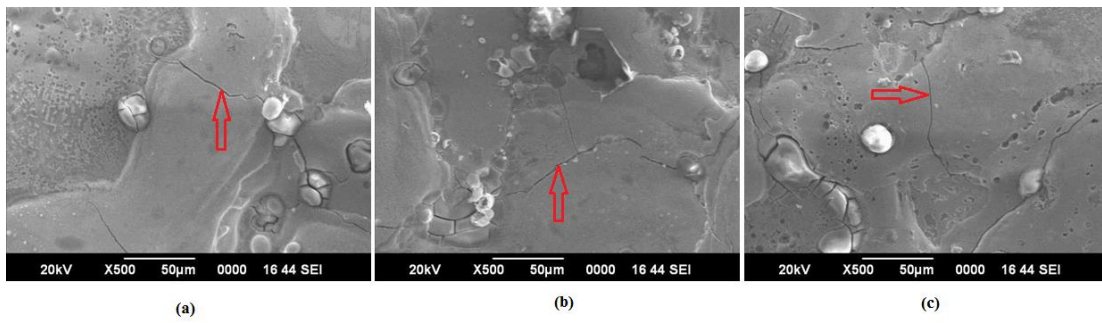


Fig. 6.6.2: SEM micrographs revealing existence of surface cracks on the EDMed **Inconel 601** work surface (a) ( $SCD \sim 0.0064 \mu\text{m}/\mu\text{m}^2$ ) at  $I_p=6\text{A}$ , and (b) ( $SCD \sim 0.0086 \mu\text{m}/\mu\text{m}^2$ ) at  $I_p=8\text{A}$ , and (c) ( $SCD \sim 0.012 \mu\text{m}/\mu\text{m}^2$ ) at  $I_p=10\text{A}$

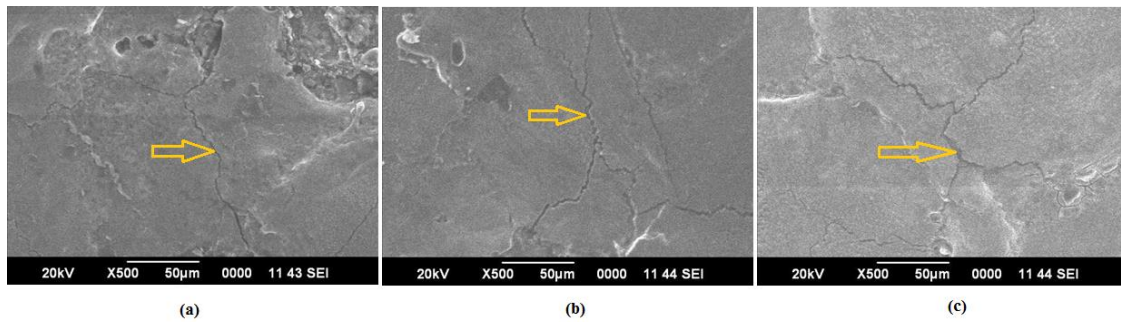


Fig. 6.6.3: SEM micrographs revealing existence of surface cracks on the EDMed **Ti-6Al-4V** work surface (a) ( $SCD \sim 0.0062 \mu\text{m}/\mu\text{m}^2$ ) at  $I_p=6\text{A}$ , and (b) ( $SCD \sim 0.0115 \mu\text{m}/\mu\text{m}^2$ ) at  $I_p=8\text{A}$ , and (c) ( $SCD \sim 0.012 \mu\text{m}/\mu\text{m}^2$ ) at  $I_p=10\text{A}$

Lee et al. (2004) reported that the formation of surface crack is basically due to the differentials of high contraction stresses exceeding the work material's ultimate tensile stress within the white layer depth. However, severity of surface cracking largely depends

on thermal conductivity, the ultimate tensile strength and also the fracture toughness of the work material. Hence, varied degree of crack intensity (surface crack density), crack opening width etc. are found with variation in work materials. In the present work, it has been found that SCD has increased with increase in peak discharge current; and, such an increasing trend has been found irrespective of the work material studied (Fig. 6.6.1-6.6.3). Increase in peak discharge current results in increase of the spark energy thereby evolution of enormous heat in the vicinity of the surface being machined. This causes huge thermal stress stimulating surface cracks to develop.

As compared to 304SS (thermal conductivity:  $14.76 \text{ W/m}^\circ\text{C}$  at  $20^\circ\text{C}$ ), the low thermal conductivity of Inconel 601 (thermal conductivity:  $11.2 \text{ W/m}^\circ\text{C}$  at  $20^\circ\text{C}$ ) obstructs the heat (that is generated during EDM operation) to be dissipated through bulk of the work material. Hence, immense heat is accumulated at the machining zone resulting evolution of huge thermal (residual) stress. When such induced residual stress exceeds ultimate tensile strength of the work surface of Inconel 601, surface cracking takes place. The fracture toughness of Inconel 601 being relatively less as compared to 304SS ( $228 \text{ MPa.m}^{1/2}$ ); severity of cracking is expected to be more for the case of the EDMed Inconel 601 work surface.

On the contrary, Ti-6Al-4V alloy exhibits very poor thermal conductivity ( $7.2 \text{ W/m}^\circ\text{C}$  at  $20^\circ\text{C}$ ). Moreover, it has a fracture toughness value much lower ( $107 \text{ MPa.m}^{1/2}$ ) as compared to 304SS. Hence, it is expected that severity of surface cracking is likely to be more for the EDMed work surface of Ti-6Al-4V. However, XRD analysis has predominantly revealed the existence of TiC layer onto the top surface of EDMed Ti-6Al-4V specimens. Hence, surface cracking that is supposed to be incurred on the EDMed work surface of Ti-6Al-4V is surely going to be influenced by the presence of TiC. As TiC exhibits high degree of brittleness and possess very low thermal conductivity (even less than that of Ti-6Al-4V alloy) as well as low fracture toughness; consequently, severity of surface cracking with relatively high crack opening width has been observed on most of the EDMed specimen of Ti-6Al-4V (Fig. 6.7).

Experimental data also has exhibited the effect of peak discharge current on WLT. It has been found that with increase in peak current, WLT has assumed approximately an increasing trend. This can be explained by the fact that increase in peak current intern increases energy input at the spark gap causing more material to be eroded out. Dielectric fluid appears increasingly inefficient to flush out the bulk of the total eroded material



(debris). During  $T_{off}$ , remaining material re-solidifies adhering on the top of machined surface forming white layer.

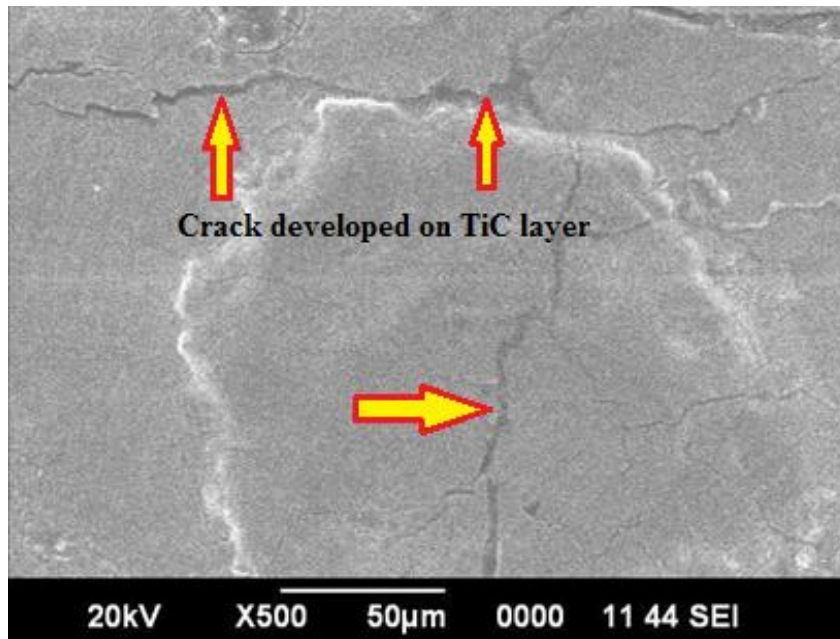


Fig. 6.7: Severity of surface cracking observed on the TiC layer deposited on the EDMed Ti-6Al-4V work surface (at  $I_p=10A$ )

SEM micrographs revealing existence of white layer on the top surface of the EDMed specimen have been arranged to infer the effect of peak discharge current on WLT for the EDMed 304SS, Inconel 601 and Ti-6Al-4V specimens. With increase in peak discharge current, it has been found that irrespective of the work material chosen, WLT has assumed an increasing trend. However, the rate of increase of WLT has been found different for different work material (Fig. 6.8.1-6.8.3).

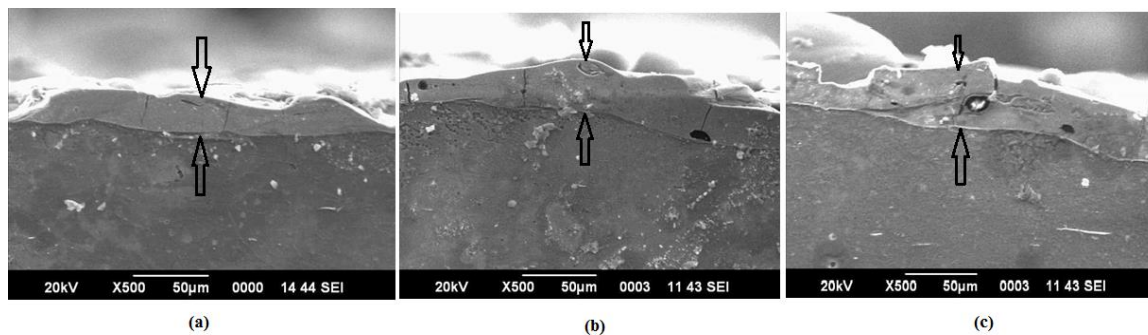


Fig. 6.8.1: SEM micrographs revealing existence of white layer on the EDMed **304SS** work surface (a) (WLT~21.875µm) at  $I_p=6A$ , and (b) (WLT~25.625µm) at  $I_p=8A$ , and (c) (WLT~32.362µm) at  $I_p=10A$

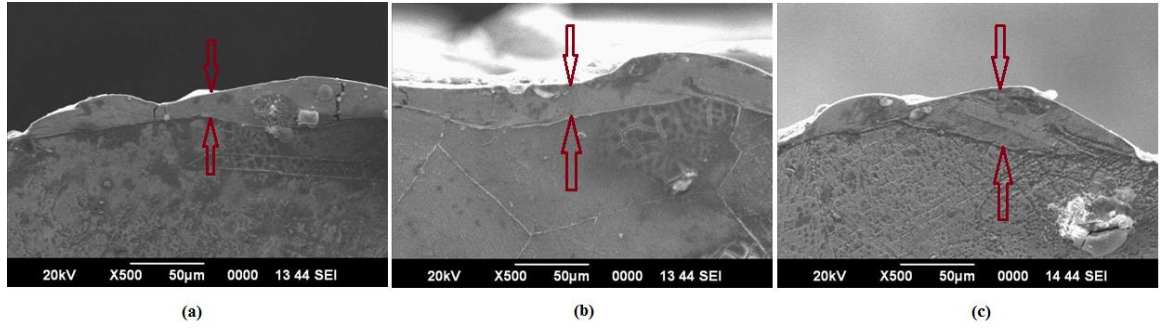


Fig. 6.8.2: SEM micrographs revealing existence of white layer on the EDMed **Inconel 601** work surface (a) (WLT~21.732µm) at  $I_p=6A$ , and (b) (WLT~25.635µm) at  $I_p=8A$ , and (c) (WLT~26.72µm) at  $I_p=10A$

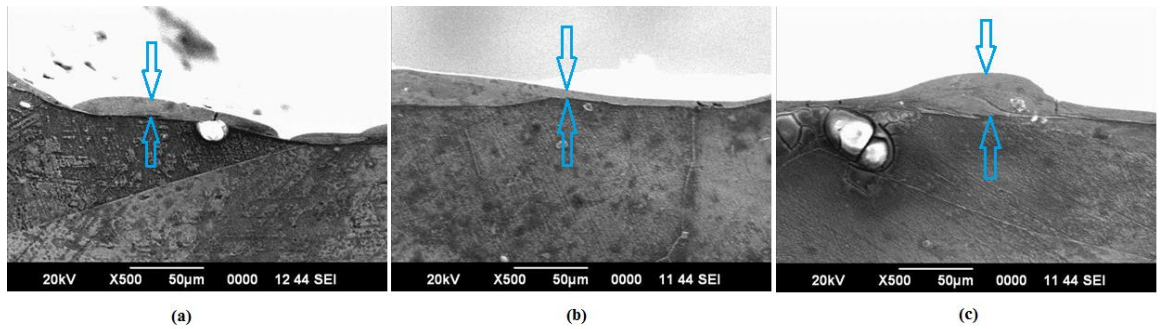


Fig. 6.8.3: SEM micrographs revealing existence of white layer on the EDMed **Ti-6Al-4V** work surface (a) (WLT~10.317µm) at  $I_p=6A$ , and (b) (WLT~14.286µm) at  $I_p=8A$ , and (c) (WLT~19.524µm) at  $I_p=10A$

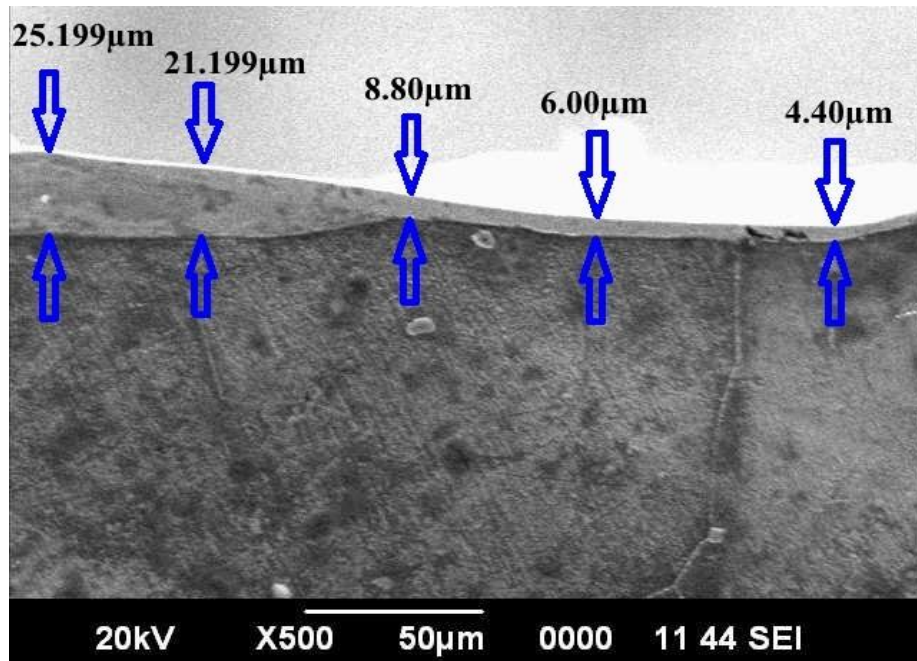


Fig. 6.9: Non-uniform deposition of the molten material (forming while layer) observed on the EDMed **Ti-6Al-4V** work surface (at  $I_p=8A$ )

It has been noticed that as compared to electro-discharge machined 304SS as well as Inconel 601 work surfaces, the white layer developed on the EDMed Ti-6Al-4V specimen has corresponded to non-uniform deposition of the molten material (Fig. 6.9). This has been caused due to low material removal rate. The poor thermal conductivity of Ti-6Al-4V has restricted heat to be dissipated thus affecting cooling of the specimen adversely. The formation of TiC layer over the machined surface also creates a barrier towards heat conduction. As a consequence of the above, molten material has deposited in a non-uniform manner onto the EDMed work surface of Ti-6Al-4V.

## 6.5 Conclusions

The conclusions drawn from the aforesaid research have been pointed out below.

- ▲ EDMed work surface of 304SS has exhibited FeC precipitates.
- ▲ Grain refinement has been found attributed to the EDMed work sample of Inconel 601 at crystallographic plane in the direction  $[1\ 1\ 1]$ . Moreover, precipitates of  $\text{Cu}_{0.81}\text{Ni}_{0.19}$  and NiC have been observed at crystallographic planes in directions:  $[1\ 1\ 1]$  and  $[2\ 0\ 0]$ .
- ▲ Highly intense layer of TiC has been formed on the EDMed work surface of Ti-6Al-4V. Such carbide precipitation has been found increased with increase in peak discharge current.
- ▲ Peak discharge current has shown positive effect on SCD as well WLT. Irrespective of the work material chosen; it has been experimentally noticed that with increase in peak discharge current, SCD and WLT have assumed an increasing trend.
- ▲ Severity of surface cracking has been found predominant for the EDMed Ti-6Al-4V due to presence of brittle TiC layer with very poor thermal conductivity.
- ▲ Non-uniform deposition of molten material (white layer) has been found on the EDMed Ti-6Al-4V work surface mainly due to low material removal rate, formation of TiC and above all very low thermal conductivity of Ti-6Al-4V as well as TiC.
- ▲ EDS analysis has revealed significant Carbon enrichment onto the EDMed surfaces of 304SS, Inconel 601 and Ti-6Al-4V due to dielectric cracking. Such Carbon enrichment has been attributed to the deposition of carbide layer and consequently increase in micro-hardness of the EDMed work surface as compared to 'as received' parent material.

## Chapter 7

# Machining Performance Optimization during EDM of Inconel 718: Application of Satisfaction Function Approach Integrated with Taguchi Method

### 7.1 Coverage

The present work aims to determine an appropriate setting of process parameters (viz. gap voltage, peak discharge current, pulse-on time, duty factor and flushing pressure) for achieving optimal machining performance during electro-discharge machining of super alloy Inconel 718 by using Copper tool electrode. Experiments have been performed based on  $L_{25}$  orthogonal array design of experiment by varying each of the aforesaid process parameters at five different levels. The machining performance has been evaluated in terms of Material Removal Rate (MRR), Electrode Wear Rate (EWR), Surface Roughness ( $R_a$ ), Surface Crack Density (SCD), White Layer Thickness (WLT), and Micro-Hardness (MH) of the EDMed Inconel 718 end product.

In this part of work, a novel optimization route (combining satisfaction function, distance measure approach in conjugation with Taguchi's philosophy) has been introduced. Application feasibility of aforementioned approach has been compared to that of Principal Component Analysis (PCA) and Combined Quality Loss (CQL) concept integrated with Taguchi method. Additionally, morphology of the EDMed work surface of Inconel 718 has been investigated.

## 7.2 Scope of the Work

Literature depicts that a considerable volume of work has been carried out by the pioneers to investigate machining and machinability of Inconel super alloys of different grades (Thakur et al., 2009; Rahman et al., 1997; Ho and Newman, 2003; Newton et al., 2009; Li et al., 2003; Sengottuvel et al., 2013; Li et al., 2014; Ramakrishnan and Karunamoorthy, 2008; Kuppan et al., 2008; Newton et al., 2009; Kumar et al., 2011; Kuppan et al., 2011; Ay et al., 2013; Li et al., 2003; Lin et al., 2013; Sengottuvel et al., 2013; Ahmad and Lajis, 2013; Mohanty et al., 2014a; Dhanabalan et al., 2014; Mohanty et al., 2014b; Li et al., 2014; Li et al., 2015; Nayak and Mahapatra, 2015; Sharma et al., 2015; Bozdana and Ulutas, 2016). Owing to the difficulties in conventional machining, non-conventional machining routes like EDM, WEDM, micro-machining etc. have been recommended to get quality end product. During electro-discharge machining there are several controllable parameters viz. OCV (also called gap voltage), peak discharge current, pulse-on time, duty factor, flushing pressure etc. on the EDM setup (Jameson, 2001). Proper tuning (controlling) of these parameters surely results satisfactory machining yield. However, these parameters interact in a complicated manner and hence affect the machining responses (outputs). In this context, research interest has been evolved to search for a suitable machining environment (setting of controllable process parameters) to satisfy multi-requirements of process performance yields in terms of Material Removal Rate (MRR), Electrode Wear Rate (EWR), roughness average ( $R_a$ ), Surface Crack Density (SCD), While Layer Thickness (WLT) and micro-hardness of the EDMed end product of Inconel 718.

Literature survey reveals that most of the past researchers have considered MRR, EWR, and surface roughness of the EDMed Inconel as the major focus towards evaluating machining performance; aspects of surface crack and white layer formation (and their quantification) have not been emphasized intensively. Hence, it is indeed a necessity to optimize aforementioned EDM responses simultaneously and thereby to select the most appropriate setting of process parameters for achieving satisfactory machining performance. This invites a multi-response optimization problem in which the optimal solution (parameters setting) needs to be determined from the discrete domain of the controllable process parameters under consideration.

Since, controllable process parameters assume a discrete domain of variation (as per specification and provision of factorial adjustment on the EDM setup), application of



Taguchi method seems fruitful in this context. However, traditional Taguchi approach (Phadke, 1998; Phadke 1989; Park, 1996; Yang and Tarng, 1988; Ghani et al., 2004; Pang et al., 2014) fails to solve multi-response optimization problem. As the current problem is associated with multiple performance characteristics (responses) of EDM, it is necessary to aggregate multi-performance features into an equivalent single index; which can finally be optimized by Taguchi method.

Literature is rich in addressing a variety of multi-response optimization problems in manufacturing domain. Application of grey-Taguchi (Datta et al., 2008), TOPSIS-Taguchi (Singh et al., 2011), desirability function based Taguchi (Singh et al., 2013), and Utility based Taguchi (Singh et al., 2006) approaches etc. have been recommended in existing literature. However, these approaches rely on their own principle (philosophy to search the optimal solution); and hence, the expected outcome may be different for different approaches. Thus, the expertise of the Decision-Maker (DM) plays an important role to recommend the most suitable compromise solution from amongst the set of possible optimal solutions. Hence, research is still being continued to develop alternative approaches to provide reliable outcome of such a multi-response optimization problem.

In course of optimizing multi-responses simultaneously, the aggregation of multi-responses must be carried out to compute a unique performance index so as to convert the present problem into an equivalent single objective optimization case. Then Taguchi method can be attempted to optimize the unique quantitative index.

However, in such a multi-response optimization problem, assignment of priority weight to individual responses is very important whilst converting multi-responses into a unique performance index. This is because, assignment of response priority weight solely depends on the discretion of the DM; and it can vary according to the variation of human perception from a Decision-Maker to another one. Another drawback of aforementioned approaches is that these methods assume negligible response correlation which seems practically invalid. In order to overcome this, application of Principal Component Analysis (PCA) has been prescribed by past researchers (Datta et al., 2009). This technique is capable of eliminating response correlation and thus it converts correlated responses into uncorrelated quality indices. The uncorrelated quality indices (also called principal components or PCs) can now be treated as ‘new response variables’ to go for optimization by different Taguchi based multi-response optimization approaches.

In this context, the present work aims to develop an integrated approach towards multi-response optimization in a case experimental study focusing on EDM of Inconel 718

super alloys. Principal Component Analysis (PCA) integrated with satisfaction function and distance based approach has been proposed herein in amalgamation with Taguchi method to optimize machining performance features during EDM of Inconel 718. The optimal setting thus obtained has been verified to that of using Principal Component Analysis (PCA) and Combined Quality Loss (CQL) based Taguchi approach already highlighted in existing literature resource (Routara et al., 2010). Optimal setting has been verified finally by confirmatory test. Apart from that, surface morphology of EDMed Inconel 718 work surface has been studied in detail with the help of scanning electron microscopy.

## 7.3 Data Analysis: Methodology

### 7.3.1 Satisfaction Function

Martel and Aouni (1990) used the concept of the satisfaction functions as a powerful tool to aggregate simultaneously several quality characteristics. The satisfaction functions are not necessarily linear and symmetric as in the case of fuzzy membership functions. The general shape of the satisfaction function is shown in Fig. 7.1, where  $S(x)$  is the satisfaction function associated with deviation  $x$ ;  $x_{id}$  the indifference threshold;  $x_o$  is the dissatisfaction threshold; and  $x_v$  is the veto threshold (Cherif et al., 2008). The DM is fully satisfied when the deviation  $x$  is within the interval  $[0, x_{id}]$ . Therefore, within the range of indifference  $[0, x_{id}]$ , the deviation  $x$  is not penalized and the DM's satisfaction level will be at its maximal value of 1. Outside this interval, where  $x \in [x_{id}, x_o]$ , the DM's satisfaction function is decreasing monotonously. Besides, any solution leading to a deviation that exceeds the veto threshold  $x_v$  will be rejected. Briefly, satisfaction function converts the deviations in the interval of  $[x_{id}, x_v]$  to a satisfaction value in the interval of  $[0, 1]$ . In this work, satisfaction function approach has been used to convert of the machining performance parameters viz. MRR, EWR,  $R_a$ , SCD, WLT and MH to satisfaction values between 0 and 1, regardless of their physical units. When no information about the preference of the DM is available, the satisfaction function is assumed to be linear (Suh, 1990; Chen, 1997; Chen, 2001; Fiat et al., 2008; Kentli and Kar, 2011).

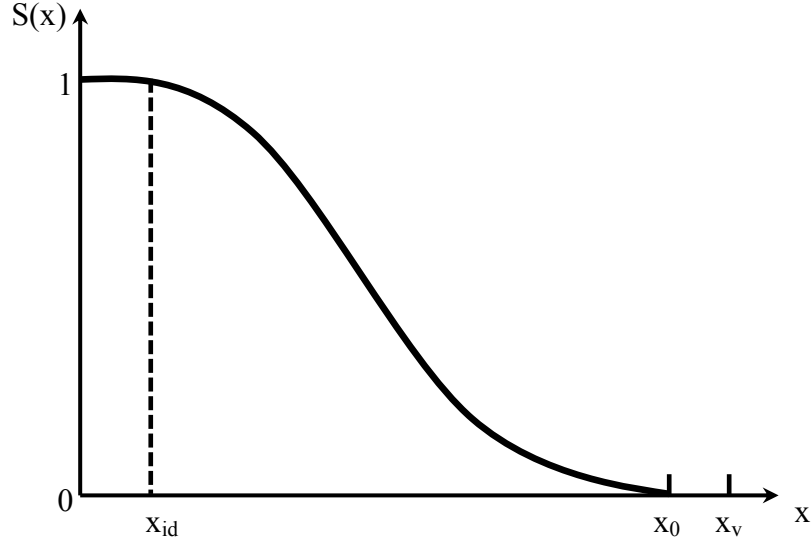


Fig. 7.1: General shape of the satisfaction function

Using the values obtained from the satisfaction functions for each of the machining characteristics, a distance function has been explored to combine these values into a composite number. This function is similar to Euclidean norm. The parametric setting which corresponds to the minimum distance  $d_T$  from the ideal point (ideal satisfaction values for each of the performance characteristics) is the most suitable one.

$$d_T = \left[ \sum_{i=1}^n (1 - S_i)^2 \right]^{1/2} \quad (7.1)$$

Assume that there exist a total  $n$  number of performance characteristics;  $S_i$  is the satisfaction value of  $i^{th}$  response.

When the value of EWR,  $R_a$ , SCD, WLT and MH (individually) is at the minimum of the set, it provides the best satisfaction, and when it is at the maximum, it provides zero satisfaction. Similarly, when the MRR is at the minimum of the set, it provides zero satisfaction, and when it is at the maximum it provides the maximum satisfaction.

How the satisfaction function is to be used is shown in Fig. 7.2.1 in the case where the maximum satisfaction is obtained from the minimum value of the performance characteristics, such as EWR,  $R_a$ , SCD, WLT and MH. Fig. 7.2.2 shows the case where the maximum satisfaction is obtained from the maximum value of the performance characteristic, say MRR.



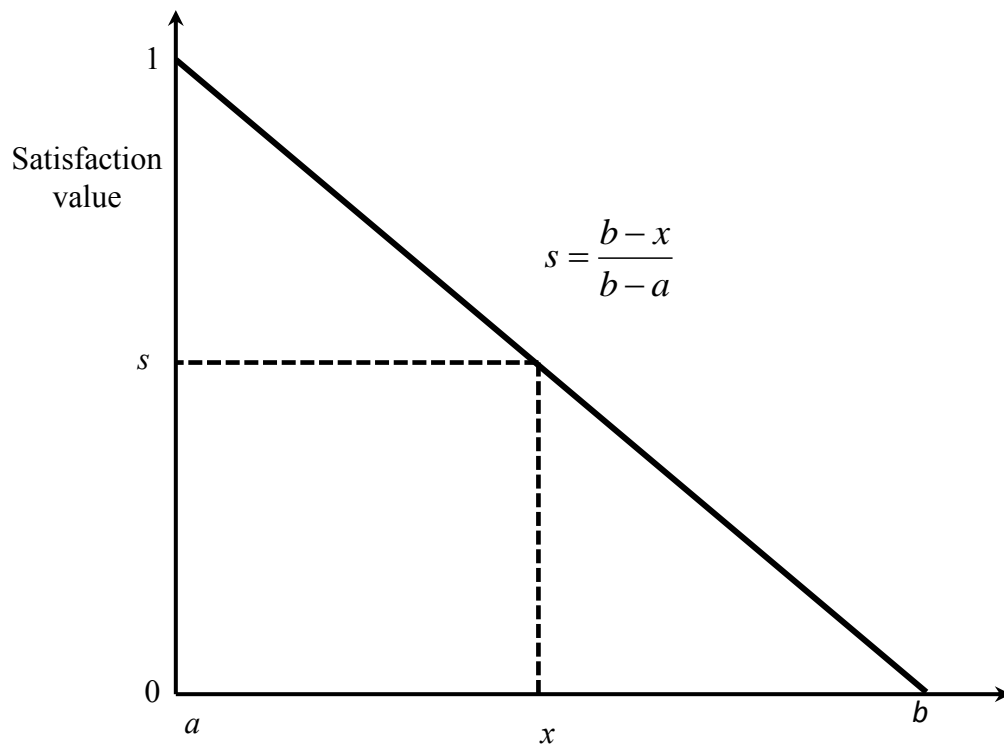


Fig. 7.2.1: Degree of satisfaction chart for a characteristic where the minimum value provides the best satisfaction (Lower-is-Better; LB)

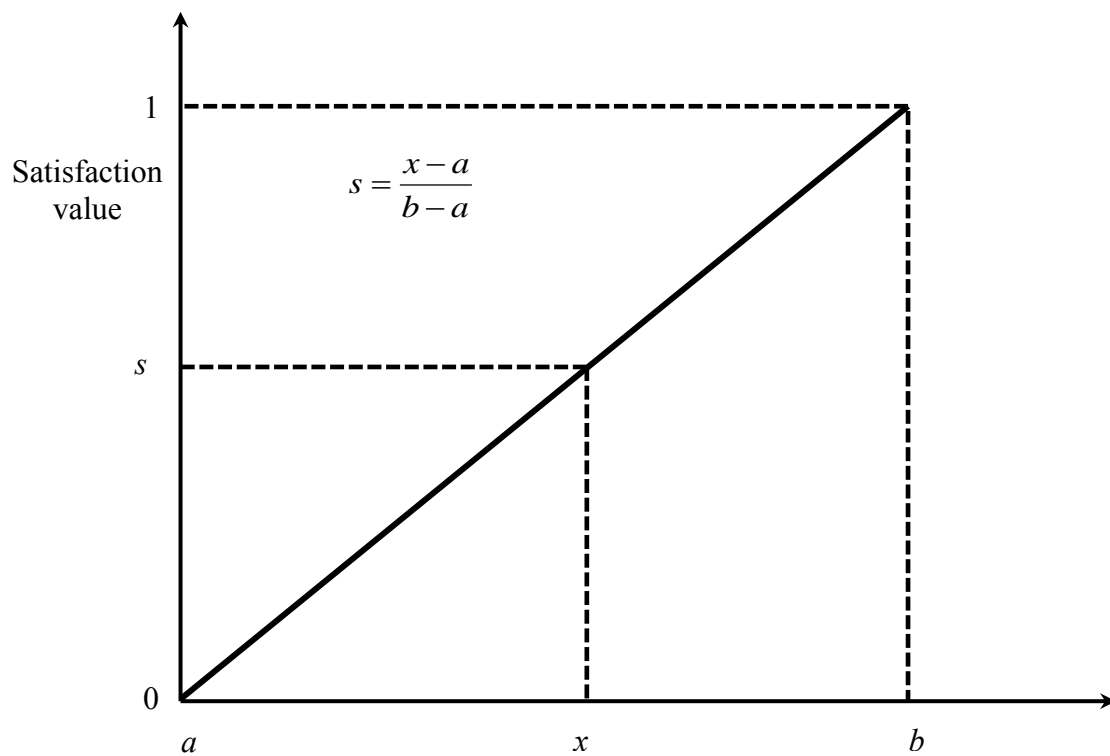


Fig. 7.2.2: Degree of satisfaction chart for a characteristic where the maximum value provides the best satisfaction (Higher-is-Better; HB)

### 7.3.2 Proposed Optimization Module

A satisfaction function and distance based approach has been attempted herein in conjugation with Taguchi's philosophy for optimization of EDM performance features on Inconel 718. Principal Component Analysis (PCA) has been carried out to eliminate response-correlation and to transform correlated responses into lesser number of uncorrelated quality indices, called major principal components (PCs). Quality Loss (QL) concept has been introduced herein representing the absolute deviation of individual PCs with respect to the ideal values. Satisfaction values corresponding to the QL of individual PCs for each experimental run have been computed next. A minimum value of QL yields maximum satisfaction; as QL corresponds to Lowe-is-Better (LB) criteria. Now, satisfaction values of individual PCs have been utilized to compute a unique distance measure ( $d_T$ ). This distance measure represents the deviation of the machining yield from the ideal satisfaction value. Finally,  $d_T$  has been optimized (minimized) by Taguchi method. The optimal parametric setting thus obtained has been compared to that of PCA and Combined Quality Loss (CQL) based Taguchi optimization approach (Routara et al., 2010). The flow chart of aforesaid two optimization approaches has been depicted in APPENDIX, provided at the end of this chapter.

## 7.4 Results and Discussion

Experimental data as depicted in Table 2.12 of Chapter 2 (Phase V), have been normalized first. Normalization has been carried out to eliminate criteria conflict and dimensional effect. For normalizing the dataset of MRR (which corresponds to HB criteria), the following formula has been used.

$$x_i^* = \frac{x_i}{x_{\max}} \Big|_{i=1,2,\dots,n} \quad (7.2)$$

Here  $x_i^*$  is the normalized data for  $i^{th}$  experimental run ( $i = 1, 2, \dots, n$ );  $x_i$  is the experimental data for  $i^{th}$  experimental run;  $x_{\max}$  is the maximum value of the data series  $x_i | i = 1, 2, \dots, n$ .

For normalizing the dataset of EWR, Ra, SCD, WLT and MH (all correspond to LB criteria), the following formula has been used.

$$x_i^* = \frac{x_{\min}}{x_i} \Big|_{i=1,2,\dots,n} \quad (7.3)$$

Here  $x_i^*$  is the normalized data for  $i^{th}$  experimental run ( $i = 1, 2, \dots, n$ );  $x_i$  is the experimental data for  $i^{th}$  experimental run;  $x_{\min}$  is the minimum value of the data series  $x_i | i = 1, 2, \dots, n$ .

It is to be noted that after normalization, the criteria requirement of the normalized responses appear as Higher-is-Better (HB); and the ideal normalized data corresponds to a value unity. The normalized data have been depicted in Table 7.1.

As the present research aims at optimizing multi-response features in relation to EDM of Inconel 718 by applying a satisfaction function and distance measure based Taguchi approach; the specific requirements of Taguchi method need to be examined first. Multi-objective optimization by Taguchi method can be applicable only in the case where responses are uncorrelated. Hence, a correlation test has been carried out on exploring normalized dataset of the responses (Table 7.1) and results obtained has been furnished in Table 7.2. Pearson's correlation coefficients between two response pairs (along with p-value) have been shown in Table 7.2. The non-zero value of correlation coefficient of all response pairs indicates the existence of correlation to some extent. The correlation between MRR ~ SCD and EWR ~  $R_a$  appears significant (at 95% confidence level) with correlation coefficient 0.697 (p-value 0) and 0.422 (p-value 0.032), respectively.

Table 7.1: Normalized data

Sl. No.	Normalized response data					
	MRR	EWR	$R_a$	SCD	WLT	MH
Ideal sequence	1.000	1.000	1.000	1.000	1.000	1.000
1	0.100	0.100	0.561	0.354	0.864	0.803
2	0.158	0.500	0.337	0.337	0.850	0.909
3	0.431	0.500	0.234	0.371	0.982	0.799
4	0.544	0.143	0.216	0.412	0.895	0.760
5	0.989	0.100	0.281	0.397	0.942	0.905
6	0.055	0.071	0.571	0.364	0.873	0.901
7	0.170	0.083	0.485	0.368	0.975	0.681
8	0.302	0.250	0.264	0.368	0.950	0.907
9	0.435	0.200	0.278	0.359	0.820	0.943
10	1.000	0.077	0.222	1.000	0.938	0.898
11	0.059	1.000	0.719	0.296	0.838	0.894
12	0.113	1.000	0.386	0.344	0.829	0.904
13	0.205	1.000	0.294	0.333	0.828	0.868
14	0.552	0.500	0.250	0.602	0.856	0.869
15	0.892	0.167	0.219	0.448	0.872	0.903
16	0.026	1.000	0.500	0.326	0.909	0.918
17	0.055	0.500	0.405	0.357	0.921	1.000
18	0.253	0.500	0.296	0.519	0.918	0.914
19	0.503	0.500	0.376	0.667	0.891	0.903
20	0.550	1.000	0.216	0.509	0.884	0.858
21	0.015	1.000	1.000	0.359	0.946	0.932
22	0.081	1.000	0.376	0.479	1.000	0.946
23	0.209	0.333	0.291	0.412	0.940	0.938
24	0.282	0.250	0.232	0.483	0.843	0.883
25	0.539	0.500	0.206	0.560	0.873	0.816

Table 7.2: Check for response correlation

Correlation between response pairs	Pearson's correlation coefficient	p-value	Remark
MRR ~ EWR	-0.287	0.156	Insignificant
MMR ~ R <sub>a</sub>	-0.237	0.244	Insignificant
MRR ~ SCD	0.697	0.000	<b>Significant</b>
MRR ~ WLT	0.189	0.355	Insignificant
MRR ~ MH	0.027	0.894	Insignificant
EWR ~ R <sub>a</sub>	0.422	0.032	<b>Significant</b>
EWR ~ SCD	-0.013	0.949	Insignificant
EWR ~ WLT	0.017	0.933	Insignificant
EWR ~ MH	0.354	0.076	Insignificant
R <sub>a</sub> ~ SCD	0.08	0.697	Insignificant
R <sub>a</sub> ~ WLT	0.252	0.214	Insignificant
R <sub>a</sub> ~ MH	0.276	0.173	Insignificant
SCD ~ WLT	0.328	0.102	Insignificant
SCD ~ MH	0.211	0.300	Insignificant
WLT ~ MH	0.44	0.830	Insignificant

Table 7.3: Results of PCA

Eigen analysis of the correlation matrix						
	PC1	PC2	PC3	PC4	PC5	PC6
Eigenvalue	1.9102	1.8211	0.9606	0.5739	0.5087	0.2254
Eigenvector	0.657 - 0.261 - 0.139 0.616 0.316 0.035	0.062 - 0.530 - 0.570 - 0.240 - 0.295 - 0.495	0.199 0.180 - 0.313 0.128 - 0.712 0.554	- 0.188 - 0.513 - 0.192 - 0.288 0.370 0.667	- 0.034 0.581 - 0.697 - 0.084 0.409 - 0.026	0.699 0.131 0.185 - 0.675 0.050 0.031
Accountability proportion (AP)	0.318	0.304	0.160	0.096	0.085	0.038
Cumulative Accountability proportion (CAP)	0.318	0.622	0.782	0.878	0.962	1.000

In order to eliminate response correlation, Principal Component Analysis (PCA) [Su and Tong, 1997; Tong and Wang, 2002; Fung and Kang, 2005; Tong et al., 2005; Liao, 2006; Sibaliya and Majstorovic, 2009; Gauri and Pal, 2014] has been carried out on the dataset of Table 7.1; results have been depicted in Table 7.3. It has been seen from Table 7.3 that first three principal components (PC1, PC2 and PC3) could take care 31.8%, 30.4% and 16% data variation, respectively. Rest of the principal components viz. PC4, PC5 and PC6 have corresponded to very low accountability proportion i.e. 9.6%, 8.5% and 3.8%, respectively. Hence, first three principal components (PC1, PC2, and PC3) have been

considered as major principal components (with cumulative accountability proportion 87.8%) and considered for further analysis.

By utilizing normalized response data from Table 7.1 and the components of eigenvector of PC1, PC2 and PC3 obtained from the PCA result in Table 7.3; the values of major principal components have been computed as shown in Table 7.4. Table 7.4 has represented values of individual principal components in all experimental settings including ideal situation. Thus, by exploring PCA, correlated multi-response features (i.e. MRR, EWR,  $R_a$ , SCD, WLT, MH) have been transformed into three uncorrelated quality indices called principal components PC1, PC2 and PC3 to be utilized further in course of Taguchi based optimization approach. Now, Quality Loss (QL) estimates for individual principal components have been computed for each of the experimental runs as shown in Table 7.5.

**Table 7.4:** Computed major Principal Components (PCs)

Sl. No.	Major Principal Components (PCs)		
	PC1	PC2	PC3
Ideal sequence	1.224	-2.068	0.036
1	0.481	-1.104	-0.263
2	0.435	-1.229	-0.042
3	0.687	-1.146	-0.106
4	0.853	-0.905	-0.097
5	1.159	-0.973	0.008
6	0.469	-1.151	-0.231
7	0.582	-1.023	-0.373
8	0.655	-1.082	-0.105
9	0.708	-1.032	0.020
10	1.550	-1.067	0.101
11	0.157	-1.697	-0.097
12	0.265	-1.517	0.037
13	0.330	-1.438	0.063
14	0.869	-1.200	0.070
15	1.096	-0.970	0.076
16	0.207	-1.614	-0.068
17	0.395	-1.345	-0.082
18	0.636	-1.266	-0.033
19	0.872	-1.318	0.023
20	0.693	-1.427	0.133
21	0.162	-1.926	-0.241
22	0.384	-1.618	-0.049
23	0.593	-1.170	-0.086
24	0.682	-1.049	-0.020
25	0.844	-1.145	0.035

**Table 7.5:** Computed Quality Loss (QL) estimates

Sl. No.	Quality loss (QL) estimates			Combined Quality Loss (CQL) [Lower-is-Better]	Corresponding S/N ratio [dB]	Predicted S/N ratio [dB]
	QL(1)	QL(2)	QL(3)			
1	0.743	0.964	0.299	0.738	2.63887	8.52912
2	0.789	0.839	0.078	0.663	3.56973	
3	0.537	0.922	0.142	0.606	4.35055	
4	0.371	1.163	0.133	0.630	4.01319	
5	0.065	1.095	0.028	0.458	6.78269	
6	0.755	0.917	0.267	0.718	2.87751	
7	0.642	1.045	0.409	0.751	2.48720	
8	0.569	0.986	0.141	0.643	3.83578	
9	0.516	1.036	0.016	0.616	4.20839	
10	0.326	1.001	0.065	0.535	5.43292	
11	1.067	0.371	0.133	0.605	4.36489	
12	0.959	0.551	0.001	0.604	4.37926	
13	0.894	0.630	0.027	0.614	4.23663	
14	0.355	0.868	0.034	0.489	6.21382	
15	0.128	1.098	0.040	0.487	6.24942	
16	1.017	0.454	0.104	0.611	4.27918	
17	0.829	0.723	0.118	0.642	3.84930	
18	0.588	0.802	0.069	0.565	4.95903	
19	0.352	0.750	0.013	0.437	7.19037	
20	0.531	0.641	0.097	0.485	6.28517	
21	1.062	0.142	0.277	0.544	5.28802	
22	0.840	0.450	0.085	0.534	5.44917	
23	0.631	0.898	0.122	0.631	3.99941	
24	0.542	1.019	0.056	0.628	4.04081	
25	0.380	0.923	0.001	0.513	5.79765	

For example, (for *Run No. 1*) QL(1) i.e. quality loss estimate for PC1 has been computed as the absolute value of the deviation of PC1 with respect to the ideal value i.e.  $|1.224 - 0.481|$ . Now, satisfaction values with respect to the quality loss of individual principal components have been computed and shown in [Table 7.6](#). In computing satisfaction values of quality loss estimates (corresponding to three major PCs), the Lowe-is-Better (LB) criteria requirement has been used (refer to [Fig. 7.2.1](#)). Next, the total distance measure ( $d_T$ ) for each of the experimental runs has been computed (using [Eq. 7.1](#)) and shown in [Table 7.6](#). The total distance measure ( $d_T$ ) has been treated as single objective function and finally optimized (minimized) by Taguchi method. [Table 7.7](#) has exhibited mean response (S/N ratio of  $d_T$ ) values for different factorial settings; the same has been plotted in [Fig. 7.3](#) in order to predict the optimal setting. The optimal setting has appeared as ( $A_4B_5C_1D_5E_3$ ) i.e. OCV=80V,  $I_p$ =11A,  $T_{on}$ =100 $\mu$ s,  $\tau$  =85% and  $F_p$ =0.4 bar. The predicted S/N ratio of  $d_T$  as obtained through Taguchi analysis at the

setting ( $A_4B_5C_1D_5E_3$ ) appears as (-1.55193 dB); which has been found the highest as compared to the entries of S/N ratios for all experimental settings (refer to [Table 7.6](#)). This has inferred satisfactory prediction of the optimal setting. This has further been validated by confirmatory test to be discussed in later sections.

**Table 7.6:** Computed satisfaction values

Sl. No.	Satisfaction value			Total distance measure $d_T$ [Lower-is-Better]	Corresponding S/N ratio [dB]	Predicted S/N ratio [dB]
	$S_{QL(1)}$	$S_{QL(2)}$	$S_{QL(3)}$			
Ideal sequence	1.000	1.000	1.000	0.000	-	-
1	0.304	0.171	0.269	1.474	-3.36995	-1.55193
2	0.261	0.279	0.809	1.438	-3.15518	
3	0.497	0.207	0.653	1.372	-2.74708	
4	0.652	0.000	0.675	1.456	-3.26323	
5	0.939	0.058	0.932	1.375	-2.76605	
6	0.292	0.212	0.347	1.457	-3.26919	
7	0.398	0.101	0.000	1.473	-3.36405	
8	0.467	0.152	0.655	1.415	-3.01513	
9	0.516	0.109	0.961	1.424	-3.07020	
10	0.694	0.139	0.841	1.354	-2.63237	
11	0.000	0.681	0.675	1.450	-3.22736	
12	0.101	0.526	0.998	1.426	-3.08239	
13	0.162	0.458	0.934	1.413	-3.00284	
14	0.667	0.254	0.917	1.291	-2.21852	
15	0.880	0.056	0.902	1.380	-2.79758	
16	0.047	0.610	0.746	1.436	-3.14309	
17	0.223	0.378	0.711	1.411	-2.99054	
18	0.449	0.310	0.831	1.334	-2.50312	
19	0.670	0.355	0.968	1.235	-1.83334	
20	0.502	0.449	0.763	1.246	-1.91036	
21	0.005	0.878	0.323	1.416	-3.02127	
22	0.213	0.613	0.792	1.330	-2.47703	
23	0.409	0.228	0.702	1.395	-2.89148	
24	0.492	0.124	0.863	1.423	-3.06410	
25	0.644	0.206	0.998	1.325	-2.44432	

## 7.5 Comparative Analysis

A comparative analysis has been made to validate application potential of satisfaction function and distance based approach in combination with Taguchi philosophy. The optimal setting as obtained in aforesaid part of data analysis has been compared to that obtained by exploring Combined Quality Loss (CQL) (adapted from PCA) based Taguchi method ([Routara et al., 2010](#)). In Weighted Principal Component Analysis (WPCA)

(Liao, 2006), accountability proportions of individual principal components are treated as priority weights, thus facilitating computation of Composite Principal Component (CPC).

$$CPC = PC1 \times w_1 + PC2 \times w_2 + \dots + PCi \times w_i + \dots + PCn \times w_n \quad (7.3)$$

Assuming there are a total  $n$  number of principal components and  $w_i$  is the accountability proportion (treated as priority weight) of  $i^{th}$  principal component i.e.  $PCi$ . Also,  $\sum_{i=1}^n w_i = 1$ .

**Table 7.7:** Mean response (S/N ratio of  $d_T$ ) table: Prediction of optimal setting by optimizing  $d_T$

Level	Mean response values at different factorial levels				
	A	B*	C	D	E
1	-3.060	-3.206	-2.640	-2.865	-3.047
2	-3.070	-3.014	-2.789	-3.000	-2.880
3	-2.866	-2.832	-2.863	-2.734	-2.663
4	-2.476	-2.690	-2.990	-2.990	-2.785
5	-2.780	-2.510	-2.970	-2.664	-2.877
Delta	0.594	0.696	0.349	0.336	0.384
Rank	2	1	4	5	3

\*The most significant factor

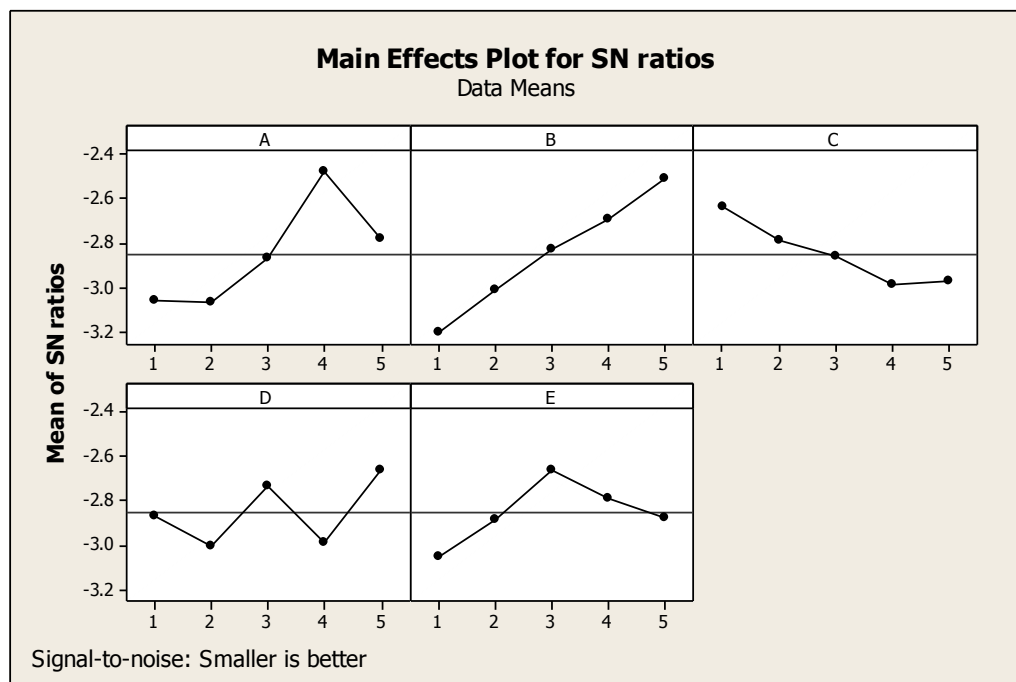


**Fig. 7.3:** Prediction of optimal setting ( $A_4B_5C_1D_5E_3$ ) by optimizing (minimizing)  $d_T$

This CPC is finally optimized (maximized) by using Taguchi method. However, in the present data analysis, (refer to Table 7.4), the values of PC1 for all experimental runs have appeared positive; whereas, for values of PC2, all have appeared as negative; and for



PC3 combination of negative and positive values. Thus, difficulty has been experienced in computing CPC. Therefore, quality loss estimates (corresponding to individual PCs) have been computed as depicted in Table 7.5.

A Combined Quality Loss (CQL) (corresponding to individual experimental runs) has been computed by aggregating quality loss estimates of individual PCs (using Eq. 7.4) as shown in Table 7.5.

$$CQL = QL(1) \times w_1^N + QL(2) \times w_2^N + QL(3) \times w_3^N \quad (7.4)$$

Here, QL(1), QL(2) and QL(3) have been the quality loss estimates for major principal components (PC1, PC2 and PC3). Also,  $w_1 = 0.318, w_2 = 0.304, w_3 = 0.160$  have been the weights (accountability proportion) of principal components (PC1, PC2 and PC3), respectively. Since all principal components (PC1 to PC6) have not been considered here, therefore,  $w_1 + w_2 + w_3 \neq 1$ . Thus, normalized weights have been explored in (Eq. 7.4), so as to satisfy the condition  $w_1^N + w_2^N + w_3^N \neq 1$ .

Finally, Taguchi method has been explored to optimize (minimize) CQL. Table 7.8 has represented mean response (S/N ratio of CQL) values at different factorial levels. The same has been plotted in Fig. 7.4. The predicted optimal setting has appeared as (A<sub>4</sub>B<sub>5</sub>C<sub>1</sub>D<sub>5</sub>E<sub>3</sub>) [i.e. OCV=80V, I<sub>p</sub>=11A, T<sub>on</sub>=100μs, τ =85% and F<sub>p</sub>=0.4 bar] by optimizing CQL through Taguchi method. Taguchi predicted S/N ratio value of CQL (at the optimal setting) has appeared as (8.52912 dB) which has been found to be the highest as compared to all S/N ratio entries of CQL for all experimental runs (refer to Table 7.5). This has indicated pleasant prediction result. It has also been observed that the optimal setting has appeared the same in aforesaid two approaches (i) optimization of d<sub>T</sub> in satisfaction function and distance based Taguchi method and (ii) optimization of CQL in PCA based Taguchi method.

**Table 7.8:** Mean response (S/N ratio of CQL) table:  
Prediction of optimal setting by optimizing CQL

Level	Mean response values at different factorial levels				
	A	B*	C	D	E
1	4.271	3.890	4.939	4.302	4.123
2	3.768	3.947	4.777	4.312	4.580
3	5.089	4.276	4.306	4.618	5.328
4	5.313	5.133	4.461	4.599	4.572
5	4.915	6.110	4.873	5.525	4.752
Delta	1.544	2.220	0.633	1.222	1.205
Rank	2	1	5	3	4

\*The most significant factor

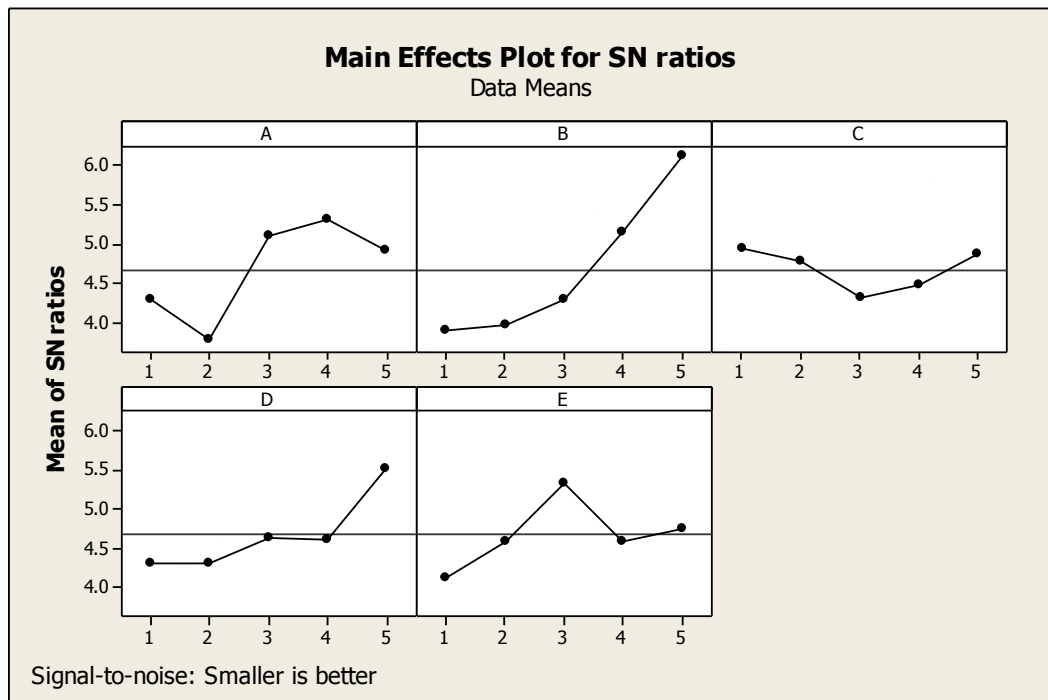


Fig. 7.4: Prediction of optimal setting ( $A_4B_5C_1D_5E_3$ ) by optimizing (minimizing) CQL

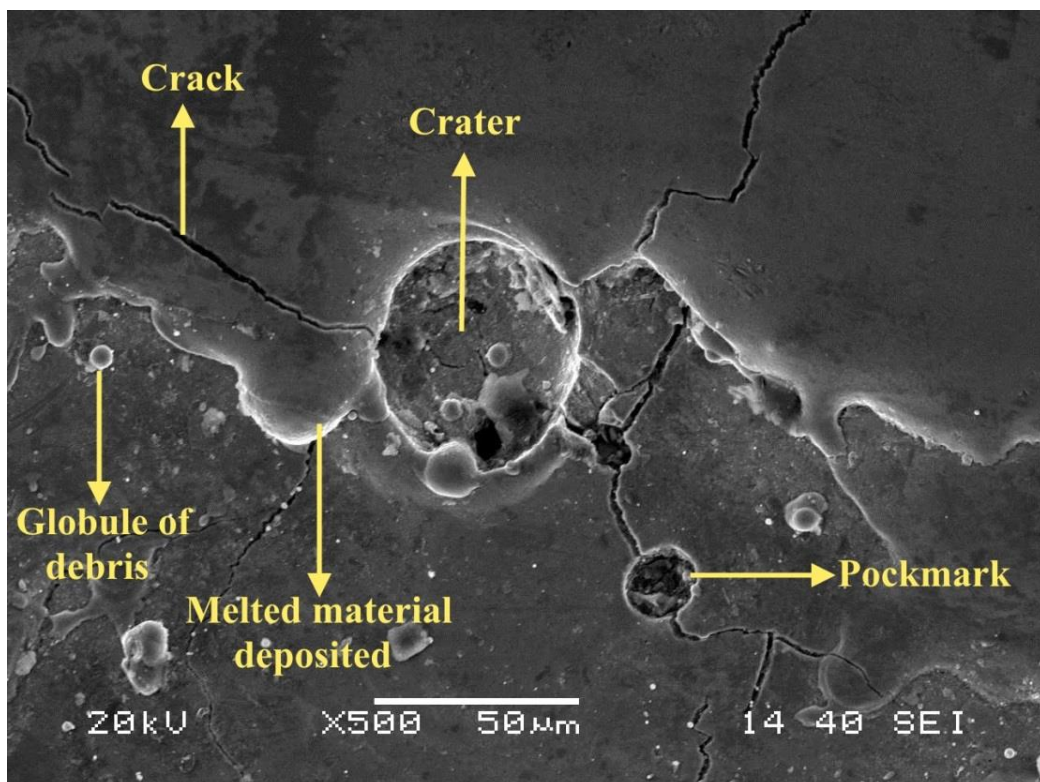


Fig. 7.5: Characteristics of EDMed work surface of Inconel 718 obtained at parameters setting [OCV=50V,  $I_p$ =11A,  $T_{on}$ =500 $\mu$ s,  $\tau$ =85% and  $F_p$ =0.6bar]

## 7.6 Study of the characteristics of EDMed work surface of Inconel 718

It has been observed that EDM process has produced much damage on the machined Inconel 718 work surface such as globules of debris, pockmarks, melted drops, craters of varying sizes and cracks (Fig. 7.5) resulting an uneven surface profile. Fig. 7.6a, b has depicted characteristics of the EDMed Inconel 718 work surface as compared to ‘as received’ parent material. As compared to the work surface before machining, the EDMed surface has appeared disappointing due to uneven surface texture, melted metal deposition, formation of white layer, pockmarks, surface cracks etc.; the causes behind formation of such surface irregularities has clearly been reported in (Hasçalik and Çaydaş, 2007; Rao et al., 2014).

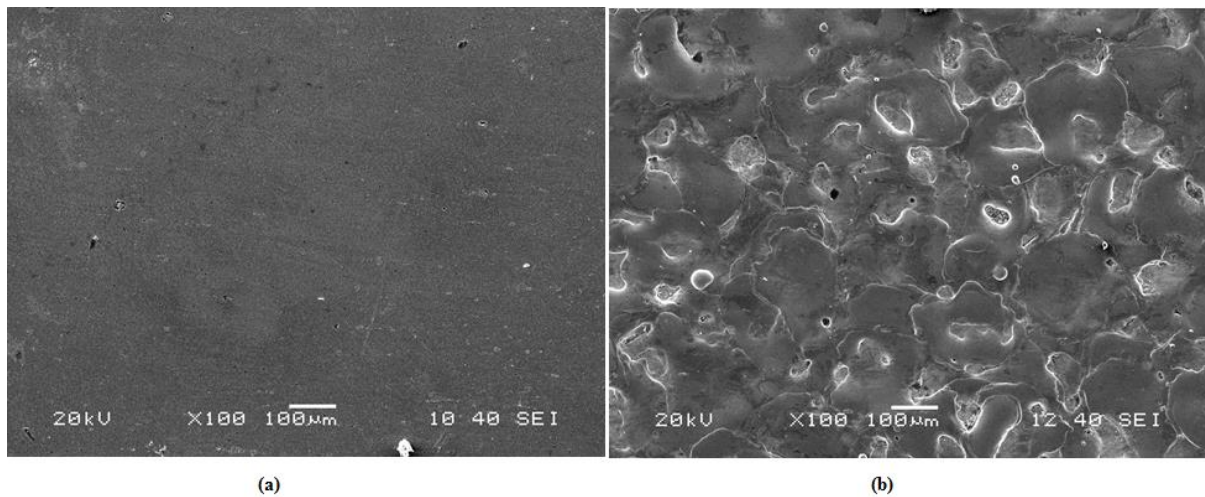


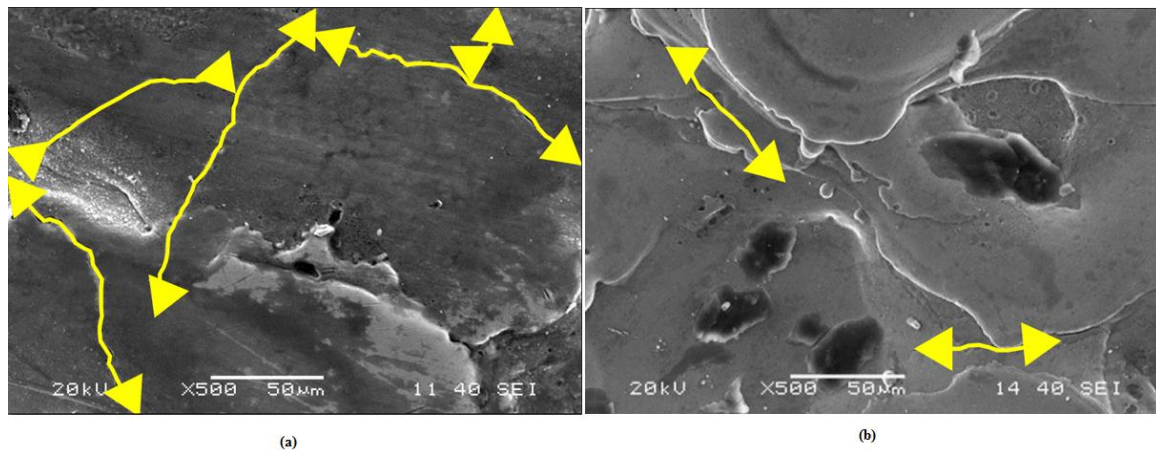
Fig. 7.6: SEM micrographs of Inconel 718 before and after machining: (a) ‘As received’ Inconel 718, and (b) EDMed work surface obtained at parameters setting ( $A_1B_1C_1D_1E_1$ ) i.e. [OCV=50V,  $I_p=3A$ ,  $T_{on}=100\mu s$ ,  $\tau=60\%$  and  $F_p=0.2$  bar]

Table 7.9: Results of confirmatory test

Setting(s)	Experimental data					
	MRR [mm <sup>3</sup> /min]	EWR [mm <sup>3</sup> /min]	$R_a$ [µm]	SCD [µm/µm <sup>2</sup> ]	WLT [µm]	MH [HV <sub>0.05</sub> ]
$A_2B_3C_4D_5E_1$	26.92124	0.044793	8.067	0.0152	17.523	388.9667
$A_4B_5C_1D_5E_3$ (Optimal)	54.67643468	0.156950673	3.9000	0.00407	5.4120	319.5667

## 7.7 Confirmatory Test

In order to validate the predicted optimal setting, confirmatory test has been conducted on that particular setting i.e. ( $A_4B_5C_1D_5E_3$ ) [ $OCV=80V$ ,  $I_p=11A$ ,  $T_{on}=100\mu s$ ,  $\tau=85\%$  and  $F_p=0.4$  bar] and corresponding response features have been noted down. Table 7.9 has depicted a comparative study on the values of machining performance characteristics obtained by exploring the optimal setting ( $A_4B_5C_1D_5E_3$ ) to that of obtained by using an arbitrary setting i.e.  $A_2B_3C_4D_5E_1$  (apart from the optima). It has been observed that optimal setting has produced better results in terms of higher MRR and lesser extent of  $R_a$ , SCD, WLT and MH. The SEM images revealing improvement in SCD and WLT (reduced) in optimal setting (as compared to setting  $A_2B_3C_4D_5E_1$ ) have also been provided in Fig. 7.7a, b and Fig. 7.8a, b, respectively.



**Fig. 7.7:** Comparison on SCD of EDMed work surface of Inconel 718 obtained at parameters setting (a)  $A_2B_3C_4D_5E_1$  [ $OCV=60V$ ,  $I_p=7A$ ,  $T_{on}=400\mu s$ ,  $\tau=85\%$  and  $F_p=0.2$  bar], and (b)  $A_4B_5C_1D_5E_3$  i.e. Optimal Setting [ $OCV=80V$ ,  $I_p=11A$ ,  $T_{on}=100\mu s$ ,  $\tau=85\%$  and  $F_p=0.4$  bar]

However, it seems that the setting  $A_2B_3C_4D_5E_1$  offers better result in term as of EWR ( $0.044793 \text{ mm}^3/\text{min}$ ) as compared to the optimal which corresponds to EWR value of  $0.156950673 \text{ mm}^3/\text{min}$ . As, EWR corresponds to Lower-is-Better (LB) criteria, apparently it seems that the selected arbitrary setting is better as compared to the predicted optimal. However, it is to be noted that optimization is nothing but searching a compromise solution. In case of multi-response optimization problem, where multiple responses are aggregated to compute a single index for final optimization; 100% fulfillment of all the responses cannot be possible simultaneously. It is said that the optimal setting is capable of satisfying the responses up to the maximum possible extent.



This has been well understood from Table 7.9 in the sense that the predicted optimal setting has been found superior (as compared to the setting  $A_2B_3C_4D_5E_1$ ) as it has satisfied the requirements of majority of the response features viz. MRR,  $R_a$ , SCD, WLT and MH.

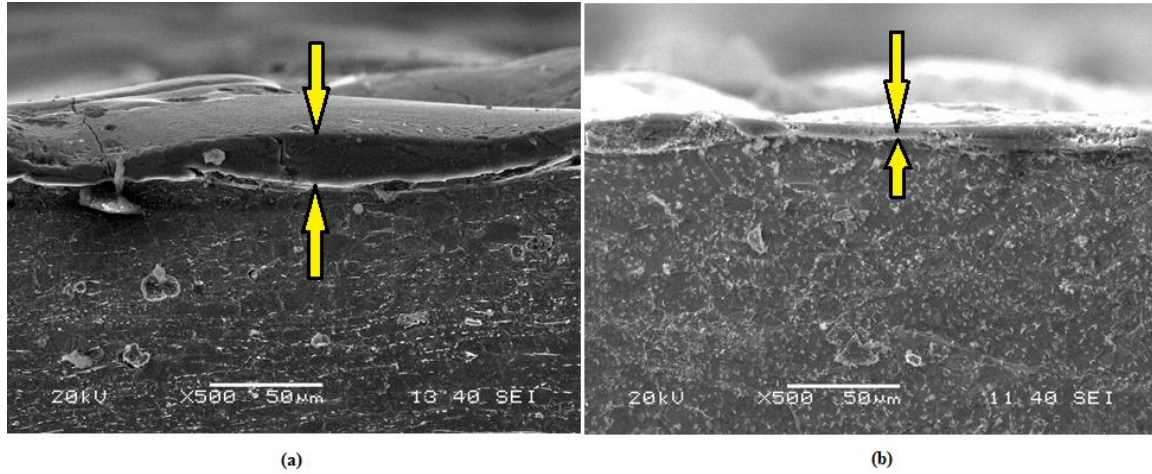


Fig. 7.8: Comparison on WLT obtained onto the top surface EDMed Inconel 718 obtained at parameters setting (a)  $A_2B_3C_4D_5E_1$  [OCV=60V,  $I_p=7A$ ,  $T_{on}=400\mu s$ ,  $\tau=85\%$  and  $F_p=0.2bar$ ], and (b) and  $A_4B_5C_1D_5E_3$  i.e. Optimal Setting [OCV=80V,  $I_p=11A$ ,  $T_{on}=100\mu s$ ,  $\tau=85\%$  and  $F_p=0.4bar$ ]

## 7.8 Conclusions

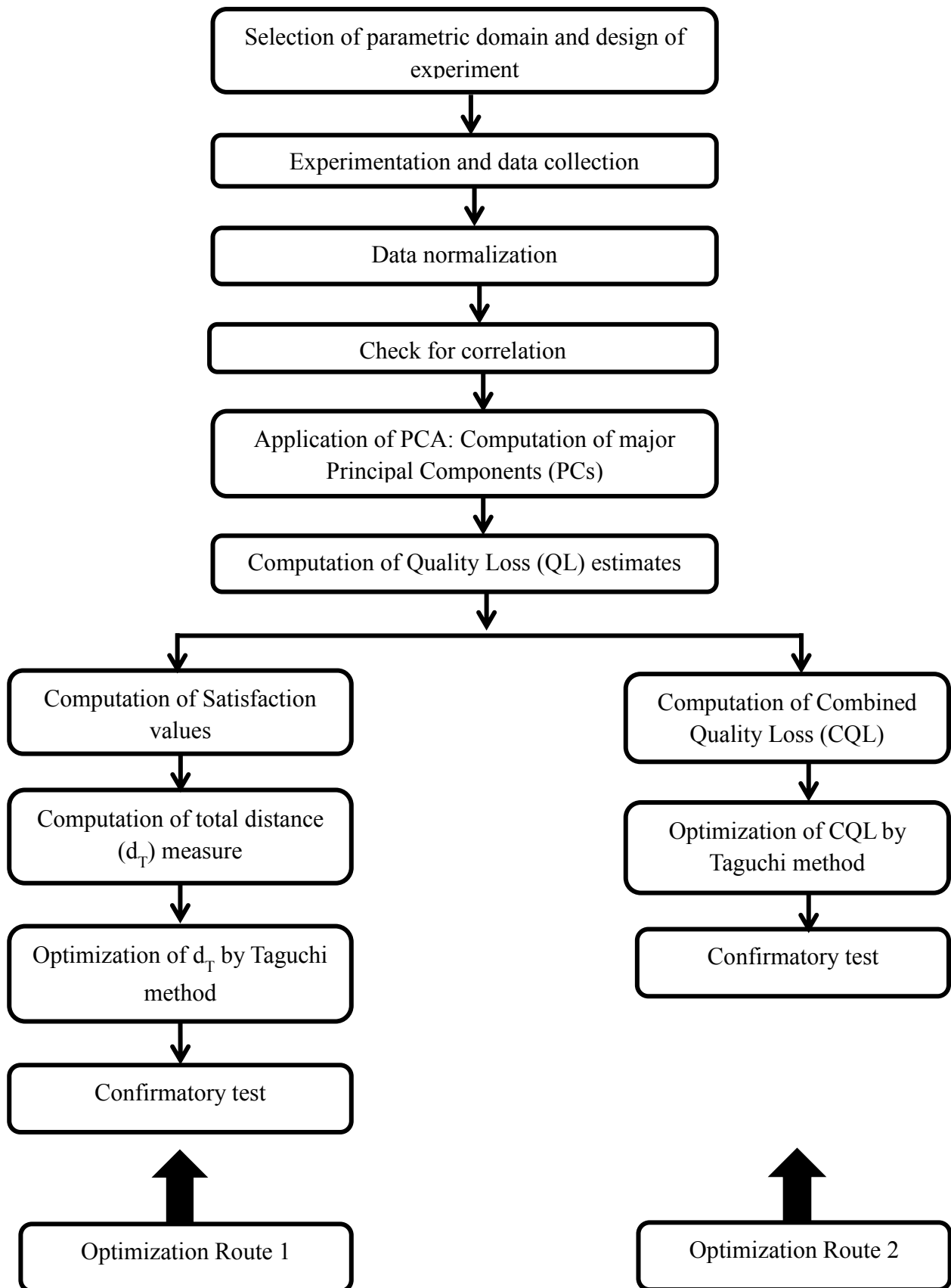
The conclusions of the aforesaid work have been pointed out below.

- ▲ The proposed satisfaction function and distance based approach in conjugation with Taguchi's philosophy has been demonstrated herein to determine the best suitable combination of EDM parameters (viz. gap voltage, peak current, pulse-on-time, duty factor and flashing pressure) to improve machining performances in terms of MRR, EWR,  $R_a$ , SCD, WLT, and MH. Owing to the inability of Taguchi method to solve multi-response optimization problem, the proposed satisfaction function and distance measure based approach seems helpful in aggregating multiple response features into an equivalent single index (i.e.  $d_T$  in the present case) which has been optimized finally by Taguchi method.
- ▲ Application potential of proposed satisfaction function and distance measure based Taguchi optimization route has been verified by Combined Quality Loss (CQL) concept (adapted from PCA) based Taguchi approach. The optimal setting has appeared the same in both the cases. With the EDM setup utilized herein and within

selected parametric domain, the optimal machining environment has been obtained as: OCV=80V,  $I_p=11A$ ,  $T_{on}=100\mu s$ ,  $\tau =85\%$  and  $F_p=0.4$  bar to maximize MRR and minimize EWR,  $R_a$ , SCD, WLT and MH. Optimal result has also been verified by confirmatory test.

- ▲ Before analysing experimental data to go for applying Taguchi based optimization routes, it is customary to check for response correlation. Hence, application of PCA has been recommended at this stage to eliminate response correlation and to convert correlated responses into equal or lesser number of uncorrelated quality indices called principal components. This helps in reduction of number of responses in the case where responses are very large in number. Based on accountability proportion, major principal components can be considered and treated as uncorrelated responses to go for further optimization computations.
- ▲ Mean response tables (mean S/N ratio of  $d_T$  and mean S/N ratio of CQL) have indicated that peak current ( $I_p$ ) has been found to be the most significant parameter to influence machining performances.
- ▲ SEM images of the EDMed work surfaces of Inconel 718 have also been analysed herein. It has been observed that by proper tuning of process parameters surface defects, irregularities, formation of cracks, white layer etc. can be controlled. Confirmatory experiment has revealed that by utilizing optimal setting of process parameters, formation of surface cracks, and white layer could be minimized to a major extent.
- ▲ The proposed satisfaction function and distance measure based approach (in conjugation with Taguchi's philosophy) seems more practical than CQL based Taguchi approach; the former does not require assignment of response weight in computing  $d_T$ . Whilst in case of computing CQL, accountability proportions of major principal components are assumed as individual response weights. In practice assignment of exact weight of the response is indeed difficult since it depends on perception of the Decision-Makers.

APPENDIX: Flowchart of the optimization modules attempted herein



## Chapter 8

# Machining Performance Optimization during Electro-Discharge Machining of Inconel 601, 625, 718 and 825 Super Alloys

### 8.1 Coverage

Nickel-based super alloy (such as Inconel) is widely used in aerospace, nuclear, and chemical industries because of their excellent mechanical and chemical properties at elevated temperatures. Inconel comes under the category of '*difficult-to-cut*' materials. Difficulty is faced whilst machining of Inconel because of its poor thermal conductivity, high toughness, high hardness, and extremely high work hardening behaviour. Moreover, it contains highly abrasive carbide particles which tend to stick on the tool surface, resulting inferior surface finish. Moreover, enormous heat is generated during machining which leads to reduction in tool life. Hence, machining and machinability aspects of Inconel have become a predominant research agenda today.

Technological advances have led to an extensive usage of high strength, high hardness materials in manufacturing industries. In course of machining '*difficult-to-cut*' materials, conventional manufacturing processes are increasingly being replaced by the advanced techniques such as electro-discharge machining, ultrasonic machining, electro-chemical machining and laser machining. Amongst these, EDM has found widespread application in MEMS (Micro-Electro-Mechanical Systems); tool and die, automobile and aerospace industries. Therefore, promoting the quality of the EDMed product and thereby achieving satisfactory machining performance; a thorough understanding of the relationship between the EDM parameters and the machined surface integrity in consideration with the particular tool-work combination has become an important research focus. EDM is an electro-thermal machining process, where electrical energy is used to generate electrical spark and material removal mainly occurs due to thermal energy of the spark. It has



become an excellent option to machine ‘*difficult-to-cut*’ materials and high temperature resistant alloys; super alloy Inconel, in the present case.

An experimental investigation on assessing machining performance during electro-discharge machining of Inconel 625, 718, 601 and 825 has been delineated herein. Attempt has been made on evaluating optimal machining parameters setting to achieve satisfactory machining yield. Based on 5-factor-4-level  $L_{16}$  orthogonal array, experiments have been carried out by varying gap voltage, peak current, pulse-on time, duty factor and flushing pressure (each varied at four discrete levels) to examine the extent of machining performance in terms of material removal rate, electrode wear rate, surface roughness, and surface crack density of the EDMed end products obtained by utilizing different parameters settings (for different grades of Inconel viz. 601, 625, 718, 825, respectively). An integrated optimization route combining satisfaction function approach, Fuzzy Inference System (FIS) in conjugation with Taguchi’s philosophy has been proposed for simultaneous optimization of aforementioned multiple performance indices. The most favourable machining parameters setting has been obtained as: [gap voltage= 90V, Peak current= 5A, Pulse-on time= 200 $\mu$ s, duty factor = 70%, flushing pressure= 0.6 bar] for Inconel 625; [gap voltage = 90V, Peak current = 5A, Pulse-on time = 200 $\mu$ s, duty factor = 85%, flushing pressure = 0.4 bar] for Inconel 718; [gap voltage = 80V, Peak current = 7A, Pulse-on time = 500 $\mu$ s, duty factor = 80%, flushing pressure = 0.3 bar] for Inconel 601; and [gap voltage = 80V, Peak current = 5A, Pulse-on time = 300 $\mu$ s, duty factor = 85%, flushing pressure = 0.4 bar] for Inconel 825. In addition to that, analysis of SEM micrographs has been carried out to understand surface irregularities in terms of surface cracks, white layer for the EDMed Inconel end products (of different grades).

## 8.2 Scope of the Work

Rapid innovations and advancements in the field of space research, missile and nuclear industry require highly complicated and precise components made out of advanced materials such as super alloys. However, super alloys (for example Inconel) are difficult to be processed through traditional machining routes, from the standpoint of production economics as well as environmental hazards and safety (Yao et al., 2005). Aforementioned challenges have imposed an impulsive motivation towards development of non-traditional machining alternatives (Jain, 2008). The fact is well attributed that

traditional manufacturing/production processes are unsuitable to machine innovative materials such as super alloys like Inconel, as well as to produce intricate geometrical shapes in the hard and high temperature-resistant alloys (Singh et al., 2005). On the contrary, non-traditional machining routes have been found advantageous in this respect. In view of the widespread application of super alloy Inconel especially over automotive and aerospace industries and the challenges being faced thereof whilst machining of this super alloy; the increasing need for better understanding on (i) aspects of machining complexity and possible solution, and (ii) extent of machinability of different grades of Inconel has motivated to define the present research problem.

Literature has depicted that substantial volume of work has been carried out by pioneer researchers for understanding of machining and machinability aspects of Inconel (different grades) in EDM, WEDM, micro-machining etc. (Feyzi and Safavi, 2013; Hewidy et al., 2005; Sharma et al., 2015; Torres et al., 2016; Rodrigues et al., 2015; Ramakrishnan and Karunamoorthy, 2008; Newton et al., 2009; Rajesha et al., 2010; Rajesha et al., 2012; Lin et al., 2013; Li et al., 2013; Ay et al., 2013; Ahmad and Lajis, 2013; Li et al., 2015; Aggarwal et al., 2015). Influence of process variables on various performance attributes has been experimentally investigated and mathematically analyzed. Effort has also been made to optimize process responses towards determining the most favorable process environment (parameters setting) for EDM of Inconel work material. It is felt that the ease of machining i.e. the extent of machinability would tend to vary for Inconel of different grades due to variation in their chemical composition, mechanical properties etc. Process parameters also interact in a complicated manner; thereby, influencing EDM performance characteristics. However, aforementioned studies have considered a particular grade of Inconel alloy (especially Inconel 718). Literature has been found sparse to deliver a consolidated database comparing machinability aspects of different grades of Inconel for electro-discharge machining.

Based on extensive literature review, specific research gaps/questions have been identified as mentioned below.

1. Is there a unique optimal setting of process parameters which can simultaneously satisfy multi-requirements of process performance yields in terms of MRR, EWR,  $R_a$  and SCD during EDM of different grades of Inconel super alloy?

2. In deriving the most favourable (optimal) setting of process parameters, it seems necessary to aggregate multi-performance features into a unique quality index which can finally be optimized using Taguchi method. Literature is rich enough in addressing application of Taguchi based optimization approaches like grey-Taguchi, desirability function based Taguchi, utility theory based Taguchi, TOPSIS (Technique for Order Preference by Similarity to Ideal Solution) based Taguchi etc. in optimizing process/product in the domain of manufacturing. However, these approaches consider priority weight of individual responses in course of aggregating multiple response variables into a unique performance index. As assignment of response priority weight is absolutely based on the personal judgment of the Decision-Maker (DM); the weights set may vary from person to person. This invites uncertainties in decision making. It is worth of investigating whether optimal parameters' setting is sensitive to the change in weights of the response variables. In order or avoid this limitation, the present work proposes application of satisfaction function integrated with Fuzzy Inference System (FIS) for logical aggregation of multi-performance features into a unique performance index. Such an aggregation is performed in FIS internal hierarchy, and it does not require utilizing response priority weight assigned by the Decision-Makers.
3. Most of the earlier studies ([Ay et al. 2013](#); [Sengottuvel et al., 2013](#); [Mohanty et al., 2014a, b](#); [Aggarwal et al., 2015](#)) focused on multi-response optimization in machining of Inconel considering the objective functions like MRR, EWR and  $R_a$ . Few studies have emphasized on dimensional deviation and form tolerances of the EDMed end product. Aspects of formation of surface cracks as well as white layer have still been untouched. Therefore, in the present work, a unified attempt has been made to include surface crack density in the list of response functions (including MRR, EWR and  $R_a$ ) to be optimized simultaneously. Apart from this, few micrographic analyses have been carried out on selected specimens of the EDMed Inconel work material to check whether variation in Inconel grades (i.e. variation in chemical constituents) influences thickness of the white layer generated during EDM onto the machined surface.

To address these issues, present work aims to perform an experimental study to compare machining behaviour of Inconel 601, 625, 718 and 825, respectively, during EDM with a graphite electrode. The specific objective of the current work is to determine a suitable parameters setting consisting of gap voltage, peak current, pulse-on time, duty factor and

flushing pressure, for achieving satisfactory machining yield in terms of MRR, EWR,  $R_a$ , SCD etc. for electro-discharge machining of Inconel 601, 625, 718 and 825, respectively. In accomplishing this, application of satisfaction function approach, Fuzzy Inference System (FIS) integrated with Taguchi method is aimed to be attempted to determine an optimal process environment (for each grade of Inconel) to ensure high MRR, lesser extent of EWR,  $R_a$  as well as SCD.

## 8.3 Data Analysis

### 8.3.1 Methodology

#### 8.3.1.1 Fuzzy Inference System (FIS)

Fuzzy logic is a mathematical theory of inexact reasoning that facilitates modelling of the reasoning process of human in linguistic terms (Zadeh, 1976; Cox, 1992; Mendel, 1995; Yager and Filev, 1999). It seems very efficient in defining the relationship between system inputs and desired output(s). Fuzzy controllers and fuzzy reasoning have found particular applications in extremely complicated industrial systems that cannot be modelled precisely even under various assumptions and approximations (Tzeng and Chen, 2007). A fuzzy system is basically composed of a fuzzifier, an inference engine, a knowledge base (rule and data base), and a defuzzifier (Fig. 8.1).

The execution of fuzzy inference system involves exploration of membership functions, fuzzy logic operators, and IF-THEN rules considering relationships of inputs with respect to output(s).

The parameters of the IF-THEN rules (referred to as antecedents or premises in fuzzy modelling) define a fuzzy region of the input space; whilst the output parameters (also used as consequents in fuzzy modelling) specify the corresponding output. Two types of FISs, the Mamdani FIS and the Sugeno FIS, have been widely used in various applications. Aforesaid two types of inference systems vary somewhat in the way by which output(s) is/are determined. Literature depicts that Mamdani FIS is intuitive and its rule base can easily be interpreted. The Mamdani FIS can be used directly for both Multi-Input-Single Output (MISO) systems and Multi-Input-Multiple-Output (MIMO) systems (Kovac et al., 2014). In terms of usage, Mamdani FIS is more widely used; mostly because it provides reasonable results with a relatively simple structure, and also due to the intuitive and interpretable nature of the rule base.

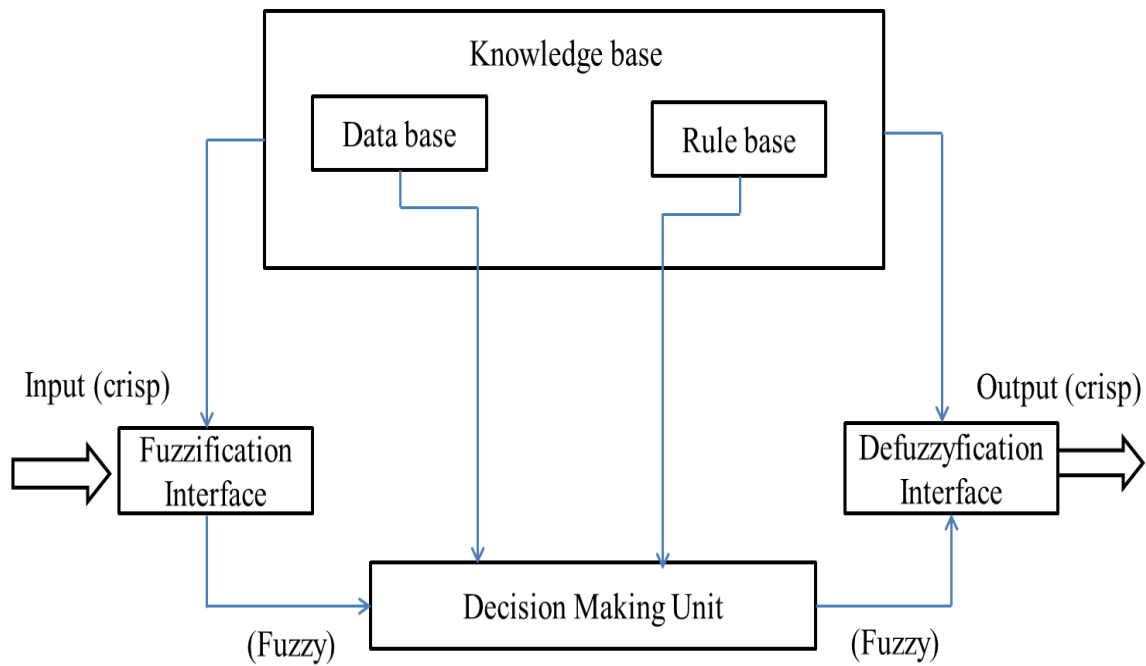


Fig. 8.1: FIS architecture

### 8.3.1.2 Taguchi Method

Taguchi method pioneered by *Dr. Genichi Taguchi* in 1940s is an engineering methodology for improving productivity in manufacturing processes at an economic cost. According to Taguchi, a robust design is one that is created with a system of design tools to reduce variability in product (or process), while simultaneously guiding the performance towards an optimal setting. A product that is robustly designed is expected to provide customer satisfaction even when subjected to extreme conditions on the manufacturing floor or in the service environment. Taguchi method is based on performing evaluation or experiments to test the sensitivity of a set of response variables with respect to a set of control parameters (or independent variables) by considering experiments as per orthogonal array design of experiment aiming to attain the optimum setting of the control parameters. Orthogonal array provides the best set of well balanced (minimum) experiments; thus, reducing experimental time and execution cost. In Taguchi method, experimental data are transferred into Signal-to-Noise (S/N) ratios which are assessed statistically by ANOVA to determine significant process control parameters and to obtain the optimal parameters setting to maximize process performance/product quality etc. The concepts behind Taguchi methodology are summarized below (Lin et al., 2009).

⇒ Quadratic quality loss functions (Fig. 8.2.1-8.2.3) are used to quantify the loss incurred by the customer due to deviation from target performance.

- ⇒ Taguchi technique uses S/N ratio as a performance measure to choose control levels of process parameters. The S/N ratio considers both the mean and the variability of response data. The change in quality characteristics of a product response to a factor introduced in the experimental design is the signal of the desired effect. The effect of the external factors of the outcome of the quality characteristic under test is termed as noise. Taguchi recommends the use of S/N ratio to measure the quality characteristics deviating from the desired value. The S/N ratio for each level of process parameters is computed based on the S/N analysis and converted into a single metric. The aim in any experiment is to determine the highest possible S/N ratio for the result irrespective of the type of the quality characteristics. A high value of S/N implies that signal is much higher than the random effect of noise factors. In the Taguchi method of optimization, the S/N ratio is used as the quality characteristic of choice.
- ⇒ Orthogonal arrays are used for gathering dependable information about control factors (design parameters) with a reduced number of experiments.

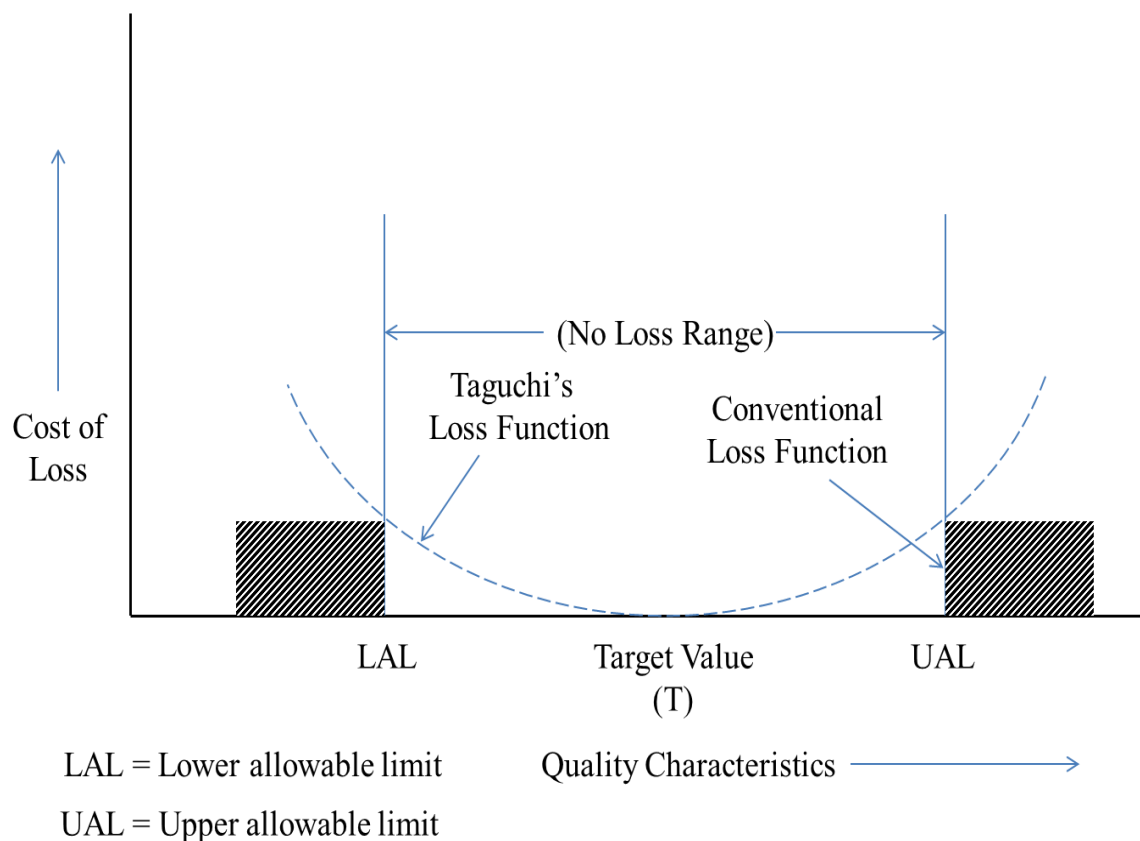


Fig. 8.2.1: Taguchi's loss function of Target-the-Best (TB) type

The different S/N ratio characteristics have been depicted in (Fig. 8.2.1-8.2.3), for Nominal-the-Best (NB) or Target-the-Best (TB), Lower-is-Better (LB) and Higher-is-Better (HB) types, respectively. The computation formulae for converting experimental (response) data into corresponding S/N ratio have been provided in (Eq. 8.1-8.3).

$$S / N|_{HB} = -10 \log \frac{1}{n} \left[ \sum_{i=1}^n \frac{1}{y_i^2} \right] \quad (8.1)$$

$$S / N|_{LB} = -10 \log \frac{1}{n} \left[ \sum_{i=1}^n y_i^2 \right] \quad (8.2)$$

$$S / N|_{NB} = -10 \log \left[ \frac{\mu^2}{\sigma^2} \right] \quad (8.3)$$

Here  $y_i$  is the response value obtained at  $i^{th}$  experimental trial;  $n$  be the total number of trials for a particular parameters setting;  $\mu$  is the mean response value and  $\sigma$  indicates standard deviation.



Fig. 8.2.2: Taguchi's loss function of Lower-is-Better (LB) type



Fig. 8.2.3: Taguchi's loss function of Higher-is-Better (HB) type

### 8.3.1.3 Proposed Optimization Route

An integrated optimization route combining satisfaction function approach, Fuzzy Inference System (FIS) and Taguchi method has been proposed in this work for optimizing multiple response characteristics of EDM on Inconel super alloys. As traditional Taguchi approach alone cannot solve multi-response optimization problem; application of grey relational analysis (Chiang and Hsieh, 2009; Kuram and Ozelik, 2013), desirability function approach (Sait et al., 2009), utility theory (Walia et al., 2006), TOPSIS (*Technique for Order Preference by Similarity to Ideal Situation*) (Şimşek et al., 2013) etc. have been recommended in literature for logical and systematic aggregation of multi-response features into a unique performance index; which is to be optimized finally by Taguchi method. Literature provides immense evidence on application of grey-Taguchi, desirability-Taguchi, utility-Taguchi etc. for multi-response optimization problems mostly in manufacturing environment. However, limited application of satisfaction function has been noticed in existing literature; that too in the field of industrial decision making (Kentli and Kar, 2011).

In this context, present work explores satisfaction function approach to convert experimental data into satisfaction scores of individual responses. Satisfaction scores of individual responses are to be fed as inputs to a fuzzy inference engine; thereby, obtaining aggregated unique output termed as combined satisfaction score ( $S_c$ ). The combined satisfaction score needs to be optimized (maximized) by Taguchi method. The flowchart of the proposed optimization route has been provided in Fig. 8.3.

FIS plays an important role in aggregating multi-inputs into a single output which is treated as unique objective function in Taguchi's optimization module. The additional advantage of exploring FIS is that the inference engine operates under a rule-base in relation to the mapping of inputs versus output and provides a single output. Such an aggregation does not require assignment of response priority weight which often appears uncertain and depends on the Decision-Makers' perceptions.

Thus, proposed optimization route seems advantageous as compared to grey-Taguchi, utility-Taguchi etc. which consider priority weight of individual responses whilst combining multi-performance features into a unique index measure (for example, grey relational grade, overall utility degree, overall desirability etc.).

The theories of satisfaction function approach and related computational formulae have already been discussed in Chapter 7 (Section 7.3.1).



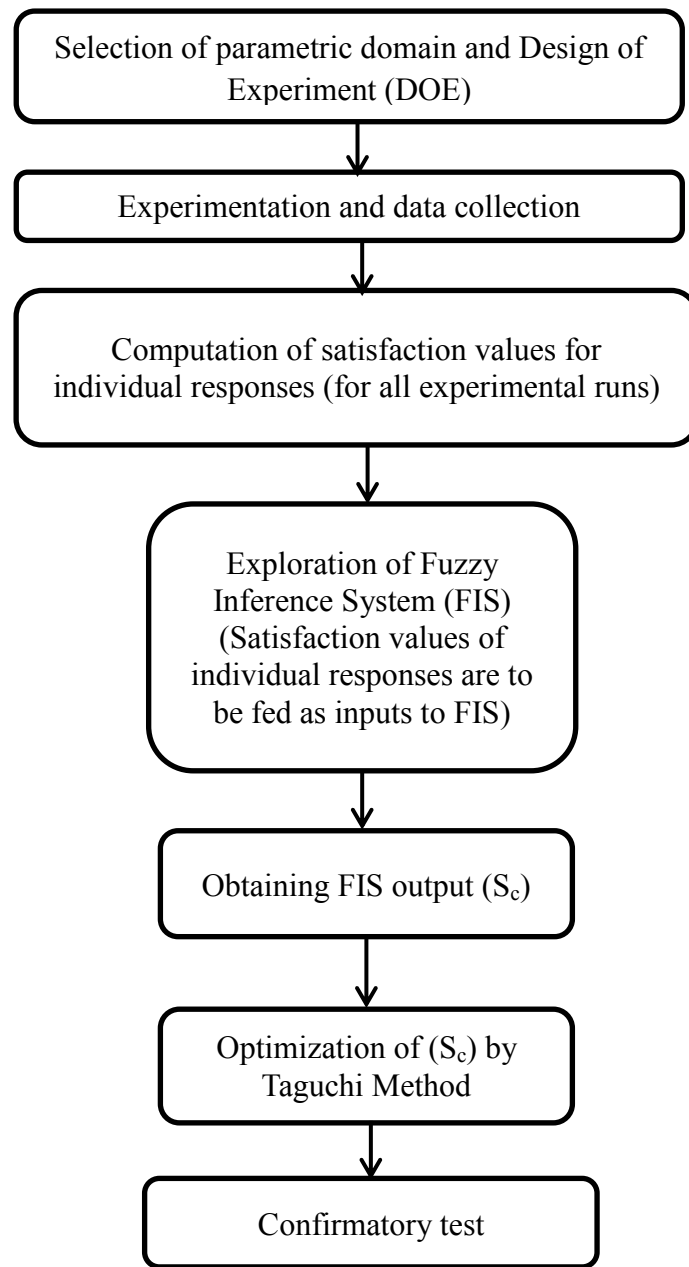


Fig. 8.3: Flowchart of the proposed optimization route

## 8.3.2 Results and Discussion

### 8.3.2.1 Machining Performance Optimization

Experimental data (refer to [Table 2.16](#) of Chapter 2, Phase VI) in relation to process responses viz. MRR, EWR,  $R_a$  and SCD obtained by experimenting at different parametric settings (for Inconel 625, 718, 601 and 825, respectively) have been utilized herein to obtain the most favourable parameters setting (for each of the Inconel grades) to satisfy multi-requirements of process performance yields, simultaneously. The most suitable process environment (parametric setting) is to be selected so as to optimize various process responses up to the maximum possible extent. In order to increase productivity, MRR should correspond to Higher-is-Better (HB) type; whereas, to ensure extended tool life, EWR should be as less as possible (Lower-is-Better; LB type). In order to ensure quality and performance of the end product up to the desired level,  $R_a$  and SCD of the EDMed work surface of Inconel need to be minimized to the maximum possible extent. Thus, it is understood that  $R_a$  and SCD both correspond to LB type. Since traditional Taguchi approach fails to solve multi-response optimization problem; in order to satisfy aforesaid responses of contradicting requirements simultaneously, it seems necessary to aggregate individual response data into an equivalent single performance index. Once a multi-response optimization problem is approximated to the problem of optimizing a single performance measure; Taguchi method can be applied at this stage to get the optimal solution. Since different response features considered herein are contradicting in nature (also correspond to different unit/dimension), a logical normalization is indeed required to convert raw experimental data into corresponding normalized values. Once data are normalized, the problem of criteria conflict and also unit effect are automatically eliminated; normalized data of all individual responses come under a common domain in between [0,1]. In this work, satisfaction function approach has been attempted to convert individual response data (experimentally obtained) into their corresponding satisfaction measures. While converting experimental data of EWR,  $R_a$  and SCD into corresponding satisfaction score ( $S_{EWR}, S_{R_a}, S_{SCD}$ ) the satisfaction chart for LB type (refer to [Fig. 7.2.1](#) of [Chapter 7](#)); and for converting experimental data of MRR in corresponding satisfaction score  $S_{MRR}$ , the satisfaction chart of HB type (refer to [Fig. 7.2.2](#) of [Chapter 7](#)); and for has been used. Computed satisfaction scores of individual responses for all experimental runs have been depicted in [Table 8.1.1-8.1.4](#), for Inconel 625, 718, 601 and 825, respectively. Satisfaction scores of individual responses

$(S_{MRR}, S_{EWR}, S_{R_a}, S_{SCD})$  have been fed as inputs to a Fuzzy Inference System (FIS) for logical aggregation of inputs into a unique performance index i.e. combined satisfaction score ( $S_c$ ). The FIS predicted combined satisfaction score has been treated as single objective function and finally optimized (maximized) by Taguchi method.

**Table 8.1.1:** Satisfaction values (corresponding to each response) for all experimental runs:  
Computed combined satisfaction score ( $S_c$ )

Run No.	<b>Inconel 625</b>						
	Satisfaction values (Higher-is-Better)				$S_c$ (Combined satisfaction score) as FIS output	S/N ratio of $S_c$ [dB]	Predicted S/N ratio (at optimal setting) [dB]
	$S_{MRR}$	$S_{EWR}$	$S_{R_a}$	$S_{SCD}$			
1	0.120	1.000	0.571	0.000	0.506	-5.91699	-4.85072
2	0.058	0.750	0.483	0.932	0.444	-7.05234	
3	0.102	0.250	0.244	0.970	0.437	-7.19037	
4	0.275	0.250	0.117	0.842	0.438	-7.17052	
5	0.051	0.750	0.976	0.759	0.445	-7.03280	
6	0.429	0.500	0.415	0.782	0.493	-6.14306	
7	0.224	0.250	0.576	0.323	0.438	-7.17052	
8	0.569	0.000	0.376	1.000	0.484	-6.30309	
9	0.008	0.750	0.732	0.842	0.467	-6.61366	
10	0.035	1.000	0.663	0.827	0.43	-7.33063	
11	0.529	0.750	0.302	0.925	0.493	-6.14306	
12	0.437	0.250	0.151	0.714	0.438	-7.17052	
13	0.000	1.000	1.000	0.880	0.5	-6.02060	
14	0.056	0.750	0.571	0.489	0.555	-5.11414	
15	0.291	0.500	0.341	0.684	0.472	-6.52116	
16	1.000	0.500	0.000	0.361	0.5	-6.02060	

The proposed FIS architecture has been shown in Fig. 8.4. FIS transforms crisp inputs into corresponding linguistic values (Fuzzifier), explores a linguistic rule-base for understanding of relational mapping in between inputs and output (rule base/ inference engine), predicts linguistic output and finally defuzzifies linguistic output into a crisp score (defuzzifier). In order to fuzzify crisp inputs i.e.  $(S_{MRR}, S_{EWR}, S_{R_a}, S_{SCD})$ , three triangular membership functions viz. Low (L), Medium (M) and High (H) have been selected for each of the inputs (Fig. 8.5.1-8.5.4). Similarly, aforesaid three membership functions (L, M, H) (Fig. 8.6) have been chosen for obtaining output i.e. ( $S_c$ ) in terms of fuzzy number. A set of 81 fuzzy rules (Table 8.2; Fig. 8.7) has been utilized so as to capture the relationship of inputs/output with the inference engine.

**Table 8.1.2:** Satisfaction values (corresponding to each response) for all experimental runs:  
Computed combined satisfaction score ( $S_c$ )

Run No.	<b>Inconel 718</b>						
	Satisfaction values (Higher-is-Better)				$S_c$ (Combined satisfaction score) as FIS output	S/N ratio of $S_c$ [dB]	Predicted S/N ratio (at optimal setting) [dB]
	$S_{MRR}$	$S_{EWR}$	$S_{R_a}$	$S_{SCD}$			
1	0.046	1.000	0.735	0.000	0.555	-5.1141	-2.54596
2	0.157	0.500	0.386	0.266	0.484	-6.3031	
3	0.074	0.500	0.318	0.633	0.467	-6.6137	
4	0.487	0.000	0.283	0.190	0.42	-7.5350	
5	0.033	1.000	0.601	0.823	0.429	-7.3509	
6	0.188	0.500	0.359	0.810	0.478	-6.4114	
7	0.304	0.500	0.740	0.468	0.458	-6.7827	
8	0.447	0.000	0.063	0.709	0.308	-10.2290	
9	0.000	1.000	1.000	0.101	0.675	-3.4139	
10	0.062	1.000	0.744	0.734	0.508	-5.8827	
11	0.535	0.500	0.013	1.000	0.5	-6.0206	
12	0.642	0.000	0.000	0.709	0.384	-8.3134	
13	0.019	1.000	0.856	0.177	0.606	-4.3505	
14	0.196	0.500	0.552	1.000	0.5	-6.0206	
15	0.455	0.500	0.466	0.025	0.498	-6.0554	
16	1.000	0.000	0.036	0.608	0.488	-6.2316	

**Table 8.1.3:** Satisfaction values (corresponding to each response) for all experimental runs:  
Computed combined satisfaction score ( $S_c$ )

Run No.	<b>Inconel 601</b>						
	Satisfaction values (Higher-is-Better)				$S_c$ (Combined satisfaction score) as FIS output	S/N ratio of $S_c$ [dB]	Predicted S/N ratio (at optimal setting) [dB]
	$S_{MRR}$	$S_{EWR}$	$S_{R_a}$	$S_{SCD}$			
1	0.167	1.000	0.649	0.103	0.511	-5.83158	-2.15811
2	0.220	0.667	0.417	0.782	0.5	-6.02060	
3	0.146	0.667	0.354	1.000	0.472	-6.52116	
4	0.219	0.333	0.266	0.667	0.446	-7.01330	
5	0.059	0.667	0.631	0.385	0.51	-5.84860	
6	0.343	0.667	0.214	0.628	0.497	-6.07287	
7	0.140	0.667	0.192	0.333	0.441	-7.11123	
8	0.306	0.333	0.347	0.705	0.47	-6.55804	
9	0.000	1.000	0.683	0.000	0.533	-5.46546	
10	0.025	1.000	0.513	0.474	0.78	-2.15811	
11	0.459	0.667	0.203	0.038	0.414	-7.65999	
12	0.750	0.333	0.255	0.218	0.47	-6.55804	
13	0.021	1.000	1.000	0.128	0.648	-3.76850	
14	0.218	0.667	0.827	0.244	0.464	-6.66964	
15	0.553	0.333	0.000	0.513	0.472	-6.52116	
16	1.000	0.000	0.170	0.513	0.529	-5.53089	

**Table 8.1.4:** Satisfaction values (corresponding to each response) for all experimental runs:  
Computed combined satisfaction score ( $S_c$ )

Run No.	<b>Inconel 825</b>						
	Satisfaction values (Higher-is-Better)				$S_c$ (Combined satisfaction score) as FIS output	S/N ratio of $S_c$ [dB]	Predicted S/N ratio (at optimal setting) [dB]
	$S_{MRR}$	$S_{EWR}$	$S_{Ra}$	$S_{SCD}$			
1	0.184	0.750	0.472	0.798	0.482	-6.33906	-4.52813
2	0.163	0.500	0.493	0.000	0.5	-6.02060	
3	0.028	0.500	0.313	1.000	0.465	-6.65094	
4	0.222	0.250	0.176	0.220	0.433	-7.27024	
5	0.010	1.000	0.754	0.615	0.543	-5.30400	
6	0.398	0.500	0.514	0.037	0.5	-6.02060	
7	0.090	0.500	0.363	1.000	0.481	-6.35710	
8	0.155	0.250	0.000	0.642	0.408	-7.78680	
9	0.000	1.000	0.704	0.514	0.588	-4.61245	
10	0.078	0.750	0.458	0.706	0.516	-5.74701	
11	0.816	0.250	0.271	0.138	0.434	-7.25021	
12	0.950	0.000	0.324	0.798	0.41	-7.74432	
13	0.042	0.750	1.000	0.523	0.441	-7.11123	
14	0.190	0.750	0.810	0.606	0.478	-6.41144	
15	0.536	0.500	0.444	0.505	0.498	-6.05541	
16	1.000	0.250	0.197	0.514	0.457	-6.80168	

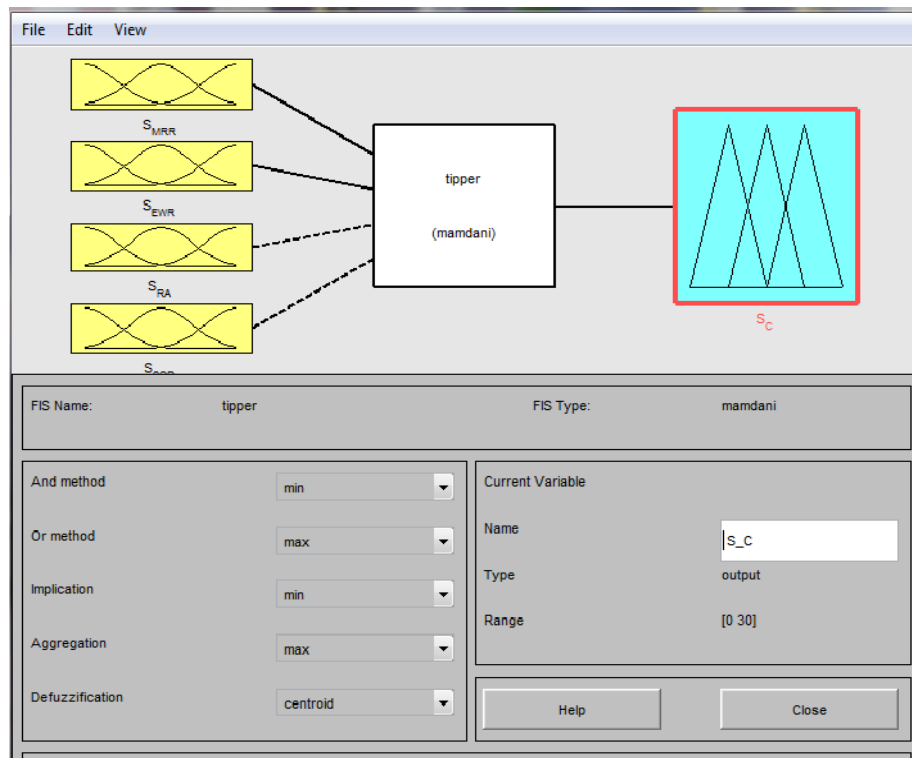


**Fig. 8.4:** Proposed FIS architecture

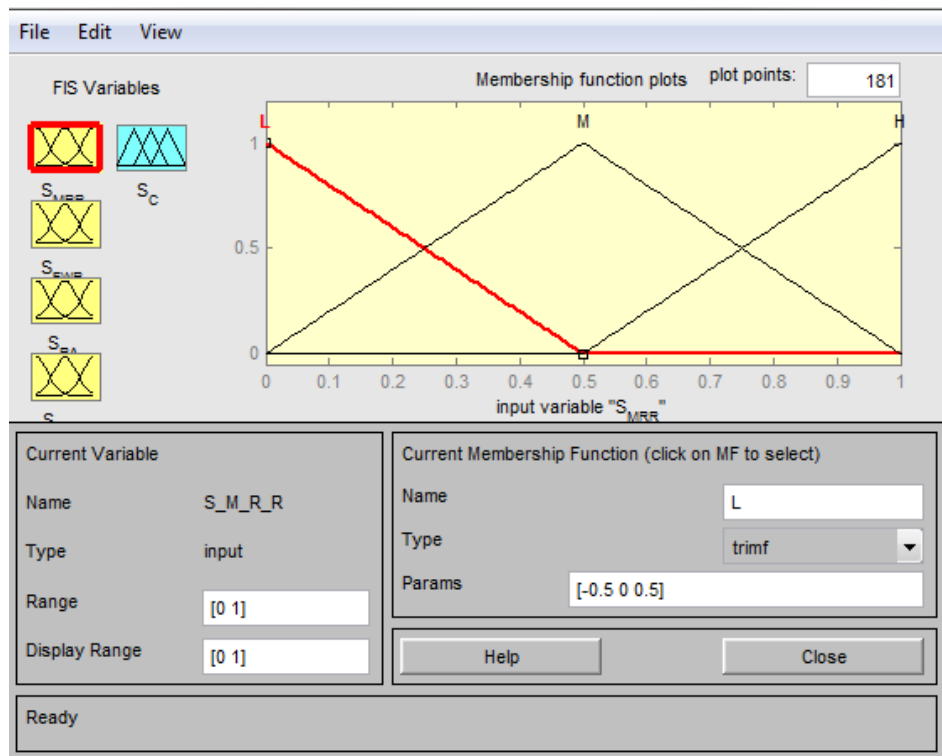


Fig. 8.5.1: Membership Functions (MFs) for  $S_{MRR}$

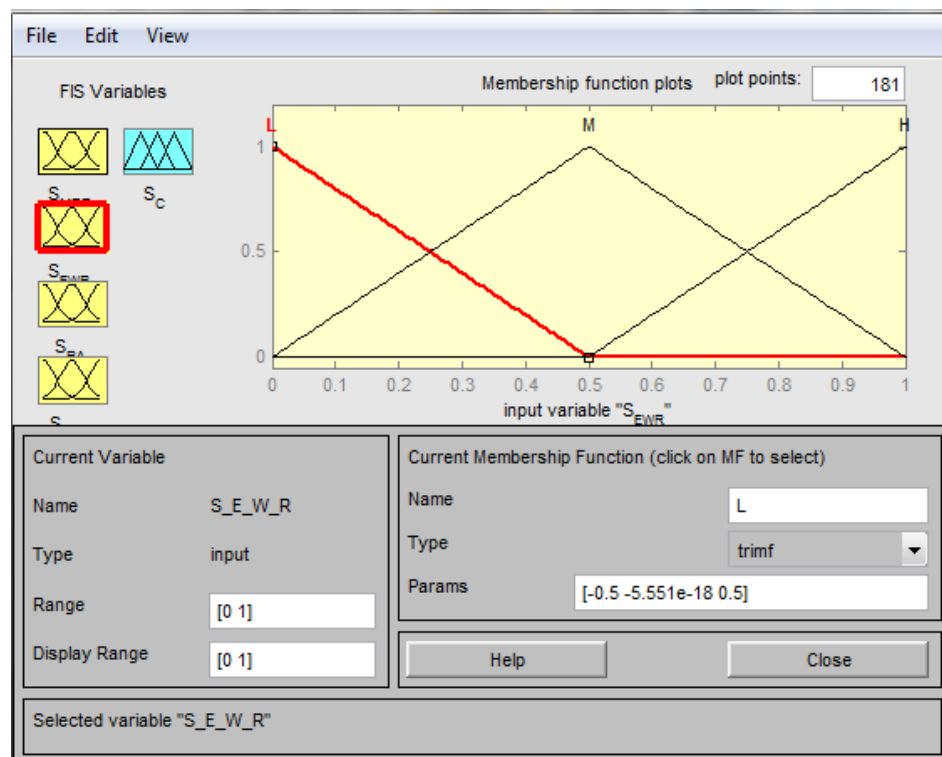


Fig. 8.5.2: Membership Functions (MFs) for  $S_{EWR}$

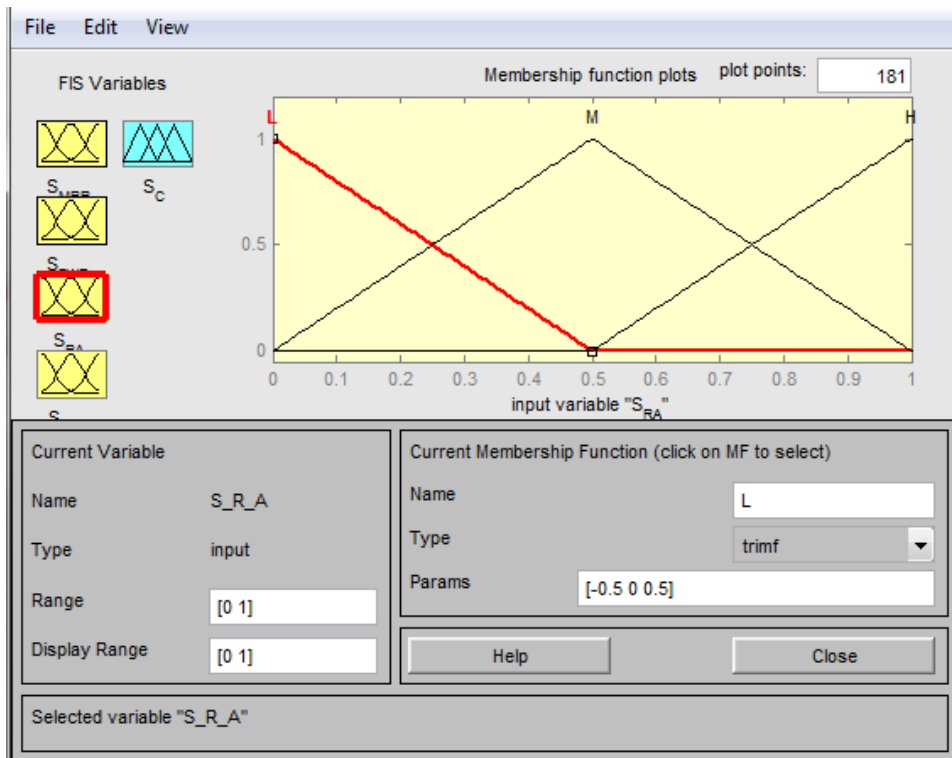


Fig. 8.5.3: Membership Functions (MFs) for  $S_{R_a}$

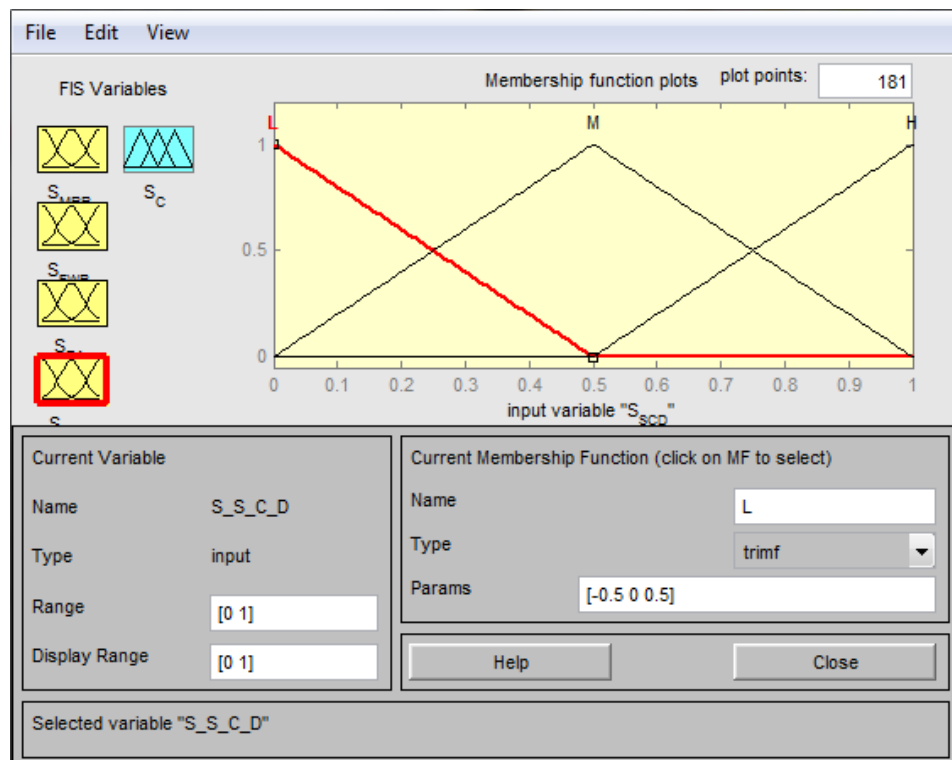


Fig. 8.5.4: Membership Functions (MFs) for  $S_{SCD}$

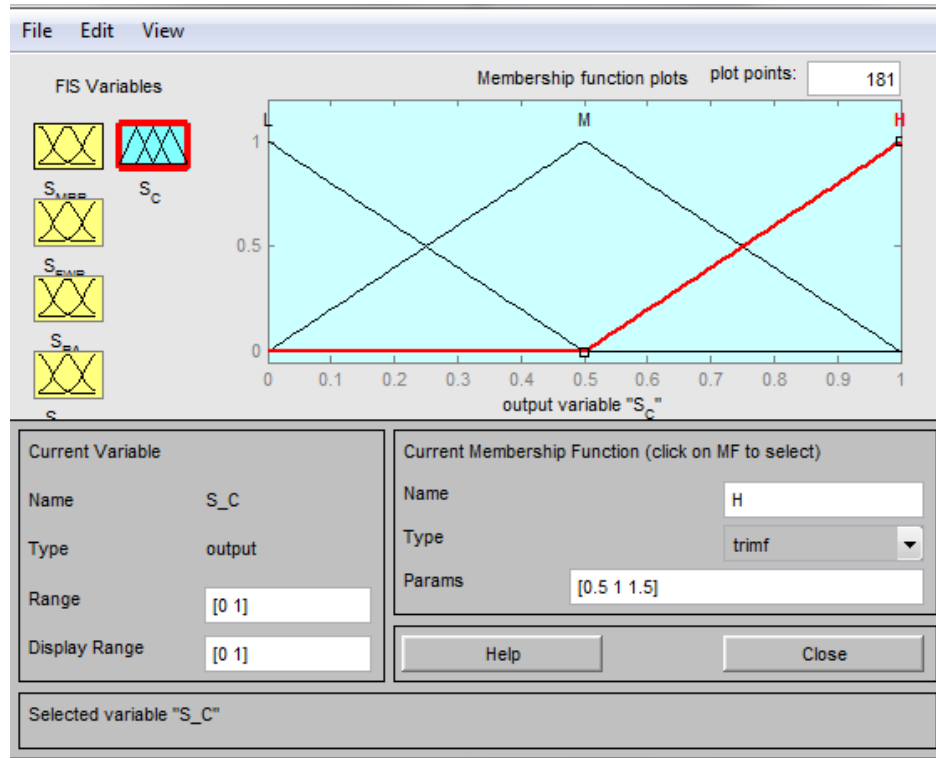


Fig. 8.6: Membership Functions (MFs) for  $S_c$

Table 8.2: Fuzzy rule matrix

Rule no.	IF	IF	IF	IF	THEN
	$S_{MRR}$	$S_{EWR}$	$S_{R_a}$	$S_{SCD}$	$S_c$
1	L	L	L	L	L
2	L	L	L	M	L
3	L	L	L	H	L
4	L	L	M	L	M
5	L	L	M	M	L
6	L	L	M	H	L
7	L	L	H	L	L
8	L	L	H	M	L
9	L	L	H	H	L
10	L	M	L	L	L
11	L	M	L	M	L
12	L	M	L	H	L
13	L	M	M	L	M
14	L	M	M	M	M
15	L	M	M	H	M
16	L	M	H	L	L
17	L	M	H	M	L
18	L	M	H	H	M
19	L	H	L	L	M
20	L	H	L	M	M
21	L	H	L	H	M
22	L	H	M	L	M
23	L	H	M	M	H
24	L	H	M	H	L
25	L	H	H	L	H
26	L	H	H	M	M
27	L	H	H	H	M
28	M	L	L	L	M
29	M	L	L	M	L
30	M	L	L	H	L



31	M	L	M	L	L
32	M	L	M	M	L
33	M	L	M	H	M
34	M	L	H	L	M
35	M	L	H	M	M
36	M	L	H	H	L
37	M	M	L	L	L
38	M	M	L	M	M
39	M	M	L	H	M
40	M	M	M	L	M
41	M	M	M	M	M
42	M	M	M	H	M
43	M	M	H	L	M
44	M	M	H	M	M
45	M	M	H	H	M
46	M	H	L	L	M
47	M	H	L	M	L
48	M	H	L	H	M
49	M	H	M	L	M
50	M	H	M	M	L
51	M	H	M	H	M
52	M	H	H	L	M
53	M	H	H	M	H
54	M	H	H	H	H
55	H	L	L	L	M
56	H	L	L	M	M
57	H	L	L	H	L
58	H	L	M	L	L
59	H	L	M	M	H
60	H	L	M	H	L
61	H	L	H	L	L
62	H	L	H	M	M
63	H	L	H	H	M
64	H	M	L	L	M
65	H	M	L	M	M
66	H	M	L	H	M
67	H	M	M	L	L
68	H	M	M	M	L
69	H	M	M	H	M
70	H	M	H	L	M
71	H	M	H	M	H
72	H	M	H	H	H
73	H	H	L	L	M
74	H	H	L	M	M
75	H	H	L	H	M
76	H	H	M	L	M
77	H	H	M	M	M
78	H	H	M	H	H
79	H	H	H	L	M
80	H	H	H	M	H
81	H	H	H	H	H

Based on that defuzzifier module, FIS has been provided crisp scores of ( $S_c$ ) as unique output. The FIS predicted combine satisfaction scores (with respect to each experimental run number) have been presented in [Table 8.1.1-8.1.4](#), for Inconel 625, 718, 601 and 825, respectively.

The optimal setting of process parameters has been determined by maximizing ( $S_c$ ) through Taguchi method. According to Taguchi's philosophy, the objective function value i.e. ( $S_c$ ) has been converted into corresponding S/N ratio by using HB formulation ([Eq. 8.1](#)). Optimal setting has been determined by maximizing S/N ratio. The computed

S/N ratios of ( $S_c$ ) for all experimental runs have been furnished in Table 8.1.1-8.1.4, for Inconel 625, 718, 601 and 825, respectively. Optimal parametric combinations have been determined by mean S/N ratio plots (of  $S_c$ ) as depicted in Fig. 8.8.1-8.8.4, for Inconel 625, 718, 601 and 825, respectively. The optimal setting appears as:  $A_4B_1C_1D_1E_4$  (for Inconel 625),  $A_4B_1C_1D_4E_2$  (for Inconel 718),  $A_3B_2C_4D_3E_1$  (for Inconel 601) and  $A_3B_1C_2D_4E_2$  (for Inconel 825).

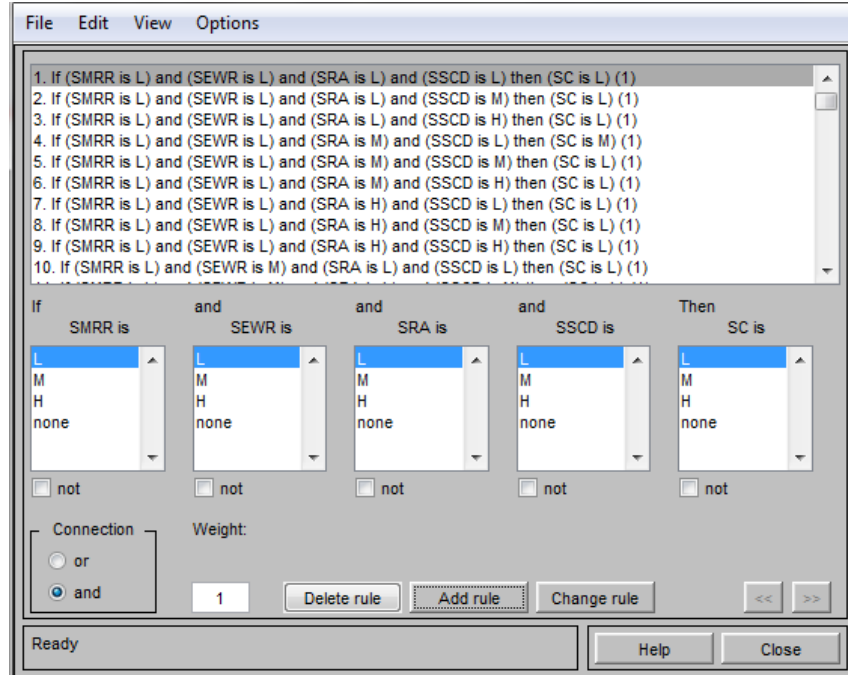


Fig. 8.7: Fuzzy (linguistic) rule base

The predicted S/N ratio (of  $S_c$ ) obtained at setting  $A_4B_1C_1D_1E_4$  (for Inconel 625) is (-4.85072 dB); at setting  $A_4B_1C_1D_4E_2$  (for Inconel 718) is (-2.54596 dB); and at setting  $A_3B_1C_2D_4E_2$  (for Inconel 825) is (-4.52813dB), each seems the maximum as compared to all computed S/N ratio entries of  $S_c$  (for sixteen experimental runs and for the particular Inconel grade) as depicted in Table 8.1.1-8.1.4, respectively. Since S/N ratio always corresponds to HB type, the maximum value (as compared to the sixteen experimental settings) obtained at predicted optimal setting confirms that the proposed optimization route performs satisfactorily.

The predicted S/N ratio of  $S_c$  as obtained at setting  $A_3B_2C_4D_3E_1$  (for Inconel 601) appears (-2.15811dB). This value is found more as compared to all computed S/N ratio entries for sixteen experimental runs, except for Run No. 10 (refer to Table 8.1.3).

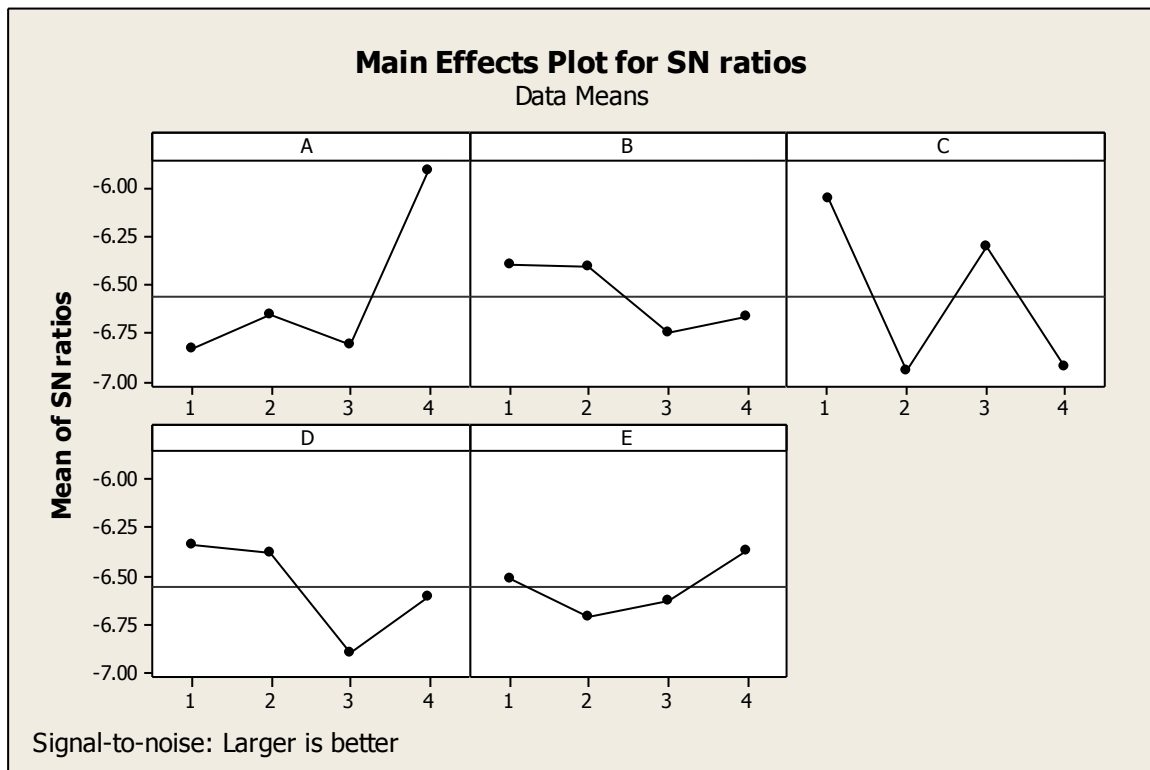


Fig. 8.8.1: S/N ratio plot: Evaluation of optimal setting (Optimization of  $S_c$ )  
[Optimal setting:  $A_4B_1C_1D_1E_4$ ] (Inconel 625)

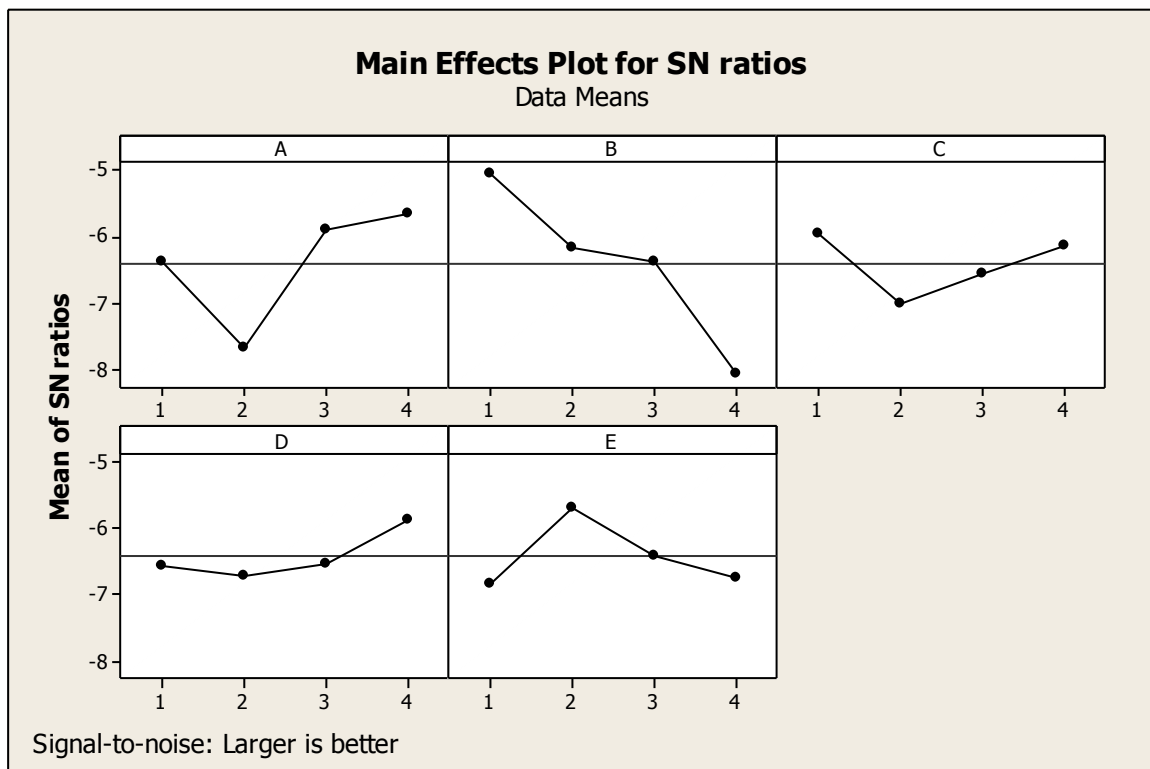


Fig. 8.8.2: S/N ratio plot: Evaluation of optimal setting (Optimization of  $S_c$ )  
[Optimal setting:  $A_4B_1C_1D_4E_2$ ] (Inconel 718)

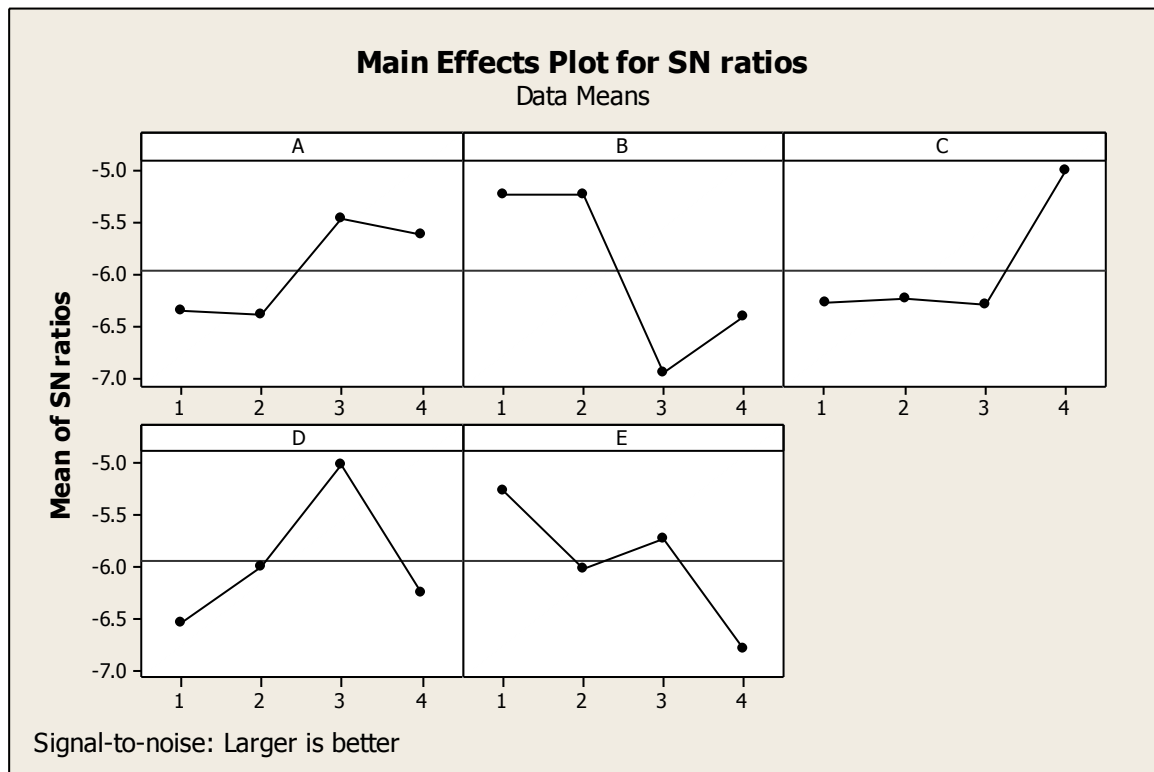


Fig. 8.8.3: S/N ratio plot: Evaluation of optimal setting (Optimization of  $S_c$ )  
[Optimal setting:  $A_3B_2C_4D_3E_1$ ] (Inconel 601)

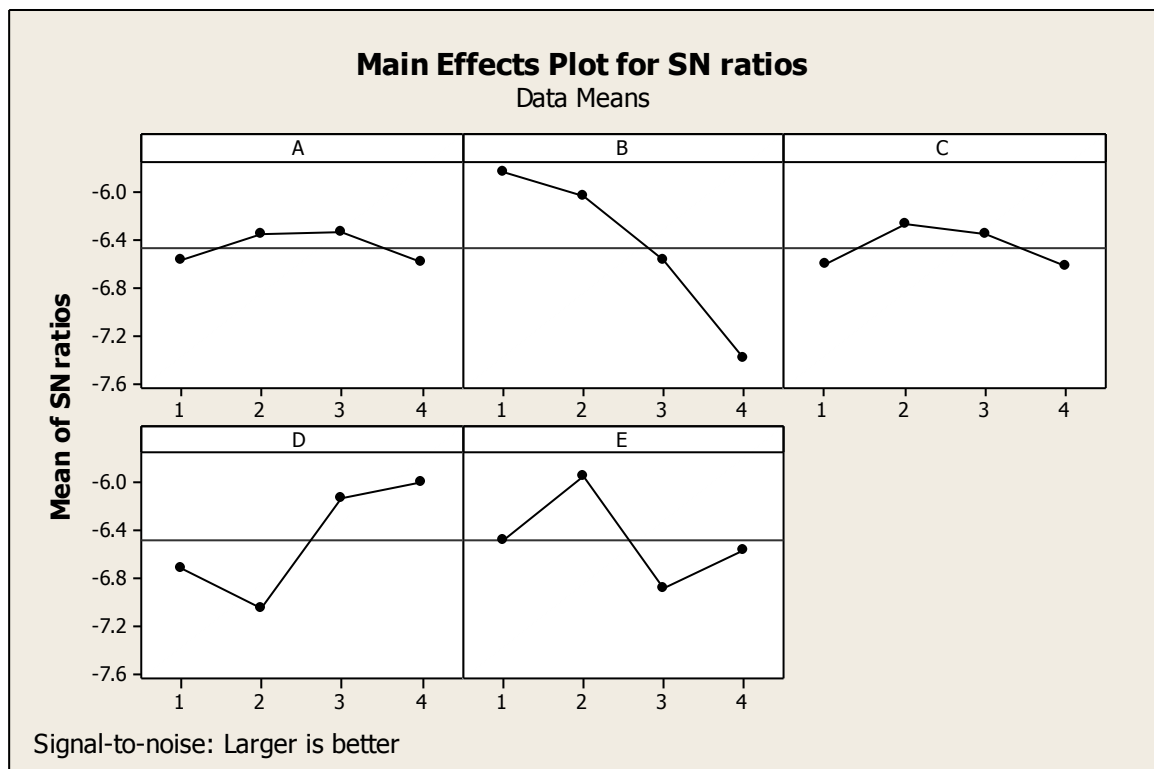


Fig. 8.8.4: S/N ratio plot: Evaluation of optimal setting (Optimization of  $S_c$ )  
[Optimal setting:  $A_3B_1C_2D_4E_2$ ] (Inconel 825)

In Run No. 10, it has been observed that S/N ratio of  $S_c$  exactly matches to that of predicted optimal setting. Hence, the setting corresponding to Run No. 10 i.e.  $A_3B_2C_4D_3E_1$  is considered as optimal setting. This has also been found evident from mean S/N ratio plot of  $S_c$  (Fig. 8.8.3). Taguchi's optimal prediction can be treated as a reliable solution if it is found that the predicted S/N ratio of the response assumes the maximum value at optimal setting as compared to that obtained in all experimental runs included in orthogonal array design of experiment. This is because, S/N ratio corresponds to HB requirements; higher values are more preferred.

The predicted optimal setting may be one of the settings that are included in orthogonal array (16 runs as indicated in Table 2.16 of Chapter 2; Phase VI); it may be a different setting beyond 16 runs of OA; since apart from 16 settings, the remaining  $(4^5 - 16)$  settings are not experimented. In case on Inconel 601, it has been found that predicted optimal setting is  $A_3B_2C_4D_3E_1$  and it corresponds to Run No. 16 of the OA. Optimal results have further been verified by confirmatory tests.

While comparing the optimal machining parameters settings for different grades of Inconel considered herein, it has been found that the optimal parameters settings appear almost similar for Inconel 625 and Inconel 718; both possesses optimal parameters: OCV=90V,  $I_p=5$  A and  $T_{on}=200$   $\mu$ s. The variation only has been observed for the values of duty factor and flushing pressure. For Inconel 625 optimal parametric setting includes  $\tau=70\%$  and  $F_p=0.6$  bar; whereas, Inconel 718 corresponds to optimal values of  $\tau$  and  $F_p$  i.e. 85% and 04 bar, respectively. As energy per spark depends on the value of gap voltage, peak discharge current and pulse-on time, equal heat input is attributed (since values of OCV,  $I_p$  and  $T_{on}$  are same) for Inconel 625 as well as Inconel 718 to produce optimized machining response. This may also be attributed due to the fact that the chemical composition of aforesaid two grades of Inconel appears almost similar. Moreover, both the Inconel grades correspond to nearly same thermal conductivity i.e.  $10.8 \text{ W/m}^0\text{C}$  (20-100  $^0\text{C}$ ) for Inconel 625 and  $11.4 \text{ W/m}^0\text{C}$  at 100  $^0\text{C}$  for Inconel 718.

From mean response tables (Table 8.3.1-8.3.4 and Table 8.4.1-8.4.4), it has been found that duty factor ( $\tau$ ) and dielectric flushing circulation pressure ( $F_p$ ) are not so much significant as compared to other electrical parameters (OCV,  $I_p$ , and  $T_{on}$ ) whilst influencing most of the machining responses. Hence, slight variation of  $\tau$  and  $F_p$  in the optimal parameters settings for Inconel 625 and Inconel 718 can be accepted.

Table 8.3.1: Mean response table of MRR (for Inconel 625)

Level	Variation of MRR expressed in [mm <sup>3</sup> /min] due to factorial variation				
	A [OCV]	B (I <sub>p</sub> )	C (T <sub>on</sub> )	D (τ)	E (F <sub>p</sub> )
1	5.228	2.595	15.880	7.192	8.439
2	10.246	5.385	7.198	9.428	10.364
3	8.395	9.360	6.478	9.648	8.110
4	10.761	17.290	5.074	8.362	7.716
Delta	5.533	14.695	10.806	2.456	2.648
%Contribution	5.533	14.695	10.806	2.456	2.648
Rank	3	1	2	5	4

Table 8.3.2: Mean response table of EWR (for Inconel 625)

Level	Variation of EWR expressed in [mm <sup>3</sup> /min] due to factorial variation				
	A [OCV]	B (I <sub>p</sub> )	C (T <sub>on</sub> )	D (τ)	E (F <sub>p</sub> )
1	0.12127	0.06615	0.09923	0.12128	0.11027
2	0.15438	0.08820	0.12127	0.11027	0.12127
3	0.09923	0.14333	0.14335	0.11025	0.13230
4	0.09923	0.17643	0.11025	0.13230	0.11025
Delta	0.05515	0.11028	0.04412	0.02205	0.02205
%Contribution	21.74	43.47	17.39	8.69	8.69
Rank	2	1	3	4	5

Table 8.3.3: Mean response table of R<sub>a</sub> (for Inconel 625)

Level	Variation of R <sub>a</sub> expressed in [μm] due to factorial variation				
	A [OCV]	B (I <sub>p</sub> )	C (T <sub>on</sub> )	D (τ)	E (F <sub>p</sub> )
1	9.117	5.933	9.333	8.342	8.200
2	7.533	7.892	8.200	7.842	8.475
3	8.375	9.033	8.250	8.317	8.442
4	8.267	10.433	7.508	8.792	8.175
Delta	1.583	4.500	1.825	0.950	0.300
%Contribution	17.28	49.13	19.92	10.37	3.27
Rank	3	1	2	4	5

Table 8.3.4: Mean response table of SCD (for Inconel 625)

Level	Variation of SCD expressed in [μm/μm <sup>2</sup> ] due to factorial variation				
	A [OCV]	B (I <sub>p</sub> )	C (T <sub>on</sub> )	D (τ)	E (F <sub>p</sub> )
1	0.01897	0.01985	0.02123	0.02303	0.01975
2	0.01858	0.01802	0.01782	0.01568	0.01992
3	0.01710	0.01845	0.01713	0.01840	0.01698
4	0.02008	0.01840	0.01855	0.01762	0.01808
Delta	0.00298	0.00183	0.00410	0.00735	0.00295
%Contribution	15.51	9.52	21.34	38.26	15.35
Rank	3	5	2	1	4

Table 8.4.1: Mean response table of MRR (for Inconel 718)

Level	Variation of MRR expressed in [mm <sup>3</sup> /min] due to factorial variation				
	A [OCV]	B (I <sub>p</sub> )	C (T <sub>on</sub> )	D (τ)	E (F <sub>p</sub> )
1	6.99	1.929	14.637	10.220	8.867
2	8.575	5.772	10.974	9.994	12.296
3	10.604	11.587	6.639	10.070	8.211
4	13.886	20.775	7.814	9.780	10.690
Delta	6.886	18.846	7.998	0.440	4.084
%Contribution	18.00	49.26	20.90	1.15	10.67
Rank	3	1	2	5	4

Table 8.4.2: Mean response table of EWR (for Inconel 718)

Level	Variation of EWR expressed in [mm <sup>3</sup> /min] due to factorial variation				
	A [OCV]	B (I <sub>p</sub> )	C (T <sub>on</sub> )	D (τ)	E (F <sub>p</sub> )
1	0.08820	0.04410	0.08820	0.08820	0.07717
2	0.08820	0.07717	0.08820	0.08820	0.08820
3	0.07717	0.08820	0.08820	0.07717	0.08820
4	0.08820	0.13230	0.07717	0.08820	0.08820
Delta	0.01103	0.08820	0.01103	0.01103	0.01103
%Contribution	8.33	66.65	8.33	8.33	8.33
Rank	~*	1	~	~	~

\*Same ranking order for A, C, D, E

Table 8.4.3: Mean response table of R<sub>a</sub> (for Inconel 718)

Level	Variation of R <sub>a</sub> expressed in [μm] due to factorial variation				
	A [OCV]	B (I <sub>p</sub> )	C (T <sub>on</sub> )	D (τ)	E (F <sub>p</sub> )
1	9.167	6.433	10.242	8.600	8.633
2	9.092	8.575	9.667	9.917	8.350
3	9.100	9.508	8.775	9.208	9.517
4	8.817	11.658	7.492	8.450	9.675
Delta	0.350	5.225	2.750	1.467	1.325
%Contribution	3.14	47.00	24.73	13.19	11.91
Rank	5	1	2	3	4

Table 8.4.4: Mean response table of SCD (for Inconel 718)

Level	Variation of SCD expressed in [μm/μm <sup>2</sup> ] due to factorial variation				
	A [OCV]	B (I <sub>p</sub> )	C (T <sub>on</sub> )	D (τ)	E (F <sub>p</sub> )
1	0.01795	0.01793	0.01533	0.01580	0.01720
2	0.01455	0.01455	0.01650	0.01585	0.01725
3	0.01508	0.01590	0.01528	0.01457	0.01550
4	0.01653	0.01572	0.01700	0.01787	0.01415
Delta	0.00340	0.00338	0.00173	0.00330	0.00310
%Contribution	22.80	22.66	11.60	22.13	20.79
Rank	1	2	5	3	4

Table 8.5.1: Mean response table of MRR (for Inconel 601)

Level	Variation of MRR expressed in [mm <sup>3</sup> /min] due to factorial variation				
	A [OCV]	B (I <sub>p</sub> )	C (T <sub>on</sub> )	D (τ)	E (F <sub>p</sub> )
1	8.305	3.955	18.795	12.814	10.879
2	9.131	8.767	15.462	10.493	13.545
3	12.466	13.015	7.602	12.435	12.688
4	17.275	21.440	5.317	11.433	10.065
Delta	8.970	17.485	13.477	2.321	3.480
%Contribution	19.61	38.23	29.46	5.07	7.60
Rank	3	1	2	5	4

Table 8.5.2: Mean response table of EWR (for Inconel 601)

Level	Variation of EWR expressed in [mm <sup>3</sup> /min] due to factorial variation				
	A [OCV]	B (I <sub>p</sub> )	C (T <sub>on</sub> )	D (τ)	E (F <sub>p</sub> )
1	0.08820	0.05513	0.09923	0.08820	0.08820
2	0.09923	0.07717	0.11025	0.08820	0.09923
3	0.07717	0.09923	0.08820	0.09923	0.08820
4	0.11025	0.14333	0.07717	0.09923	0.09922
Delta	0.03308	0.08820	0.03307	0.01103	0.01103
%Contribution	18.75	50.00	18.74	6.25	6.25
Rank	2	1	3	~ <sup>*</sup>	~

\*Same ranking order for D, E

Table 8.5.3: Mean response table of R<sub>a</sub> (for Inconel 601)

Level	Variation of R <sub>a</sub> expressed in [μm] due to factorial variation				
	A [OCV]	B (I <sub>p</sub> )	C (T <sub>on</sub> )	D (τ)	E (F <sub>p</sub> )
1	10.192	7.308	11.208	9.658	10.592
2	10.875	9.550	11.058	9.558	10.700
3	10.267	12.308	9.008	10.233	9.883
4	9.492	11.658	9.550	11.375	9.650
Delta	1.383	5.000	2.200	1.817	1.050
%Contribution	12.07	43.66	19.21	15.86	9.17
Rank	4	1	2	3	5

Table 8.5.4: Mean response table of SCD (for Inconel 601)

Level	Variation of SCD expressed in [μm/μm <sup>2</sup> ] due to factorial variation				
	A [OCV]	B (I <sub>p</sub> )	C (T <sub>on</sub> )	D (τ)	E (F <sub>p</sub> )
1	0.01693	0.02070	0.01940	0.02015	0.01840
2	0.01790	0.01775	0.01820	0.01868	0.01873
3	0.02048	0.01822	0.01810	0.01727	0.01805
4	0.01917	0.01780	0.01878	0.01837	0.01930
Delta	0.00355	0.00295	0.00130	0.00288	0.00125
%Contribution	29.75	24.72	10.89	24.14	10.47
Rank	1	2	4	3	5



**Table 8.6.1:** Mean response table of MRR (for Inconel 825)

Level	Variation of MRR expressed in [mm <sup>3</sup> /min] due to factorial variation				
	A [OCV]	B (I <sub>p</sub> )	C (T <sub>on</sub> )	D (τ)	E (F <sub>p</sub> )
1	4.945	2.724	16.060	9.991	7.144
2	5.295	6.376	11.502	8.517	8.996
3	12.638	10.335	3.566	8.151	10.009
4	12.174	15.617	3.925	8.394	8.904
Delta	7.694	12.893	12.494	1.840	2.866
%Contribution	20.36	34.12	33.06	4.86	7.58
Rank	3	1	2	5	4

**Table 8.6.2:** Mean response table of EWR (for Inconel 825)

Level	Variation of EWR expressed in [mm <sup>3</sup> /min] due to factorial variation				
	A [OCV]	B (I <sub>p</sub> )	C (T <sub>on</sub> )	D (τ)	E (F <sub>p</sub> )
1	0.13230	0.06615	0.14333	0.13233	0.12127
2	0.12127	0.11025	0.13233	0.14332	0.12127
3	0.13233	0.14333	0.11025	0.11025	0.14335
4	0.12127	0.18745	0.12127	0.12127	0.12128
Delta	0.01105	0.12130	0.03308	0.03307	0.02207
%Contribution	5.00	54.99	14.99	14.99	10.05
Rank	5	1	2	3	4

**Table 8.6.3:** Mean response table of R<sub>a</sub> (for Inconel 825)

Level	Variation of R <sub>a</sub> expressed in [μm] due to factorial variation				
	A [OCV]	B (I <sub>p</sub> )	C (T <sub>on</sub> )	D (τ)	E (F <sub>p</sub> )
1	9.758	6.267	9.758	8.542	9.950
2	9.342	7.817	8.433	9.025	9.042
3	9.042	9.908	8.875	9.125	8.108
4	7.400	11.550	8.475	8.850	8.442
Delta	2.358	5.283	1.325	0.583	1.842
%Contribution	20.70	46.37	11.63	5.11	16.17
Rank	2	1	4	5	3

**Table 8.6.4:** Mean response table of SCD (for Inconel 825)

Level	Variation of SCD expressed in [μm/μm <sup>2</sup> ] due to factorial variation				
	A [OCV]	B (I <sub>p</sub> )	C (T <sub>on</sub> )	D (τ)	E (F <sub>p</sub> )
1	0.02020	0.01903	0.02165	0.01698	0.01847
2	0.01945	0.02203	0.02048	0.02215	0.02017
3	0.01982	0.01850	0.01818	0.01797	0.01928
4	0.01985	0.01978	0.01903	0.02223	0.02140
Delta	0.00075	0.00353	0.00348	0.00525	0.00293
%Contribution	4.70	22.14	21.83	32.93	18.38
Rank	5	2	3	1	4

N.B.: Delta = (Maximum variation – minimum variation)

While comparing the optimal parameters settings obtained for Inconel 601 as well as Inconel 825, it has been observed that Inconel 825 corresponds to lesser peak current as well as lesser pulse-on time as compared to Inconel 601; OCV being same i.e. 80V for both the cases. The optimal values of  $I_p$  and  $T_{on}$  appears as 5A and 300 $\mu$ s, respectively (for Inconel 825); while Inconel 601 assumes optimal values  $I_p=7$ A and  $T_{on}=500\mu$ s. Low values of  $I_p$  and  $T_{on}$  results in reduced energy per spark and hence Inconel 825 experiences less heat input as compared to Inconel 601. If we consider thermal conductivity of Inconel 601 and Inconel 825; it can be seen that these are approximately same i.e. 14.3 W/m  $^{\circ}$ C (at 200  $^{\circ}$ C) for Inconel 601 and 13.8 W/m  $^{\circ}$ C (at 200  $^{\circ}$ C) for Inconel 825. Hence, requirement of high heat input to produce optimal machining performance may be explained by their chemical composition. It has been found that as compared to Inconel 825, the Ni content of Inconel 601 is substantially high. Ni behaves like a heat resistant substance in turn results in requirement of high heat input to Inconel 601. Moreover, presence of considerable amount of Al in Inconel 601 may induce the possibility of nonconductive oxide layer on the surface being machined. Such oxide layer may behave like an insulator and resists material melting during operation. As a consequence, high value of heat input seems necessary to produce desired machining yield for Inconel 601. The variation in the optimal values of  $\tau$  and  $F_p$  for Inconel 601 and Inconel 825 does not bear any alarming indication since from mean response tables (Table 8.5.1-8.5.4 and Table 8.6.1-8.6.4)  $\tau$  and  $F_p$  have been found insignificant on affecting EDM performance.

In addition to that, the levels of significance of process control parameters on MRR, EWR,  $R_a$  and SCD have been determined through mean value tables of individual responses. Percentage contribution of significant input factors for different response parameters has also been furnished herein (Table 8.3.1-8.3.4; 8.4.1-8.4.4; 8.5.1-8.5.4; 8.6.1-8.6.4). It has been observed that peak discharge current ( $I_p$ ) has appeared as the most significant process parameter on influencing MRR, EWR and  $R_a$  separately.

### 8.3.2.2 Analysis of SEM Micrographs

SEM micrographs revealing surface structure of 'as received' Inconel specimens have been provided in Fig. 8.9. Observations of the EDMed surface revealed surface irregularities in terms of voids, globules of debris, an uneven fusing structure (melted metal deposition), shallow craters and pockmarks, as well as surface cracks. Cracks are

developed while high thermal stresses generated during operation exceed the fracture strength of the material due to excessive plastic deformation. Pockmarks are formed during solidification of molten metal while entrapped gases get released. Such surface irregularities of substantial extent may be detrimental for the fatigue life of the part component while put in service. Fig. 8.10 depicts various surface irregularities as visualized from SEM micrographs of EDMed Inconel of different grades obtained at a common parameters setting i.e. [OCV=60V;  $I_p$ =5A;  $T_{on}$ =200  $\mu$ s;  $\tau$ =70%;  $F_p$ =0.3bar]. Additionally, SEM micrographs revealing existence of white layer on the surface of EDMed Inconel specimens (of different grades) have also been provided in Fig. 8.11.1-8.11.4.

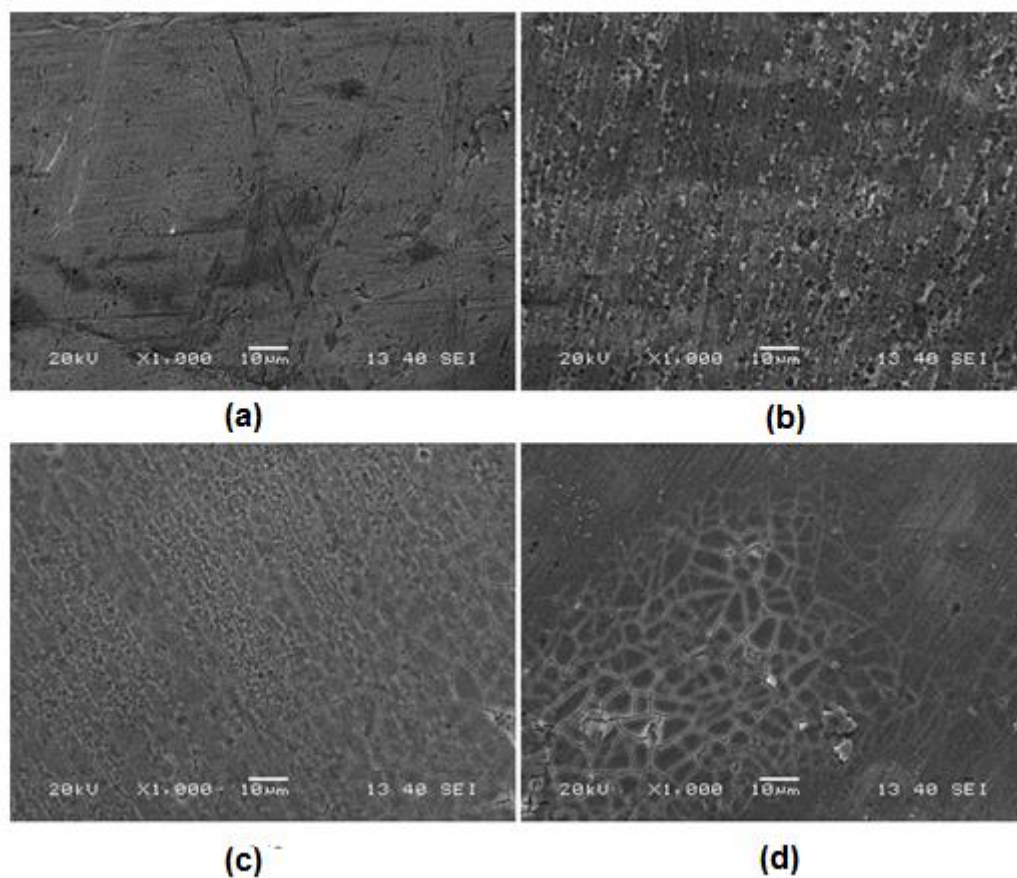
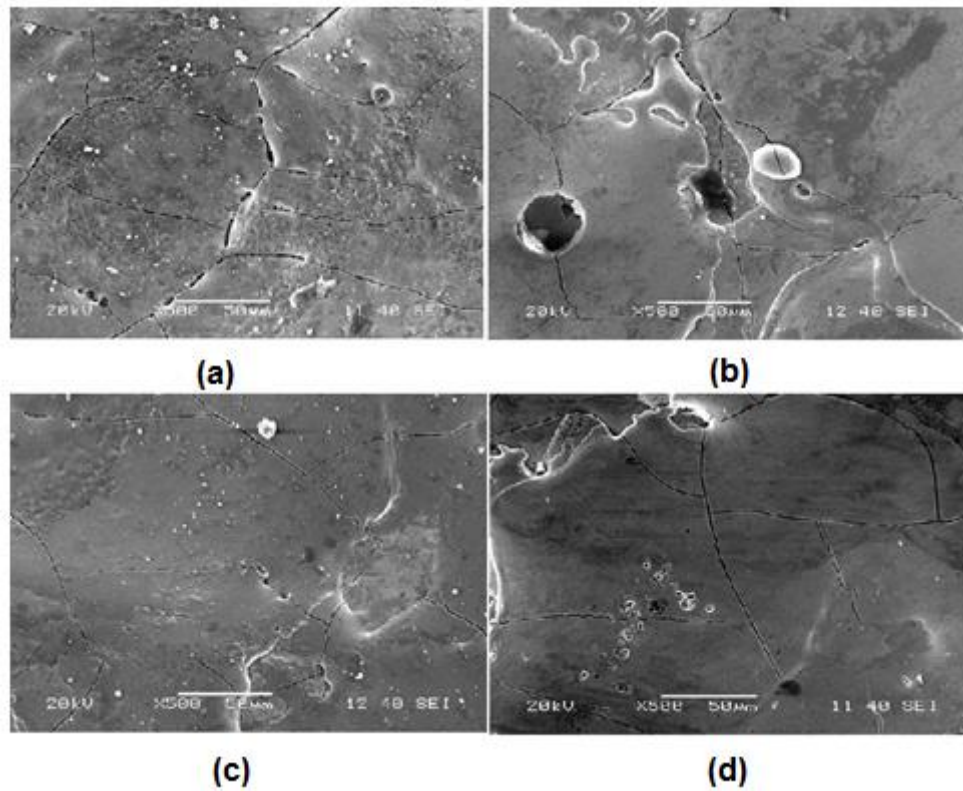


Fig. 8.9: SEM micrographs revealing surface structure of ‘as received’ (a) Inconel 625, (b) Inconel 728, (c) Inconel 601, and (d) Inconel 825

It is true that the formation of white layer is inevitable during EDM operation performed on any work material. However, depending on the properties of the workpiece material along with the setting of process control parameters, the white layer thickness may vary. It is to be noted that in the present experimental scheme, the white layer thickness has not been considered as an output response and therefore, not included in the list of

objectives/responses for simultaneous optimization with other responses considered herein like MRR, EWR,  $R_a$  and SCD.



**Fig. 8.10:** SEM micrographs revealing surface structure of the EDMed specimens of (a) Inconel 625, (b) Inconel 718, (c) Inconel 601, and (d) Inconel 825 obtained at parameters setting: [OCV=60V,  $I_p$ =5A,  $T_{on}$ =200 $\mu$ s,  $\tau$ =70%,  $F_p$ =0.3bar]

To exhibit the dependence of control parameters on WLT i.e. to analyse the relationship between the white layer and the working conditions; it requires measurement of WLT (after surface grinding/polishing/etching of the EDMed surface and viewing under SEM) obtained on the EDMed end product in all experimental runs for four types of Inconel grades.

Here, SEM images of white layer, developed on EDMed component of four Inconel grades, have been grabbed through exploring a common parameters setting i.e. [OCV=90V,  $I_p$ =11A,  $T_{on}$ =200  $\mu$ s,  $\tau$ =80%,  $F_p$ =04 bar] (off course, this is not the optimal setting). Variation of the value of WLT obtained on EDMed component of different grades of Inconel reveals its dependency on the property of work material (process parameters setting being the same).



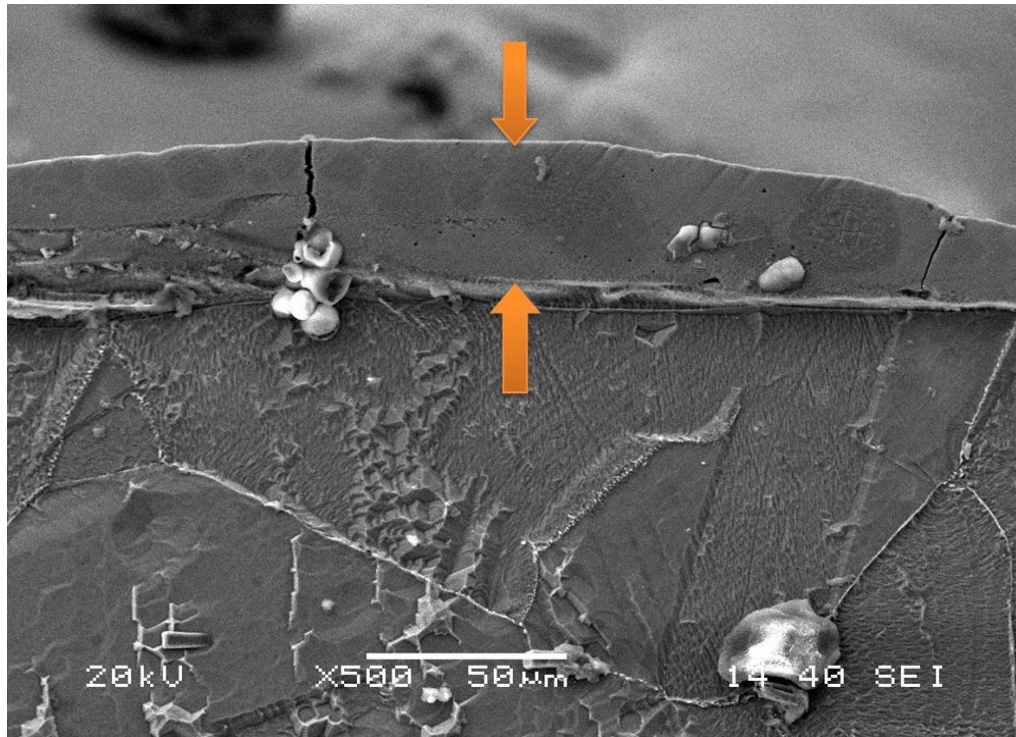


**Fig. 8.11.1:** SEM micrograph revealing White Layer Thickness (WLT~32.016  $\mu\text{m}$ ) of EDMed Inconel 601 obtained at Run No. 16 i.e. [OCV=90V,  $I_p$ =11A,  $T_{on}$ =200  $\mu\text{s}$ ,  $\tau$ =80%,  $F_p$ =04 bar]

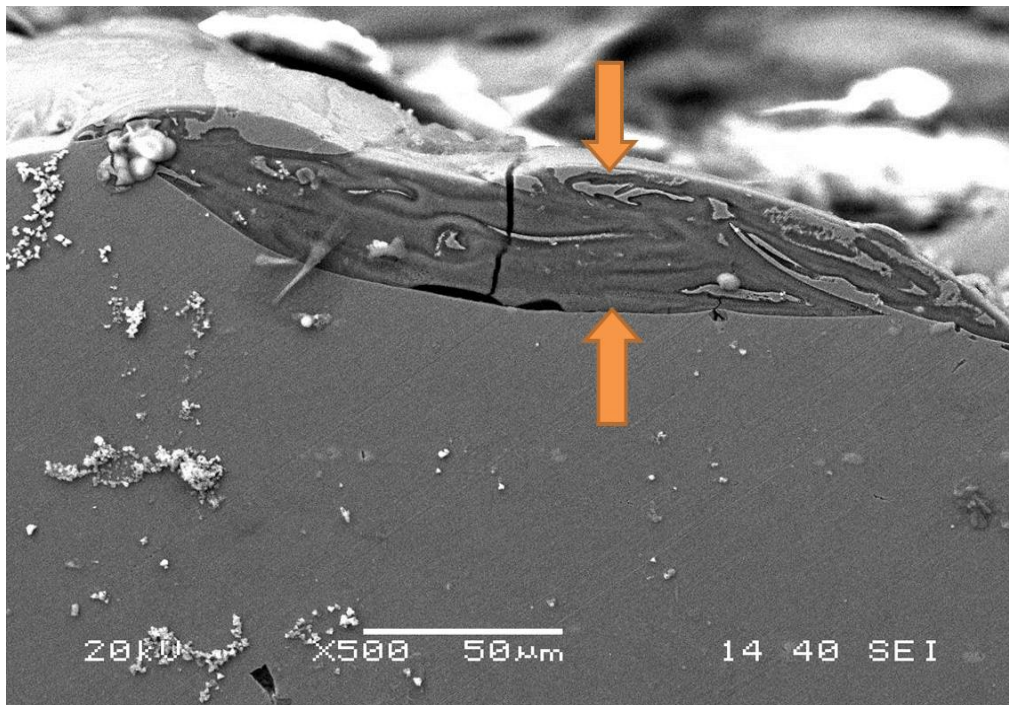


**Fig. 8.11.2:** SEM micrograph revealing White Layer Thickness (WLT~28.189  $\mu\text{m}$ ) of EDMed Inconel 625 obtained at Run No. 16 i.e. [OCV=90V,  $I_p$ =11A,  $T_{on}$ =200  $\mu\text{s}$ ,  $\tau$ =80%,  $F_p$ =04 bar]

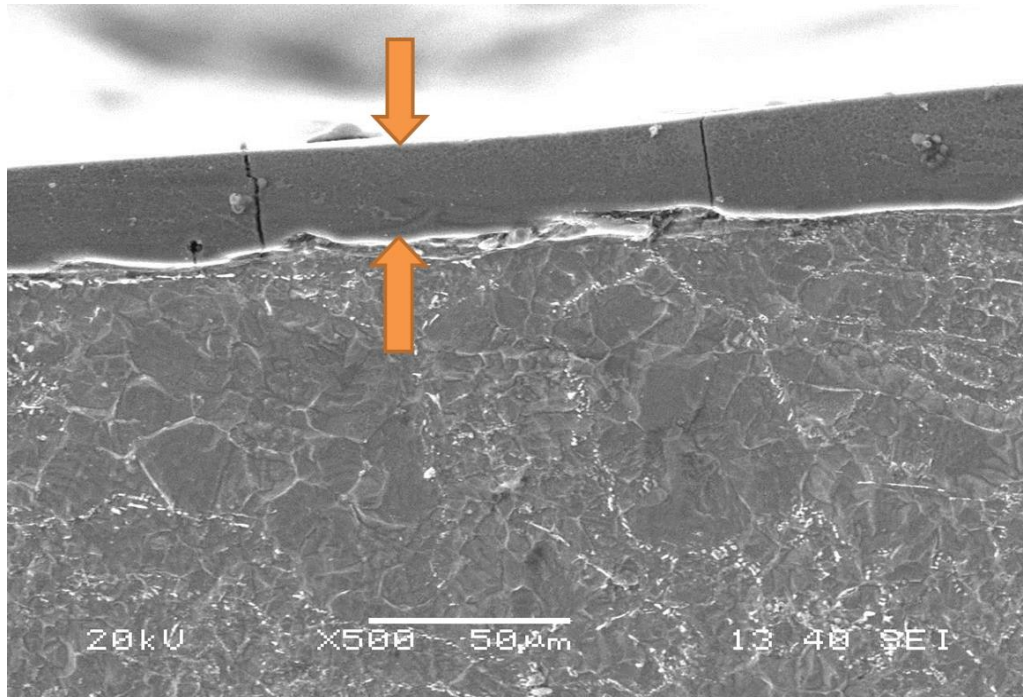


**Fig. 8.11.3:** SEM micrograph revealing White Layer Thickness (WLT~25.426  $\mu\text{m}$ ) of EDMed Inconel 718 obtained at Run No. 16 i.e. [OCV=90V,  $I_p$ =11A,  $T_{on}$ =200  $\mu\text{s}$ ,  $\tau$ =80%,  $F_p$ =04 bar]

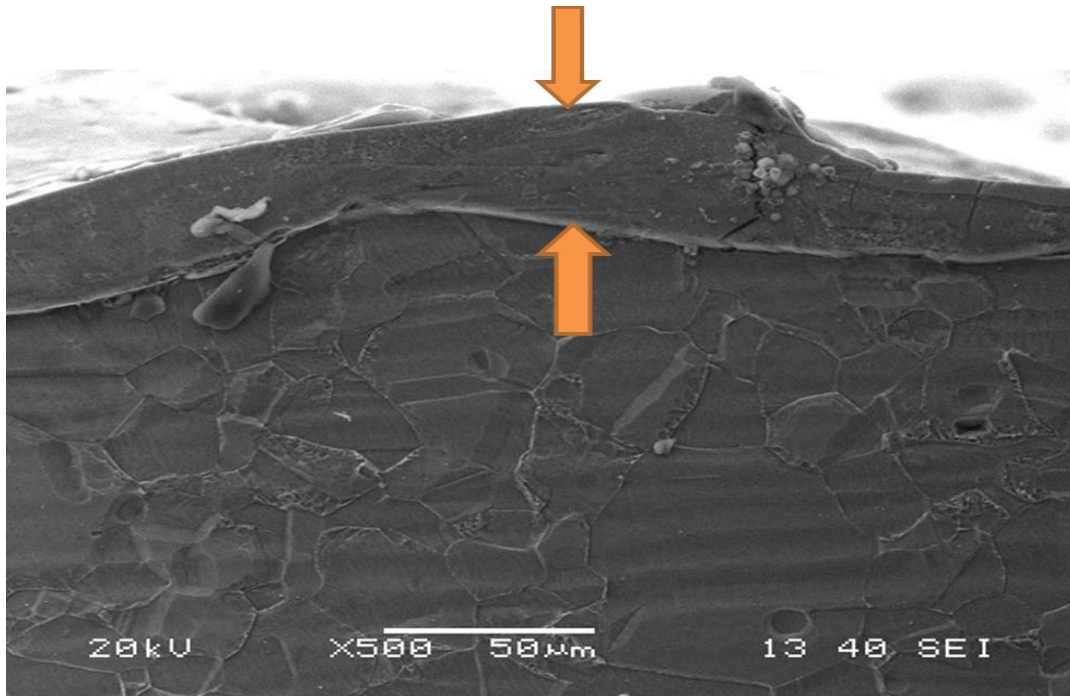


**Fig. 8.11.4:** SEM micrograph revealing White Layer Thickness (WLT~30.692  $\mu\text{m}$ ) of EDMed Inconel 825 obtained at Run No. 16 i.e. [OCV=90V,  $I_p$ =11A,  $T_{on}$ =200  $\mu\text{s}$ ,  $\tau$ =80%,  $F_p$ =04 bar]

The SEM images shown herein only reveal existence of white layer on the EDMed work piece. In the present case, the HAZ has not been found beneath the white layer. This may be attributed due to the fact that EDM operates under pulse-mode, and the pulse-on time being too small (in the order of  $\mu\text{s}$ ); time seems insufficient for substantial amount of heat conduction through the work piece; since Inconel possesses very low thermal conductivity. Continuous flushing of dielectric also reduces the extent of such heat transfer. Hence, HAZ could not be identified. It could not be distinguished prominently from the base material.

## 8.4 Conclusions

Conclusions drawn from the aforesaid research have been pointed out below.

- ▲ Application of satisfaction function, fuzzy inference system in conjugation with Taguchi's philosophy has been demonstrated herein as an efficient optimization route for simultaneous optimization of multi-requirements of process performance yield in relation to MRR, EWR,  $R_a$  and SCD during EDM of different grades of Inconel.
- ▲ The present work proposes an integrated optimizing route combining satisfaction function, fuzzy inference system and Taguchi method for simultaneous optimization of multi-performance features (multi-response) through a case experimental study of EDM of different grades of Inconel super alloy. As compared to existing literature, the complex mathematical formulation and tedious procedural steps delineated in grey-fuzzy, utility-fuzzy and desirability fuzzy approaches, the proposed optimization module is quite easier; however, application of which is hardly found in existing literature before. This seems to be the unique contribution of the present dissertation deserves mention.
- ▲ FIS has been explored for logical aggregation of multi-inputs to compute a unique output (combined satisfaction function i.e.  $S_c$  in the present case) that is the prerequisite of Taguchi's optimization approach. FIS works under the relationship mapping between multi-inputs with respect to the single output; however, while aggregating multi-input to transform a unique output, it does not consider priority weightages of individual inputs. Therefore, assignment of response priority weightage is not required in the proposed optimization module. As exact priority weights is difficult to assign for individual responses, Decision-Makers' judgement is required

for assigning response priority weightage; however, Decision-Maker' judgement may vary depending on individuals' perception thus inviting uncertainty in decision making.

- ▲ Literature highlights exploration of (i) grey relation analysis combined with FIS, (ii) utility theory combined with FIS and also (iii) desirability function approach combined with FIS etc. towards for aggregation of multi-performance features (process output responses) to compute a unique performance index (generally called Multi-Performance Characteristic Index, MPCI). However, the proposed satisfaction function approach in combination with fuzzy inference system has been found a unique conceptualization aiming for logical aggregation of multi-responses into an equivalent single performance index; i.e. combined satisfaction score  $S_c$ , which is to optimized (maximized) finally by Taguchi method.
- ▲ Within selected experimental domain and on the machining setup explored herein the optimal setting for simultaneously satisfying MRR, EWR,  $R_a$  and SCD has been obtained as ( $A_4B_1C_1D_1E_4$ ) i.e. [OCV= 90V,  $I_p$ = 5A,  $T_{on}$ = 200 $\mu$ s,  $\tau$  = 70%,  $F_p$ = 0.6 bar] for Inconel 625; ( $A_4B_1C_1D_4E_2$ ) i.e. [OCV= 90V,  $I_p$  = 5A,  $T_{on}$ = 200 $\mu$ s,  $\tau$  = 85%,  $F_p$  = 0.4 bar] for Inconel 718; ( $A_3B_2C_4D_3E_1$ ) i.e. [OCV= 80V,  $I_p$ = 7A,  $T_{on}$  = 500 $\mu$ s,  $\tau$  = 80%,  $F_p$  = 0.3 bar] for Inconel 601; ( $A_3B_1C_2D_4E_2$ ) i.e. [OCV = 80V,  $I_p$  = 5A,  $T_{on}$  = 300 $\mu$ s,  $\tau$  = 85%,  $F_p$  = 0.4 bar] for Inconel 825. It has been observed that optimal parametric combination varies from one Inconel grade to another due to differences in their mechanical properties, chemical composition and consequently the ease of machining.
- ▲ Analysis of SEM micrographs reveals surface irregularities in terms of cracks, crater globules of debris pockmarks etc. on the surface of the EDMed Inconel specimens; these can be substantially reduced by proper tuning process control parameters set to the optimal level. It has been found that the SCD varies from 0.0148 ~ 0.0281  $\mu$ m/ $\mu$ m<sup>2</sup> for the EDMed surface of Inconel 625 whilst experimented as per  $L_{16}$  design of experiment. For Inconel 718, the variation of SCD appears in the range of 0.0122~0.0201  $\mu$ m/ $\mu$ m<sup>2</sup>. The range of SCD as observed for Inconel 601 and Inconel 825 is 0.0141~0.0219  $\mu$ m/ $\mu$ m<sup>2</sup> and 0.0148~0.0257  $\mu$ m/ $\mu$ m<sup>2</sup>, respectively. For a common parametric setting i.e. [OCV=90V,  $I_p$ =11A,  $T_{on}$ =200  $\mu$ s,  $\tau$ =80%,  $F_p$ =0.4 bar], the white layer thickness has been found maximum for Inconel 601 (~32.016  $\mu$ m) and minimum for Inconel 718 (~25.426  $\mu$ m).





## Chapter 9

# Summary and Contribution

### 9.1 Executive Summary

In *Chapter 3*, aspects of machinability of Inconel 718 super alloy have been experimentally investigated during electro-discharge machining using Copper tool electrode. Based on five-factor-five-level  $L_{25}$  orthogonal array design of experiment, experiments have been conducted by varying the following controllable process parameters viz. gap voltage, peak discharge current, pulse-on time, duty factor, and flushing pressure. Machining performance has been evaluated in terms of multiple responses such as roughness average, surface crack density, white layer thickness (observed on the EDMed work surface), and micro-hardness of the white layer. In addition to this, SEM images of the EDMed work surfaces of Inconel 718 have been analyzed in view of various surface irregularities. Effects of process parameters on EDM performance outputs have been graphically presented. Finally, utility theory coupled with Taguchi method has been attempted to determine the most appropriate setting of process parameters to ensure satisfactory machining yield during execution of EDM operation on Inconel 718.

In *Chapter 4*, effects of cryogenic treatment of the electrode material on improving machining yield during electro-discharge machining of Inconel 825 super alloys have been investigated. The extent of machining performance has been evaluated in terms of multiple response features viz. surface crack density and white layer thickness developed onto the top surface of the EDMed Inconel 825 work material. Based on three controllable process parameters namely, peak discharge current, pulse duration and duty factor, EDM experiments have been conducted using Non-Treated Tool (NTT), and Cryogenically Treated Tool (CTT), respectively. Attempt has been made to compare chemical composition, metallurgical aspects, residual stress and micro-hardness of the EDMed Inconel 825 work surface obtained by using CTT with respect to that of obtained

using NTT. Morphology of the EDMed Inconel 825 work surface has been examined through analysis of SEM micrographs. Moreover, effects of cryogenic treatment of tool electrode has been discussed from the viewpoint of shape retention capability, wear and extent of Carbon deposition onto the bottom surface of the tool electrode during electro-discharge machining on Inconel 825 work material.

In **Chapter 5**, the extent of machinability of Inconel super alloy 825 has been investigated during electro-discharge machining using deep Cryogenically Treated Workpiece (CTW) as compared to the case of EDM using Non-Treated Workpiece (NTW). Effects of cooling rate (ramp-down) followed during cryogenic treatment cycle of the work material have also been examined in purview of various EDM performance features.

In **Chapter 6**, an experimental investigation has been carried out focusing surface integrity and metallurgical characteristics of the EDMed work surface of Inconel 601 super alloy in comparison with EDMed 304SS as well as EDMed Titanium alloy Ti-6Al-4V. Degree of severity of surface cracks and depth of white layer thus formed onto the EDMed work surface have been studied for aforesaid three work materials upon execution of EDM operation. Comparison on machinability of aforesaid three work materials has been made with relevance to EDS, XRD analysis and micro-hardness test data.

In **Chapter 7**, machinability aspects of Inconel 718 work material have been experimentally investigated during electro-discharge machining using Copper tool electrode. Based on five-factor-five-level  $L_{25}$  orthogonal array design of experiment, experiments have been conducted by varying the following controllable process parameters viz. gap voltage, peak discharge current, pulse-on time, duty factor, and flushing pressure. Machining performance has been evaluated in terms of multiple responses such as material removal rate, electrode wear rate, roughness average (of the EDMed surface), surface crack density, white layer thickness, and micro-hardness of the white layer. Objective functions have been selected in such a way that except MRR (which has corresponded to Higher-is-Better (HB) requirement); all the response variables have corresponded to Lower-is-Better (LB) requirement. Aforesaid multiple response variables of conflicting requirements have been optimized simultaneously with a goal to determine the best setting of controllable process parameters within selected

experimental domain. Owing to the limitation of Taguchi's optimization philosophy, the concept of 'satisfaction function' has been articulated in this research to obtain satisfaction values of individual responses; thus, facilitating aggregation of multi-response features into an equivalent single index. A distance measure value has been computed next which basically determines the separation of each experimental setting (alternative) with respect to the ideal expectation (satisfaction). Finally, this distance function has been optimized using Taguchi method.

In order to validate the proposed satisfaction function and distance measure approach integrated with Taguchi method, the optimal setting, thus obtained from the aforesaid research, has been compared to that of an established optimization procedure i.e. Principal Component Analysis (PCA) and Combined Quality Loss (CQL) concept integrated with Taguchi method. It has been observed that both the approaches have converged to the same result. Optimal setting has been verified through confirmatory test. In addition to this, SEM micrographs of EDMed work surfaces of Inconel 718 have been critically analyzed and important inferences have been drawn.

In **Chapter 8**, an experimental investigation on assessing machining performance during electro-discharge machining of Inconel 625, 718, 601 and 825 has been delineated. Based on 5-factor-4-level  $L_{16}$  orthogonal array, experiments have been carried out by varying gap voltage, peak current, pulse-on time, duty factor and flushing pressure (each varied at four discrete levels) to examine the extent of machining performance in terms of material removal rate, electrode wear rate, surface roughness, and surface crack density of the EDMed end products obtained by utilizing different parameters settings (for Inconel of different grades, respectively). An integrated optimization module combining satisfaction function approach and Fuzzy Inference System (FIS) in conjugation with Taguchi's philosophy has been proposed for simultaneous optimization of aforementioned multiple performance indices. Analysis of SEM micrographs has been carried out to understand surface irregularities in terms of surface cracks, formation of white layer etc. for the EDMed Inconel end products (of different grades). Aspects of machinability have thus been studied by comparing machining responses obtained during EDM of Inconel 625, 718, 601 and 825, respectively.

## 9.2 Research Contribution

- ✓ Surface Integrity (morphology and topography) of the EDMed work surface of Inconel has been studied in detail.
- ✓ Metallurgical characteristics of the EDMed Inconel work surface have been studied with respect to unaffected parent material.
- ✓ Ease of electro-discharge machining of Inconel using deep cryogenically treated electrode/workpiece has been studied.
- ✓ Machinability of Inconel has been compared to that of 304SS as well as Ti-6Al-4V for electro-discharge machining.
- ✓ The most appropriate setting of EDM process parameters has been determined towards optimizing multiple indicators (measures) of machining yield.

## 9.3 Limitations of the Present Work

The limitations of the present work have also been presented below.

- ☑ For calculation of dislocation density  $\delta$ , by considering the highest intensity peak, the value of  $a$  (the lattice parameter) has been calculated herein from the value of  $d$  (the inter planer spacing). However, apart from exploring a single  $d$  value, it would be more scientific to use *two-five* peaks to be analyzed with proper extrapolation. Moreover, the equation used herein for computing the values of dislocation density has indeed been an approximated one collected from literature.
- ☑ Peak broadening during cryogenic treatment of the specimens is hugely contributed by the lattice strain; however, this has been ignored in the present work. In reality, peak broadening (due to cryogenic treatment) of tool/work material is affected by (a) crystallite size, and (b) micro-strain (ignoring instrumental broadening). In order to capture the ‘strain-effect’, it is required to anneal the ‘as received’ sample first and then to compare peak broadening of the test samples (with respect to the annealed one) and by using *Williamson Hall plot* crystallite size and strain to be computed. However, in during execution of the present experimental work, such as approach has been attempted; but it has been observed that the plots of the points have not approximately indicated a straight line (exhibiting highly scattered plots). Therefore, the data (crystallite size only) have been used. However, it would be more scientific to confirm the crystallite size by FESEM/TEM in consideration with the strain part.

## 9.4 Future Scope

The research can be extended in the following directions.

- ⇒ Effects of tool electrode (viz. Copper, Tungsten Carbide, Copper Tungsten, graphite, brass etc.) as well as dielectric medium (viz. EDM oil, Kerosene, distilled water, used transformer oil etc.) are to be studied on influencing EDM performance on Inconel work material.
- ⇒ Ease of machining of cryogenically treated Inconel work material using cryogenically treated tool electrode may be investigated and compared with the case of EDM with (a) normal tool and NTW/CTW, (b) normal workpiece and NTT/CTT.
- ⇒ Effects of Shallow Cryogenic Treatment (SCT) and Deep Cryogenic Treatment (DCT) on tool/work material may be investigated on assessing ease of machining of Inconel super alloys by electro-discharge machining using different combinations of tool/work material (non-treated and cryogenically treated).
- ⇒ Aspects of tool life, quantitative evaluation of tool shape retention capability, corner size machining accuracy of the EDMed hole need to be investigated in detail while executing EDM operation on Inconel super alloys.
- ⇒ Machinability of Inconel needs to be compared to that of other super alloys (like Ti-6Al-7Nb, Nimonic etc.) in the context of EDM/WEDM operations.
- ⇒ Application of evolutionary algorithms (like Genetic Algorithm, Particle Swarm Optimization, Ant-Colony Optimization, Harmony Search Algorithm and many others) may be attempted for optimization of EDM response outputs in the context of machining of Inconel super alloys.



# References

- Abdulkareem S, Khan AA and Konneh M. (2009) Reducing electrode wear ratio using cryogenic cooling during electrical discharge machining, *International Journal of Advanced Manufacturing Technology*, **45**(11–12): 1146–1151.
- Abdulkareem S, Khan AA, Konneh M (2010) Cooling effect on electrode and process parameters in EDM, *Materials and Manufacturing Processes*, **25**(6): 462–466.
- Agarwal V, Khangura SS and Garg RK (2015) Parametric modeling and optimization for wire electrical discharge machining of Inconel 718 using response surface methodology, *International Journal of Advanced Manufacturing Technology*, **79**(1-4): 31-47.
- Ahmad S, Lajis MA (2013) Electrical discharge machining (EDM) of Inconel 718 by using copper electrode at higher peak current and pulse duration, *2<sup>nd</sup> International Conference on Mechanical Engineering Research (ICMER 2013): IOP Conference Series: Materials Science and Engineering*, 50(1), 012062, DOI: 10.1088/1757-899X/50/1/012062.
- Akhbarizadeh A, Shafyei A and Golozar MA (2009) Effects of cryogenic treatment on wear behavior of D6 tool steel, *Materials and Design*, **30**(8): 3259–3264.
- Akincioglu S, Gökaya H, Uygur İ (2015) A review of cryogenic treatment on cutting tools, *International Journal of Advanced Manufacturing Technology*, **78**(9): 1609–1627.
- Alias A, Abdullah B, Abbas NM (2012) Influence of machine feed rate in WEDM of Titanium Ti-6Al-4V with constant current (6A) using brass wire, *Procedia Engineering*, **41**: 1806-1811.
- Altug M, Erdem M, Ozay C (2015) Experimental investigation of kerf of Ti-6Al-4V exposed to different heat treatment processes in WEDM and optimization of parameters using genetic algorithm, *International Journal of Advanced Manufacturing Technology*, **78**(9):1573–1583.
- Amini K, Akhbarizadeh A, Javadpour S (2012) Investigating the effect of holding duration on the microstructure of 1.2080 tool steel during the deep cryogenic heat treatment, *Vacuum*, **86**(10): 1534-1540.
- Amorim FL, Stedile LJ, Torres RD, Soares PC, Laurindo CAH (2014) Performance and surface integrity of Ti-6Al-4V after sinking EDM with special graphite electrodes, *Journal of Materials Engineering and Performance*, **23**(4): 1480–1488.
- Ashtiani HRR, Zarandooz R (2016) Microstructural and mechanical properties of resistance spot weld of Inconel 625 super alloy, *International Journal of Advanced Manufacturing Technology*, **84**(1): 607-619.
- ASM Handbook, Properties and Selection: Nonferrous Alloys and Special Purpose Materials, vol. 2, 1993.



- Ay M, Çaydaş U and Haşçalık A (2013) Optimization of micro-EDM drilling of Inconel 718 super alloy, *International Journal of Advanced Manufacturing Technology*, **66**(5): 1015–1023.
- Barron RF (1985) Cryogenic systems, Oxford Science Publications, New York, pp. 21-24.
- Bensely A, Prabhakaran A, Lal DM and Nagarajan G (2006) Enhancing the wear resistance of case carburized steel (En 353) by cryogenic treatment, *Cryogenics*, **45**(12): 747–754.
- Bhattacharyya B, Gangopadhyay S, Sarkar BR (2007) Modelling and analysis of EDM<sub>ED</sub> job surface integrity, *Journal of Materials Processing Technology*, **189**(1): 169-177.
- Bozdana AT, Ulutas T (2016) The effectiveness of multi-channel electrodes on drilling blind holes on Inconel 718 by EDM process, *Materials and Manufacturing Processes*, **31**(4): 504-513.
- Bozkurt B, Gadalla AM, Eubank PT (1996) Simulation of erosions in a single discharge EDM process, *Material and Manufacturing Process*, **11**(4): 555-563.
- Bruyn HED (1970) Some aspects of the influence of gap flushing on the accuracy in finishing by spark erosion, *Annals of the CIRP*, **16**: 147-157.
- Chen L (2001) Multi-objective design optimization based on satisfaction metrics, *Engineering Optimization*, **33**(5): 601–617.
- Chen LH (1997) Designing robust products with multiple quality characteristics, *Computers and Operations Research*, **24**(10): 937–944.
- Chen SL, Yan BH, Huang FY (1999) Influence of kerosene and distilled water as dielectrics on the electric discharge machining characteristics of Ti–6Al–4V, *Journal of Materials Processing Technology*, **87**(1-3): 107–111.
- Cherif MS, Chabchoub H, Aouni B (2008) Quality control system design through the goal programming model and the satisfaction functions, *European Journal of Operational Research*, **186**(3): 1084–1098.
- Chiang YM, Hsieh HH (2009) The use of the Taguchi method with grey relational analysis to optimize the thin-film sputtering process with multiple quality characteristic in color filter manufacturing, *Computers and Industrial Engineering*, **56**(2): 648-661.
- Cox E (1992) Fuzzy fundamentals, *Spectrum, IEEE*, **29**(10): 58-61.
- Crookall JR, Khor BC (1972) Residual stresses and surface effects in electro discharge machining, Proceedings of the 13<sup>th</sup> International Machine Tool Design and Research Conference, Birmingham, pp. 331–338.
- Crookall JR, Khor BC (1975) Electro-discharge machined surfaces, *Proceedings of the Fifteenth International Machine Tool Design and Research Conference*, 373-384, Macmillan Education UK.
- Cullity BD (1978) Elements of X-Ray Diffraction, Addison Wesley, 2<sup>nd</sup> Ed., pp. 470.

- D'Urso G, Maccarini G, Ravasio C (2014) Process performance of micro-EDM drilling of stainless steel, *The International Journal of Advanced Manufacturing Technology*, **72**(9): 1287-1298.
- Das D, Dutta AK, Ray KK (2008) On the enhancement of wear resistance of tool steels by cryogenic treatment, *Journal Philosophical Magazine Letters*, **88**(11): 801–811.
- Das D, Dutta AK, Toppo V, Ray KK (2007) Effect of deep cryogenic treatment on the carbide precipitation and tribological behavior of D2 Steel, *Materials and Manufacturing Processes*, **22**(4): 474-480.
- Datta S, Bandyopadhyay A, Pal PK (2008) Grey based Taguchi method for optimization of bead geometry in submerged arc bead-on-plate welding, *International Journal of Advanced Manufacturing Technology*, **39**(11-12): 1136-1143.
- Datta S, Nandi G, Bandyopadhyay A, Pal PK (2009) Application of PCA based hybrid Taguchi method for multi-criteria optimization of submerged arc weld: A case study, *International Journal of Advanced Manufacturing Technology*, **45**(3-4): 276-286.
- Dhanabalan S, Sivakumar K, Narayanan CS (2014) Analysis of form tolerances in electrical discharge machining process for Inconel 718 and 625, *Materials and Manufacturing Processes*, **29**(3): 253-259.
- Dhobe MM, Chopde IK, Gogte CL (2014) Optimization of wire electro discharge machining parameters for improving surface finish of cryo-treated tool steel using DOE, *Materials and Manufacturing Processes*, **29**(11-12): 1381-1386.
- Ebeid SJ, Hewidy MS, El-Taweel TA, Youssef AH (2004) Towards higher accuracy for ECM hybridized with low-frequency vibrations using the response surface methodology, *Journal of Materials Processing Technology*, **149**(1), 432-438.
- Ekmekci (2009) White layer composition, heat treatment, and crack formation in electric discharge machining process, *Metallurgical and Materials Transactions B*, **40**(1): 70-81.
- Ekmekci B (2007) Residual stresses and white layer in electric discharge machining (EDM), *Applied Surface Science*, **253**(23): 9234–9240.
- Ekmekci B, Elkoca O, Tekkaya AE, Erden A (2005) Residual stress state and hardness depth in electric discharge machining: de-ionized water as dielectric liquid, *Machining Science and Technology*, **9**(1): 39-61.
- Ekmekci B, Tekkaya AE, Erden A (2006) A semi-empirical approach for residual stresses in electric discharge machining (EDM), *International Journal of Machine Tools and Manufacture*, **46**(7): 858-868.
- Erden A, Bilgin S (1980) Role of impurities in electric discharge machining, Proceedings of the Twenty-First International Machine Tool Design and Research Conference, pp. 345-350, Macmillan Education, UK.

- Ezugwu EO, Wang ZM (1997) Titanium alloys and their machinability—a review, *Journal of Materials Processing Technology*, **68**: 262–274.
- Feyzi T, Safavi SM (2013) Improving machinability of Inconel 718 with a new hybrid machining technique, *International Journal of Advanced Manufacturing Technology*, **66**(5-8): 1025–1030.
- Fiat O, Cosset F, Bessaudou A (2008) Calculation of weights from equal satisfaction surfaces, *Chemometrics and Intelligent Laboratory Systems*, **90**(1): 25–30.
- Firouzdor V, Nejati E, Khomamizadeh F (2008) Effect of deep cryogenic treatment on wear resistance and tool life of M2 HSS drill, *Journal of Materials Processing Technology*, **206**(1-3): 467–472.
- Fung CP, Kang PC (2005) Multi-response optimization in friction properties of PBT composites using Taguchi method and principal component analysis, *Journal of Materials Processing Technology*, **170**(3): 602–610.
- Gaikwad V, Jatti VS (2016) Optimization of material removal rate during electrical discharge machining of cryo-treated NiTi alloys using Taguchi's method, *Journal of King Saud University-Engineering Sciences*, (Article in Press),
- Gauri SK, Pal S (2014) The principal component analysis (PCA)-based approaches for multi-response optimization: some areas of concerns, *International Journal of Advanced Manufacturing Technology*, **70**(9-12): 1875–1887.
- Ghani JA, Choudhury IA, Hassan HH (2004) Application of Taguchi method in the optimization of end milling parameters, *Journal of Materials Processing Technology*, **145**(1): 84–92.
- Gill SS, Singh J (2010) Effect of deep cryogenic treatment on machinability of titanium alloy (Ti-6246) in electric discharge drilling, *Materials and Manufacturing Processes*, **25**(6): 378–385.
- Goyal A (2017) Investigation of material removal rate and surface roughness during wire electrical discharge machining (WEDM) of Inconel 625 super alloy by cryogenic treated tool electrode, *Journal of King Saud University – Science*, (Published Online), DOI: <https://doi.org/10.1016/j.jksus.2017.06.005>
- Guu YH, Chou CY, Chiou ST (2005) Study of the effect of machining parameters on the machining characteristics in electrical discharge machining of Fe-Mn-Al alloy, *Materials and Manufacturing Processes*, **20**(6): 905–916.
- Guu YH, Hocheng H (2001) Effects of workpiece rotation on machinability during electrical-discharge machining, *Materials and Manufacturing Processes*, **16**(1): 91–101.
- Guu YH, Hocheng H, Chou CY, Deng CS (2003) Effect of electrical discharge machining on surface characteristics and machining damage of AISI D2 tool steel, *Materials Science and Engineering A*, **358**(1-2): 37–43.

- Guu YH, Hou MTK (2007) Effect of machining parameters on surface textures in EDM of Fe-Mn-Al alloy, *Materials Science and Engineering: A*, **466**(1): 61-67.
- Hands BA (1986) Cryogenic Engineering, Academic Press, London, pp. 100-106.
- Haron CHC, Jawaid A (2005) The effect of machining on surface integrity of titanium alloy Ti-6Al-4V, *Journal of Materials Processing Technology*, **166**(2): 188-192.
- Hascalik A, Caydas U (2007a) A comparative study of surface integrity of Ti-6Al-4V alloy machined by EDM and AECG, *Journal of Materials Processing Technology*, **190**(1-3): 173-180.
- Hascalik A, Caydas U (2007b) Electrical discharge machining of Titanium alloy (Ti-6Al-4V), *Applied Surface Science*, **253**(22): 9007-9016.
- Hasçalık A, Çaydaş U (2004) Experimental study of wire electrical discharge machining of AISI D5 tool steel, *Journal of Materials Processing Technology*, **148**(3): 362-367.
- Hewidy MS, El-Taweel TA, El-Safty MF (2005) Modelling the machining parameters of wire electrical discharge machining of Inconel 601 using RSM, *Journal of Materials Processing Technology*, **169**(2): 328-336.
- Ho KH, Newman ST (2003) State of the art electrical discharge machining (EDM), *International Journal of Machine Tools and Manufacture*, **43**(13): 1287-1300.  
<http://dx.doi.org/10.1016/j.jksues.2016.04.003>.  
<http://dx.doi.org/10.1063/1.4712089>.
- Huang CA, Hsu FY, Yao SJ (2004) Microstructure analysis of the martensitic stainless steel surface fine-cut by the wire electrode discharge machining (WEDM), *Materials Science and Engineering: A*, **371**(1): 119-126.
- Huang JT, Liao YS, Hsue WJ (1999) Determination of finish-cutting operation number and machining-parameters setting in wire electrical discharge machining, *Journal of Materials Processing Technology*, **87**(1): 69-81.
- Hui Z, Liu Z, Cao Z, Qiu M (2016) Effect of cryogenic cooling of tool electrode on machining Titanium alloy (Ti-6Al-4V) during EDM, *Materials and Manufacturing Processes*, **31**(4): 475-482.
- Imran M, Mativenga PT, Kannan S, Novovic D (2008) An experimental investigation of deep-hole micro-drilling capability for a nickel-based super alloy, *Proc IMechE Part B: Journal of Engineering Manufacture*, **222**(12): 1589-1596.
- Isaak C-J, Reitz W (2008) The effects of cryogenic treatment on the thermal conductivity of GRCo-84, *Materials and Manufacturing Processes*, **23**(1): 82-91.
- Jabbaripour B, Sadeghi MH, Faridvand S, Shabgard MR (2012) Investigating the effects of EDM parameters on surface integrity, MRR and TWR in machining of Ti-6Al-4V, *Machining Science and Technology*, **16**(3): 419-444.

- Jacob R, Nair HG, Isac J (2015) Structural and Morphological Studies of Nanocrystalline Ceramic  $\text{BaSr}_{0.9}\text{Fe}_{0.1}\text{TiO}_4$ , *International Letters of Chemistry, Physics and Astronomy*, **41**: 100-117.
- Jafferson JM, Hariharan P (2013) Machining performance of cryogenically treated electrodes in microelectric discharge machining: A comparative experimental study, *Materials and Manufacturing Processes*, **28**(4): 397-402.
- Jameson EC (2001) Description and development of EDM, Published by SME, Dearborn, Michigan, pp. 16.
- Josef S, Miloš J, Petr H, Michal B, Lothar W (2011) The effect of microstructure on fatigue performance of Ti-6Al-4V alloy after EDM surface treatment for application in orthopaedics, *Journal of Mechanical Behaviour of Biomedical Materials*, **4**: 1955–1962.
- Kahng CH, Rajurkar KP (1977) Surface characteristics behaviour due to rough and fine cutting by EDM, *Annals of the CIRP*, **26**(1): 77-82.
- Kalsi NS, Sehgal R, Sharma VS (2010) Cryogenic treatment of tool materials: A review, *Materials and Manufacturing Processes*, **25**(10): 1077–1100.
- Kao JY, Tsao CC, Wang SS, Hsu CY (2010) Optimization of the EDM parameters on machining Ti-6Al-4V with multiple quality characteristics, *International Journal of Advanced Manufacturing Technology*, **47**(1): 395-402.
- Kapoor J, Singh S, Khamba JS (2012) Effect of cryogenic treated brass wire electrode on material removal rate in wire electrical discharge machining, *Proceedings of the Institution of Mechanical Engineers, Part C: Journal of Mechanical Engineering Science*, (Published Online), DOI: 10.1177/0954406212438804.
- Kentli A, Kar AK (2011) A satisfaction function and distance measure based multi-criteria robot selection procedure, *International Journal of Production Research*, **49**(19): 5821-5832.
- Keskin Y, Halkacı HS, Kizil M (2006) An experimental study for determination of the effects of machining parameters on surface roughness in electrical discharge machining (EDM), *International Journal of Advanced Manufacturing Technology*, **28**(11-12): 1118-1121.
- Khan MAR, Rahman MM, Kadirgama K (2015) An experimental investigation on surface finish in die-sinking EDM of Ti-5Al-2.5Sn, *International Journal of Advanced Manufacturing Technology*, **77**(9): 1727–1740.
- Khanna R, Singh H (2016) Comparison of optimized settings for cryogenic-treated and normal D-3 steel on WEDM using grey relational theory, *Proceedings of the Institution of Mechanical Engineers, Part L: Journal of Materials Design and Applications*, **230**(1): 219-232.

- Kibri G, Sarkar B, Pradhan B, Bhattacharyya B (2010) Comparative study of different dielectrics for micro-EDM performance during microhole machining of Ti-6Al-4V alloy, *International Journal of Advanced Manufacturing Technology*, **48**(5): 557-570.
- Koenig LW, Weill R, Wertheim R, Jutzler WI (1977) The flow fields in the working gap with electro-discharge machining, *Annals of the CIRP*, **25**(1): 71-76.
- Kolli M, Kumar A (2015) Effect of dielectric fluid with surfactant and graphite powder on Electrical Discharge Machining of titanium alloy using Taguchi Method, *Engineering Science and Technology, an International Journal*, **18**(4): 524-535.
- Kovac P, Rodic D, Pucovsky V, Savkovic B, Gostimirovic M (2014) Multi-output fuzzy inference system for modeling cutting temperature and tool life in face milling, *Journal of Mechanical Science and Technology*, **28**(10): 4247-4256.
- Kruth JP, Bleys P (2000) Measuring residual stress caused by wire EDM of tool steel, *International Journal of Electrical Machining*, **5**: 23-28.
- Kruth JP, Tönshoff HK, Klöcke F, Stevens L, Bleys P, Beil A (1988) Surface and sub-surface quality in material removal processes for tool making, Proceedings of the 12<sup>th</sup> International Symposium for Electro-machining, pp. 33-64.
- Kumar A, Maheshwari S, Sharma C, Beri, N (2011) Analysis of machining characteristics in additive mixed electric discharge machining of nickel-based super alloy Inconel 718, *Materials and Manufacturing Processes*, **26**(8): 1011-1018.
- Kumar S, Batish A, Singh R and Sing TP (2014) A hybrid Taguchi artificial neural network approach to predict surface roughness during electric discharge machining of titanium alloys, *Journal of Mechanical Science and Technology*, **28**(7): 2831-2844.
- Kumar S, Batish A, Singh R, Singh TP (2016a) Machining performance of cryogenically treated Ti-5Al-2.5 Sn titanium alloy in electric discharge machining: A comparative study, Proceedings of the Institution of Mechanical Engineers, Part C: Journal of Mechanical Engineering Science, 0954406215628030.
- Kumar S, Singh R, Batish A, Singh TP (2015) Modeling the tool wear rate in powder mixed electro-discharge machining of titanium alloys using dimensional analysis of cryogenically treated electrodes and workpiece, *Proceedings of the Institution of Mechanical Engineers, Part E: Journal of Process Mechanical Engineering*, (Published Online), DOI: 10.1177/0954408915593875.
- Kumar S, Singh R, Batish A, Singh TP and Singh R (2016b) Investigating surface properties of cryogenically treated titanium alloys in powder mixed electric discharge machining, *Journal of the Brazilian Society of Mechanical Sciences and Engineering*, (Published Online) DOI: 10.1007/s40430-016-0639-y.
- Kuppan P, Narayanan S, Rajadurai A (2011) Effect of process parameters on material removal rate and surface roughness in electric discharge drilling of Inconel 718 using graphite

- electrode, *International Journal of Manufacturing Technology and Management*, **23**(3/4): 214-233.
- Kuppan P, Rajadurai A, Narayanan S (2008) Influence of EDM process parameters in deep hole drilling of Inconel 718, *International Journal of Advanced Manufacturing Technology*, **38**(1): 74–84.
- Kuram E, Ozcelik B (2013) Multi-objective optimization using Taguchi based grey relational analysis for micro-milling of Al 7075 material with ball nose end mill, *Measurement*, **46**(6): 1849-1864.
- Lal DM, Renganarayanan S, Kalanidhi A (2001) Cryogenic treatment to augment wear resistance of tool and die steels, *Cryogenics*, **41**(3): 149–55.
- Lee HT, Hsu FC, Tai TY (2004) Study of surface integrity using the small area EDM process with a copper-tungsten electrode, *Materials Science and Engineering A*, **364**(1-2): 346–356.
- Lee HT, Tai TY (2003) Relationship between EDM parameters and surface crack formation, *Journal of Materials Processing Technology*, **142**(3): 676-683.
- Lee HT, Yur JP (2000) Characteristic analysis of EDMed surfaces using the Taguchi approach, *Materials and Manufacturing Processes*, **15**(6): 781-806.
- Lee LC, Lim LC, Narayanan V, Venkatesh VC (1988) Quantification of surface damage of tool steels after EDM, *International Journal of Machine Tools and Manufacture*, **28**(4): 359-372.
- Lee LC, Lim LC, Wong YS (1992) Towards crack minimisation of EDMed Surfaces, *Journal of Materials Processing Technology*, **32**(1–2): 45–54.
- Lee LC, Lim LC, Wong YS, Lu HH (1990) Towards a better understanding of the surface features of electro-discharge machined tool steels, *Journal of Materials Processing Technology*, **24**: 513-523.
- Leskovsek V, Kalin M, Vizintin J (2006) Influence of deep-cryogenic treatment on wear resistance of vacuum heat-treated HSS, *Vacuum*, **80**(6): 507–18.
- Li L, Guo YB, Wei XT, Li W (2003) Surface integrity characteristics in wire-EDM of Inconel 718 at different discharge energy, *Procedia CIRP*, **6**: 220–225.
- Li L, Guo YB, Wei XT, Li W (2013) Surface integrity characteristics in wire-EDM of Inconel 718 at different discharge energy, *Procedia CIRP*, **6**: 220-225.
- Li L, Li ZY, Wei XT and Cheng X (2015) Machining characteristics of Inconel 718 by sinking-EDM and wire-EDM, *Materials and Manufacturing Processes*, **30**(8): 968-973.
- Li L, Wei XT, Li ZY (2014) Surface integrity evolution and machining efficiency analysis of W-EDM of nickel-based alloy, *Applied Surface Science*, **313**: 138-143.
- Liao HC (2006) Multi-response optimisation using weighted principal component, *International Journal of Advanced Manufacturing Technology*, **27**(7-8): 720–725.

- Liao YS, Huang JT, Chen YH (2004) A study to achieve a fine surface finish in Wire-EDM, *Journal of Materials Processing Technology*, **149**(1): 165-171.
- Lin M-Y, Tsao C-C, Hsu C-Y, Chiou A-H, Huang P-C, Lin Y-C (2013) Optimization of micro milling electrical discharge machining of Inconel 718 by Grey-Taguchi method, *Transactions of Nonferrous Materials Society of China*, **23**(3): 661–666.
- Lin YC, Chen YF, Wang DA, Lee HS (2009) Optimization of machining parameters in magnetic force assisted EDM based on Taguchi method, *Journal of Materials Processing Technology*, **209**(7): 3374-3383.
- Lin YC, Yan BH, Chang YS (2000) Machining characteristics of titanium alloy (Ti-6Al-4V) using a combination process of EDM with USM, *Journal of Materials Processing Technology*, **104**(3): 171-177.
- Lingadurai K, Nagasivamuni B, Muthu Kamatchi M, Palavesam J, Selection of Wire Electrical Discharge Machining Process Parameters on Stainless Steel AISI Grade-304 using Design of Experiments Approach, *Journal of The Institution of Engineers (India): Series C*, 93(2) (2012):163–170.
- Luis CJ, Puertas I, Villa G (2005) Material removal rate and electrode wear study on the EDM of silicon carbide, *Journal of Materials Processing Technology*, **164**: 889-896.
- Lütjering G, Williams JC (2007) Titanium. Springer
- Makenzi MM, Ikua BW (2012) A review of flushing techniques used in electrical discharge machining, *Proceedings of the Mechanical Engineering Conference on Sustainable Research and Innovation, Kenya*, **4**:162-165, May 3-4, 2012.
- Mamalis AG, Vosniakos GC, Vaxevanidis NM, Prohaszka J (1987) Macroscopic and microscopic phenomena of electro-discharge machined steel surfaces: an experimental investigation, *Journal of Mechanical Working Technology*, **15**(3): 335-356.
- Manikandan R, Venkatesan R (2012) Optimizing the machining parameters of micro-EDM for Inconel 718, *Journal of Applied Sciences*, **12**(10): 971-977.
- Manohar M, Selvaraj T, Sivakumar D, Gopinath S, George KM (2014) Experimental study to assess the effect of electrode bottom profiles while machining Inconel 718 through EDM process, *Procedia Materials Science*, **6**: 92-104.
- Martel JM, Aouni B (1990) Incorporating the decision-maker's preferences in the goal programming model, *Journal of Operational Research Society*, **41**(12): 1121–1132.
- Mendel JM (1995) Fuzzy logic systems for engineering: a tutorial, *Proceedings of the IEEE*, **83**(3): 345-377.
- Mohanty A, Talla G, Gangopadhyay S (2014a) Experimental Investigation and Analysis of EDM Characteristics of Inconel 825, *Materials and Manufacturing Processes*, **29**(5): 540-549.
- Mohanty CP, Mahapatra SS, Singh MR (2014b) An experimental investigation of machinability of Inconel 718 in electrical discharge machining, *Procedia Materials Science*, **6**: 605-611.



- Molinari M, Pellizzari M, Gialanella S, Straffellini G, Stiasny KH (2001) Effect of deep cryogenic treatment on the mechanical properties of tool steels, *Journal of Materials Processing Technology*, **118**(1-3): 350–355.
- Muthukumar V, Rajesh N, Venkatasamy R, Sureshbabu A, Senthilkumar N (2014) Mathematical modeling for radial overcut on electrical discharge machining of Incoloy 800 by response surface methodology, *Procedia Materials Science*, **6**: 1674-1682.
- Nadig DS, Ramakrishnan V, Sampathkumaran P, Prashanth CS (2012) Effect of cryogenic treatment on thermal conductivity properties of copper, *AIP Conference Proceedings*, **1435**(1): 133- 139.
- Nadig DS, Ramakrishnan V, Sampathkumaran P, Prashanth CS (2011) Effect of cryogenic treatment on thermal conductivity properties of copper, *AIP Conference Proceedings*, 13–17 June 2011, Location: Spokane, Washington, USA.
- Natarajan N, Suresh P (2015) Experimental investigations on the microhole machining of 304 stainless steel by micro-EDM process using RC-type pulse generator, *International Journal of Advanced Manufacturing Technology*, **77**(9): 1741-1750.
- Nayak BB, Mahapatra SS (2015) Optimization of WEDM process parameters using deep cryo-treated Inconel 718 as work material, *Engineering Science and Technology an International Journal*, (Article in Press) DOI: 10.1016/j.jestch.2015.06.009.
- Nayak D, Sahu SN, Mula S (2016) Metallurgical approach towards explaining optimized EDM process parameters for better surface integrity of AISI D2 tool steel, *Transactions of the Indian Institute of Metals*, (Published Online), DOI: 10.1007/s12666-016-0910-z.
- Newton TR, Melkote SN, Watkins TR, Trejo RM, Reister L (2009) Investigation of the effect of process parameters on the formation and characteristics of recast layer in wire-EDM of Inconel 718, *Materials Science and Engineering: A*, **513–514**: 208–215.
- Ogata I, Mukoyama Y (1991) Residual stress on surface machined by wire electric discharge, *International journal of the Japan Society for Precision Engineering*, **25**(4): 273-278.
- Opitz H (1960) Metallurgical aspects and surface characteristics, *Proceedings of Spark Machining Symposium*, pp. 237-251, Birmingham, UK.
- Pang JS, Ansari MNM, Zaroog OS, Ali MH, Sapuan SM (2014) Taguchi design optimization of machining parameters on the CNC end milling process of halloysite nanotube with aluminium reinforced epoxy matrix (HNT/Al/Ep) hybrid composite, *HBRC Journal*, **10**(2): 138–144.
- Park SH (1996) *Robust design and analysis for quality engineering*, Chapman and Hall, London.
- Patil PI, Tated RG (2012) Comparison of effects of cryogenic treatment on different types of steels: A review, *IJCA Proceedings on International Conference in Computational Intelligence (ICCIA 2012)*, **9**: 10-29, March 2012.

- Petr H, Lucie B, Josef S, Markéta B, Katarína N, Miloš J (2012) Surface treatment by electric discharge machining of Ti–6Al–4V alloy for potential application in orthopaedics, *Journal of Mechanical Behaviour of Biomedical Materials*, **7**: 96–105.
- Phadke MS (1989) Quality engineering using robust design, Prentice-Hall, Englewood Cliffs, NJ.
- Phadke MS (1998) Quality engineering using design of experiments, quality control, robust design, and the Taguchi method, Wadsworth and Books, California.
- Prabhu S, Vinayagam BK (2011) AFM surface investigation of Inconel 825 with multi wall carbon nano tube in electrical discharge machining process using Taguchi analysis, *Archives of Civil and Mechanical Engineering*, **11**(1): 149-169.
- Pradhan MK, Biswas CK (2010) Neuro-fuzzy and neural network-based prediction of various responses in electrical discharge machining of AISI D2 steel, *International Journal of Advanced Manufacturing Technology*, **50**(5): 591-610.
- Prihandana GS, Sriani T, Mahardika M, Hamdi M, Miki N, Wong YS, Mitsui K (2014) Application of powder suspended in dielectric fluid for fine finish micro-EDM of Inconel 718, *International Journal of Advanced Manufacturing Technology*, **75**(1-4): 599-613.
- Rahman M, Seah WKH, Teo TT (1997) The Machinability of Inconel 718, *Journal of Materials Processing Technology*, **63**(1-3): 199-204.
- Rajendran S, Marimuthu K, Sakthivel M (2013) Study of crack formation and resolidified layer in EDM process on T90Mn2W50Cr45 tool steel, *Materials and Manufacturing Processes*, **28**(6): 664-669.
- Rajesha S, Sharma AK, Kumar P (2010) Some aspects of surface integrity study of electro discharge machined Inconel 718, Proceedings of the 36<sup>th</sup> International MATADOR Conference, Springer London, pp. 439-444.
- Rajesha S, Sharma AK, Kumar P (2012) On electro discharge machining of Inconel 718 with hollow tool, *Journal of Materials Engineering and Performance*, **21**(6): 882-891.
- Rajyalakshmi G, Ramaiah PV (2003) Multiple process parameter optimization of wire electrical discharge machining on Inconel 825 using Taguchi grey relational analysis, *International Journal of Advanced Manufacturing Technology*, **69**(5): 1249–1262.
- Ramakrishnan R, Karunamoorthy L (2008) Modeling and multi-response optimization of Inconel 718 on machining of CNC WEDM process, *Journal of Materials Processing Technology*, **207**(1-3): 343–349.
- Ramanujam R, Venkatesan K, Saxena V, Pandey R, Harsha T, Kumar G (2014) Optimization of machining parameters using fuzzy based principal component analysis during dry turning operation of Inconel 625–A hybrid approach, *Procedia Engineering*, **97**: 668-676.
- Ramasawmy H, Blunt L, Rajurkar KP (2005) Investigation of the relationship between the white layer thickness and 3D surface texture parameters in the die sinking EDM process, *Precision Engineering*, **29**(4): 479-490.

- Ramkumar KD, Mithilesh P, Varun D, Reddy ARG, Arivazhagan N, Narayanan S, Kumar KG (2014) Characterization of microstructure and mechanical properties of Inconel 625 and AISI 304 dissimilar weldments, *ISIJ International*, **54**(4), 900-908.
- Rao GKM, Satyanarayana S, Praveen M (2008) Influence of machining parameters on electric discharge machining of maraging steels - An experimental investigation, Proceedings of the World Congress on Engineering, Vol. II, July 2-4, 2008, London, UK.
- Rao P, Ramji K, Satyanarayana B (2014) Experimental investigation and optimization of wire EDM parameters for surface roughness, MRR and white layer in machining of aluminium alloy, *Procedia Materials Science*, **5**: 2197-2206.
- Rao RV, Kalyankar VD (2013) Parameter optimization of modern machining processes using teaching-learning-based optimization algorithm, *Engineering Applications of Artificial Intelligence*, **26**(1): 524-531.
- Rebelo JC, Dias AM, Kremer D, Lebrun JL (1998) Influence of EDM pulse energy on the surface integrity of martensitic steels, *Journal of Materials Processing Technology*, **84**(1): 90-96.
- Reddy TVS, Sornakumar T, Reddy MV, Venkatram R (2009) Machinability of C45 steel with deep cryogenic treated tungsten carbide cutting tool inserts, *International Journal of Refractory Metals and Hard Materials*, **27**(1): 181-185.
- Reed-Hill R, Abbaschian R (1991) Physical Metallurgy Principles, 3<sup>rd</sup> Edition, Boston: PWS-Kent Publishing.
- Rodrigues MA, Hassui A, da Silva RHL, Loureiro D (2015) Tool life and wear mechanisms during Alloy 625 face milling, *International Journal of Advanced Manufacturing Technology*, (Published online) DOI: 10.1007/s00170-015-8056-4.
- Routara BC, Mohanty SD, Datta S, Bandyopadhyay A, Mahapatra SS (2010) Combined quality loss (CQL) concept in WPCA-based Taguchi philosophy for optimization of multiple surface quality characteristics of UNS C34000 brass in cylindrical grinding, *International Journal of Advanced Manufacturing Technology*, **51**(1-4): 135-143.
- Saha SK, Choudhury SK (2009) Experimental investigation and empirical modelling of the dry electric discharge machining process, *International Journal of Machine Tools and Manufacture*, **49**: 297-308.
- Sait AN, Aravindan S, Haq AN (2009) Optimisation of machining parameters of glass-fibre-reinforced plastic (GFRP) pipes by desirability function analysis using Taguchi technique, *International Journal of Advanced Manufacturing Technology*, **43**(5-6): 581-589.
- Seah KHW, Rahman M, Yong KH (2003) Performance evaluation of cryogenically treated tungsten carbide cutting tool inserts, *Proceedings of the Institution of Mechanical Engineers Part B-Journal of Engineering Manufacture*, **217**(1): 29-43.

- Sengottuvel P, Satishkumar S, Dinakaran D (2013) Optimization of multiple characteristics of EDM Parameters based on desirability approach and fuzzy modeling, *Procedia Engineering*, **64**: 1069-1078.
- Shankar V, Rao KBS, Mannan S L (2001) Microstructure and mechanical properties of Inconel 625 super alloy, *Journal of Nuclear Materials*, **288**(2): 222-232.
- Sharma N, Singh A, Sharma R (2014) Modelling the WEDM Process Parameters for Cryogenic Treated D-2 Tool Steel by integrated RSM and GA, *Procedia Engineering*, **97**: 1609-1617.
- Sharma P, Chakradhar D, Narendranath S (2015) Evaluation of WEDM performance characteristics of Inconel 706 for turbine disk application, *Materials and Design*, **88**: 558-566.
- Sibaliya TV, Majstorovic VD (2009) Multi-response optimisation of thermosonic copper wire-bonding process with correlated responses, *International Journal of Advanced Manufacturing Technology*, **42**(3-4): 363–371.
- Sidhu TS, Prakash S, Agrawal RD (2006) Studies of the metallurgical and mechanical properties of high velocity oxy-fuel sprayed stellite-6 coatings on Ni-and Fe-based superalloys, *Surface and Coatings Technology*, **201**(1): 273-281.
- Simao J, Lee HG, Aspinwall DK, Dewes RC, Aspinwall EM (2003) Workpiece surface modification using electrical discharge machining, *International Journal of Machine Tools and Manufacture*, **43**(2): 121–128.
- Şimşek B, İç YT, Şimşek EH (2013) A TOPSIS-based Taguchi optimization to determine optimal mixture proportions of the high strength self-compacting concrete, *Chemometrics and Intelligent Laboratory Systems*, **125**: 18-32.
- Singh A, Datta S, Mahapatra SS (2011) Application of TOPSIS in the Taguchi method for optimal machining parameter selection, *Journal for Manufacturing Science and Production*, **11**: 49-60.
- Singh A, Datta S, Mahapatra SS, Singha T, Majumdar G (2013) Optimization of bead geometry of submerged arc weld using fuzzy based desirability function approach, *Journal of Intelligent Manufacturing*, **24**(1): 35-44.
- Singh H, Kumar P (2006) Optimizing multi-machining characteristics through Taguchi's approach and utility concept, *Journal of Manufacturing Technology Management*, **17**(2): 255 – 274.
- Singh P, Kumar A, Kaushal A, Kaur D, Pandey A and Goyal RN (2008) In situ high temperature XRD studies of ZnO nanopowder prepared via cost effective ultrasonic mist chemical vapour deposition, *Bulletin of Materials Science*, **31**(3): 573-577.

- Singh S, Maheshwari S, Pandey PC (2004) Some investigations into the electric discharge machining of hardened tool steel using different electrode materials, *Journal of Materials Processing Technology*, **149**(1-3): 272-277.
- Singh S, Pandey PC (2002) Surface finish quality in electric discharge machining—a review, Proceedings of the National Seminar on Emerging Convergent Technologies and System, SECTAS-2002, pp. 462-467, DEI, Dyalbagh, India.
- Sivaprakasam P, Hariharan P, Gowri S (2014) Modeling and analysis of micro-WEDM process of titanium alloy (Ti-6Al-4V) using response surface approach, *Engineering Science and Technology, an International Journal*, **17**: 227-235.
- Spur G, Schönbeck J (1993) Anode erosion in wire-EDM—a theoretical model, *CIRP Annals-Manufacturing Technology*, **42**(1): 253-256.
- Srivastava V, Pandey PM (2012a) Effect of process parameters on the performance of EDM process with ultrasonic assisted cryogenically cooled electrode, *Journal of Manufacturing Processes*, **14**(3): 393-402.
- Srivastava V, Pandey PM (2012b) Performance evaluation of electrical discharge machining (EDM) process using cryogenically cooled electrode, *Materials and Manufacturing Processes*, **27**(6): 683-688.
- Srivastava V, Pandey PM (2014) Statistical modelling and material removal mechanism of electrical discharge machining process with cryogenically cooled electrode, *Procedia Materials Science*, **5**: 2004-2013.
- Su CT, Tong LI (1997) Multi-response robust design by principal component analysis, *Total Quality Management*, **8**(6): 409–416.
- Subbaiah YPV, Prathap P, Reddy KTP (2006) Structural, electrical and optical properties of ZnS films deposited by close-spaced evaporation, *Applied Surface Science*, **253**(5): 2409–2415.
- Suh NP (1990) The principles of design. Oxford: Oxford University Press.
- Sundaram MM, Yildiz Y, Rajurkar KP (2009) Experimental study of the effect of cryogenic treatment on the performance of electro-discharge machining, Proceedings of the International Manufacturing Science and Engineering Conference, West Lafayette, October 4–7, 2009.
- Tai TY, Lu SJ (2009) Improving the fatigue life of electro-discharge-machined SDK11 tool steel via the suppression of surface cracks, *International Journal of Fatigue*, **31**(3): 433-438.
- Thakur DG, Ramamoorthy B, Vijayaraghavan L (2009) Study on the machinability characteristics of superalloy Inconel 718 during high speed turning, *Materials and Design*, **30**(5): 1718–1725.

- Thirumalai R, Senthilkumaar JS (2013) Multi-criteria decision making in the selection of machining parameters for Inconel 718, *Journal of Mechanical Science and Technology*, **27**(4): 1109-1116.
- Thomson PF (1989) Surface damage in electro-discharge machining, *Materials Science and Technology*, **5**: 1153-1157.
- Tiwary AP, Pradhan BB, Bhattacharyya B (2015) Study on the influence of micro-EDM process parameters during machining of Ti-6Al-4V superalloy, *International Journal of Advanced Manufacturing Technology*, **76**(1): 151-160.
- Tomlinson WJ, Adkin JR (1992) Microstructure and properties of electro discharge machined surfaces, *Surface Engineering*, **8**(4): 283-288.
- Tong LI, Wang CH (2002) Multi-response optimisation using principal component analysis and grey relational analysis, *International Journal of Industrial Engineering-Theory Applications and Practice*, **9**(4): 343-350.
- Tong LI, Wang CH, Chen HC (2005) Optimisation of multiple responses using principal component analysis and technique for order preference by similarity to ideal solution, *International Journal of Advanced Manufacturing Technology*, **27**(3): 407-414.
- Tönshoff HK, Brinksmeier E (1980) Determination of the mechanical and thermal influences on machined surfaces by microhardness and residual stress analysis, *CIRP Annals-Manufacturing Technology*, **29**(2): 519-530.
- Torres A, Puertas I, Luis CJ (2016) EDM machinability and surface roughness analysis of INCONEL 600 using graphite electrodes, *International Journal of Advanced Manufacturing Technology*, **84**(9): 2671-2688.
- Trucks H-E (1983) How cryogenics is used for the treatment of metals, *Manufacturing Engineering*, **91**(6): 54-55.
- Tsai HC, Yan BH, Huang FY (2003) EDM performance of Cr/Cu-based composite electrodes, *International Journal of Machine Tools and Manufacture*, **43**(3): 245-252.
- Tsai Y-Y, Masuzawa T (2004) An index to evaluate the wear resistance of the electrode in micro-EDM, *Journal of Materials Processing Technology*, **149**(1-3): 304-309.
- Tzeng YF, Chen FC (2007) Multi-objective optimisation of high-speed electrical discharge machining process using a Taguchi fuzzy-based approach, *Materials and Design*, **28**(4): 1159-1168.
- Upadhyay C, Datta S, Masanta M, Mahapatra SS (2016) An Experimental Investigation Emphasizing Surface Characteristics of Electro-Discharge Machined Inconel 601, *Journal of the Brazilian Society of Mechanical Sciences and Engineering*, (Published Online) DOI: 10.1007/s40430-016-0643-2.

- Vinila VS, Jacob R, Mony A, Nair HG, Issac S, Rajan S, Nair AS and Isac J (2014) XRD studies on nano-crystalline ceramic superconductor PbSrCaCuO at different treating temperatures, *Crystal Structure Theory and Applications*, **3**(1): 1-9.
- Vinothkumar TS, Kandaswamy D, Prabhakaran G, Rajadurai A (2015) Effect of dry cryogenic treatment on Vickers hardness and wear resistance of new martensitic shape memory nickel-titanium alloy, *European Journal of Dentistry*, **9**(4): 513–517.
- Walia RS, Shan HS, Kumar P (2006) Multi-response optimization of CFAAFM process through Taguchi method and utility concept, *Materials and Manufacturing Processes*, **21**(8): 907-914.
- Wallbank J (1980) Effect of EDM on material properties of die steels, *Metallurgia*, **47**(7): 356-362.
- Wang F, Liu Y, Shen Y, Ji R, Tang Z, Zhang Y (2013) Machining performance of Inconel 718 using high current density electrical discharge milling, *Materials and Manufacturing Processes*, **28**(10): 1147-1152.
- Wang K, Zhang Q, Liu Q, Zhu G, Zhang J (2016) Experimental study on micro electrical discharge machining of porous stainless steel, *International Journal of Advanced Manufacturing Technology*, (Published Online), DOI: 10.1007/s00170-016-9611-3.
- Wells PW, Willey PCT (1975) The effects of variation in dielectric flow rate in the gap on wear ratio and surface finish during electro-discharges, *Proceedings of IEE Conference*, **133**: 110-117, UK.
- Williams RE, Rajurkar KP (1991) Study of wire electrical discharge machined surface characteristics, *Journal of Materials Processing Technology*, **28**(1-2): 127-138.
- Wong YS, Lim LC, Lee LC (1995) Effects of flushing on electro-discharge machined surfaces, *Journal of Materials Processing Technology*, **48**(1): 299-305.
- Xavior MA, Adithan M (2009) Determining the influence of cutting fluids on tool wear and surface roughness during turning of AISI 304 austenitic stainless steel, *Journal of Materials Processing Technology*, **209**(2): 900-909.
- Yadav US, Yadava V (2014) Parametric study on electrical discharge drilling of aerospace nickel alloy, *Materials and Manufacturing Processes*, **29**(3): 260-266.
- Yadav US, Yadava V (2015) Experimental investigation on electrical discharge drilling of Ti-6Al-4V alloy, *Machining Science and Technology*, **19**(4): 515-535.
- Yager RR, Filev DP (1994) *Essentials of fuzzy modeling and control*. New York.
- Yan BH, Tsai HC, Huang FY (2005) The effect in EDM of a dielectric of a urea solution in water on modifying the surface of Titanium, *International Journal of Machine Tools and Manufacture*, **45**(2): 194-200.

- Yang WH, Tarng YS (1988) Design optimisation of cutting parameters for turning operations based on the Taguchi method, *Journal of Materials Processing Technology*, **84**(1-3): 122-129.
- Yao YL, Cheng GJ, Rajurkar KP, Kovacevic R, Feiner S, Zhang W (2005) Combined research and curriculum development of nontraditional manufacturing, *European Journal of Engineering Education*, **30**(3): 363-376.
- Yildiz Y, Sundaram MM, Rajurkar KP, Altintas A (2015) Correlation of surface roughness and recast layer thickness in electrical discharge machining, *Proceedings of the Institution of Mechanical Engineers, Part E: Journal of Process Mechanical Engineering*, (Published online) DOI: 0954408915600949.
- Yildiz Y, Sundaram MM, Rajurkar KP, Nalbant M (2011) The effects of cold and cryogenic treatments on the machinability of beryllium-copper alloy in electro discharge machining, *Proceedings of the 44<sup>th</sup> CIRP Conference on Manufacturing Systems*, Madison, WI, May 31–June 3, 2011.
- Zadeth LA (1976) A fuzzy algorithmic approach to definition of complex and imprecise concept, *International Journal of Man-Machine Studies*, **8**: 249-291.
- Zeid OA (1967) On the effect of electro-discharge machining parameters on the fatigue life of AISI D6 tool steel, *Journal of Materials Processing Technology*, **68**(1): 27-32.

Websites:

<http://www.hightempmetals.com/index.php>  
<http://megamex.com>  
<http://www.californiametal.com/>  
<http://www.kennametal.com>  
<http://www.EDMtodayMagazine.com>  
<http://www.specialmetals.com>





# Dissemination

## Internationally Indexed Journals (*Web of Science, SCI, Scopus*)<sup>1</sup>

**Rahul**, Kumar Abhishek, Saurav Datta, Bibhuti Bhusan Biswal, Siba Sankar Mahapatra, *Machining Performance Optimization for Electro Discharge Machining of Inconel 601, 625, 718 and 825: An Integrated Optimization Route Combining Satisfaction Function, Fuzzy Inference System and Taguchi Approach*, **Journal of the Brazilian Society of Mechanical Sciences and Engineering**. (**Published Online**) DOI: [10.1007/s40430-016-0659-7](https://doi.org/10.1007/s40430-016-0659-7)

**Rahul**, Saurav Datta, Bibhuti Bhusan Biswal, Siba Sankar Mahapatra, 2017, *A Novel Satisfaction Function and Distance Based Approach for Machining Performance Optimization during Electro-Discharge Machining on Super Alloy Inconel 718*, **The Arabian Journal for Science and Engineering**, 42: 1999-2020. DOI: [10.1007/s13369-017-2422-5](https://doi.org/10.1007/s13369-017-2422-5)

**Rahul**, Saurav Datta, , Bibhuti Bhusan Biswal, Siba Sankar Mahapatra, 2017, *Electrical Discharge Machining of Inconel 825 using Cryogenically Treated Copper Electrode: Emphasis on Surface Integrity and Metallurgical Characteristics*, **Journal of Manufacturing Processes**, 26: 188-202. (<http://dx.doi.org/10.1016/j.jmapro.2017.02.020>)

**Rahul**, Kumar Abhishek, Saurav Datta, Bibhuti Bhusan Biswal, Siba Sankar Mahapatra, 2017, *Machining Performance Optimization during EDM of Inconel 718: A Case Experimental Investigation*, **International Journal of Productivity and Quality Management**, 21(4): 460-489. (<https://doi.org/10.1504/IJPQM.2017.085255>)

**Rahul**, Saurav Datta, Manoj Masanta, Bibhuti Bhusan Biswal, Siba Sankar Mahapatra, *Analysis on Surface Characteristics of Electro-Discharge Machined Inconel 718*, **International Journal of Materials and Product Technology**. (**Accepted**)

Chandramani Upadhyay, **Rahul**, Saurav Datta, Siba Sankar Mahapatra, Bibhuti Bhusan Biswal, *An Experimental Investigation on Electro Discharge Machining (EDM) of Inconel 601*, **International Journal of Industrial and Systems Engineering**. (**Accepted**)

## Conferences<sup>1</sup>

**Rahul**, Chandramani Upadhyay, Saurav Datta, Bibhuti Bhusan Biswal, Siba Sankar Mahapatra, *Machining Performance Optimization for Electro Discharge Machining of Inconel 625: A Case Experimental Study*, **4<sup>th</sup> Asia Conference on Mechanical and Materials Engineering (ACMME 2016)**, during July 14-16, 2016, **Kuala Lumpur, Malaysia**.

**Rahul**, Saurav Datta, Bibhuti Bhusan Biswal, Siba Sankar Mahapatra, *Analysis of Surface Characteristics of Electro-Discharge Machined of Super Alloy Inconel 601: A Multi-Response Optimization Route Combining TOPSIS and Taguchi Method*, **International Conference on Evolutions in Manufacturing: Technologies and Business Strategies for Global Competitiveness**, November 12-13, 2016, organized by Department Of Production Engineering, **Birla Institute of Technology Mesra, Ranchi & The Institution of Engineers (India), Jharkhand State Centre** (Under the Aegis of Production Engineering Division Board, IEI).

**Rahul**, Saurav Datta, Bibhuti Bhusan Biswal, Siba Sankar Mahapatra, *Optimization of Surface Roughness, Surface Crack Density and White Layer Thickness of Electro-Discharge Machined Super Alloy Inconel 718: Application of TOPSIS Integrated with Taguchi Method*, **4<sup>th</sup> International Conference on Production and Industrial Engineering (CPIE 2016)**, held during December 19-21, 2016 at **Dr. B.R. Ambedkar NIT, Jalandhar**.

**Rahul**, Saurav Datta, Bibhuti Bhusan Biswal, Siba Sankar Mahapatra, *Optimization of EDM Responses on Super Alloy Inconel 718: Use of Satisfaction Function Approach Combined with Taguchi Philosophy*, **7<sup>th</sup> International Conference on Materials Processing and Characterization (ICMPC 2017)**, 17-19 March 2017, **GRIET, Hyderabad**.

**Rahul**, Ankur Srivastava, Dileep Mishra, Suman Chatterjee, Saurav Datta, Bibhuti Bhusan Biswal, Siba Sankar Mahapatra, *Multi-Response Optimization during Electro-Discharge Machining of Super Alloy Inconel 718: Application of PCA-TOPSIS*, **7<sup>th</sup> International Conference on Materials Processing and Characterization (ICMPC 2017)**, during March 17-19, 2017, at **GRIET, Hyderabad**.

## Article under Review <sup>2</sup>

**Rahul**, Saurav Datta, Bibhuti Bhusan Biswal, Siba Sankar Mahapatra, *Machinability Analysis of Inconel 601, 625, 718 and 825 in Electro Discharge Machining: An Experimental Investigation*, for consideration in: **Measurement**.

**Rahul**, Saurav Datta, Manoj Masanta, Bibhuti Bhusan Biswal, Siba Sankar Mahapatra, *On Electro-Discharge Machining of Cryogenically Treated Super Alloy Inconel 825 using Cooper Tool Electrode: A Case Experimental Research*, for consideration in: **International Journal of Materials and Product Technology**.

**Rahul**, Saurav Datta, Bibhuti Bhusan Biswal, *Effect of Cryogenic Treatment of Tool Electrode and Workpiece Material on Evaluating Machinability of Super Alloy Inconel 825 during Electro-Discharge Machining*, for consideration in: **Measurement**.

---

<sup>1</sup>Articles already published, in press, or formally accepted for publication.

<sup>2</sup>Articles under review/communicated/ to be communicated.



## **Resume**

### **PERSONAL DETAILS**

**Name:** RAHUL

**Father's Name:** Mr. Ram Kamal Choudhary

**Date of Birth:** Oct 20, 1988

**Gender:** Male

**Permanent Address:** Gayatri Puram Ward No. 19, Nakaha No. 1, Basharatpur, 273004  
Gorakhpur, Uttar Pradesh, India

**Mobile No.:** +91 9583640120/ +91 9439709541

**Email:** rahulkumar589@gmail.com

### **ACADEMIC QUALIFICATION**

<b>Exam/Degree</b>	<b>Institute/University</b>	<b>Department/Field</b>	<b>Year</b>	<b>% Marks /CGPA</b>
Ph. D. ( <i>Dissertation being submitted</i> )	National Institute of Technology Rourkela, Odisha, India	Industrial Design	2017	8.77/10
M. Tech.	Sant Longowal Institute of Engineering and Technology ( <i>Deemed University</i> ), Sangrur, Punjab	Mechanical Engineering (Specialization in Welding and Fabrication)	2013	6.92/10
B. Tech.	Gautam Buddha Technical University, Uttar Pradesh	Mechanical Engineering	2011	68.58
Diploma (Engg.)	Government Polytechnic, Gorakhpur, Uttar Pradesh	Mechanical Production Engineering	2007	71.13
High School (+2 Standard)	Jawahar Navodaya Vidyalaya Gorakhpur, Uttar Pradesh	Science	2004	73.40

---

**Rahul**